UCLA

· Department of Physics ·

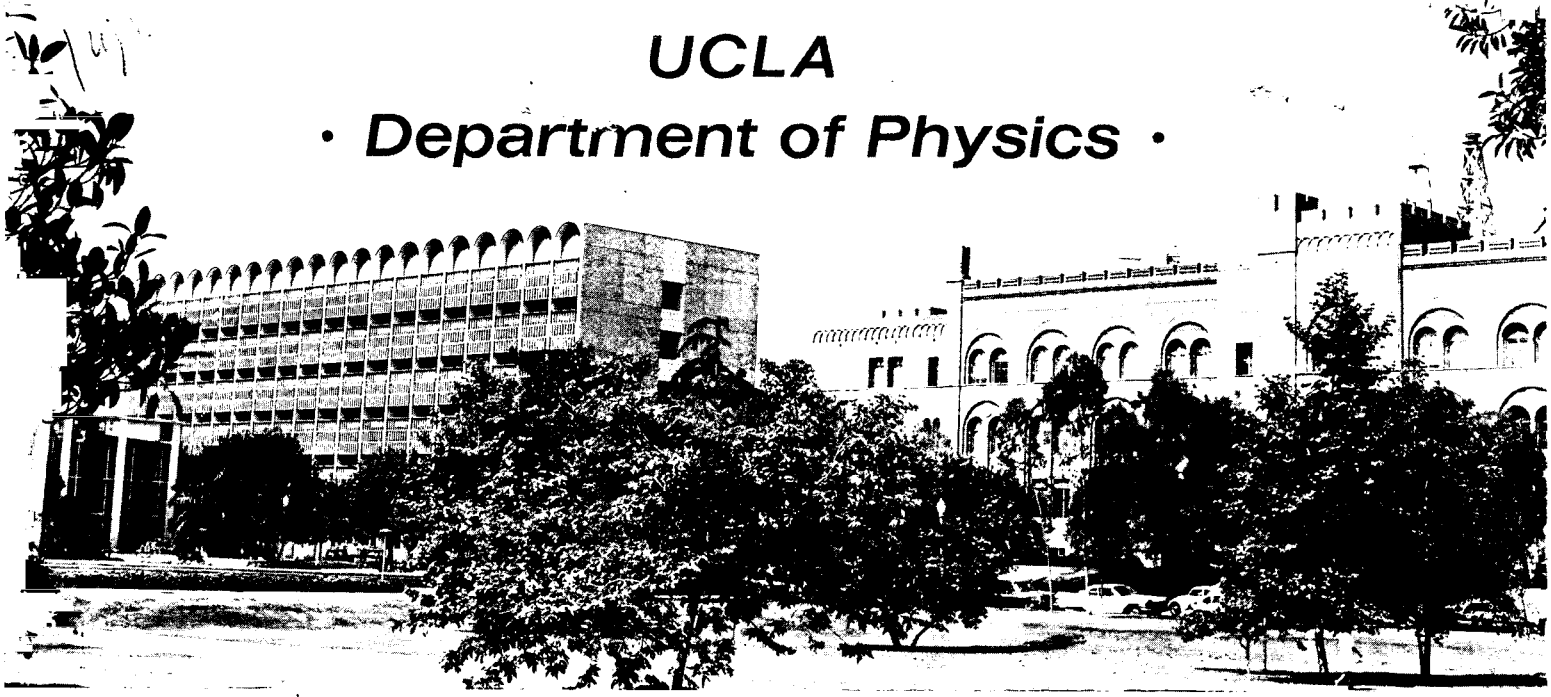

(NASA-CR-125416) ELECTROMAGNETIC PLASMA WAVE PROPAGATION ALONG A MAGNETIC FIELD Ph.D. Thesis C.L. Olson (California Univ.) Jun. 1970 264 p CSCL 20I

N72-15666

Unclas

G3/25 13525

(CATEGORY)

RECEIVED
NASA STI FACILITY
INPUT BRANCH

LOS ANGELES 90024

CALIFORNIA

Reproduced by
NATIONAL TECHNICAL
INFORMATION SERVICE
U S Department of Commerce
Springfield VA 22151

Plasma Physics Group
Department of Physics
University of California
Los Angeles, California 90024

Electromagnetic Plasma Wave Propagation Along a Magnetic Field

Craig Lee Olson

June 1970

A dissertation submitted in partial satisfaction of the requirements for the degree Doctor of Philosophy in Physics.

Partially supported by the Office of Naval Research, Grant #N00014-69-A-0200-4023; the National Science Foundation, Grant #GP-6817; the Atomic Energy Commission, Contract AT(04-3)-34, Project #157; and the National Aeronautics and Space Administration, Contract #NGR-05-007-190.

Copyright by

Craig Lee Olson

1970

PRECEDING PAGE BLANK NOT FILMED

TABLE OF CONTENTS

LIST OF FIGURES

PART I

PART II

APPENDICES

ACKNOWLEDGMENTS

I am deeply grateful to Professor Burton D. Fried for introducing me to, and supporting my research efforts in, theoretical plasma physics. I also graciously acknowledge Professor Fried for originally suggesting the transverse echo problem (which forms Part II of this dissertation), for consultation during the course of my research activities, and for a thorough, critical evaluation of the preliminary draft of this dissertation. I wish to thank Professor Charles F. Kennel for his enthusiastic response to the preliminary draft of this dissertation and for his pertinent comments concerning the subtleties of performing the Fourier-Laplace inversion in Part I. I am also grateful to Professor Alfred Y. Wong for providing experimental motivation for the research contained in this dissertation.

Numerous discussions with Dr. George L. Johnston and Dr. C. L. Hedrick are gratefully acknowledged and pleasantly remembered. Specifically I am thankful to Dr. Johnston for his suggestion to first Fourier-Laplace invert the first-order terms in the echo problem and then solve the second-order Vlasov equation (thereby avoiding a convolution integral which defied further rigorous manipulation). Discussions with Dr. Newell Booth on experimental considerations are also gratefully acknowledged.

The research in this dissertation was supported in part by the Office of Naval Research through Contract NONR 4756(01).

Extensive use of the University of California Mathematical On-Line Computing System is gratefully acknowledged.

PRECEDING PAGE BLANK NOT FILMED
xi, xii,

ABSTRACT OF THE DISSERTATION

Electromagnetic Plasma Wave Propagation

Along a Magnetic Field

by

Craig Lee Olson

Doctor of Philosophy in Physics

University of California, Los Angeles, 1970

Professor Burton D. Fried, Chairman

Part I: Steady-state excitation of transverse plasma waves along a magnetic field.

The linearized response of a Vlasov plasma to the steady-state excitation of transverse plasma waves along an external magnetic field is examined. Previous research is reviewed. Assuming a delta-function excitation mechanism, and performing a detailed Vlasov-Maxwell equation analysis using Fourier-Laplace transforms, the plasma response is found to consist of three terms: a branch-cut term, a free-streaming term, and a dielectric-pole term(s). These terms are examined analytically, and numerically evaluated for a case in which the driving frequency (ω_1) is slightly below the electron cyclotron frequency (ω_{ce}). In addition to the least-damped pole term, it is shown that the free-streaming term is always significant and the branch-cut term is significant when $\omega_1 \simeq \omega_{ce}$. The infinite sequence of pole terms (that result from the infinite number of roots of the appropriate transverse dispersion relation) is shown to be negligible except at positions very close to the place of excitation. Effects of Krook model collisions are investigated,

as well as effects of a finite-width excitation mechanism.

Part II: Steady-state transverse plasma wave echoes.

The phenomenon of plasma wave echoes, introduced by Gould, Malmberg, O'Neil, and Wharton for the case of longitudinal electrostatic waves, is extended to the case of transverse plasma waves that propagate along an external magnetic field. It is shown that a transverse echo results in lowest order only when one excitation is transverse and the other is longitudinal. For this case, the second-order (nonlinear) plasma echo response is computed from the Vlasov-Maxwell equations up to an integral over the velocity variable v_z. Transverse echo characteristics are discussed and several experiments are suggested. The integral over v_z is evaluated by the method of steepest descent; the results are explained physically and also evaluated numerically for some specific cases. Several extensions are considered: (1) effects of Fokker-Planck collisions and finite-width excitation mechanisms, (2) effects of temperature anisotropy ($T_\perp \neq T_z$), and (3) effects of propagation just off-axis ($k_\perp \neq 0$). Lastly, transverse echoes for the case of no external magnetic field are examined.

In addition, several appendices concerning Part I and Part II are presented, the most important of these being (1) a thorough investigation of the roots of the transverse dispersion relation ($\underline{k} \parallel \underline{B}_o$) for real ω and complex k, and (2) the method of steepest descent as used in evaluating the branch-cut and phase-mixing integrals that occur in Part I and Part II.

I. STEADY-STATE EXCITATION OF TRANSVERSE PLASMA WAVES ALONG AN EXTERNAL MAGNETIC FIELD

1. Introduction

A sizable portion of the plasma physics research done to date involves the theory of waves in plasmas. Of fundamental interest are calculations or experiments concerning the damping (or growth) of the basic types of wave motion a plasma can support. Two types of problems are readily discernible: (1) the initial-value problem in which a wave is imposed on the plasma at some specific time, and it is desired to know how the plasma response decays (or grows) in time; and (2) the steady-state problem in which a wave is continuously excited at some point in a plasma, and it is desired to know how the plasma response decays (or grows) in distance. We will be concerned with the steady-state problem since it should be more readily realizable experimentally.

Purely longitudinal waves which experience spatial Landau damping have been examined in theory extensively (since Landau's original paper[1]) by Gould[2] and by Johnston,[3] et al.[4,5] and in experiment by Wong, D'Angelo, and Motley, et al.[6] However, the corresponding work for purely transverse waves that propagate along an external magnetic field (and therefore experience cyclotron damping when the driving frequency is near the cyclotron frequency) has received relatively little attention to date.

Thus the problem to which we address ourselves is that of determining the response of a Vlasov plasma (a hot correlationless plasma) to a localized steady-state excitation of transverse electromagnetic waves

that propagate along an external magnetic field. We are specifically interested in obtaining the form of the response when the excitation frequency is just below the electron cyclotron frequency, i.e., when electron cyclotron damping is significant. One primary objective of this theoretical calculation is to obtain the cyclotron-damped response and see if it is adequately represented by consideration of just the "least-damped root" of an appropriate transverse dispersion relation. We will find in general that it is not.

Another motivation for this work is that the response of a single transverse excitation should be well understood before embarking on studies of the nonlinear response of two spatially separated excitations, such as occur in Part II of this dissertation where we shall investigate transverse plasma wave echoes. The production of an echo (as will be explained in Part II) depends on the free-streaming term of the first-order distribution function produced by the first of the two excitations. Thus in computing the response of a single transverse excitation now, we will pay particular attention to the transverse free-streaming waves that are produced.

We present a brief summary of previous research. First we review work on the related problem of the steady-state excitation of longitudinal plasma waves. Experimental verification of spatial Landau damping was reported by Wong, D'Angelo, and Motley[6] who compared their experimental results with a simple theory that involved just the least-damped root of the appropriate longitudinal dispersion relation. Use of just the least-damped root in this case was questioned by Gould[2] who rigorously investigated the first-order (linear) response for the problem

assuming an idealized dipole-grid excitation mechanism. Gould's results showed that the true response was indeed more complicated than that obtained from considering just the least-damped root and that the response was approximately exponentially damped only over a restricted region in space. Further theoretical work including the effects of finite spacing of the pair of excitation grids and also a calculation of the second-order (nonlinear) response was performed by Johnston.[3]

The longitudinal dispersion relation mentioned above has an infinite number of roots. Fried and Gould[7] have examined in detail the loci of the roots of this dispersion relation for real k and complex ω. Their results are pertinent to initial value problems in which a fixed real k is imposed at a specific time and then the initial perturbation decays (or grows) in time. Similarly, Kuehl, Stewart, and Yeh[8] and Derfler and Simonen[9] have examined the roots of the longitudinal dispersion relation for real ω and complex k. Their results are pertinent to steady-state problems (as discussed above) in which a fixed real ω is continuously excited and the resultant spatial perturbations decay (or grow) in distance. We shall comment more on their results in Appendix D.

We now consider the transverse excitation problem which we find has only been partially investigated in the past. The principal paper is that of Shafranov[10] who considered a related problem, the half-space problem. (The full-space problem that we shall consider is different than the half-space problem in that, in addition to other effects, free-streaming waves are produced by those particles that pass through the excitation region. In the half-space problem particles never pass

through the excitation region but are reflected at the half-space boundary where the excitation is applied.) Shafranov obtained a branch-cut term and a pole term for the response (as we shall find also). However, we note the following errors and inadequacies in his work:

(i) The saddle-point contours for the k (actually kc/ω) inversion integral are drawn to the wrong asymptotes. Also the primitive contour was closed in some unexplained manner whereas it should really be deformed away from its initial position. In addition the resultant saddle point contributions contain phase factors that do not occur in usual saddle point theory.

(ii) Only one root of the appropriate transverse dispersion relation is considered whereas in fact there are an infinite number of them.

(iii) Useful values of the cyclotron damped root are not given. A cubic equation is given, which if solved, gives the value of the cyclotron-damped root at $\omega = \omega_{ce}$ (ω_{ce} is the electron cyclotron frequency). The only other expression given for the value of the cyclotron-damped root is an asymptotic result which cannot be derived rigorously as we shall show in Appendix C.

(iv) No estimates are given for the range of validity of the branch-cut term. In addition it is stated that the branch-cut term is the most important term at large distances from the place of excitation for $\omega_{ce} < \omega < \omega_R$ (ω_R is the right-hand cutoff frequency); we shall find that the branch-cut term is significant only very close to the place of excitation.

Thus Shafranov's work represents only a first attempt at solving the problem.

Other research on the half-space problem includes Sach's[11] work on the effects of collisions on ion cyclotron waves. In this work two least-damped roots were obtained by keeping two terms in the asymptotic expansion (of the plasma dispersion function that occurs in the dispersion relation) with the result that the roots are not valid unless the collision frequency is appropriately high. Another related work is that of Platzman and Buchsbaum[12] on the reflection and transmission of transverse waves into a semi-infinite plasma. In this work a Lorentzian zero-order distribution function was used (to simplify numerical calculations) and attention was focused on determining the effects of collisions on the reflection and transmission coefficients. Lastly we note that in an experiment directly related to our problem, Crawford et al.[13] have attempted to measure spatial electron cyclotron damping but were unsuccessful because of high collision rates. The results they did obtain were compared with a simple, least-damped root theory. Clearly a thorough rigorous theoretical investigation of the steady-state transverse excitation problem is still needed, and that is what we shall present shortly.

The transverse dispersion relation mentioned above has previously been only partially examined. (We state explicitly that, as used henceforth, the transverse dispersion relation refers to wave propagation exactly along the external magnetic field.) Many authors[14-19] have derived the transverse dispersion relation but all of them considered real k and complex ω and then, at most, obtained an asymptotic expression for the value of the least-damped root. Recently Kamimura and Hasegawa[20] have presented numerical results concerning the value

of the least-damped root (for real k and complex ω) for several choices of the pertinent parameters. At present, however, there exists no work that classifies and examines the infinite number of roots of the transverse dispersion relation for real k and complex ω.

Previous work on the roots of the transverse dispersion relation for real ω and complex k is even scarcer. Only isolated instances may be found such as in Stix[17] and in Shafranov[10] (as mentioned above); in both of these the value of the cyclotron-damped root is given exactly at $\omega = \omega_{ce}$. Also, in Shafranov an asymptotic result is given for ω far from ω_{ce}, a result which, as we shall show in Appendix C, cannot be derived rigorously and is therefore incorrect. Crawford et al.[13] have presented some numerical results for the cyclotron-damped root (for $\omega_{pe}^2/\omega_{ce}^2 = 40$ where ω_{pe} is the electron plasma frequency) but no detailed study of the behavior of this root was made. Thus a classification and thorough investigation of the infinite number of roots of the transverse dispersion relation for real ω and complex k is still needed and that is what we will present in Appendix C.

We have performed a detailed theoretical investigation of the steady-state transverse excitation problem assuming an external excitation of the form

$$\underline{E}_{ext}(z,t) = E_1(z)\left[\hat{e}_x \cos(\omega_1 t) + \hat{e}_y \sin(\omega_1 t)\right] \tag{1.1}$$

$$E_1(z) = \mathcal{J}_1 \delta(z) \tag{1.2}$$

Before commencing with our presentation we summarize the most important

results that will be obtained:

(1) From a rigorous derivation starting with the Vlasov-Maxwell equations we find that the first-order (linear) current response consists of three terms as given in Eq. (2.85); a branch-cut term, a free-streaming term, and a dielectric-pole term.

(2) Numerical evaluation of these terms for a specific case in which ω_1 is slightly below ω_{ce} (with $\omega_{pe}/\omega_{ce} = 0.4$, $c/a = 1120$; these being typical values for the UCLA Q machine) shows that, in addition to the pole term, the branch-cut and free-streaming terms have significant amplitudes and penetration distances (see Figs. 7a-f). Thus the plasma response is not correctly given by consideration of just a "least-damped root."

(3) An analytical investigation of the three terms shows that the penetration lengths of both the branch-cut and free-streaming terms would approach infinity as ω_1 approached ω_{ce} were it not for the fact that certain dielectric functions are present (in these terms) which effectively shield these terms and actually cause their penetration lengths to go to zero as ω_1 approaches ω_{ce} , provided $(\omega_{pe}^2/\omega_{ce}^2)(c/a) \gg 1$. If $(\omega_{pe}^2/\omega_{ce}^2)(c/a) \ll 1$ then no such shielding effect occurs. In addition we show that the infinite number of residue terms (that occur because the transverse dispersion relation has an infinite number of roots) is negligible except at distances extremely close to $z = 0$.

(4) The physical nature of transverse free-streaming waves and of the free-streaming term in (2.85) is discussed. Explanations are given for (i) why transverse free-streaming waves have negative phase

velocities, (ii) why transverse free-streaming waves experience no cyclotron damping, (iii) why the free-streaming term in (2.85) has an accompanying pole contribution for $\omega_l < 0$ or $\omega_l > \omega_{ce}$ but <u>not</u> for $0 < \omega_l < \omega_{ce}$, and (iv) why the free-streaming term in (2.85) always diverges at $z = 0$ and how this divergence can be removed.

(5) Effects of collisions on the three terms in (2.85) are examined using the Krook model. It is shown that previous work by Crawford et al.[13] (concerning the locus of points where cyclotron damping equals collisional damping on a T_e vs. ω_l/ω_{ce} plot) is in error (see Fig. 10). The correct loci are then computed (see Fig. 11). From the results it is shown that cyclotron damping measurements (with negligible collision interference) are just barely feasible on the UCLA Q machine (for $n_e = 10^{10}$ cm^{-3}). In general, cyclotron-damping measurements would be more feasible at higher energies ($T_e > 0.2$ eV) and lower densities ($n_e < 10^{10}$ cm^{-3}).

(6) Effects of a finite-width excitation mechanism on the three terms in (2.85) are examined. In place of (1.2), we consider two choices of $E_1(z)$ [square-shaped in (7.3) and Gaussian-shaped in (7.11)]. Both choices yield qualitatively the same results which are: (i) the divergence of the free-streaming term at $z = 0$ is removed, and (ii) that when the width of the excitation region is greater than the characteristic length of a specific term in (2.85), then that term is reduced in amplitude. Thus, under certain conditions it is possible to diminish the size of the branch-cut and free-streaming terms while leaving the dielectric-pole term essentially unchanged.

In the course of obtaining the above results we shall refer to

Appendices A, B, C, E. Appendix A contains the solution of the linearized Vlasov equation and Appendix B examines symmetry properties of the transverse dispersion relation. A thorough investigation of the roots of the transverse dispersion relation for real ω and complex k is given in Appendix C, as mentioned earlier. Lastly, Appendix E contains an explanation of the method of steepest descent and a detailed account of the paths of steepest descent used in evaluating branch-cut and phase-mixing integrals. Material relegated to the appendices is actually text material in the usual sense and it contains many results, both analytical and numerical, that should be of general interest. This material was placed in the appendices because it must be referred to both now in Part I (the single transverse excitation problem) and later in Part II (the transverse echo problem).

We proceed to give the results of our investigation of the single transverse excitation problem.

2. Derivation of the Linear Response from the Vlasov-Maxwell Equations

2.1 Formulation of the problem and method of solution using Fourier-Laplace transforms.

We wish to compute the response of a hot correlationless plasma in an external magnetic field to the spatial excitation of transverse electromagnetic waves that propagate along the direction of the external magnetic field. The plasma is described by Maxwell's equations, and the Vlasov equation which for a plasma in external magnetic and electric fields is

$$\frac{\partial f}{\partial t} + \underline{v}\cdot\frac{\partial f}{\partial \underline{x}} + \frac{q}{m}\left[\underline{E}_{TOTAL} + \frac{1}{c}\underline{v}\times\underline{B}_{TOTAL}\right]\cdot\frac{\partial f}{\partial \underline{v}} = 0 \qquad (2.1)$$

where $f = f(\underline{x},\underline{v},t)$ is the distribution function (normalized to unity) of the species whose particles have charge q and mass m, c is the speed of light, and the subscripts on $\underline{E}$ and $\underline{B}$ are used to emphasize that these are the total fields (plasma fields plus external fields). Taking the zero-order external magnetic field to be $\underline{B}_o = B_o\hat{e}_z$ and using cylindrical coordinates for the velocity $\underline{v}$ (as shown in Fig. 1) we find

$$\frac{\partial f}{\partial t} + \underline{v}\cdot\frac{\partial f}{\partial \underline{x}} - \Omega\frac{\partial f}{\partial \phi} + \frac{q}{m}\left[\underline{E}_p + \underline{E}_{ext} + \frac{1}{c}\underline{v}\times\left(\underline{B}_p + \underline{B}_{ext}\right)\right]\cdot\frac{\partial f}{\partial \underline{v}} = 0 \qquad (2.2)$$

where $\Omega = qB_o/mc$ (a signed quantity) is the cyclotron frequency, and the subscripts (p) and (ext) refer to (plasma) and (external), respectively.

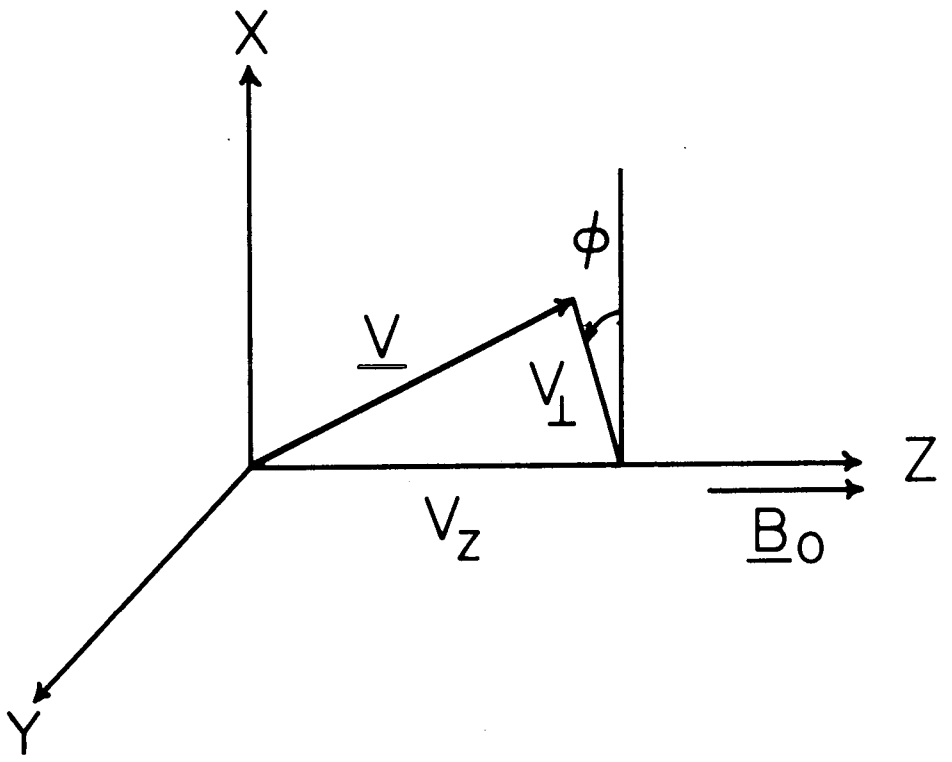

FIGURE 1. CYLINDRICAL COORINATES USED FOR THE VELOCITY VECTOR $\underline{V}$.

We assume a perturbation expansion of f , $\underline{E}_p$, and $\underline{B}_p$ with

$$\begin{aligned} f(\underline{x},\underline{v},t) &= f_0(\underline{v}) + f_1(\underline{x},\underline{v},t) + f_2(\underline{x},\underline{v},t) + \cdots \\ \underline{E}_p(\underline{x},\tau) &= \underline{E}_1(\underline{x},\tau) + \underline{E}_2(\underline{x},t) + \cdots \\ \underline{B}_p(\underline{x},t) &= \underline{B}_1(\underline{x},\tau) + \underline{B}_2(\underline{x},\tau) + \cdots \end{aligned} \tag{2.3}$$

where 0, 1, 2, refer to terms of zero, first, second order. We take $\underline{E}_{ext}$ and $\underline{B}_{ext}$ to be first order. Then in zeroth order, (2.3) is

$$-\Omega \frac{\partial f_0(\underline{v})}{\partial \phi} = 0 \tag{2.4}$$

which means the zero-order velocity distribution is

$$f_0(\underline{v}) = f_0(v_z, v_\perp) \tag{2.5}$$

In first order (2.3) is

$$\frac{\partial f_1}{\partial t} + \underline{v}\cdot\frac{\partial f_1}{\partial \underline{x}} - \Omega \frac{\partial f_1}{\partial \phi} + \frac{q}{m}\left[\underline{E}_1 + \underline{E}_{ext} + \frac{1}{c}\underline{v}\times\left(\underline{B}_1 + \underline{B}_{ext}\right)\right]\cdot\frac{\partial f_0}{\partial \underline{v}} = 0 \tag{2.6}$$

To obtain the first-order (linear) response we must solve (2.6) together with the appropriate Maxwell equations,

$$\nabla\times\left(\underline{E}_1 + \underline{E}_{ext}\right) = -\frac{1}{c}\frac{\partial}{\partial t}\left(\underline{B}_1 + \underline{B}_{ext}\right) \tag{2.7a}$$

$$\nabla\times\left(\underline{B}_1 + \underline{B}_{ext}\right) = \frac{4\pi}{c}\left(\underline{J}_1 + \underline{J}_{ext}\right) + \frac{1}{c}\frac{\partial}{\partial t}\left(\underline{E}_1 + \underline{E}_{ext}\right) \tag{2.7b}$$

where

$$\underline{J}_1 = nq\int f_1\,\underline{v}\,d^3v \tag{2.8}$$

and n is the density of the species under consideration. To handle all means of excitation we have kept $\underline{E}_{ext}$, $\underline{B}_{ext}$, $\underline{J}_{ext}$ (all first-order terms) in (2.7) but will later consider their effects individually.

We shall use Fourier-Laplace transforms to solve (2.6) - (2.8). For an arbitrary function $F(z)$ the Fourier transform and its inversion are defined by

$$F(k) \equiv \int_{-\infty}^{+\infty} dz\ F(z)\, e^{-ikz}$$

$$F(z) \equiv \int_{-\infty}^{+\infty} \frac{dk}{2\pi}\ F(k)\, e^{+ikz} \tag{2.9}$$

Similarly for an arbitrary function $F(t)$, the Laplace transform and its inversion are defined by

$$F(\omega) \equiv \int_{0}^{\infty} dt\ F(t)\, e^{+i\omega t} \qquad \mathrm{Im}\,\omega > 0$$

$$F(t) \equiv \int_{-\infty+i\delta}^{+\infty+i\delta} \frac{d\omega}{2\pi}\ F(\omega)\, e^{-i\omega t} \tag{2.10}$$

where in the former we have assumed $\mathrm{Im}\,\omega > 0$ initially to insure causality (then $e^{+i\omega t} \to 0$ for $t \to \infty$) and in the latter we require δ to be such that the ω contour is above all singularities of $F(\omega)$. The combined Fourier-Laplace transform pair and its inversion may be written

$$F(k,\omega) = \int_0^{\infty} d\tau \int_{-\infty}^{+\infty} dz\, F(z,t)\, e^{-i(kz-\omega\tau)} \qquad \text{Im}\,\omega > 0 \tag{2.11}$$

$$F(z,t) = \int_{-\infty+i\delta}^{+\infty+i\delta} \frac{d\omega}{2\pi} \int_{-\infty}^{+\infty} \frac{dk}{2\pi}\, F(k,\omega)\, e^{+i(kz-\omega\tau)} \tag{2.12}$$

Using (2.11) we shall transform Eqs. (2.6), (2.7) to k, ω space, solve these equations in k, ω space (a relatively easy task), and then use (2.12) to transform back to z, t space (a relatively difficult task).

2.2 Solution in transform space (k,ω)

Taking Fourier-Laplace transforms of (2.7a,b) gives

$$\underline{k} \times \left(\underline{E}_{,} + \underline{E}_{ext}\right) = \frac{\omega}{c}\left(\underline{B}_{,} + \underline{B}_{ext}\right) \tag{2.13a}$$

$$-\underline{k} \times \left(\underline{B}_{,} + \underline{B}_{ext}\right) = \frac{4\pi i}{c}\left(\underline{J}_{,} + \underline{J}_{ext}\right) + \frac{\omega}{c}\left(\underline{E}_{,} + \underline{E}_{ext}\right) \tag{2.13b}$$

where we have assumed Im ω > 0 and

$$\underline{E}_{,}(t=0) = \underline{E}_{ext}(\tau=0) = 0$$
$$\underline{B}_{,}(\tau=0) = \underline{B}_{ext}(t=0) = 0 \tag{2.14}$$

In (2.13a,b) $\underline{B}$, $\underline{E}$, and $\underline{J}$ are all now functions of k, ω. Combining (2.13a,b) we obtain

$$(\underline{E}_1 + \underline{E}_{ext})(k^2c^2 - \omega^2) - c^2\underline{k}\left[\underline{k}\cdot(\underline{E}_1 + \underline{E}_{ext})\right] = 4\pi i\omega(\underline{J}_1 + \underline{J}_{ext}) \tag{2.15}$$

Since we are dealing with transverse sources, $\underline{k}\cdot\underline{J}_{ext} = \underline{k}\cdot\underline{E}_{ext} = 0$ which implies $\underline{k}\cdot\underline{E}_1 = \underline{k}\cdot\underline{J}_1 = 0$. Thus (2.15) is

$$(\underline{E}_1 + \underline{E}_{ext})(k^2c^2 - \omega^2) = 4\pi i\omega(\underline{J}_1 + \underline{J}_{ext}) \tag{2.16}$$

Equations (2.13a) and (2.16) summarize Maxwell's equations for our problem.

We now solve (2.5) for f_1 which will be used later in computing $\underline{J}_1$. Taking Fourier-Laplace transforms of (2.6) gives

$$i(\underline{k}\cdot\underline{v} - \omega)f_1 - \Omega\frac{\partial f_1}{\partial\phi} = -g(\phi) \tag{2.17}$$

$$g(\phi) \equiv -\frac{q}{m}\left[(\underline{E}_1 + \underline{E}_{ext}) + \frac{1}{\omega}\underline{v}\times\underline{k}\times(\underline{E}_1 + \underline{E}_{ext})\right]\cdot\frac{\partial f_0}{\partial\underline{v}} \tag{2.18}$$

where we have used (2.13a) to eliminate $\underline{B}_1 + \underline{B}_{ext}$. Expanding the triple vector product in (2.18) we obtain

$$g(\phi) = \frac{q}{m}\left[\left(1 - \frac{kv_z}{\omega}\right)(\underline{E}_1 + \underline{E}_{ext})\cdot\frac{\partial f_0}{\partial\underline{v}} + \frac{\underline{k}}{\omega}\underline{v}\cdot(\underline{E}_1 + \underline{E}_{ext})\frac{\partial f_0}{\partial v_z}\right] \tag{2.19}$$

where we have explicitly used

$$\underline{k} = k\hat{e}_z \tag{2.20}$$

In Appendix A it is shown that (2.17) has the solution [taking into account the necessary periodicity in ϕ , $f_1(\phi+2\pi) = f_1(\phi)$, and the fact that $k_\perp = 0$]

$$f_1(\phi) = \frac{\frac{1}{\Omega}}{e^{2\pi i \nu} - 1} \int_0^{2\pi} d\phi' g(\phi+\phi') e^{i\nu\phi'} \tag{2.21}$$

where

$$\nu = \frac{\omega - k v_z}{\Omega} \tag{2.22}$$

To perform the integral in (2.21) we need expressions for $\underline{E}\cdot\underline{v}$ and $\underline{E} \cdot \frac{\partial}{\partial \underline{v}}$ [which occur in (2.19)] in terms of ϕ . To this end it is useful to change to rotating coordinates.

In terms of the unit vectors

$$\hat{e}_\pm \equiv \frac{1}{\sqrt{2}} (\hat{e}_x \pm i \hat{e}_y) \tag{2.23}$$

the velocity vector $\underline{v}$ is

$$\underline{v} = \hat{e}_+ v_- + \hat{e}_- v_+ + \hat{e}_z v_z \tag{2.24}$$

where

$$\begin{aligned} v_\pm &\equiv \frac{1}{\sqrt{2}} (v_x \pm i v_y) \\ &= \frac{1}{\sqrt{2}} (v_\perp \cos\phi \pm i\, v_\perp \sin\phi) \\ &= \frac{1}{\sqrt{2}} v_\perp e^{\pm i\phi} \end{aligned} \tag{2.25}$$

Also

$$\frac{\partial}{\partial \underline{v}} = \hat{e}_+ \frac{\partial}{\partial v_+} + \hat{e}_- \frac{\partial}{\partial v_-} + \hat{e}_z \frac{\partial}{\partial v_z} \tag{2.26}$$

where

$$\frac{\partial}{\partial v_\pm} = \frac{1}{\sqrt{2}} e^{\mp i\phi} \frac{\partial}{\partial v_\perp} \mp \frac{i}{\sqrt{2}\, v_\perp} e^{\mp i\phi} \frac{\partial}{\partial \phi} \tag{2.27}$$

Now writing $\underline{E} = \hat{e}_{-\sigma} E_\sigma$ with summation over $\sigma = \pm 1$ implied, and noting that

$$\begin{aligned} \hat{e}_\pm \cdot \hat{e}_\pm &= 0 \\ \hat{e}_\pm \cdot \hat{e}_\mp &= 1 \end{aligned} \tag{2.28}$$

we obtain

$$\underline{E} \cdot \underline{v} = E_\sigma \frac{v_\perp}{\sqrt{2}} e^{-i\sigma\phi}$$

$$\underline{E} \cdot \frac{\partial}{\partial \underline{v}} = E_\sigma \frac{1}{\sqrt{2}} e^{-i\sigma\phi} \left\{ \frac{\partial}{\partial v_\perp} - i \frac{\sigma}{v_\perp} \frac{\partial}{\partial \phi} \right\} \tag{2.30}$$

Thus $g(\phi)$ in (2.19) becomes

$$g(\phi) = \frac{q}{m} \frac{1}{\sqrt{2}} \left(E_{1\sigma} + E_{ext\,\sigma} \right) e^{-i\sigma\phi} \left[\left(1 - \frac{k v_z}{\omega} \right) \frac{\partial f_0}{\partial v_\perp} + \frac{k v_\perp}{\omega} \frac{\partial f_0}{\partial v_z} \right] \tag{2.31}$$

There is no $\partial f_0 / \partial \phi$ term because of (2.4). Performing the ϕ' integration in (2.21) we find

$$f_1(\phi) = \frac{q \left(E_{1\sigma} + E_{ext\,\sigma} \right) e^{-i\sigma\phi}}{m \sqrt{2}\, i \left(\omega - k v_z - \sigma \Omega \right)} \left[\left(1 - \frac{k v_z}{\omega} \right) \frac{\partial f_0}{\partial v_z} + \frac{k v_\perp}{\omega} \frac{\partial f_0}{\partial v_z} \right] \tag{2.32}$$

We may now compute $\underline{J}_1$ as given by (2.8),

$$\underline{J}_1 = nq \int f_1 \underline{v}\, d^3v \tag{2.8}$$

Noting that

$$\underline{v}\, d^3v = \left[\hat{e}_+ \frac{1}{\sqrt{2}} v_\perp e^{-i\phi} + \hat{e}_- \frac{1}{\sqrt{2}} v_\perp e^{+i\phi} + \hat{e}_z v_z\right] v_\perp\, d\phi\, dv_z\, dv_\perp \tag{2.33}$$

we see that since $f_1(\phi) \sim e^{-i\sigma\phi}$ the only term of $\underline{v}\, e^{-i\sigma\phi}\, d^3v$ that survives the ϕ integration in (2.8) equals $e_{-\sigma}(v_\perp/\sqrt{2})\, 2\pi$. Therefore writing $\underline{J}_1 = e_{-\sigma} J_{1\sigma}$ we obtain

$$J_{1\sigma} = \sum_{e,i} \frac{inq^2}{m}(E_{1\sigma} + E_{ext\,\sigma}) \left\{ -\pi \int_{-\infty}^{+\infty} dv_z \int_0^{\infty} v_\perp^2\, dv_\perp \frac{\left[\left(1 - \frac{kv_z}{\omega}\right)\frac{\partial f_o}{\partial v_\perp} + \frac{kv_\perp}{\omega}\frac{\partial f_o}{\partial v_z}\right]}{(\omega - kv_z - \sigma\Omega)} \right\} \tag{2.34}$$

where we have explicitly indicated a sum over species (e = electron, i = ion). We assume the zero-order distribution function is an anisotropic Maxwellian

$$f_o(v_z, v_\perp) = f_o(v_z)\, f_o(v_\perp) = \left[\frac{1}{\sqrt{\pi}a} e^{-\frac{v_z^2}{a^2}}\right]\left[\frac{1}{\pi b^2} e^{-\frac{v_\perp^2}{b^2}}\right] \tag{2.35}$$

($a = [\overline{v_z^2}]^{1/2} = [2\kappa T_z/m]^{1/2}$, $b = [\overline{v_\perp^2}]^{1/2} = [2\kappa T_\perp/m]^{1/2}$, κ = Boltzmann's constant). Then (2.34) reduces to

$$J_{1\sigma} = \sum_{e,i} \frac{inq^2}{m}(E_{1\sigma} + E_{ext\,\sigma}) \left\{ \int_{-\infty}^{+\infty} \frac{dv_z\, f_o(v_z)\left[1 - \frac{kv_z}{\omega}\left(1 - \frac{T_\perp}{T_z}\right)\right]}{(kv_z - \omega + \sigma\Omega)} \right\} \tag{2.36}$$

Returning to Maxwell's equations and writing $\underline{J}_{ext} = \hat{e}_{-\sigma} J_{ext\,\sigma}$ we find (2.16) is

$$(E_{1\sigma} + E_{ext\,\sigma})(k^2c^2 - \omega^2) = 4\pi i\omega(J_{1\sigma} + J_{ext\,\sigma}) \tag{2.37}$$

We must now decide whether to consider (1) an external field source or (2) an external current source:

(1) External field source ($\underline{E}_{ext} \neq 0$, $\underline{J}_{ext} = 0$)

Using Maxwell's equations for just the plasma fields, (2.37) is

$$E_{1\sigma}(k^2c^2 - \omega^2) = 4\pi i\omega J_{1\sigma} \tag{2.38}$$

and since $E_{total\,\sigma} = E_{1\sigma} + E_{ext\,\sigma}$ we find using (2.36) that

$$E(k,\omega)_{TOTAL\,\sigma} = \frac{E_{ext\,\sigma}(k,\omega)}{\epsilon_T(k,\omega,\sigma)} \tag{2.39}$$

where $\epsilon_T(k,\omega,\sigma)$, the transverse dielectric function, is

$$\epsilon_T(k,\omega,\sigma) = 1 - \sum_{e,i} \frac{\omega_p^2\,\omega}{(k^2c^2 - \omega^2)} \int_{-\infty}^{+\infty} \frac{dv_z\, f_o(v_z)\left[1 - \frac{kv_z}{\omega}\left(1 - \frac{T_\perp}{T_z}\right)\right]}{(kv_z - \omega + \sigma\Omega)} \tag{2.40}$$

($\omega_p^2 = 4\pi nq^2/m$ is the plasma frequency).

(2) External current source ($\underline{J}_{ext} \neq 0$, $\underline{E}_{ext} = 0$)

Using Maxwell's equations for the total fields, (2.37) is

$$E_{1\sigma}(k^2c^2 - \omega^2) = 4\pi i\omega(J_{1\sigma} + J_{ext\,\sigma}) \tag{2.41}$$

and using (2.36) we find

$$E_{\substack{\text{TOTAL}\\ \sigma}}(k,\omega) = E_{1\sigma}(k,\omega) = \frac{\left[\dfrac{4\pi i\omega}{k^2c^2-\omega^2}\right] J_{ext\,\sigma}(k,\omega)}{\epsilon_T(k,\omega,\sigma)} \tag{2.42}$$

where $\epsilon_T(k,\omega,\sigma)$ is still given by (2.40). Had we considered $J_{\text{total }\sigma} = J_{1\sigma} + J_{\text{ext }\sigma}$ we would have found

$$J_{\substack{\text{TOTAL}\\ \sigma}}(k,\omega) = \frac{J_{ext\,\sigma}(k,\omega)}{\epsilon_T(k,\omega,\sigma)} \tag{2.43}$$

where again $\epsilon_T(k,\omega,\sigma)$ is given by (2.40).

Noting the similarity of the results for an external field source or an external current source, we arbitrarily choose to consider the former and will therefore continue with (2.39) and (2.40). Then specializing to the case of isotropic temperature ($T_\perp = T_z$) and performing the integral over v_z in (2.40), we obtain

$$\epsilon_{T_\pm}(k,\omega,\sigma) = 1 - \frac{\omega}{(k^2c^2-\omega^2)}\left[\frac{\omega_{pe}^2}{ka} Z_\pm\left(\frac{\omega+\sigma\omega_{ce}}{ka}\right) + \frac{\omega_{pi}^2}{kA} Z_\pm\left(\frac{\omega-\sigma\omega_{ci}}{kA}\right)\right] \tag{2.44}$$

where ω_{pe}, $\omega_{ce} = |\Omega B_o/mc|$, a all refer to the electrons; ω_{pi}, $\omega_{ci} = |\Omega B_o/Mc|$, A all refer to the ions; and Z is the plasma dispersion function[21] defined by

$$Z_\pm(\zeta) = \frac{1}{\sqrt{\pi}}\int_{-\infty}^{+\infty} \frac{dt\, e^{-t^2}}{t-\zeta} \tag{2.45}$$

for $\text{Im}\,\zeta \gtrless 0$ and its analytic continuation for $\text{Im}\,\zeta \lesseqgtr 0$. The ± signs

refer to different branches of the Z function; the choice of which branch to use will be discussed shortly.

To complete the solution of our problem in k, ω space we explicitly specify the external field source to be

$$\underline{E}_{ext}(z,t) = E_1(z)\left[\hat{e}_x \cos(\omega_1 t) + \hat{e}_y \sin(\omega_1 t)\right] \tag{2.46}$$

so $\omega_1 > 0$ corresponds to a right-hand excitation while $\omega_1 < 0$ corresponds to a left-hand excitation. Writing $\underline{E}_{ext} = \hat{e}_{-\sigma} E_{ext\,\sigma}$ we find

$$E_{ext\,\sigma}(z,t) = E_1(z)\, e^{i\sigma\omega_1 t} \tag{2.47}$$

Taking Fourier-Laplace transforms of (2.47) gives

$$E_{ext\,\sigma}(k,\omega) = \frac{i E_1(k)}{(\omega + \sigma\omega_1)} \tag{2.48}$$

We have now solved our problem in k, ω space since we now have expressions for $f_1(k,\omega)$, $\epsilon_{T_\pm}(k,\omega,\sigma)$, and $E_{ext\,\sigma}(k,\omega)$. Equations (2.32), (2.39), and (2.48) combine to give

$$f_1(k,\underline{v},\omega) = \left[\frac{q e^{-i\sigma\phi}}{m\sqrt{2}} \frac{\partial f_0}{\partial v_\perp}\right] \frac{E_1(k)}{(\omega+\sigma\omega_1)(\omega - k v_z - \sigma\Omega)\,\epsilon_{T_\pm}(k,\omega,\sigma)} \tag{2.49}$$

We proceed to perform the inverse Fourier-Laplace transform to obtain $f_1(z,\underline{v},t)$ to be used in calculating $\underline{J}_1(z,t)$, the final (current) response.

2.3 Inversion of solution to position space (z,t)

The inverse transform of (2.49) is

$$f_1(z,v,t) = B\int_{-\infty+i\delta}^{+\infty+i\delta}\frac{d\omega}{2\pi}\int_{-\infty}^{+\infty}\frac{dk}{2\pi}\frac{E_1(k)\,e^{i(kz-\omega t)}}{(\omega+\sigma\omega_1)\left(k-\left[\frac{\omega-\sigma\Omega}{v_z}\right]\right)\epsilon_{T_\pm}(k,\omega,\sigma)}$$

$$B = \left[\frac{q\,e^{-i\sigma\phi}}{m\sqrt{2}(-v_z)}\frac{\partial f_0}{\partial v_\perp}\right] \qquad (2.50)$$

where $\delta > 0$ is chosen so the primitive ω contour, as shown in Fig. 2a, is above all singularities of the integrand of (2.50). The primitive k contour lies along the real k axis, as shown in Fig. 3a. The proper manipulation of these contours will show us whether to use $\epsilon_{T_+}(k,\omega,\sigma)$ or $\epsilon_{T_-}(k,\omega,\sigma)$ in (2.50).

Branch-cut considerations

We reconsider the Z function of (2.45). As defined, the real axis of the ζ plane is a branch cut of $Z(\zeta)$. If initially $\mathrm{Im}\,\zeta > 0$ then $Z_+(\zeta)$ should be used and its analytic continuation for $\mathrm{Im}\,\zeta \leq 0$. If instead $\mathrm{Im}\,\zeta < 0$ initially, then $Z_-(\zeta)$ should be used and its analytic continuation for $\mathrm{Im}\,\zeta \geq 0$. Regions where $Z_\pm(\zeta)$ are originally defined are shown in Fig. 4a. Note that $Z_\pm(\zeta)$ must be analytically continued across the branch cut (the real ζ axis) into the region where $Z_\mp(\zeta)$ is originally defined. [A convenient representation of $Z_\pm(\zeta)$ that illustrates these points is

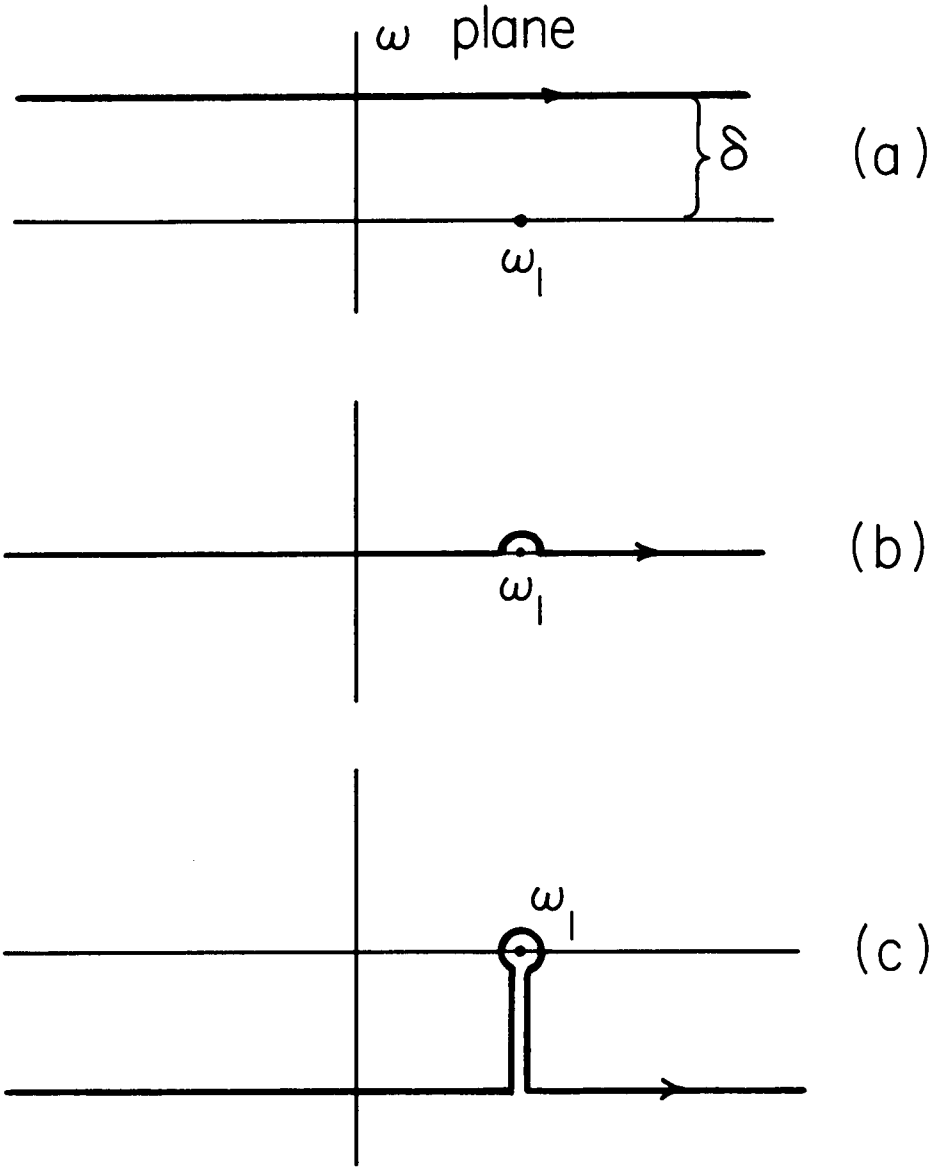

FIGURE 2. CONTOUR IN THE ω PLANE.

(a) Primitive contour (Im $\omega = \delta > 0$).
(b) Contour lowered ($\delta \to 0$) and deformed around pole at $\omega = \omega_1$ (only the pole at $\omega = \omega_1$ is shown).
(c) Contour lowered below the real axis (so on horizontal part $\exp(-i\omega t) \sim \exp(-|\text{Im } \omega| t) \to 0$ as $t \to \infty$).

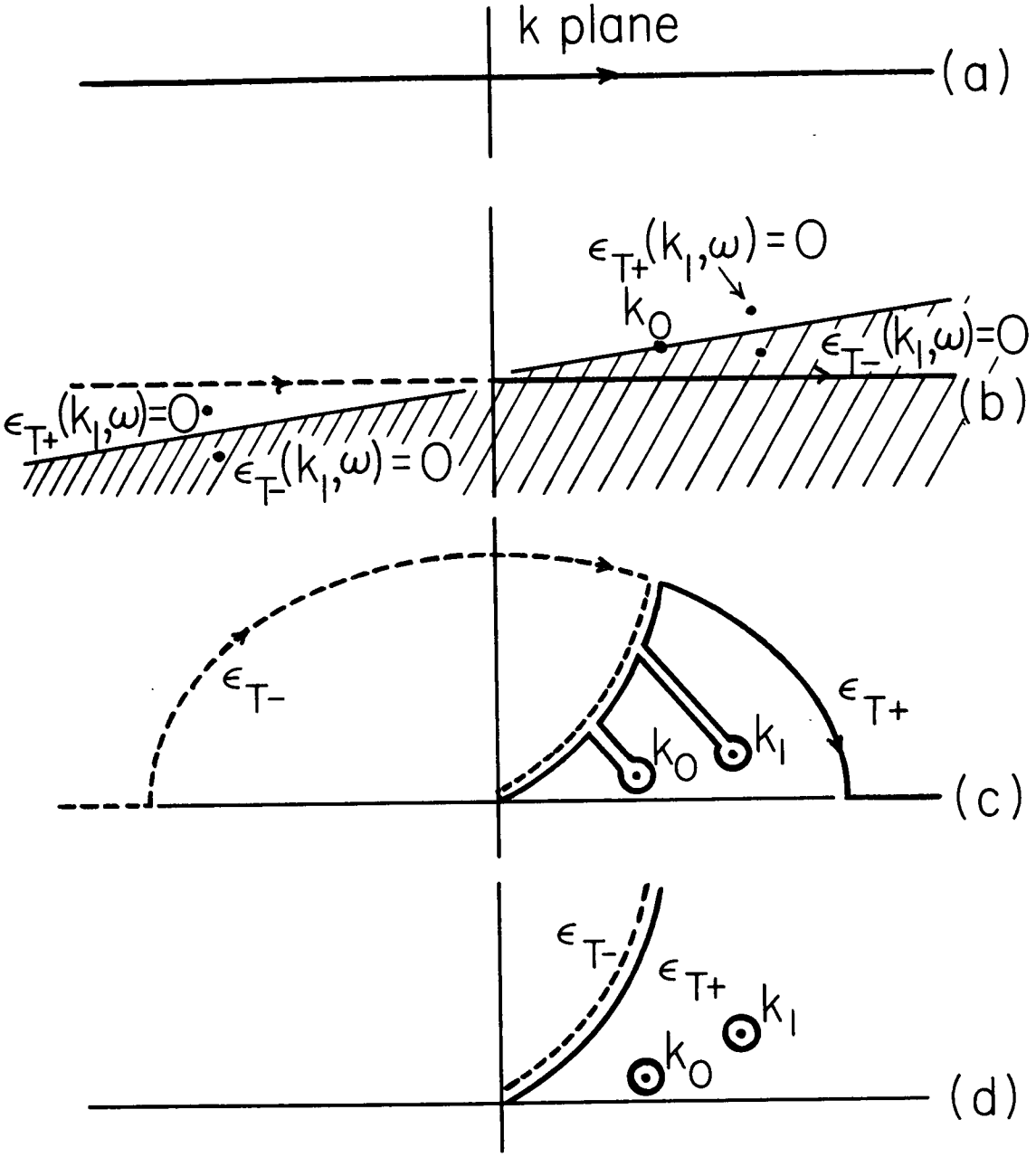

FIGURE 3. CONTOUR IN THE K PLANE.

(a) Primitive contour.
(b) Primitive contour with $\epsilon_{T\pm}$ specified. Also shown, for Re $\omega > \omega_{ce}$, are the branch cuts, the pole at $k_o=(\omega-\omega_{ce})/v_z$ (for $v_z>0$), and the least-damped roots of $\epsilon_{T\pm}(k_1,\omega)=0$.
(c) Contour pulled above for $z>0$. The path of steepest descent has been chosen for the branch-cut integral.
(d) Net result: branch-cut integral plus two residue terms.

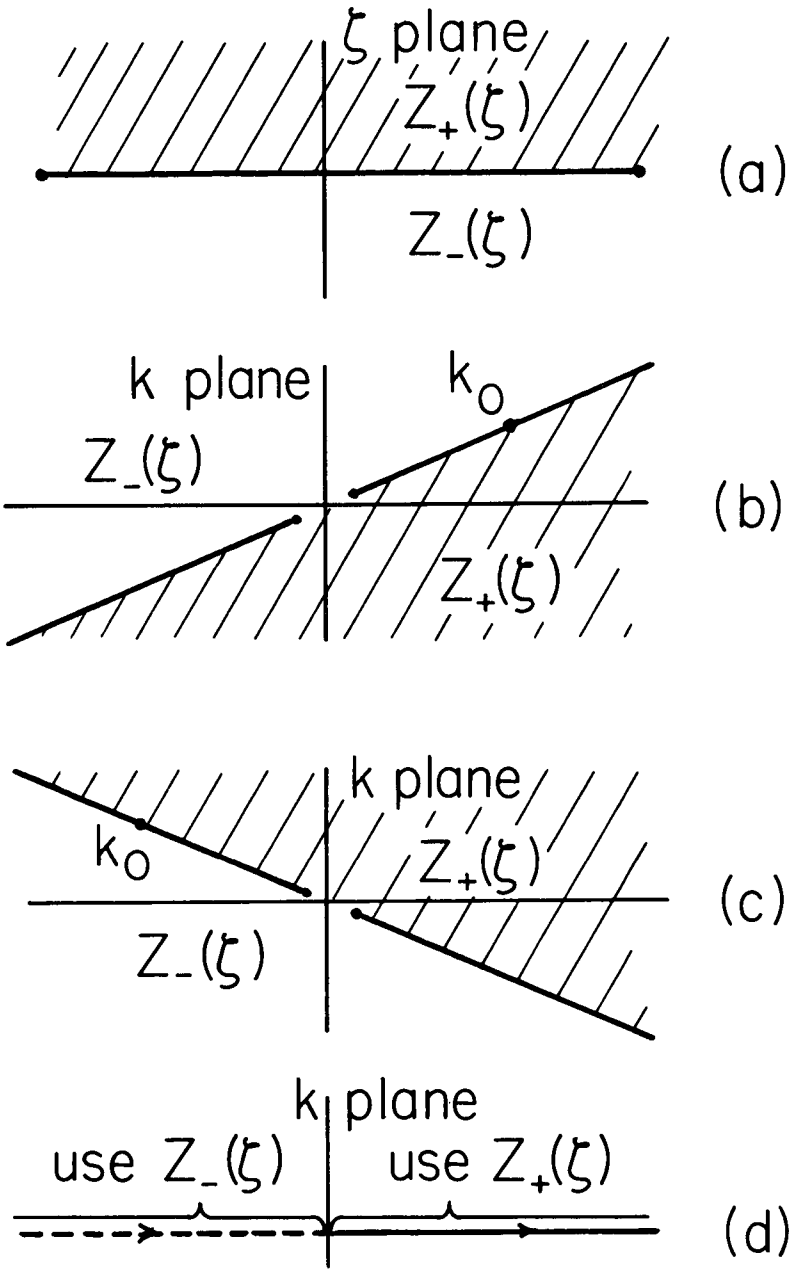

FIGURE 4. BRANCH CUTS IN THE ζ AND K PLANES.

(a) Branch cut in the ζ plane.

(b) Mapping of the branch cut in the ζ_e plane to the k plane, $k=(\omega-\omega_{ce})/\zeta_e a$, for Re $\omega > \omega_{ce}$. Also shown is the pole at $k_o=(\omega-\omega_{ce})/v_z$ for $v_z>0$.

(c) Branch cut in the k plane for Re $\omega < \omega_{ce}$.

(d) Resultant choice of $Z_\pm(\zeta)$ along the primitive contour in the k plane.

$$Z_{\pm}(\zeta) = \frac{1}{\sqrt{\pi}} P\int_{-\infty}^{+\infty} \frac{d\tau\, e^{-\tau^2}}{\tau - \zeta} + i\sqrt{\pi}\,\sigma_{\pm}(\zeta)\, e^{-\zeta^2} \tag{2.51}$$

where $\sigma_+(\zeta) = 0$	and $\sigma_-(\zeta) = -2$	for	$\operatorname{Im}\zeta > 0$
1	-1		$= 0$
2	0		< 0

and P stands for principal part.]

We set $\sigma = -1$ for now. Then the arguments of the Z functions that occur in $\varepsilon_{T_\pm}(k,\omega,\sigma)$ in (2.44) are

$$\zeta_e \equiv \frac{\omega - \omega_{ce}}{ka} \qquad \zeta_i \equiv \frac{\omega + \omega_{ci}}{kA} \tag{2.52}$$

where e, i, refer to electron, ion. Consider ζ_e . The branch cut in the ζ_e plane (the real ζ_e axis) maps onto the k plane according to

$$k = \frac{\omega - \omega_{ce}}{\zeta_e a} \tag{2.53}$$

Recalling that initially $\operatorname{Im}\omega = \delta > 0$ and considering a <u>single</u> point on the primitive ω contour (i.e., an ω of the form $\operatorname{Re}\omega + i\delta$) we find the branch cut in the k plane for $\operatorname{Re}\omega > \omega_{ce}$ to be as shown in Fig. 4b. Note that the points $\zeta_e = \pm\infty$ when mapped onto the k plane pinch the origin. If instead we have $\operatorname{Re}\omega < \omega_{ce}$ then the branch cut in the k plane would be as shown in Fig. 4c. The variable ζ_i gives similar branch cuts (i.e., like Fig. 4b for $\operatorname{Re}\omega > -\omega_{ci}$ and like Fig. 4c for $\operatorname{Re}\omega < -\omega_{ci}$). In any case note that along the primitive

contour in the k plane (the real k axis in Fig. 3a) we now know that for both ζ_e and ζ_i we should use Z_+ (and therefore ε_{T_+}) for $k > 0$ and Z_- (and therefore ε_{T_-}) for $k < 0$. This result is shown both in Figs. 4c and 3b where for clarity we have drawn a dashed line for that part of the contour where ε_{T_-} is to be used and left a solid line for that part of the contour where ε_{T_+} is to be used.

We may now calculate the integrals over k and ω that occur in (2.50). We shall perform the k integration and then the ω integration since we have found this ordering to present fewer complications than the reverse ordering.

The k integration

In Fig. 3b we show the primitive k contour with the choice of ε_{T_+} or ε_{T_-} specified according to the above discussion. For a typical point on the ω contour (we have chosen $\mathrm{Re}\,\omega > \omega_{ce}$ and $\mathrm{Im}\,\omega = \delta \ll \mathrm{Re}\,\omega$ for this figure) the branch cut is shown as well as the pole at

$$k_o \equiv \frac{\omega - \omega_{ce}}{v_z} \tag{2.54}$$

for $v_z > 0$ and also the poles at k_1, where

$$\varepsilon_{T_\pm}(k_1, \omega) = 0 \tag{2.55}$$

Only the least-damped roots of (2.55) in the ζ_e plane are considered now. [The roots of $\varepsilon_{T_\pm}(k,\omega) = 0$ are discussed in Appendix C.]

In Fig. 3c we have pulled the contour above for $Z > 0$ being careful to deform the ε_{T_+} side of the contour around the poles at k_o

and k_1 . Only the ϵ_{T_+} side of the contour "sees" the poles where $\epsilon_{T_+}(k_1,\omega) = 0$. Note that if $\text{Re}\,\omega < \omega_{ce}$ then the ϵ_{T_-} side of the contour would deform around the pole at k_o for $v_z > 0$. (If $v_z < 0$, the pole at k_o lies in the lower-half plane and is missed altogether.) We have chosen to deform the ϵ_{T_+} and ϵ_{T_-} paths to meet along a curved path that will presently be shown to be the path of steepest descent (P.S.D.) for this portion of the integral. This integral will be called the branch-cut integral but note it is <u>not</u> evaluated along the branch cut. As we move the outer part of the contour (the semi-circle in Fig. 3c) out to infinity, the contribution to the integral from this section of the contour becomes negligibly small (since the integrand goes as e^{ikz}/k).

Thus we are left with the three contributions shown in Fig. 3d; the branch-cut integral and the residues from the poles at k_o and k_1 . We assume the latter to be a simple first-order pole, i.e., we assume

$$\left.\frac{\partial \epsilon_{T_\pm}(k,\omega,\sigma)}{\partial k}\right|_{k=k_1} \neq 0 \qquad (2.56)$$

Explicitly the results of the k integration are then

$$\int_{-\infty}^{+\infty} \frac{dk}{2\pi} \frac{E_1(k)\, e^{ikz}}{\left(k-\left[\frac{\omega-\sigma\Omega}{v_z}\right]\right)\epsilon_{T_\pm}(k,\omega,\sigma)} =$$

$$\int_0^{\infty}\frac{dk}{2\pi}\,\frac{E_1(k)\,e^{ikz}}{\left(k-\left[\frac{\omega-\sigma\Omega}{V_z}\right]\right)}\left\{\frac{1}{\epsilon_{T_+}(k,\omega,\sigma)}-\frac{1}{\epsilon_{T_-}(k,\omega,\sigma)}\right\}$$

P.S.D.

$$+\frac{i\,H(V_z)\,E_1\left(\frac{\omega-\sigma\Omega}{V_z}\right)e^{i\left(\frac{\omega-\sigma\Omega}{V_z}\right)z}}{\epsilon_{T_\alpha}\left(\frac{\omega-\sigma\Omega}{V_z},\omega,\sigma\right)}$$

$$+\frac{i\,E_1(k)\,e^{ik_1z}}{\left(k_1-\left[\frac{\omega-\sigma\Omega}{V_z}\right]\right)\left.\frac{\partial\epsilon_{T_\beta}(k,\omega,\sigma)}{\partial k}\right|_{k=k_1}} \qquad (2.57)$$

for $z > 0$, and where $H(v_z)$ is the Heaviside function

$$H(V_z) = 1 \quad \text{for} \quad V_z \geq 0$$

$$0 \quad \text{for} \quad < 0$$

and

$$\alpha \equiv SGN\,(Re\,\omega - \sigma\Omega)$$

$$\beta \equiv SGN\,(Re\,k_1)$$

Equation (2.57) is valid for $\sigma = \pm 1$ (not just $\sigma = -1$ as used in the preceding discussion).

The branch-cut integral in (2.57) may be evaluated as follows. From (2.44) and (2.51) we find

$$\int_{P.S.D.}^{\infty} =$$

$$\int_{P.S.D.}^{\infty} \frac{dk\, E_1(k)\, e^{ikz}\left[\frac{i2\sqrt{\pi}\,\omega_{pe}^2\,\omega}{(k_c^2 z^2 - \omega^2)ka}\right]\left\{e^{-\left(\frac{\omega+\sigma\omega_{ce}}{ka}\right)^2} + \sqrt{\frac{T_e M}{T_i m}}\, e^{-\left(\frac{\omega-\sigma\omega_{ci}}{kA}\right)^2}\right\}}{2\pi\left(k-\left[\frac{\omega-\sigma\Omega}{V_z}\right]\right)\epsilon_+(k,\omega,\sigma)\,\epsilon_-(k,\omega,\sigma)} \qquad (2.58)$$

($kT_e = \frac{1}{2} ma^2$, $kT_1 = \frac{1}{2} MA^2$). We evaluate this integral by the method of steepest descent discussed in Appendix E. For $z > 0$ the electron term of the integrand (i.e., the first term within $\{\ \}$) has a saddle point at

$$k_{se} = \left[\frac{2\{(\omega+\sigma\omega_{ce})\alpha_e\}^2}{z a^2}\right]^{\frac{1}{3}} e^{i\left(\frac{\pi}{2}-\alpha_e\frac{\pi}{3}\right)}$$

$$\alpha_e = SGN(Re\,\omega + \sigma\omega_{ce}) \qquad (2.59)$$

and the ion term has a saddle point at

$$k_{si} = \left[\frac{2\{(\omega-\sigma\omega_{ci})\alpha_i\}^2}{z A^2}\right]^{\frac{1}{3}} e^{i\left(\frac{\pi}{2}-\alpha_i\frac{\pi}{3}\right)}$$

$$\alpha_i = SGN(Re\,\omega - \sigma\omega_{ci}) \qquad (2.60)$$

The correct choice of the P.S.D. and graphs of it are given in Appendix E. Computing the first term of the asymptotic expansion about the saddle point we obtain

$$\int_{P.S.D.}^{\infty} \approx$$

$$\frac{i E_l(k_{se})\,\omega_{pe}^2\, k_{se}\,\omega\, e^{-3\left[\frac{(\omega+\sigma\omega_{ce})\alpha_e z}{2a}\right]^{2/3}\left[\frac{1}{2}-i\alpha_e\frac{\sqrt{3}}{2}\right]}}{\sqrt{3}\left(k_{se}^2c^2-\omega^2\right)(\omega-\sigma\Omega)\left(k_{se}-\left[\frac{\omega-\sigma\Omega}{v_z}\right]\right)\epsilon_{T_+}(k_{se},\omega,\sigma)\,\epsilon_{T_-}(k_{se},\omega,\sigma)}$$

$$+\frac{\sqrt{\frac{T_e m}{T_i M}}\, i E_l(k_{si})\,\omega_{pe}^2\, k_{si}\,\omega\, e^{-3\left[\frac{(\omega-\sigma\omega_{ci})\alpha_i z}{2a}\right]^{2/3}\left[\frac{1}{2}-i\alpha_i\frac{\sqrt{3}}{2}\right]}}{\sqrt{3}\left(k_{si}^2c^2-\omega^2\right)(\omega-\sigma\Omega)\left(k_{si}-\left[\frac{\omega-\sigma\Omega}{v_z}\right]\right)\epsilon_{T_+}(k_{si},\omega,\sigma)\,\epsilon_{T_-}(k_{se},\omega,\sigma)} \tag{2.61}$$

which is a good approximation for

$$\left|\frac{z(\omega-\omega_{ce})}{a}\right| \gtrsim 1 \tag{2.62}$$

(as discussed in Appendix E). In using the method of steepest descent we have implicitly assumed that the integrand of (2.58) had no poles near the P.S.D. For ω near ω_1 the poles at k_o and k_1 lie near the real axis. Thus, ignoring possible interference of poles at k_1's caused by roots of $\epsilon_{T_\pm}(k_1,\omega,\sigma) = 0$ other than the least-damped ones, we conclude that use of the method of steepest descent is justified.

The ω integration

We now perform the ω integration in (2.50), which from (2.57) and (2.61) is

$$f_1(z,v,t) = B\int_{-\infty+i\delta}^{+\infty+i\delta}\frac{d\omega}{2\pi}\frac{e^{-i\omega t}}{(\omega+\sigma\omega_1)}\Bigg\{\left[\begin{array}{l}\text{Result of branch-cut}\\ \text{integral, i.e. (2.61)}\end{array}\right]$$

$$+\frac{iH(v_z)E_1\left(\frac{\omega-\sigma\Omega}{v_z}\right)e^{i\left(\frac{\omega-\sigma\Omega}{v_z}\right)z}}{\epsilon_{T_\alpha}\left(\frac{\omega-\sigma\Omega}{v_z},\omega,\sigma\right)} \qquad (2.63)$$

$$+\frac{iE_1(k_1)e^{ik_1 z}}{\left(k_1-\left[\frac{\omega-\sigma\Omega}{v_z}\right]\right)\left.\frac{\partial\epsilon_{T_\beta}(k,\omega,\sigma)}{\partial k}\right|_{k=k_1}}\Bigg\}$$

In Fig. 2a the primitive ω contour lies above all singularities of the integrand of (2.63). We let $\delta \to 0$ deforming the contour around any poles. In Fig. 2b we have lowered the contour until $\delta = 0$ and deformed it around the pole at $\omega = -\sigma\omega_1$ (this is the only pole shown in the figure). In Fig. 2c we have lowered the contour into the lower-half plane. Since for $t > 0$ the contribution from the horizontal part of the contour vanishes ($e^{-i\omega t} \sim e^{-|\text{Im }\omega|t} \to 0$ as $|\text{Im }\omega|$ or $t \to \infty$), we are left with just a residue term at $\omega = -\sigma\omega_1$. Before writing down this term we consider contributions from poles other than the one at $\omega = -\sigma\omega_1$.

The remaining poles of the integrand of (2.63) occur in the ω plane where

(i) (2.61) has poles

(ii) $\epsilon_{T_\alpha}\left(\frac{\omega-\sigma\Omega}{v_z},\omega,\sigma\right)=0$

(iii) $\omega = k_1 v_z + \sigma\Omega$

(iv) $\left.\frac{\partial\epsilon_{T_\beta}(k,\omega,\sigma)}{\partial k}\right|_{k=k_1} = 0$

In general none of these poles will occur at $\omega = -\sigma\omega_1$ so none of them will interfere with the response at frequency ω_1. However, we shall investigate all four of the above cases to determine if there is any response at frequencies other than ω_1.

CASE (i): Consider just the first (electron) term of (2.51) which has poles where any of the following are satisfied:

$$\begin{aligned} k_{se}^2 c^2 - \omega^2 &= 0 \\ \omega - k_{se} v_z + \sigma\Omega &= 0 \\ \epsilon_{T_\pm}(k_{se},\omega,\sigma) &= 0 \end{aligned} \qquad (2.64)$$

[Note from (2.59) that $k_{se} \sim (\omega+\sigma\Omega)^{2/3}$ so none of (2.64) would produce simple poles.] By the following argument we show that roots of (2.64) in the ω plane cannot produce any legitimate pole terms. First note that the position of the P.S.D. for the branch-cut integral in the k plane depended on the value of ω [see (2.59)]. Now any ω that solves (2.64) represents a pole in the k plane exactly on the P.S.D. that corresponds to that ω. Recall that in obtaining (2.61) we assumed the integrand of (2.58) contained no poles on or near the P.S.D. Thus if we could find an ω that solved (2.64) we would have to evaluate the branch-cut integral (2.58) by a different method (only

for that ω) say by integrating along the real axis in the k plane. But then the factors in (2.64) would never even occur in the calculation and thus no pole term would result from the ω that solved (2.64). We conclude that any roots of (2.64) in the ω plane can be ignored and that (2.61) is a valid representation of the branch-cut integral <u>only</u> for ω evaluated at $\omega = -\sigma\omega_1$.

<u>CASES (ii) AND (iii):</u> For definiteness we set $\sigma = -1$ and consider electron waves so $\Omega = -\omega_{ce}$. Then the residue term that results from case (ii) is

$$\frac{iE_1\left(\frac{\hat{\omega}-\omega_{ce}}{v_z}\right) e^{i\left(\frac{\hat{\omega}-\omega_{ce}}{v_z}\right)z - i\hat{\omega}t}}{(\hat{\omega}-\omega_1)\left.\frac{\partial \epsilon_{T\alpha}\left(\frac{\omega-\omega_{ce}}{v_z},\omega\right)}{\partial\omega}\right|_{\omega=\hat{\omega}}} \tag{2.65}$$

where

$$\epsilon_{T\alpha}\left(\frac{\hat{\omega}-\omega_{ce}}{v_z},\hat{\omega}\right) = 0 \qquad \alpha = \mathrm{SGN}\left(\mathrm{Re}\,\hat{\omega}-\omega_{ce}\right) \tag{2.66}$$

and the residue term that results from case (iii) is

$$\frac{(-v_z)E_1(\hat{k})\, e^{i\hat{k}z - i(\hat{k}v_z+\omega_{ce})t}}{(\hat{k}v_z+\omega_{ce}-\omega_1)\left.\frac{\partial \epsilon_{T\beta}(k,\, kv_z+\omega_{ce})}{\partial k}\right|_{k=\hat{k}}} \tag{2.67}$$

where because of (2.55) we must require

$$\epsilon_{T_\beta}(\hat{k}, \hat{k}v_z + \omega_{ce}) = 0 \qquad \beta = SGN(Re\,\hat{k}) \tag{2.68}$$

By making a change of variable in (2.65) from $\hat{\omega}$ to $\hat{k}v_z + \omega_{ce}$, i.e.,

$$\hat{\omega} = \hat{k}v_z + \omega_{ce}$$

$$v_z \frac{\partial}{\partial \omega}\bigg|_{\omega=\hat{\omega}} = \frac{\partial}{\partial k}\bigg|_{k=\hat{k}} \tag{2.69}$$

we see that the two residue terms, (2.65) and (2.67), cancel identically with the following considerations.

For reference, the roots of $\epsilon_{T_+}[(\omega-\omega_{ce}/v_z),\omega] = 0$ in the complex ω plane are shown for a typical case in Fig. C-17b in Appendix C. Note there are branches which have $\mathrm{Im}\,\omega > 0$ (corresponding to growing waves) which would be included in the ω integration. The corresponding roots of $\epsilon_{T_+}(k, kv_z+\omega_{ce}) = 0$ in the complex k plane are shown in Fig. C-17a. Note there are branches which have $\mathrm{Im}\,k < 0$ (corresponding to spatially growing waves) but it seems these branches would be excluded in the k integration since the primitive k contour runs along the real axis. In fact, however, if we review the lowering of the ω contour, and follow the pole at $k = \omega-\omega_{ce}/v_z$ [the equivalent "k" in $\epsilon_{T_+}(k, kv_z+\omega_{ce})$], we would see that since initially $\mathrm{Im}\,\omega > 0$ (and $v_z > 0$ always for $z > 0$), as $\mathrm{Im}\,\omega$ goes to zero and then becomes negative, the pole approaches the k contour from <u>above</u> and then indents it so it would be included in the final result even though

it ends up in the lower-half k plane. (If $v_z < 0$ the pole would start beneath the primitive k contour and would therefore never make a contribution.)

We conclude that the pole terms produced by cases (ii) and (iii) cancel identically.

CASE (iv): This case is not allowed in that we assumed a simple first-order pole occurred at k_1 in performing the k integration [see (2.54)]. Even if a simple pole of higher order occurred in the k integration, the term corresponding to case (iv) would be the first non-zero derivative and would therefore not produce a pole in the integrand of (2.63).

Thus in (2.63) the only pole we have to consider is the one at $\omega = -\sigma\omega_1$, which gives

$$f_1(\underline{z},\underline{v},t) = B\Bigg\{ -i\left[\text{(2.61) evaluated at } \omega = -\sigma\omega_1\right] + \frac{H(v_z)\,E_1\left(\frac{-\sigma(\omega_1+\Omega)}{v_z}\right) e^{i\left(\frac{-\sigma(\omega_1+\Omega)}{v_z}\right)z + i\sigma\omega_1 t}}{\epsilon_{T_{-\sigma\alpha}}\left(\frac{-\sigma(\omega_1+\Omega)}{v_z}, -\sigma\omega_1, \sigma\right)} + \frac{E_1(k_1)\,e^{ik_1 z + i\sigma\omega_1 t}}{\left(k_1 + \frac{\sigma(\omega_1+\Omega)}{v_z}\right)\left.\frac{\partial \epsilon_{T_{-\sigma\beta}}(k_1,-\sigma\omega_1,\sigma)}{\partial k}\right|_{k=k_1}} \Bigg\} \tag{2.70}$$

for $z > 0$ and where $\epsilon_{T_{-\sigma\beta}}(k_1,-\sigma\omega_1,\sigma) = 0$. Equation (2.70) is valid for $\sigma = \pm 1$ (not just $\sigma = -1$ as used mainly in the preceding discussion).

Final expression for $f_1(z,\underline{v},t)$

Using the symmetry properties (B.6) and (B.8) from Appendix B,

$$\left[\epsilon_{T_\pm}(-\sigma k,-\sigma\omega_1,\sigma)\right]^* = \epsilon_{T_\mp}(-\sigma k^*,-\sigma\omega_1,\sigma)$$

$$\left[\frac{\partial\epsilon_{T_\pm}(\sigma k,\sigma\omega_1,\sigma)}{\partial k}\right]^* = -\frac{\partial\epsilon_{T_\mp}(-\sigma k^*,-\sigma\omega_1,\sigma)}{\partial(-k^*)} \tag{2.71}$$

and the symmetry property

$$\left[E_1(k)\right]^* = E_1(-k^*) \tag{2.72}$$

[which follows from the fact that $E_1(z)$ is real], and then summing over $\sigma = \pm 1$ [which has been implied since (2.28)], we find $f_1(z,\underline{v},t)$ equals twice the real part of either the $\sigma = +1$ term or the $\sigma = -1$ term. We shall use the latter. Then specializing to electron waves ($\Omega = -\omega_{ce}$), and dropping the ion term in (2.61), we obtain

$$f_1(z,\underline{v},t) = \mathcal{R}e\left[B'\left\{\frac{E_1(k_{se})\omega_{pe}^2 k_{se}\omega_1\, e^{-3\left[\frac{(\omega_1-\omega_{ce})\alpha z}{2a}\right]^{2/3}\left[\frac{1}{2}-i\alpha\frac{\sqrt{3}}{2}\right]-i\omega_1 t}}{\sqrt{3}\left(k_{se}^2c^2-\omega_1^2\right)(\omega_1-\omega_{ce})\left(k_{se}-\left[\frac{\omega_1-\omega_{ce}}{v_z}\right]\right)\epsilon_{T_+}(k_{se},\omega_1)\epsilon_{T_-}(k_{se},\omega_1)}\right.\right.$$

$$\left.\left. + \frac{H(v_z)\,E_1\left(\frac{\omega_1-\omega_{ce}}{v_z}\right)e^{i\left(\frac{\omega_1-\omega_{ce}}{v_z}\right)z-i\omega_1 t}}{\epsilon_{T_\alpha}\left(\frac{\omega_1-\omega_{ce}}{v_z},\omega_1\right)}\right\}\right] \tag{2.73}$$

$$+\frac{E_1(k_1)\,e^{ik_1z-i\omega_1t}}{\left(k_1-\left[\frac{\omega_1-\omega_{ce}}{v_z}\right]\right)\frac{\partial\epsilon_{T_+}(k,\omega_1)}{\partial k}\Bigg|_{k=k_1}}$$

for $z > 0$ and where

$$B' = \left[\frac{-\sqrt{2}\,q\,e^{+i\phi}}{m v_z}\,\frac{\partial f_0}{\partial v_\perp}\right]$$

$$k_{se} = \left[\frac{2\{(\omega_1-\omega_{ce})\alpha\}^2}{2e^2}\right]^{\frac{1}{3}} e^{i\left(\frac{\pi}{2}-\alpha\frac{\pi}{3}\right)} \qquad (2.74)$$

$$\alpha = \mathrm{SGN}\,(\omega_1-\omega_{ce})$$

$$\epsilon_{T_+}(k_1,\omega_1) = 0$$

Equation (2.73) gives the first-order perturbation to the electron's zero-order distribution function. Note that although $f_1(z,\underline{v},t)$ in (2.73) is for electrons, both ions and electrons enter into the dielectric functions [see (2.44)]. The first term of (2.73) will be called the branch-cut term (since it came from the branch-cut integral), the second term will be called the free-streaming term (for reasons to be discussed shortly), and the last term will be called the dielectric-pole term (since it comes from the root(s) of the transverse dielectric function).

2.4 Calculation of $\underline{J}_1(z,t)$

The first-order current response is

$$\underline{J}_1(z,t) = nq \int f_1(z,\underline{v},t)\, \underline{v}\, d^3v \tag{2.75}$$

From earlier considerations [(2.33), etc.] the integration over ϕ and $v_\perp$ leave

$$\underline{J}_1(z,t) = \mathrm{Re}\left[\hat{e}_+ \omega_{pe}^2 \left\{ \frac{E_1(k_{se})\omega_{pe}^2\omega_1 e^{-3\left[\frac{(\omega_1-\omega_{ce})\alpha z}{2a}\right]^{2/3}\left[\frac{1}{2}-i\alpha\frac{\sqrt{3}}{2}\right]-i\omega_1 t}}{\sqrt{3}(k_{se}^2c^2-\omega_1^2)(\omega_1-\omega_{ce})\epsilon_{T_+}(k_{se},\omega_1)\epsilon_{T_-}(k_{se},\omega_1)} \int_{-\infty}^{+\infty} \frac{dv_z\, f_0(v_z)}{v_z-\left[\frac{\omega_1-\omega_{ce}}{k_{se}}\right]} \right.\right.$$

$$+ \int_0^\infty \frac{dv_z\, f_0(v_z) E_1\left(\frac{\omega_1-\omega_{ce}}{v_z}\right) e^{i\left(\frac{\omega_1-\omega_{ce}}{v_z}\right)z-i\omega_1 t}}{v_z\, \epsilon_{T_\alpha}\left(\frac{\omega_1-\omega_{ce}}{v_z},\omega_1\right)}$$

$$\left.\left. + \frac{E_1(k_1)e^{ik_1 z-i\omega_1 t}}{k_1 \left.\frac{\partial \epsilon_{T_+}(k,\omega)}{\partial k}\right|_{k=k_1}} \int_{-\infty}^{+\infty} \frac{dv_z\, f_0(v_z)}{v_z-\left[\frac{\omega_1-\omega_{ce}}{k_1}\right]} \right\}\right] \tag{2.76}$$

for $z > 0$. Note that only particles with $v_z > 0$ contribute to the free-streaming term but that all particles contribute to the branch-cut and dielectric pole terms.

To facilitate computation of the free-streaming term integral in (2.76) and because at present we have no other preferences, we assume an idealized delta-function source with

$$E_1(z) = \mathcal{E}_1 \delta(z) \tag{2.77}$$

so

$$E_1(k) = \Phi_1 \tag{2.78}$$

where Φ_1 is a constant with units of electric potential. Recall that $f_o(v_z)$ was assumed to be Maxwellian in (2.35). Then the integrals in the branch-cut term and the dielectric-pole term in (2.76) are of the form

$$\int_{-\infty}^{+\infty} \frac{dv_z\, f_o(v_z)}{v_z - \left[\frac{\omega_1 - \omega_{ce}}{k}\right]} = \frac{1}{a} Z\left(\frac{\omega_1 - \omega_{ce}}{ka}\right) \tag{2.79}$$

where Z is the plasma dispersion function defined earlier in (2.45).

The free-streaming term phase-mixing integral

The free-streaming term integral in (2.76) is

$$\frac{1}{\sqrt{\pi}\, a} \int_0^{\infty} \frac{dv_z\, e^{-\frac{v_z^2}{a^2}}\, e^{i\left(\frac{\omega_1 - \omega_{ce}}{v_z}\right)z}}{v_z\, \epsilon_{T_\alpha}\left(\frac{\omega_1 - \omega_{ce}}{v_z}, \omega_1\right)} \tag{2.80}$$

$$\alpha = \mathrm{SGN}\left(\omega_1 - \omega_{ce}\right)$$

and we shall perform this integral in the complex v_z/a plane by the method of steepest descent described in Appendix E. The appropriate saddle point of the integrand of (2.80) is

$$\frac{v_s}{a} = \left[\frac{(\omega_1 - \omega_{ce})\alpha z}{2a}\right]^{\frac{1}{3}} e^{-i\alpha\frac{\pi}{6}} \tag{2.81}$$

and the first term of the asymptotic expansion about this saddle point is

$$\frac{e^{-3\left[\frac{(\omega_1-\omega_{ce})\alpha z}{2a}\right]^{2/3}\left[\frac{1}{2}-i\alpha\frac{\sqrt{3}}{2}\right]}}{\sqrt{3}\, V_s\, \epsilon_{T_\alpha}\left(\frac{\omega_1-\omega_{ce}}{V_s}, \omega_1\right)} \tag{2.82}$$

which is a good approximation for

$$\left|\frac{z(\omega_1-\omega_{ce})}{a}\right| \gtrsim .12 \tag{2.83}$$

A complete account of the paths of steepest descent associated with (2.80) and an error discussion concluding with (2.83) are given in Appendix E.

The primitive contour of (2.80) in the complex v_z/a plane is shown in Fig. 5a. In Figs. 5b, c, d, the primitive contour has been deformed to the appropriate P.S.D. depending on the value of ω_1. The saddle point v_s/a [defined by (2.81)] is shown as well as the dielectric pole at

$$\frac{V_1}{a} = \frac{\omega_1-\omega_{ce}}{ka} \tag{2.84}$$

where

$$\epsilon_{T_\alpha}(k_1, \omega_1) = 0$$

Note that there is a pole contribution for $\omega_1 < 0$ or $\omega_1 > \omega_{ce}$ but <u>not</u> for $0 < \omega_1 < \omega_{ce}$. Thus the free-streaming term (2.80) has the

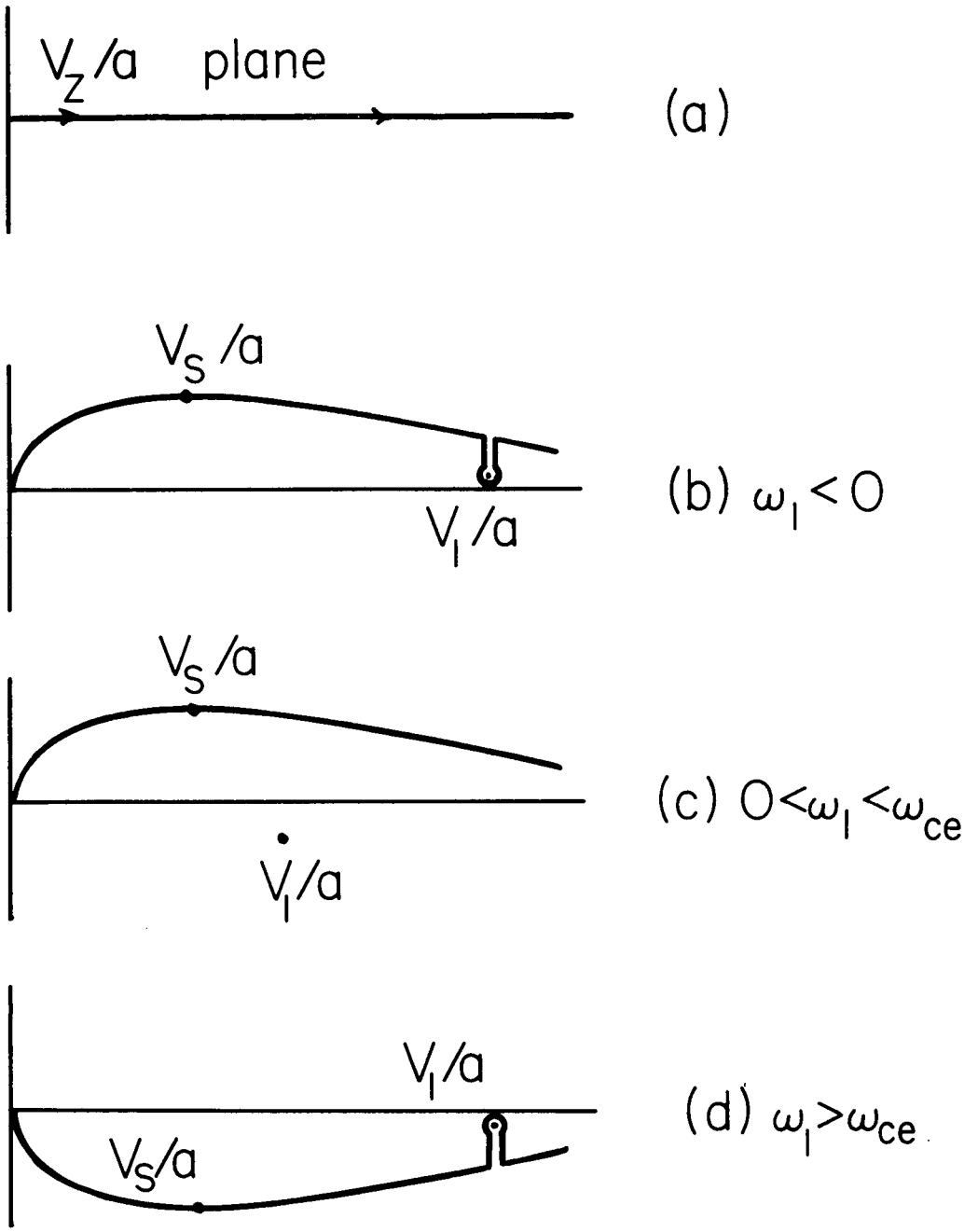

FIGURE 5. CONTOURS IN THE v_z/a PLANE USED IN EVALUATING (2.80). The primitive contour in (a) is deformed to the appropriate path of steepest descent in (b),(c),(d) according to the value of ω_1. The saddle points (v_s/a) and poles (v_1/a) are defined by (2.81),(2.84) respectively.

saddle point contribution (2.82) for all values of ω_1, and a residue contribution only for $\omega_1 < 0$ or $\omega_1 > \omega_{ce}$. These results, including the absence of a residue term for $0 < \omega_1 < \omega_{ce}$, will be discussed further in a special section on transverse free-streaming waves.

Final expression for $\underline{J}_1(z,t)$

Combining the results of the above saddle point integration with (2.79) and (2.76) we arrive at our final result for the current $\underline{J}_1(z,t)$

$$\underline{J}_1(z,t) =$$

$$\mathrm{Re}\left[\hat{e}_+ \frac{\omega_{pe}^2 \phi_1}{a}\left\{\frac{\omega_{pe}^2 \omega_1\, e^{-3\left[\frac{(\omega_1-\omega_{ce})\alpha z}{2a}\right]^{2/3}\left[\frac{1}{2}-i\alpha\frac{\sqrt{3}}{2}\right]-i\omega_1 t}}{\sqrt{3}\left(k_{se}^2c^2-\omega_1^2\right)(\omega_1-\omega_{ce})\,\epsilon_{T_+}(k_{se},\omega_1)\,\epsilon_{T_-}(k_{se},\omega_1)}\, Z_+\left(\frac{\omega_1-\omega_{ce}}{k_{se}a}\right)\right.\right.$$

$$+\frac{e^{-3\left[\frac{(\omega_1-\omega_{ce})\alpha z}{2a}\right]^{2/3}\left[\frac{1}{2}-i\alpha\frac{\sqrt{3}}{2}\right]-i\omega_1 t}}{\sqrt{3}\,\frac{v_s}{a}\,\epsilon_{T_\alpha}\left(\frac{\omega_1-\omega_{ce}}{v_s},\omega_1\right)}$$

$$\left.\left.+\frac{e^{ik_1 z-i\omega_1 t}}{k_1\left.\frac{\partial\epsilon_{T_+}(k,\omega_1)}{\partial k}\right|_{k=k_1}}\left[Z_+\left(\frac{\omega_1-\omega_{ce}}{k_1 a}\right)+2\sqrt{\pi}\,i\,S(\omega_1)\,e^{-\left(\frac{\omega_1-\omega_{ce}}{k_1 a}\right)^2}\right]\right\}\right] \tag{2.85}$$

for $z > 0$ and where

$$k_{se} = \left[\frac{2\{(\omega_1-\omega_{ce})\alpha\}^2}{2a^2}\right]^{\frac{1}{3}} e^{i\left(\frac{\pi}{2}-\alpha\frac{\pi}{3}\right)}$$

$$\frac{\gamma_s}{a} = \left[\frac{(\omega_1-\omega_{ce})\alpha 2}{2a}\right]^{\frac{1}{3}} e^{-i\alpha\frac{\pi}{6}}$$

$$\alpha = SGN(\omega_1-\omega_{ce})$$

$$S(\omega) = 1 \quad \text{for} \quad \omega_1 < 0,\ \omega_1 > \omega_{ce} \qquad (2.86)$$

$$0 \quad \text{for} \quad 0 < \omega_1 < \omega_{ce}$$

In (2.85) the terms remain in their original order, i.e., branch-cut term, free-streaming term, and then dielectric-pole term except that the $S(\omega)$ portion of the last term is the residue contribution from the free-streaming term for $\omega_1 < 0$ or $\omega_1 > \omega_{ce}$.

Before discussing the behavior of the terms in (2.85) in general, we shall present the results of a numerical evaluation of these terms for a specific case.

3. Numerical Evaluation of (2.85) for Response with Electron Cyclotron Damping

We present the results of a numerical evaluation of (2.85) for values of the excitation frequency ω_1 just slightly below ω_{ce}. This choice of frequencies was made in the interest of studying electron cyclotron damping but in addition this choice clearly illustrates the various sizes and types of terms that comprise (2.85).

First we must consider the effects of all the roots of the transverse dispersion relation. We have drawn the equivalent of Fig. 3d for $0 < \omega_1 < \omega_{ce}$ in Fig. 6, in which we display the positions of all roots of $\varepsilon_{T_\pm}(k,\omega_1) = 0$, not just the least-damped ones. (The roots of the transverse dispersion relation are discussed in Appendix C and are summarized in Fig. C-15.) Also shown in Fig. 6 is the branch-cut P.S.D. contour as chosen in Appendix E (see the discussion concerning Figs. E-1 - E-3 for details). As used earlier in Figs. 3 and 4, ε_{T_-} (ε_{T_+}) is to be used on the dashed (solid) line contours in Fig. 6.

We see from Fig. 6 that in addition to the least-damped root (marked k_1) we must consider the effects of the infinite sequence of roots and also the pure imaginary root. In the next section we shall show that the infinite sum of residues produced by the infinite sequence of roots is negligible except at positions extremely close to the place of excitation. Accordingly we shall neglect the infinite sequence of roots for now. Note that the pure imaginary root in the upper-half k plane in Fig. 6 is missed by the deformed contour altogether so it never enters the calculation for $0 < \omega_1 < \omega_{ce}$. Thus the only root we have to consider is the least-damped (cyclotron-damped) root.

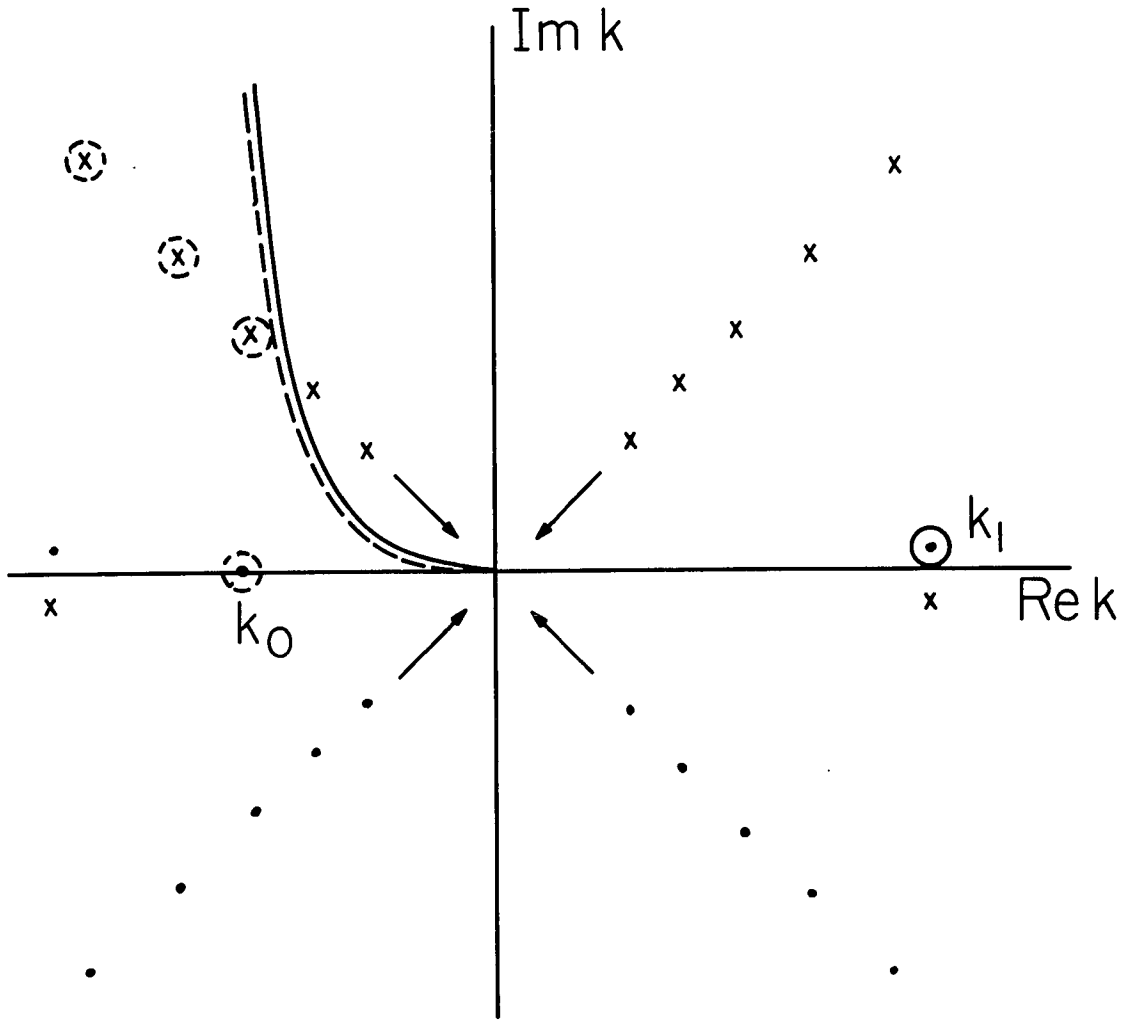

FIGURE 6. FINAL CONTOUR IN THE K PLANE FOR $0 < \omega_1 < \omega_{ce}$. Roots of $\epsilon_{T+}(k,\omega_1)=0$ are shown by dots and roots of $\epsilon_{T-}(k,\omega_1)=0$ are shown by crosses. Also shown are the branch-cut P.S.D. contour (which differs from that of Fig. 3d because now $\omega < \omega_{ce}$) and the contours that encircle the various poles (ϵ_{T-} [ϵ_{T+}] is to be used on the dashed [solid] line contours) for $z>0$.

We comment on some characteristic lengths. The branch-cut and free-streaming terms in (2.85) have the characteristic length

$$\lambda_o \equiv \frac{a}{|\omega_1 - \omega_{ce}|} \tag{3.1}$$

while the pole term has the wavelength

$$\lambda_1 \equiv \frac{2\pi}{Re\, k_1} = \frac{2\pi}{\left[\frac{Re\, k_1 c}{\omega_{ce}}\right]} \frac{c}{\omega_{ce}} \tag{3.2}$$

For our example we shall find $\lambda_1 \simeq c/\omega_{ce}$. Thus we have chosen to normalize all distances to the basic length c/ω_{ce}, i.e., we define

$$\begin{aligned} \tilde{z} &\equiv \frac{z}{\left(\frac{c}{\omega_{ce}}\right)} \\ \tilde{\lambda}_o &\equiv \frac{\lambda_o}{\left(\frac{c}{\omega_{ce}}\right)} \\ \tilde{\lambda}_1 &\equiv \frac{\lambda_1}{\left(\frac{c}{\omega_{ce}}\right)} = \frac{2\pi}{\left[\frac{Re\, k_1 c}{\omega_{ce}}\right]} \end{aligned} \tag{3.3}$$

For reference, if $f_{ce} = \omega_{ce}/2\pi = 2.25$ GHz (a typical value), then $c/\omega_{ce} \simeq 2$ cm.

In evaluating (2.85) we selected values of the plasma parameters attainable on the UCLA Q machine, i.e., $c/a = 1120$ and $\omega_{pe}/\omega_{ce} = 0.4$. Then writing

$$\underline{J}_1 = \frac{\omega_{pe}^2 \Phi_1}{a}\left[\hat{e}_x J_x + \hat{e}_y J_y\right] \tag{3.4}$$

with $\underline{J}_1$ given by (2.85) we numerically calculated J_x vs. $\tilde{z}$ for several values of ω_1/ω_{ce} in the range $0.985 \leq \omega_1/\omega_{ce} \leq 0.999$. The results are presented in Figs. 7a-f. The actual values of ω_1/ω_{ce} and the corresponding values of the parameter Γ defined by

$$\Gamma \equiv \left| \frac{\omega_1}{\omega_{ce}} - 1 \right| \frac{c}{a} \tag{3.5}$$

are given in the caption of Fig. 7. All of Figs. 7a-f are drawn to the same vertical and horizontal scales to aid in comparing the wavelengths and amplitudes of the various terms. And in each of these figures the length $\tilde{\lambda}_o$ is indicated explicitly while the length $\tilde{\lambda}_1$ (which is simply one wavelength of the pole term) is easily discernible.

We briefly note the following features in Figs. 7a-f.

Figure 7a: The branch-cut term is negligible, the free-streaming term is significant for $0 \leq \tilde{z} \lesssim 3\tilde{\lambda}_o$ and the pole term is significant from $\tilde{z} = 0$ or to large values of $\tilde{z}$ since it is only weakly damped. Note that $\tilde{\lambda}_o << \tilde{\lambda}_1$. All of these features hold for smaller values of ω_1/ω_{ce}.

Figures 7a-f: As ω_1/ω_{ce} increases, the branch-cut term grows in amplitude and penetrates further into the plasma, reaching peak penetration at about $\omega_1/\omega_{ce} = 0.996$ ($\Gamma = 4.5$). The dashed branch-cut curves computed by setting $\varepsilon_{T_+}(k_{se},\omega_1)$ equal to one in (2.85) show that if the dielectric function $\varepsilon_{T_+}(k_{se},\omega_1)$ were not present, the branch-cut term's penetration length would continue to grow with $\tilde{\lambda}_o$ approaching infinity as ω_1 approached ω_{ce}. The free-streaming term always

20

FIGURES 7a-f

In Figures 7a-f we present plots of J_x [defined in (3.4)] vs. $\tilde{Z}$ [$=Z/(c/\omega_{ce})$] for the branch-cut, free-streaming, and cyclotron-damped pole terms of (2.85). ($\omega_{pe}/\omega_{ce} = .4$, $c/a = 1120$) All figures are drawn to the same vertical and horizontal scales, which are fully labelled only in Figure 7a. In Figures 7b-f, $\epsilon_{T+}(k_{se},\omega_1)$ was set equal to one in (2.85) to produce the dashed branch-cut curves, and $\epsilon_{T-}(\omega_1-\omega_{ce}/v_s,\omega_1)$ was set equal to one in (2.85) to produce the dashed free-streaming curves. Values of ω_1/ω_{ce} , $\Gamma=|(\omega_1/\omega_{ce})-1|c/a$, $\tilde{\lambda}_o=\lambda_o/(c/\omega_{ce})=1/\Gamma$, and k_1c/ω_{ce} are as follows (values of k_1c/ω_{ce} were obtained from Figure C-5):

Figure	ω_1/ω_{ce}	Γ	$\tilde{\lambda}_o$	k_1c/ω_{ce}
7a	.985	16.8	.06	3.64 + i0.02
7b	.990	11.2	.09	4.28 + i0.145
7c	.994	6.7	.15	5.39 + i0.91
7d	.996	4.5	.22	5.76 + i1.68
7e	.9975	2.8	.36	5.89 + i2.32
7f	.999	1.1	.89	5.95 + i2.96

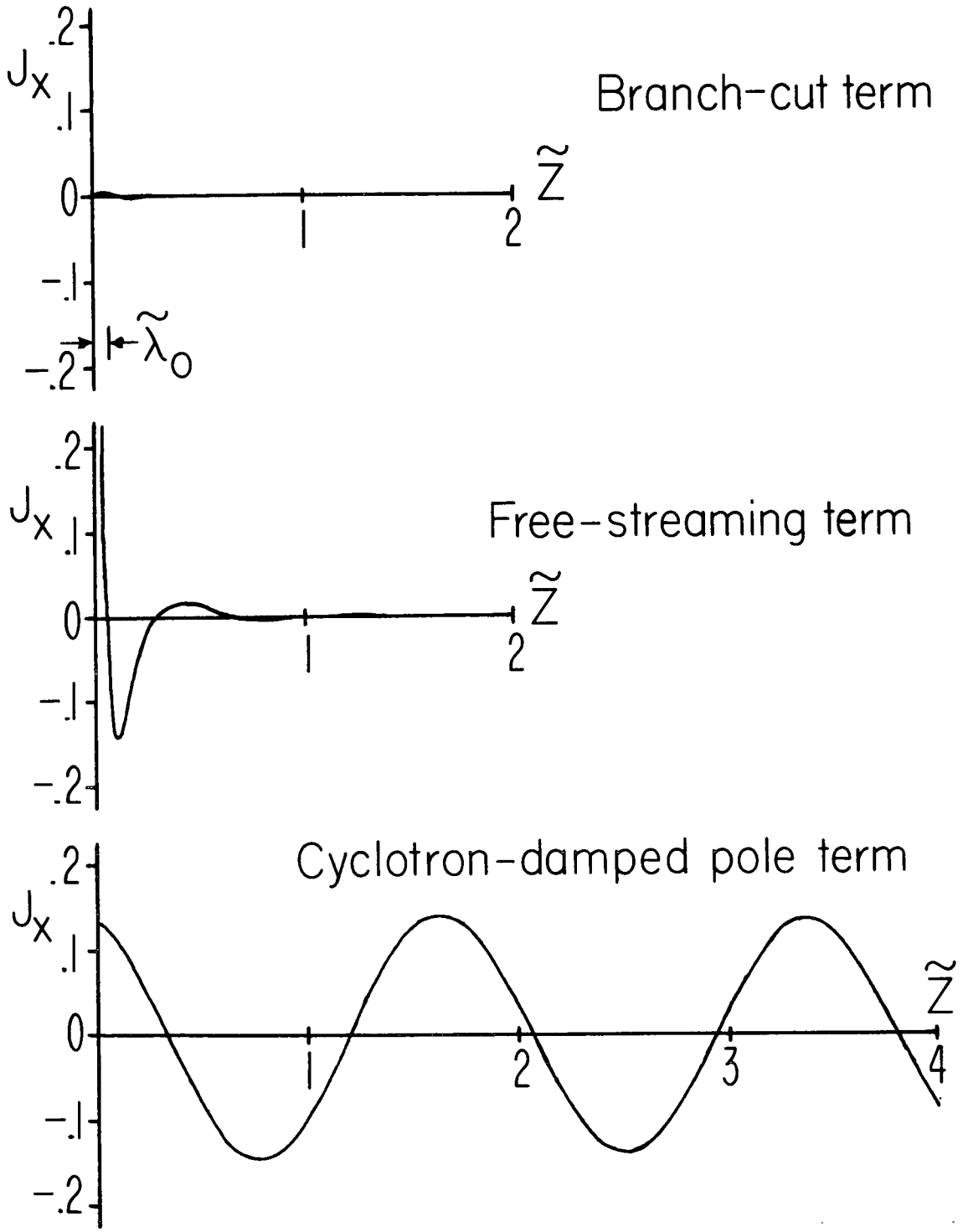

FIGURE 7a: $\omega_1/\omega_{ce} = .985$

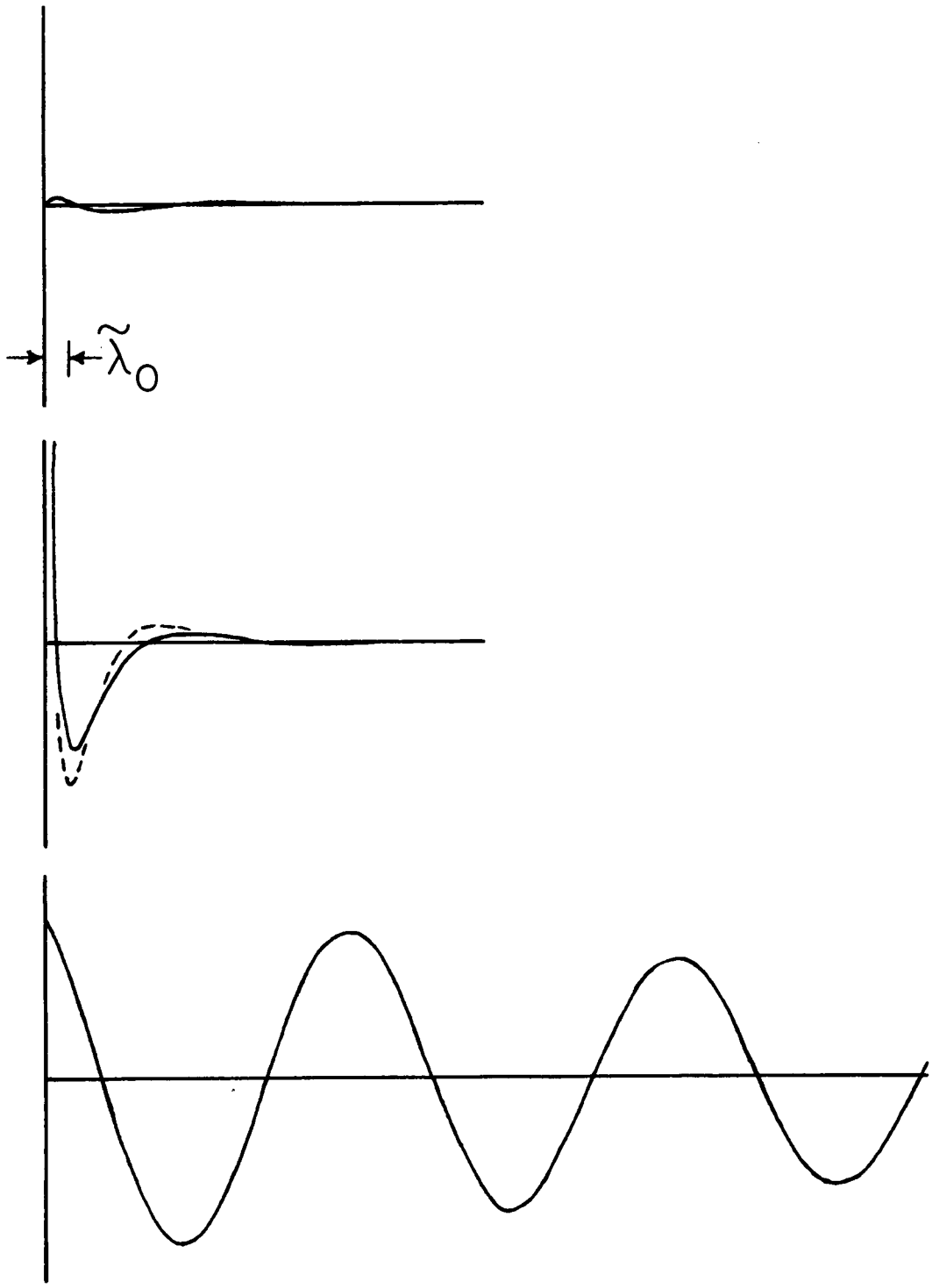

FIGURE 7b: $\omega_1/\omega_{ce} = .990$

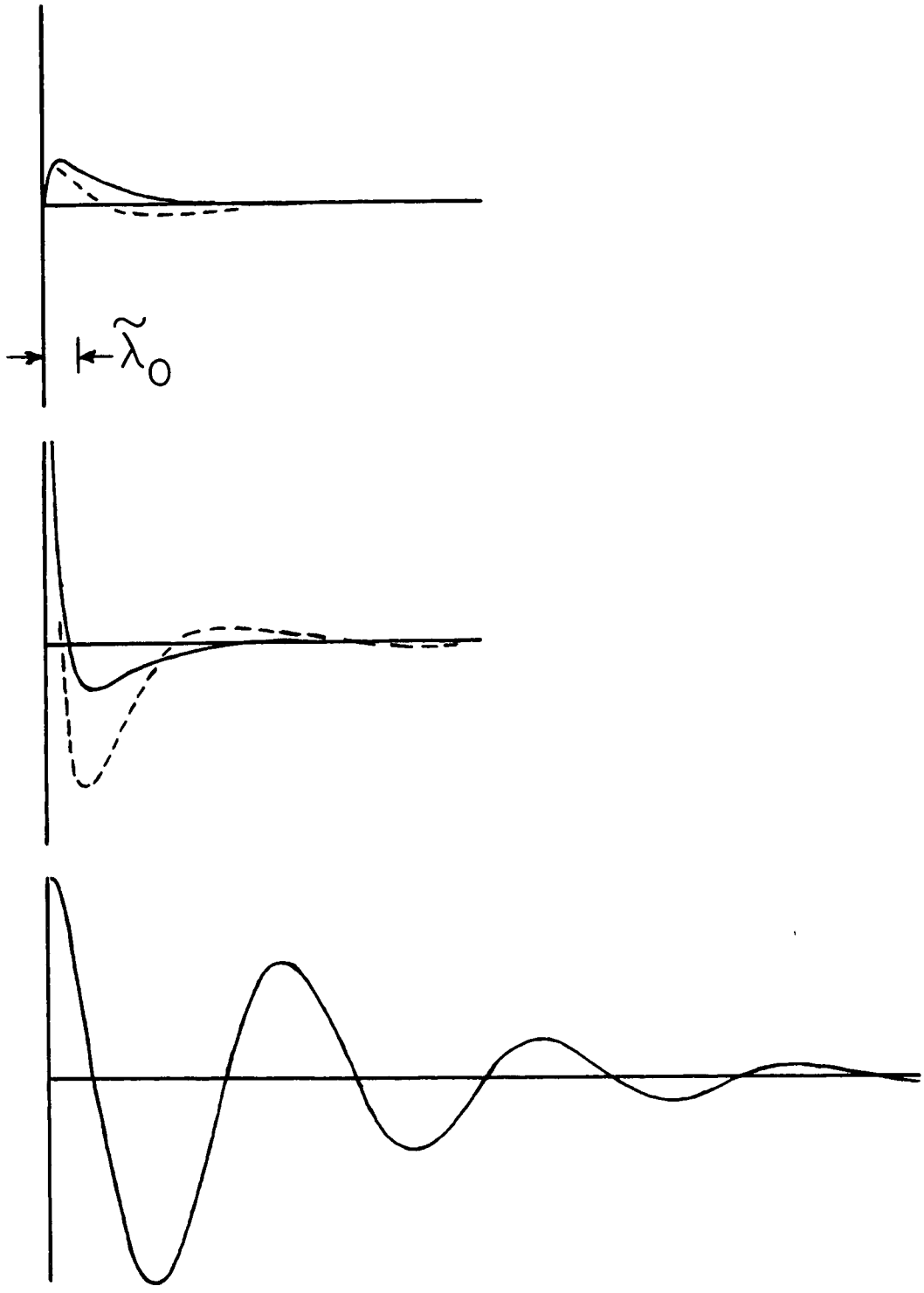

FIGURE 7c: $\omega_1/\omega_{ce} = .994$

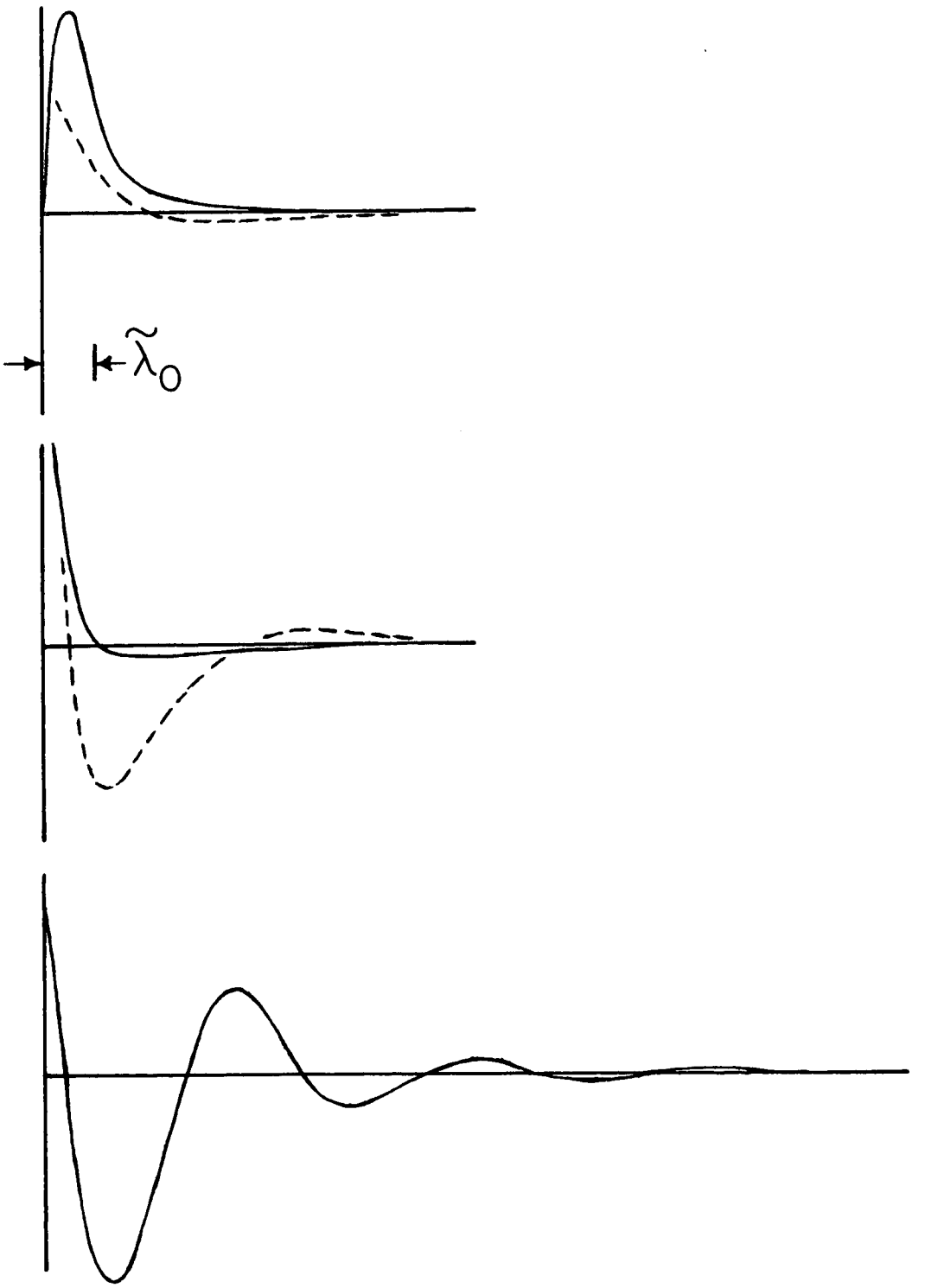

FIGURE 7d: $\omega_1/\omega_{ce} = .996$

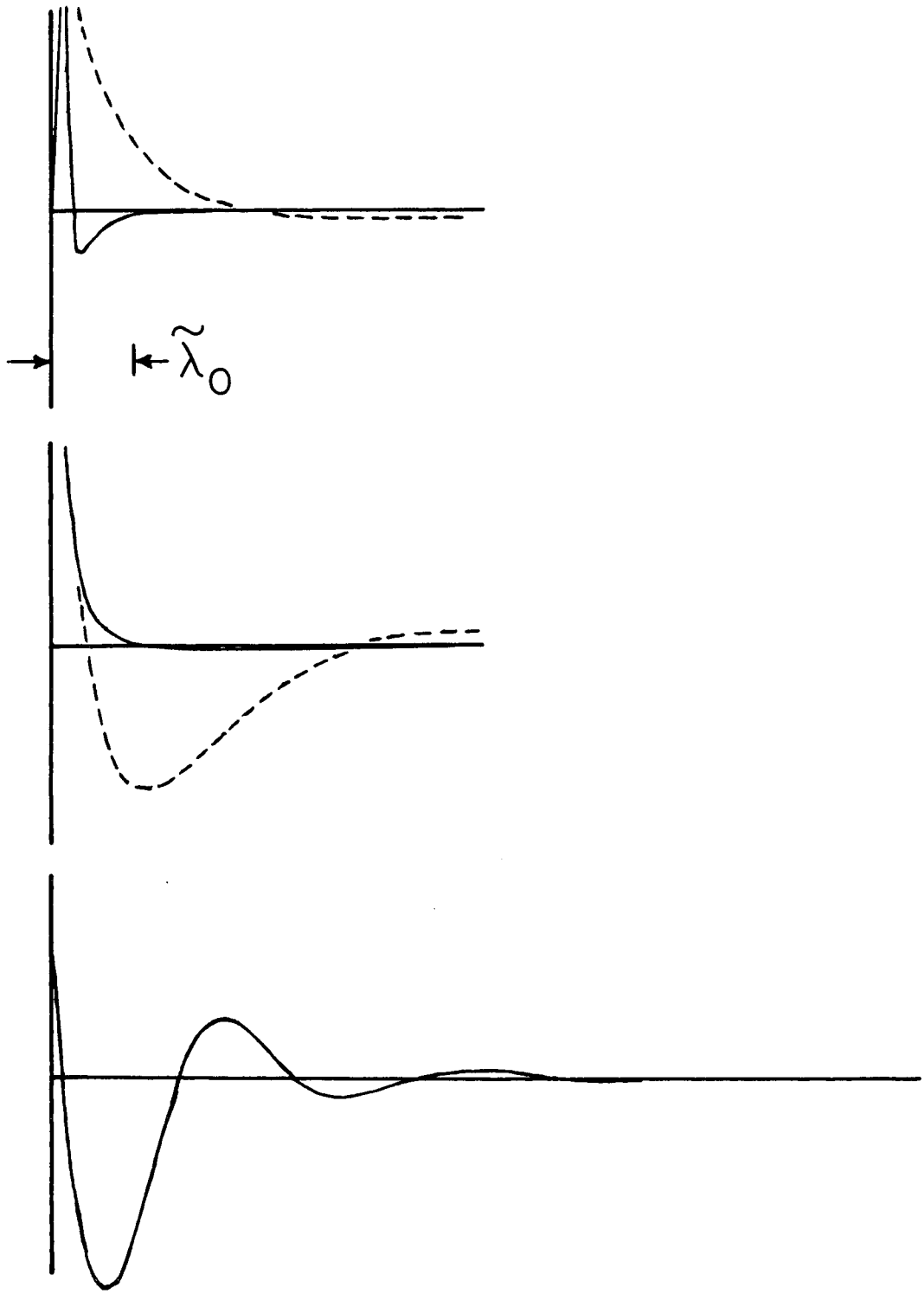

FIGURE 7e: $\omega_1/\omega_{ce} = .9975$

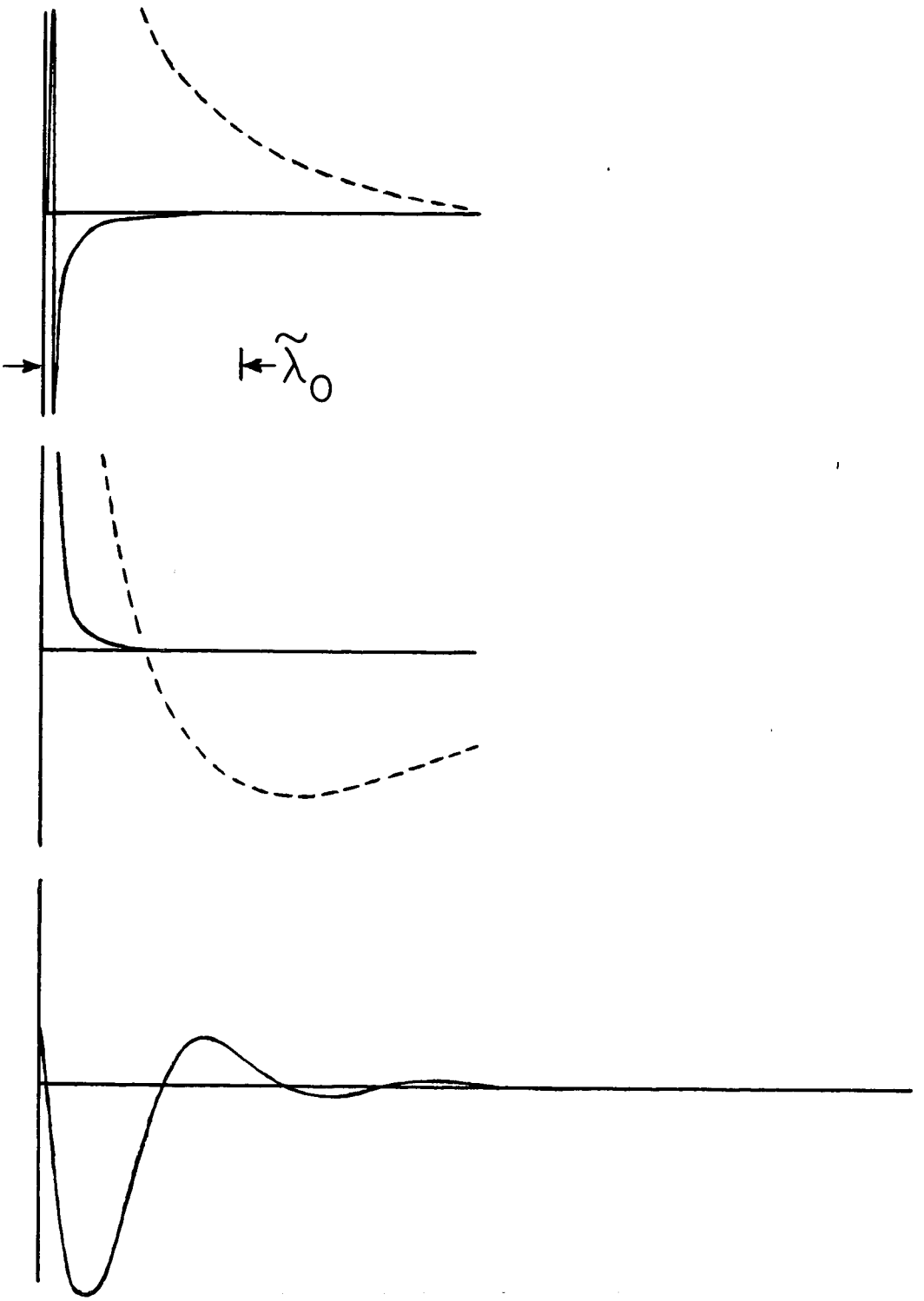

FIGURE 7f: $\omega_1/\omega_{ce} = .999$

diverges at $\tilde{z} = 0$. As ω_1/ω_{ce} increases, the free-streaming term penetrates more as its amplitude decreases; roughly, maximum penetration occurs for $\omega_1/\omega_{ce} \simeq 0.994$ ($\Gamma \simeq 6$) . The dashed free-streaming curves, computed by setting $\varepsilon_{T_-}[(\omega_1-\omega_{ce}/v_s),\omega_1]$ equal to one in (2.85), show that if the dielectric function $\varepsilon_{T_-}[(\omega_1-\omega_{ce}/v_s),\omega_1]$ were not present, the free-streaming term's penetration length would also continue to grow with $\tilde{\lambda}_o$, approaching infinity as ω_1 approached ω_{ce} . The cyclotron-damped pole term shows increased damping and a smaller wavelength as ω_1/ω_{ce} increases.

Figure 7f: The branch-cut and free-streaming terms are significant only for $0 \leq \tilde{z} << \tilde{\lambda}_o \simeq 1$ while the pole term is significant for $0 \leq \tilde{z} \lesssim 2$, the later limit being due to the heavy cyclotron damping. Note that $\tilde{\lambda}_o \simeq \tilde{\lambda}_1$. For still larger value of ω_1/ω_{ce} (i.e., $0.999 < \omega_1/\omega_{ce} \leq 1$, or equivalently $1 > \Gamma \geq 0$), the branch-cut and free-streaming terms' penetration lengths go to zero while $\tilde{\lambda}_o \to \infty$; at the same time $\tilde{\lambda}_1$ decreases (but not to zero) and the pole terms' penetration length decreases (but not to zero).

We conclude that the branch-cut and free-streaming terms attain sizable magnitudes and penetration lengths for ω_1/ω_{ce} within a certain range of values. More specifically, for the present parameter values, we shall find in a following section that collisional damping dominates cyclotron damping for $\omega_1/\omega_{ce} \lesssim 0.99$. Thus, for the present parameter values, cyclotron damping measurements would be feasible only in the range $0.99 \lesssim \omega_1/\omega_{ce} \leq 1$. And we see from Figs. 7a-f that within this range, both the branch-cut and free-streaming terms are quite significant. In fact, for $0.996 \lesssim \omega_1/\omega_{ce} \lesssim 0.998$ approximately the first

1/3 or 1/4 of the distance over which the pole term (and therefore cyclotron damping) could be measured has dominant interference from the branch-cut and free-streaming terms.

With the above specific results at our disposal, we return to (2.85) to discuss the general behavior of the three terms that comprise that equation.

4. Analytical Investigation of (2.85)

In this section we shall examine the general behavior of the three terms in (2.85) for all values of ω_1 . We shall find that the branch-cut and free-streaming terms have definite characteristics in each of the regions $\Gamma >> 1$, $\Gamma \simeq 1$, $\Gamma << 1$, where, as given earlier, $\Gamma \equiv |(\omega_1/\omega_{ce})-1| \frac{c}{a}$. [For reference, note that (1) $\Gamma >> 1$ for all values of ω_1 except those very near ω_{ce} , and (2) the Γ regions are symmetrically located about $\omega_1 = \omega_{ce}$.] The shielding effect that occurs in the branch-cut and free-streaming terms, as noted in Fig. 7, will be discussed further. Lastly, in considering the pole term, we shall investigate the infinite number of residues that occur (because there are an infinite number of roots to the transverse dispersion relation) and show that their effects are negligible in general, except at positions very near $z = 0$ (the place of excitation).

The branch-cut term in (2.85).

This term has the characteristic length $\lambda_o \equiv a/|\omega_1-\omega_{ce}|$. Observe that

$$|k_{se}| \approx \frac{1}{\lambda_o}\left(\frac{\lambda_o}{z}\right)^{\frac{1}{3}} \tag{4.1}$$

Thus at $z = 0$ (and for any ω_1 except $\omega_1 = \omega_{ce}$), the factor $(k_{se}^2c^2 - \omega_1^2) \sim k_{se}^2c^2 \to \infty$ and therefore the branch-cut terms' amplitude $\to 0$. For $z \neq 0$ the behavior of this term depends predominantly on the value of the parameter Γ :

$\Gamma >> 1$. In this region λ_o is a very small distance and the branch-cut term effectively damps out in a distance of a few λ_o

because of the exponential factor which goes as $\exp[-(z/\lambda_o)^{2/3}]$. Even for $0 \leq z < \lambda_o$ the branch-cut term is essentially negligible because, although $\varepsilon_{\Gamma_\pm}(k_{se},\omega_1) \simeq 1$, we find that

$$\left|\frac{\omega_{pe}^2}{k_{se}^2c^2-\omega_1^2}\right| \lesssim \left|\frac{\omega_{pe}^2}{k_{se}^2c^2}\right| \approx \frac{\omega_{pe}^2}{\omega_{ce}^2}\left[\frac{z}{\lambda_o\Gamma}\right]^{2/3} \ll 1 \qquad (4.2)$$

(for $\omega_{pe}^2/\omega_{ce}^2$ not too large). Thus in this region the branch-cut term is negligible in general.

$\Gamma \simeq 1$. As ω_1 approaches ω_{ce} the branch-cut terms' amplitude increases (because of the $1/(\omega_1-\omega_{ce})$ factor) and the term penetrates farther into the plasma (because λ_o increases). If there were no dielectric functions in the denominator of the branch-cut term, then both the amplitude and penetration length of this term would go to infinity at $\omega_1 = \omega_{ce}$. However, the dielectric functions are present and their shielding effect is strong enough (for $\Gamma \lesssim 1$) to damp out the branch-cut term a significant distance before the exponential factor does, i.e., before $z = \lambda_o$. (This effect was noted earlier in Fig. 7.) A result of this effect is that the branch-cut term attains a maximum penetration distance for some value of Γ larger than one. [In Fig. 7 (for $\omega_{pe}^2/\omega_{ce}^2 = 0.4$, $c/a = 1120$) maximum penetration occurred at $\Gamma \simeq 4.5$.]

$\Gamma << 1$. In this region the shielding effect described above dominates, which may be seen as follows. At $z = \lambda_o$ we find $|k_{se}| \simeq 1/\lambda_o$ and

$$\left| \epsilon_{T_\pm}(k_{se},\omega_1) \right| \approx \frac{\frac{\omega_{pe}^2}{\omega_{ce}^2}\frac{c}{a}}{\Gamma} \tag{4.3}$$

Thus at $z = \lambda_o$, the branch-cut term goes as

$$\left| \frac{\frac{\omega_{pe}^2}{\omega_{ce}^2}\frac{c}{a}}{\epsilon_{T_+}(k_{se},\omega_1)\epsilon_{T_-}(k_{se},\omega_1)\Gamma} \right| \sim \frac{\Gamma}{\frac{\omega_{pe}^2}{\omega_{ce}^2}\frac{c}{a}} \tag{4.4}$$

which, for $\omega_{pe}^2/\omega_{ce}^2$ not too small, is $<< 1$ and therefore negligible. In this case, the branch-cut term attains a sizable magnitude only for $|z| << \lambda_o$. However, for $|z| << \lambda_o$ the branch-cut term is not truly valid since then the saddle point asymptotic expansion breaks down (as shown in Appendix E). Thus, although the peak behavior near $z = 0$ of the branch-cut term in Figs. 7e,f can be explained analytically, we shall refrain from doing so because this term is not truly valid there anyway.

The above results hold for $(\omega_{pe}^2/\omega_{ce}^2)(c/a) >> 1$. If on the other hadn $(\omega_{pe}^2/\omega_{ce}^2)(c/a) << 1$, then (4.4) indicates that the branch-cut term would have a sizable magnitude at $z = \lambda_o$ and therefore a sizable penetration length (since $\lambda_o \to \infty$ for $\Gamma << 1$). In this case the branch-cut term's penetration length would simply approach infinity as ω_1 approached ω_{ce}. Thus effectively, in this case of extremely low densities and/or extremely high magnetic fields, the plasma does <u>not</u> exhibit the collective shielding effect that occurred above.

The free-streaming term in (2.85).

This term also has a characteristic length λ_o . Note that

$$\left| \frac{v_s}{\alpha} \right| \approx \left(\frac{z}{\lambda_o} \right)^{1/3} \tag{4.5}$$

A significant feature of the free-streaming term is that it always diverges at $z = 0$ due to the factor $1/v_s$. Physical reasons for the presence of this divergence and conditions under which it is removed will be discussed in a following section on transverse free-streaming waves. For $z \neq 0$, the behavior of the free-streaming term depends predominantly on the value of Γ :

$\Gamma >> 1$. In this region λ_o is a very small distance and the free-streaming term effectively damps out in a distance of a few λ_o . The dielectric function $\varepsilon_{T_\alpha}[(\omega_1 - \omega_{ce}/v_s), \omega_1] \simeq 1$ so the free-streaming term is approximately

$$\frac{e^{-\left(\frac{z}{\lambda_o}\right)^{2/3}\left(1 - i\sqrt{3}\right)}}{\left(\frac{z}{\lambda_o}\right)^{1/3}}$$

which depends only on the ratio z/λ_o . It follows that the amplitudes of this term's peaks remain approximately constant but the peaks shift to larger values of z as ω_1 approaches ω_{ce} (because then λ_o increases). Thus we find in this region that the free-streaming term is always significant for $0 \leq z \lesssim 3\lambda_o$ say.

$\Gamma \simeq 1$. As ω_1 approaches ω_{ce} the free-streaming term penetrates further into the plasma but at the same time, its amplitude decreases as the dielectric function begins to exhibit a shielding effect. This

effect dominates as $\Gamma \to 0$ and the effective penetration length recedes back to zero. From Fig. 7 we note that an "effective penetration length" is not a clearly definable quantity but that for some value of Γ larger than one (e.g., $\Gamma \simeq 6$ in Fig. 7), the free-streaming term does in some sense exhibit maximum penetration.

$\Gamma \ll 1$. In this region the shielding effect described above dominates, which may be seen as follows. For $|z| \lesssim \lambda_o$, $|v_s/a| \approx |z/\lambda_o| \lesssim 1$ and we find

$$\left| \epsilon_{T_\alpha}\left(\frac{\omega_1 - \omega_{ce}}{v_s}, \omega_1\right) \right| \approx \left(\frac{z}{\lambda_o}\right) \frac{\frac{\omega_{pe}^2}{\omega_{ce}^2}\frac{c}{a}}{\Gamma^3} \tag{4.6}$$

Thus for $|z| \lesssim \lambda_o$ the free-streaming term goes as

$$\left| \frac{1}{\left(\frac{v_s}{a}\right)\epsilon_{T_\alpha}\left(\frac{\omega_1 - \omega_{ce}}{v_s}, \omega_1\right)} \right| \approx \frac{\Gamma^3}{\left(\frac{z}{\lambda_o}\right)^{4/3}\frac{\omega_{pe}^2}{\omega_{ce}^2}\frac{c}{a}} \tag{4.7}$$

which at $z = \lambda_o$ is $\ll 1$ provided $\omega_{pe}^2/\omega_{ce}^2$ is not too small. In this case, the free-streaming term, like the branch-cut term, attains a sizable magnitude only for $|z| \ll \lambda_o$. [Equations (4.6), (4.7) for $z = \lambda_o$ may be compared to the corresponding branch-cut term Eqs. (4.3), (4.4).]

If $(\omega_{pe}^2/\omega_{ce}^2)(c/a) \ll 1$ then according to (4.7) the free-streaming term, like the branch-cut term, would have a sizable magnitude at $z = \lambda_o$ (thereby exhibiting no shielding effect) and accordingly its penetration length would approach infinity as ω_1 approached ω_{ce}.

The dielectric-pole term in (2.85).

The pole term(s) represent the collective modes of the plasma. As noted earlier, a pole term has wavelength $\lambda_1 = 2\pi/\mathrm{Re}\ k_1 = [2\pi/(\mathrm{Re}\ k_1 c/\omega_{ce})](c/\omega_{ce})$ which, for the least-damped pole, is of order c/ω_{ce} for ω_1 near ω_{ce}. The amplitude of the pole term depends mainly on the factor $Z_+(\zeta_e)$ where $\zeta_e = (\omega_1-\omega_{ce})/k_1 a$. The quantity $|Z_+(\zeta_e)|$ is largest (of order one) for ω_1 near ω_{ce}; elsewhere $|Z_+(\zeta_e)| \sim 1/\zeta_e \sim a/c$ which is typically quite small.

The waveforms produced by the pole terms are governed by the zeros of the transverse dielectric function, i.e., by the roots of $\varepsilon_T(k,\omega) = 0$ for real ω and complex k. These roots are discussed in detail in Appendix C which should be read at this time. A summary of the types of roots for the various frequency ranges is given just preceding Fig. C-14. With the results of Appendix C, the pole terms may be computed for any desired value of ω_1.

The least-damped pole and any pure imaginary poles may be readily computed. However, the infinite sequence of poles that always occurs is more difficult to evaluate. In the following we obtain an upper-bound estimate for the magnitude of the infinite sum of pole terms.

The infinite sum of pole terms.

For $0 < \omega_1 < \omega_{ce}$ the branch-cut P.S.D. contour in the k plane (as shown in Fig. 6) is such that only a portion of the infinite sequence of roots [of $\varepsilon_T(k,\omega) = 0$] is enclosed. This situation occurs whenever $\omega_1 < \omega_{ce}$ as may be seen from Fig. C-13. For $\omega_1 > \omega_{ce}$ the branch-cut P.S.D. contour (as shown in Fig. 3) is again such that only a portion of the infinite sequence of roots [now of

$\varepsilon_{T_+}(k,\omega_1) = 0$] is enclosed. In all cases the saddle point k_{se}, as given in (2.85), moves as ω_1 or z is varied, so the number of roots enclosed also varies. Thus we have chosen to evaluate the full infinite sum of residues, knowing that in any actual case the net effect will be <u>smaller</u> than the estimate we will obtain. Without loss of generality we consider $\omega_1 > \omega_{ce}$, and therefore the roots of $\varepsilon_{T_+}(k,\omega_1) = 0$.

Asymptotic expressions for the values of the roots in the infinite sequence are obtained in Appendix C. As given in (C.35) such roots of $\varepsilon_{T_+}(k,\omega_1) = 0$ in the ζ_e plane ($\zeta_e = [\omega_1 - \omega_{ce}]/ka$) are given by

$$\zeta_e = \rho e^{-i\frac{\pi}{4}}$$
$$\rho = \sqrt{2m\pi} \qquad m = 3,4,5,\cdots \tag{4.8}$$

and at such roots we have from (C.32)

$$2\sqrt{\pi}\, i\, e^{-\zeta_e^2} = \frac{D}{\zeta_e} + \frac{E}{\zeta_e^3}$$
$$D = \left[1 - \frac{\omega_1(\omega_1-\omega_{ce})}{\omega_{pe}^2}\right] \tag{4.9}$$
$$E = \left[\frac{(\omega_1-\omega_{ce})^3 c^2}{\omega_1 \omega_{pe}^2 a^2}\right]$$

We proceed to evaluate the residue terms.

For $|\zeta_e| \gtrsim 3$ we know

$$Z_+(\zeta_e) \approx -\frac{1}{\zeta_e} - \frac{1}{2\zeta_e^3} - \cdots + 2\sqrt{\pi}\, i\, e^{-\zeta_e^2} \tag{4.10}$$

so from (4.9), at a root, we have

$$Z_+(\zeta_e) \approx \frac{D-1}{\zeta_e} + \frac{E-1}{\zeta_e^3} \tag{4.11}$$

For now we assume the second term in (4.11) is negligible and take

$$Z_+(\zeta_e) \approx \frac{D-1}{\zeta_e} \tag{4.12}$$

Another result we need is

$$k\frac{\partial \epsilon_T(k,\omega_1)}{\partial k} = -\zeta_e \frac{\partial \epsilon_T(\zeta_e,\omega_1)}{\partial \zeta_e}$$

$$= \left\{ \frac{\omega_{pe}^2 \omega_1 \zeta_e^3}{\left[(\omega_1-\omega_{ce})^3 \frac{c^2}{a^2}\right] - \left[\zeta_e^2(\omega_1-\omega_{ce})\omega_1^2\right]} \cdot \right.$$

$$\left. \left[\frac{3\left[(\omega_1-\omega_{ce})^3 \frac{c^2}{a^2}\right] - \left[\zeta_e^2(\omega_1-\omega_{ce})\omega_1^2\right]}{\left[(\omega_1-\omega_{ce})^3 \frac{c^2}{a^2}\right] - \left[\zeta_e^2(\omega_1-\omega_{ce})\omega_1^2\right]} Z_1(\zeta_e) - 2\zeta_e - 2\zeta_e^2 Z_1(\zeta_e) \right] \right\} \tag{4.13}$$

To simplify this, we note that for

$$\left|(\omega_1-\omega_{ce})^3 \frac{c^2}{a^2}\right| \leq \left|\zeta_e^2(\omega_1-\omega_{ce})\omega_1^2\right|$$

i.e., for

$$\left|\frac{(\omega_1-\omega_{ce})}{\omega_1}\frac{c}{a}\right| \leq 3 \tag{4.14}$$

(since $|\zeta_e| \gtrsim 3$), we have

$$k\frac{\partial \epsilon_{T_+}(k,\omega)}{\partial k} \approx \frac{\omega_{pe}^2 \zeta_e}{-\omega_1(\omega_1-\omega_{ce})}\left[-2\zeta_e - 2\zeta_e^2 Z_1(\zeta_e)\right] \approx \frac{2D\omega_{pe}^2\zeta_e^2}{\omega_1(\omega_1-\omega_{ce})} \tag{4.15}$$

using (4.12).

We may now calculate the infinite sum of residue terms, which we shall call $\sum_\infty$. Using (4.8), (4.12), and (4.15), we find

$$\left|\sum_\infty\right| \equiv \left|\sum_k \left\{ \frac{e^{ik_1 z}}{k\frac{\partial \epsilon_{T_+}(k,\omega_1)}{\partial k}\Big|_{k=k_1}} Z_+(\zeta_e)\right\}\right| \lesssim \left|\frac{\omega_1(\omega_1-\omega_{ce})(D-1)}{2^{5/2}\pi^{3/2}\omega_{pe}^2 D}\right| \sum_{n=3}^{\infty} \frac{e^{-\frac{cz}{\sqrt{n}}}}{n^{3/2}} \tag{4.16}$$

where $c \equiv (\omega_1-\omega_{ce})/2\sqrt{\pi}a$. Since

$$\int_0^\infty \frac{e^{-\frac{cz}{\sqrt{n}}}}{n^{3/2}}\,dn = \frac{2}{cz} \tag{4.17}$$

for $cz \neq 0$, we conclude that

$$\left|\sum_\infty\right| < \left|\frac{\omega_1(D-1)}{\sqrt{2}\,\pi\,\omega_{pe}D}\right]\frac{\frac{a}{\omega_{pe}}}{z} \tag{4.18}$$

If $cz = 0$, (4.16) remains finite since

$$\sum_{n=3}^{\infty}\frac{1}{n^{3/2}} = 1.259 \tag{4.19}$$

We see that if inequality (4.14) holds (i.e., if $\Gamma \lesssim 1$) than (4.12) and the final result (4.18) hold. In the opposite limit

$$\left| \frac{\omega_1 - \omega_{ce}}{\omega_1} \right| \frac{c}{a} \gg 3 \tag{4.20}$$

(which corresponds to $\Gamma \gg 1$) we find

$$Z_+(\zeta_e) \approx \frac{E-1}{\zeta_e^3} \tag{4.21}$$

and

$$\left| \sum_{\infty} \right| < \left[\frac{2^{3/2}\, \omega_{ce}^2}{\pi\, \omega_1 \omega_{pe}} \right] \frac{\left(\frac{c}{\omega_{ce}}\right)^2 \left(\frac{a}{\omega_{pe}}\right)}{Z^3} \tag{4.22}$$

For cyclotron damping measurements we would usually have $\omega_1 \simeq \omega_{ce} \simeq \omega_{pe}$. Then at $z = a/\omega_{pe} \simeq \lambda_d$ ($\lambda_d = [4\pi ne^2/\kappa T_e]^{1/2}$ is the Debye length), we see from (4.18) that $|\sum_{\infty}| < 1$ for $\Gamma \lesssim 1$ and from (4.22) that $|\sum_{\infty}| \lesssim c^2/a^2$ for $\Gamma \gg 1$. Thus very close to the place of excitation ($z = 0$) the infinite sum of pole terms may have a significant effect. On the other hand, at $z = c/\omega_{ce}$ both (4.18) and (4.22) show that $|\sum_{\infty}| < a/c$ which is typically very small. Thus the effects of the infinite sum of pole terms is confined to a small region near the place of excitation. [To substantiate the above conclusions for the case of Fig. 7, we summed the first several thousand pole terms numerically using (4.11), (4.13) and indeed it was found that the sum was significant only extremely close to $z = 0$.]

5. Physical Picture of Transverse Free-Streaming Waves and the Free-Streaming Term in (2.85)

We wish to investigate the physical significance of transverse free-streaming waves and explain why these waves have negative phase velocities (for $z > 0$) when $0 < \omega_1 < \omega_{ce}$, and why these waves experience no cyclotron damping. Then we want to investigate the free-streaming term in (2.85) and explain why this term has no accompanying pole contribution for $0 < \omega_1 < \omega_{ce}$, and why this term diverges at $z = 0$. In addition to present considerations, free-streaming waves merit special attention since they are the basis of echo phenomenon (such as we will consider in Part II).

5.1 Physical picture of transverse free-streaming waves.

We consider the situation shown in Fig. 8a. A continuous uniform-density beam of electrons flows in the +z direction along an externally applied magnetic field $\underline{B}_o = \hat{e}_z B_o$. All particles in the beam have the same velocity v_z in the +z direction and the same magnitude of velocity $|v_\perp|$ in the perpendicular direction. The directions of the perpendicular velocities are uniformly distributed; this is represented in Fig. 8b by the uniform ring of dots plotted in perpendicular velocity space (v_x, v_y). Each dot represents a particle and the particles are uniformly spaced on a circle of radius $|v_\perp|$. Thus if the perpendicular current

$$\underline{J}_\perp = \sum_i q_i \underline{v}_{\perp i} \qquad (5.1)$$

were calculated, the result would be $\underline{J}_\perp = 0$ as illustrated in the lower portion of Fig. 8b.

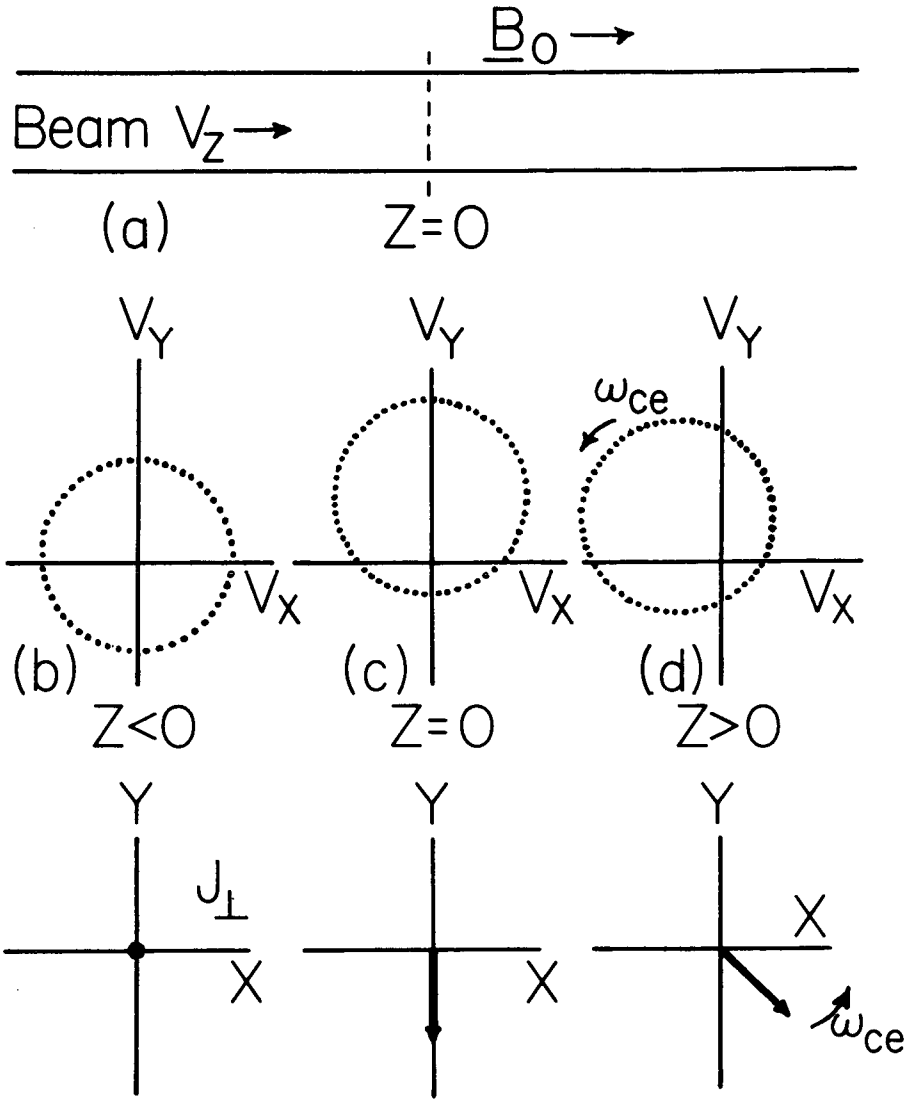

FIGURE 8. CREATION OF A TRANSVERSE FREE-STREAMING WAVE.

The beam and excitation at z=0 are shown in (a). The velocity distribution and current $J_\perp$ are shown for z<0, z=0, z>0 in (b),(c),(d) respectively.

Returning to Fig. 8a, we have placed an idealized excitation mechanism at $z = 0$ which lets particles pass through freely but subjects them to the external field

$$\underline{E}_{ext}(z,t) = \mathcal{E}_1 \left[\hat{e}_x \cos(\omega_1 t) + \hat{e}_y \sin(\omega_1 t) \right] \delta(z) \qquad (5.2)$$

[as used earlier in (2.46), (2.77)]. The effect of this external field is that as a particle passes $z = 0$ it receives a net impulsive change in its momentum, which we shall call $m\underline{\Delta v}$. If a particle passes $z = 0$ at time t we find

$$\begin{aligned} m\underline{\Delta V} &= \int_{t-\frac{\delta t}{2}}^{t+\frac{\delta t}{2}} dt\, q\underline{E}_{ext} = \frac{q}{v_z}\int_{-\frac{\delta z}{2}}^{+\frac{\delta z}{2}} dz\, \underline{E}_{ext} \\ &= \frac{q\mathcal{E}_1}{v_z}\left[\hat{e}_x \cos(\omega_1 t) + \hat{e}_y \sin(\omega_1 t)\right] \end{aligned} \qquad (5.3)$$

where δt (δz) is the time (distance) a particle spends subjected to the force $q\underline{E}_{ext}$. (Actually $\delta t, \delta z \to 0$ while $\underline{\Delta v}$ remains finite.) The important point is that all particles that pass $z = 0$ at the same time receive the same $\underline{\Delta v}$ regardless of the direction of their perpendicular velocity vectors.

In Fig. 8c we show the effect on the velocity distribution when $\underline{\Delta v}$ points upward. Each particle receives a $\underline{\Delta v}$ upward so the circle of Fig. 8b is just displaced upward a distance $\underline{\Delta v}$. If we calculate $\underline{J}_\perp$ from (5.1) we shall find a net current in the -Y direction (since $q = -e$ for electrons) and this is indicated in the lower portion of

Fig. 8c.

Now imagine what happens to the beam segment with the velocity distribution of Fig. 8c as this segment moves downstream ($z > 0$) with velocity v_z. Since every particle (electron) rotates in the right-hand direction at the cyclotron frequency ω_{ce}, it follows that the velocity vector of every particle maintains a fixed magnitude but rotates at frequency ω_{ce}. Thus, as shown in Fig. 8d, the velocity distribution is a displaced circle that rotates at frequency ω_{ce}. The net current $\underline{J_\perp}$ rotates at ω_{ce} also, as is shown in the lower portion of Fig. 8d.

In summary we note that a beam segment with $v_z > 0$ has $\underline{J_\perp} = 0$ for $z < 0$. As the segment passes $z = 0$ it obtains a net $\underline{J_\perp}$, and as it moves downstream with velocity v_z the current $\underline{J_\perp}$ rotates in the right-hand direction at frequency ω_{ce}.

The shape of the wave produced downstream depends on the relative size of ω_1 and ω_{ce}. If $\omega_1 = \omega_{ce}$ each new segment that passes $z = 0$ obtains a $\underline{J_\perp}$ exactly in phase with the $\underline{J_\perp}$'s of all the other segments that passed earlier. The established waveform, as shown in Fig. 9b, moves downstream with velocity v_z <u>and</u> rotates in the right-hand direction at frequency ω_{ce}. If $\omega_1 \neq \omega_{ce}$ then the excitation and established $\underline{J_\perp}$'s rotate at different frequencies, and the resultant waveform is a helix. For $\omega_1 < \omega_{ce}$ the waveform is as shown in Fig. 9a. (Note that this waveform occurs even if $\omega_1 = 0$.) For $\omega_1 > \omega_{ce}$ the waveform curls in the opposite direction as shown in Fig. 9c. We emphasize that all waveforms shown in Fig. 9 move downstream with velocity v_z <u>and</u> rotate in the right-hand direction at frequency ω_{ce}.

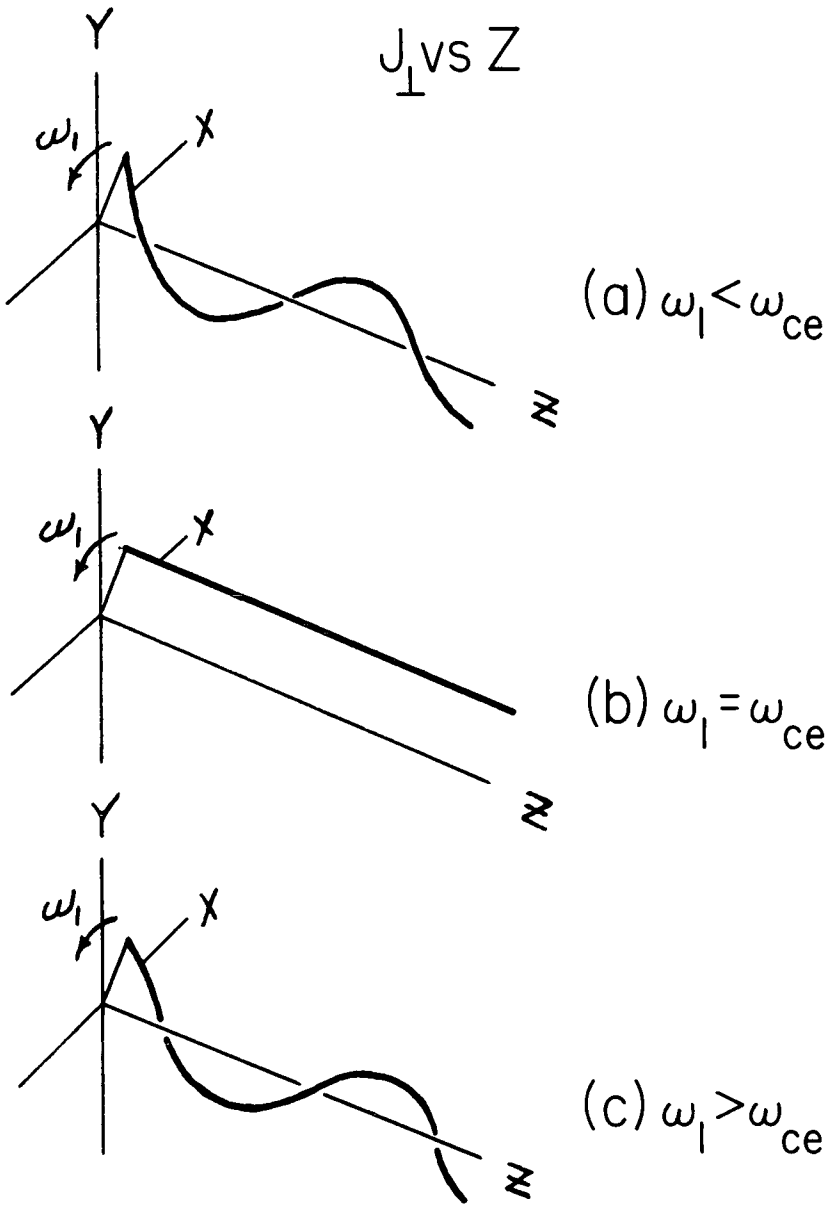

FIGURE 9. TRANSVERSE FREE-STREAMING WAVEFORMS ACCORDING TO VALUE OF ω_1 .

All established waveforms propagate with velocity v_z and simultaneously rotate at frequency ω_{ce} .

We compute the phase velocities of these waves as follows. If $\omega_{ce} = 0$ it is clear that one wavelength equals v_z times the time for one complete cycle of excitation at frequency ω_1, i.e., $\lambda = v_z(2\pi/\omega_1)$. If $\omega_{ce} \neq 0$ we find

$$\lambda = v_z\left(\frac{2\pi}{\omega_1 - \omega_{ce}}\right) \tag{5.4}$$

which can be seen by noting that an observer in a frame rotating with the electrons (at frequency ω_{ce}) sees the excitation as having a frequency $\omega_1 - \omega_{ce}$). Thus

$$k = \frac{\omega_1 - \omega_{ce}}{v_z} \tag{5.5}$$

If we consider one of the waves in Fig. 9 at some fixed z (> 0) we find the motion of the excitation at frequency ω_1 is exactly duplicated by the $\underline{J}_\perp$ of the wave (but delayed by a time z/v_z and rotated through an angle of $z\omega_{ce}/v_z$ radians). Thus the phase velocity of one of these waves would be

$$v_{PHASE} = \frac{\omega_1}{k} = v_z\left(\frac{\omega_1}{\omega_1 - \omega_{ce}}\right) \tag{5.6}$$

Note that $v_{phase} < 0$ for $0 < \omega_1 < \omega_{ce}$ which means the wave looks like it is propagating <u>toward</u> $z = 0$ whereas in fact all the particles comprising the wave are moving <u>away</u> from $z = 0$ (since $v_z > 0$). This apparent paradox may be explained as follows.

<u>Explanation of why transverse free-streaming waves have negative phase velocities (for $z > 0$) when $0 < \omega_1 < \omega_{ce}$.</u>

First consider the useful analogy of a rotating barber-shop pole.

The pole does not translate but the stripes appear to be moving upward. If the pole actually translated slowly downward (while still rotating) then the stripes would still appear to be moving upward (but slower) to a fixed observer. Thus the stripes would appear to be moving in a direction opposite to the direction the pole was moving. This situation is an exact analogy to that of transverse free-streaming waves for $0 < \omega_1 < \omega_{ce}$.

More quantitatively, consider any waveform in Fig. 9 and choose a point on it. In time Δt the point moves a distance $v_z \Delta t$ in the +z direction and it also rotates through $\omega_{ce}\Delta t$ radians in the x-y plane. Therefore to maintain constant phase (i.e., to keep up with a vector $\underline{J}_\perp$ that points in the same direction as a vector drawn to the original point), besides moving ahead $v_z \Delta t$ we must move an additional Δz due to the ω_{ce} rotation where

$$\frac{\Delta z}{\lambda} = \frac{\omega_{ce}\Delta t}{2\pi}$$

or

$$\Delta z = v_z \left(\frac{\omega_{ce}}{\omega_1 - \omega_{ce}}\right)\Delta t \tag{5.7}$$

using (5.4). Thus the phase velocity is

$$v_{PHASE} = \frac{v_z \Delta t + \Delta z}{\Delta t} = \underbrace{v_z}_{\text{from translation}} + \underbrace{\frac{\Delta z}{\Delta t}}_{\text{from rotation}} \tag{5.8}$$

$$= v_z \left(\frac{\omega_1}{\omega_1 - \omega_{ce}}\right)$$

[using (5.7)], which agrees with (5.6). But this calculation explicitly

shows that the ω_{ce} rotation can dominate the v_z translation causing the phase velocity to be negative for $0 < \omega_1 < \omega_{ce}$. Hence it is important to consider transverse free-streaming waves not as fixed waveforms that just translate, but as waveforms that translate and simultaneously rotate.

Explanation of why transverse free-streaming waves experience no cyclotron damping.

Another unique consequence of transverse free-streaming waves is that they propagate freely, experiencing no cyclotron damping. This may be seen as follows. Consider a beam of particles with velocity v_z that have established a free-streaming wave with $k = \omega_1 - \omega_{ce}/v_z$ as in (5.5). Then a test particle with velocity V in the z direction sees a Doppler-shifted frequency $\tilde{\omega}$ given by

$$\begin{aligned} \tilde{\omega} &= \omega_1 - kV = \omega_1 - \left(\frac{\omega_1 - \omega_{ce}}{v_z}\right) V \\ &= \omega_1\left(1 - \frac{V}{v_z}\right) + \omega_{ce}\left(\frac{V}{v_z}\right) \end{aligned} \tag{5.9}$$

We see from this result that $\tilde{\omega} = \omega_{ce}$ only if $V = v_z$, which means that the only particles that could cyclotron damp the wave are the very same particles that comprise the wave. Thus there is no cyclotron damping effect. It follows that when many free-streaming waves are created, each with a different v_z, they will each propagate freely, not being damped via absorption energy by particles in the other waves.

5.2 Physical picture of the free-streaming term in (2.85).

Referring back to (2.76) we see that the saddle point free-streaming

contribution to $\underline{J}_1(z,t)$ in (2.85) is just the result of a superposition of many free-streaming waves, each represented by $\exp\left(i\left[(\omega_1-\omega_{ce}/v_z)z-\omega_1 t\right]\right)$ and weighted by the factor $f_o(v_z)dv_z$. The apparent strong damping of the saddle-point contribution is due to phase mixing; all of the free-streaming waves created actually continue to propagate downstream (unless destroyed by collisions) but the sum of their $\underline{J}_\perp$'s (due to the different wavelengths and phases involved) quickly adds to zero.

Explanation of why the free-streaming term in (2.85) has an accompanying pole contribution for $\omega_1 < 0$ or $\omega_1 > \omega_{ce}$ but not for $0 < \omega_1 < \omega_{ce}$.

In (2.76) we note the presence of the dielectric function $\varepsilon_{T_\alpha}[(\omega_1-\omega_{ce}/v_z),\omega_1]$ which represents the collective effects of the plasma. We find that if some free-streaming wave has a v_z(real) such that $\omega_1-\omega_{ce}/v_z$ (real) is nearly equal to the k_1 (complex) of an allowed collective mode [i.e., $\varepsilon_{T_\alpha}(k_1,\omega_1) = 0$] then that collective mode may be excited according to the following considerations. We consider $z > 0$ as above, for which all free-streaming waves have $v_z > 0$. Then in evaluating (2.76) by the saddle-point method, we note that the v_z contour is deformed to that half of the v_z plane wherein $\exp[i(\omega_1-\omega_{ce}/v_z)z]$ represents a damped wave. Accordingly a collective mode will be excited, and a pole will result [from the root of $\varepsilon_{T_\alpha}\left((\omega_1-\omega_{ce}/v_z),\omega_1\right) = 0$ in the v_z plane] only if the k_1 of the collective mode represents a damped wave also.

For $\omega_1 > \omega_{ce}$ all free-streaming waves have positive phase velocities. In addition, the roots of $\varepsilon_{T_+}(k_1,\omega_1) = 0$ that have Re $k_1/\omega_1 > 0$

also have $\mathrm{Im}\, k_1 > 0$ (corresponding to damped waves for $z > 0$). Thus it is not surprising that when the contour in the v_z plane is deformed we pick up a residue contribution (see Fig. 5d).

For $\omega_1 < 0$ a similar result occurs (see Fig. 5b).

For $0 < \omega_1 < \omega_{ce}$ all free-streaming waves have negative phase velocities. But the roots of $\varepsilon_{\Gamma_-}(k_1,\omega_1) = 0$ that have $\mathrm{Re}\, k_1/\omega_1 < 0$ also have $\mathrm{Im}\, k_1 < 0$ (corresponding to growing waves for $z > 0$), so in effect there is no collective mode that has the characteristics of a damped free-streaming wave. Thus it is not surprising that when the contour in the v_z plane is deformed (for this case), the pole is on the "wrong" side of the contour and hence there is no residue contribution (see Fig. 5c).

Explanation of why the free-streaming term in (2.85) diverges at $z = 0$ and how this divergence can be removed.

Lastly, in (2.76) we note the presence of the factor $1/v_z$. This factor is proportional to the amount of time a particle spends traversing the excitation region, as may be noted from (5.3). It is this factor which causes the divergence of the free-streaming term at $z = 0$. Physically, this divergence may now be explained as follows.

Consider an excitation like (5.2) but which, in place of the z dependence $E_1(z) = \Phi_1\delta(z)$ has $E_1(z) = \Phi_1/\Delta$ for $-\Delta/2 \leq z \leq \Delta/2$ and is zero elsewhere (then the δ-function character is retrieved in the limit $\Delta \to 0$). Now if the time a particle (with velocity v_z) spends in the excitation region ($-\Delta/2 \leq z \leq \Delta/2$) is much smaller than one period of the excitation, i.e., if

$$\frac{\Delta}{v_z} \ll \frac{2\pi}{\omega_1} \tag{5.10}$$

then the excitation field will not have enough time to change direction as the particle passes. Consequently the particle will receive a net impulse in one (transverse) direction as a result of passing through the excitation region. As long as (5.10) holds, the smaller v_z becomes, the larger the impulse the particle receives. In the limit of an infinitesimal but non-zero Δ we find the $v_z \simeq 0$ particles receive a huge impulse as they pass $z = 0$, and accordingly the total response [as given by the free-streaming term in (2.85)] diverges at $z = 0$.

On the other hand, if Δ is really finite, then from (5.10) we conclude that the $v_z \simeq 0$ particles see a perturbing force which is spread out over the excitation region and which rotates at frequency ω_1. Accordingly the $v_z \simeq 0$ particles do not acquire a huge impulsive change in their $\underline{v}_\perp$'s with the result that at $z = 0$ the total response no longer diverges. Thus a finite-width excitation ($\Delta \neq 0$) removes the divergence. (Two examples of finite-width excitations will be considered shortly.)

It should be clear from this discussion that if collisions significantly affect the $v_z \simeq 0$ particles (as Fokker-Planck collisions do, but simple Krook model collisions do not) then the divergence of the free-streaming term in (2.85) at $z = 0$ would also be removed (even for $\Delta \to 0$).

6. Effects of Collisions on (2.85)

The Krook Model.

In the above we have neglected collisions. Now we wish to determine for what values of the temperature T_e and density n_e collisional effects are significant. Specifically we want to know when collisional damping dominates and when cyclotron damping dominates. To this end we may use the Krook, Bhatnager, Gross model for the collision term in the Landau-Boltzman equation. Then the Vlasov equation (2.1) is to be replaced by

$$\frac{\partial f}{\partial t} + \underline{v}\cdot\frac{\partial f}{\partial \underline{x}} + \frac{q}{m}\left[\underline{E}_{TOTAL} + \frac{1}{c}\underline{v}\times\underline{B}_{TOTAL}\right]\cdot\frac{\partial f}{\partial \underline{v}} = \left(\frac{\delta f}{\delta t}\right)_{COLL} \tag{6.1}$$

$$\left(\frac{\delta f}{\delta t}\right)_{COLL} = -\nu\left(f - f_o\right)$$

where ν is an effective collision frequency. An appropriate choice for ν is

$$\nu = \nu_{ee} + \nu_{ei} + \nu_{en} \tag{6.2}$$

where ν_{ee}, ν_{ei}, ν_{en} represent effective collision frequencies for electron-electron, electron-ion and electron-neutral collisions, respectively.

First consider ν_{en}. An extensive accumulation of experimental data concerning ν_{en} is presented by S. Brown.[22] From these data we conclude that for our choice of parameters (T_e = 0.2 eV, neutral gas mainly N_2, neutral gas pressure $p_o \lesssim 10^{-4}$ mm: these being typical

values for the UCLA Q machine), ν_{en} may be neglected in the following.

Now consider ν_{ee} and ν_{ei}. In the literature there exists some confusion as to what ν_{ee}, ν_{ei} should represent and whether ν_{ee} or ν_{ei} or both should be used in (6.2). Often ν in (6.1) is called an effective collision frequency for momentum transfer without any explicit indication of whether the momentum transfer occurs in electron-electron or electron-ion collisions. In other cases it is explicitly stated that ν represents a self-collision time (electron-electron collisions only).[12] In previous work on the collisional damping of transverse plasma waves, Crawford et al.[13] claim the dominant collision process is electron-ion collisions and hence use $\nu = \nu_{ei}$. Sachs[11] presents a collision term (developed by Liboff) which for $T_e = T_i$ and no net drift velocity between species reduces to $\nu = \nu_{ee}$ where ν_{ee} is Spitzer's[23] self-collision frequency. To further confound the situation we note that $\nu_{ee} \simeq \nu_{ei}$ according to Kaufman et al.[24] Perhaps the easiest (but least satisfying) solution is that of Platzman and Buchsbaum[12] who avoided the issue altogether by simply choosing a number for ν. Tanenbaum concludes that the Krook collision model is "really applicable only to cases where self-collisions are of predominant importance."[25]

Since our interest lies in determining only when collisions are significant we have, without resolving the above conflict, chosen to use $\nu = \nu_{ee}$ (self-collision frequency) with the understanding that this ν may differ from the true effective collision frequency by at most a factor of 2. Thus we shall use[24,25]

$$\nu = \nu_{ee} \approx 2.9 \cdot 10^{-6} \frac{n_e}{T_e^{3/2}} \ln_{10} \Lambda$$

$$\Lambda = 1.54 \cdot 10^{10} \frac{T_e^{3/2}}{n_e^{1/2}} \tag{6.3}$$

where n_e is the electron density in cm^{-3} and T_e is the electron temperature in eV.

Then reviewing the derivation of (2.85) when collisions are included by (6.1) we find that (2.85) should be replaced by

$$\underline{J}_1(z,t) =$$

$$\mathrm{Re}\left[\hat{e}_+ \frac{\omega_{pe}^2 \Phi_1}{a}\left\{\frac{\omega_{pe}^2 \omega_1 e^{-3\left[\frac{(\omega_1+i\nu-\omega_{ce})\alpha z}{2a}\right]^{2/3}\left[\frac{1}{2}-i\alpha\frac{\sqrt{3}}{2}\right]-i\omega_1 t}}{\sqrt{3}\left(k_{se}^2c^2-\omega_1^2\right)(\omega_1+i\nu-\omega_{ce})\,\epsilon_{T_+}(k_{se},\omega_1)\,\epsilon_{T_-}(k_{se},\omega_1)} Z\left(\frac{\omega_1+i\nu-\omega_{ce}}{k_{se}a}\right)\right.\right. \tag{6.4}$$

$$+\frac{e^{-3\left[\frac{(\omega_1+i\nu-\omega_{ce})\alpha z}{2a}\right]^{2/3}\left[\frac{1}{2}-i\alpha\frac{\sqrt{3}}{2}\right]-i\omega_1 t}}{\sqrt{3}\,\frac{v_s}{a}\,\epsilon_{T_\alpha}\left(\frac{\omega_1+i\nu-\omega_{ce}}{v_s},\omega_1\right)}$$

$$\left.\left.+\frac{e^{ik_1 z-i\omega_1 t}}{k_1\left.\frac{\partial \epsilon_{T_+}(k,\omega_1)}{\partial k}\right|_{k=k_1}}\left[Z_+\left(\frac{\omega_1+i\nu-\omega_{ce}}{k_1 a}\right)+2\sqrt{\pi}\,i\,S(\omega_1)\,e^{-\left(\frac{\omega_1+i\nu-\omega_{ce}}{k_1 a}\right)^2}\right]\right\}\right]$$

for $z > 0$ and where ν is given by (6.3). Now

$$k_{se} = \left[\frac{2\{(\omega_1 + i\nu - \omega_{ce})\alpha\}^2}{2a^2}\right]^{1/3} e^{i\left(\frac{\pi}{2} - \alpha\frac{\pi}{3}\right)}$$

$$\frac{v_s}{a} = \left[\frac{(\omega_1 + i\nu - \omega_{ce})\alpha 2}{2a}\right]^{1/3} e^{i\alpha\frac{\pi}{6}} \qquad (6.5)$$

and

$$\epsilon_{T_\pm}(k,\omega) = 1 - \frac{\omega\omega_{pe}^2}{(k^2c^2 - \omega^2)ka} Z_\pm\left(\frac{\omega + i\nu - \omega_{ce}}{ka}\right) \qquad (6.6)$$

whereas α and $S(\omega_1)$ are as given earlier.

The main effect of collisions in the transverse excitation response given by (6.4) will be in the pole term; the cyclotron-damped root of $\epsilon_{T_+}(k,\omega_1) = 0$ will be altered due to the presence of collisions. The branch-cut and free-streaming terms in (6.4) will also be affected but we defer discussion of this until later. For now we consider the effects of collisions on the cyclotron-damped root of $\epsilon_{T_+}(k,\omega) = 0$.

Cyclotron damping vs. collisional damping.

The transverse dispersion relation derived earlier for the collisionless case, as given in (2.44), is (neglecting ions)

$$\epsilon_{T_+}(k,\omega) = 1 - \frac{\omega\omega_{pe}^2}{(k^2c^2 - \omega^2)ka} Z_+\left(\frac{\omega + i\nu - \omega_{ce}}{ka}\right) = 0 \qquad (6.7)$$

When collisions are included using (6.1), the transverse dispersion relation is

$$\epsilon_{T_+}(k,\omega) = 1 - \frac{\omega\omega_{pe}^2}{(k^2c^2-\omega^2)ka} Z_+\left(\frac{\omega+i\nu-\omega_{ce}}{ka}\right) = 0 \qquad (6.8)$$

where ν is given by (6.3). For $|\zeta_\nu| \equiv |(\omega+i\nu-\omega_{ce})/ka| \gtrsim 3$, we may use the first term of the asymptotic expansion of the Z function [$Z(\zeta) = -1/\zeta$] in (6.8) to obtain

$$\epsilon_{T_+}(k,\omega) = 1 + \frac{\omega\omega_{pe}^2}{(k^2c^2-\omega^2)(\omega+i\nu-\omega_{ce})} = 0 \qquad (6.9)$$

which is simply the cold plasma dispersion relation with collisions included.

To estimate where cyclotron damping is comparable to collisional damping, Crawford et al.[13] computed the locus of points where Im k of the root of the hot plasma dispersion relation without collisions (6.7) equals Im k of the root of the cold plasma dispersion relation with collisions (6.9). We have numerically performed the same calculation for two sets of parameters with the results shown in Fig. 10; curve 1 corresponds to Crawford's parameters (and his curves), whereas curve 2 was computed for our parameters. These loci show that for a given ω, as T_e increases, collisional damping decreases and cyclotron damping increases. However, these loci contain a major flaw and that is the following. Use of the cold plasma dispersion relation (6.7) as an approximation for the hot plasma dispersion relation (6.9) is justified only for $|\zeta_\nu| \gtrsim 3$. But along the hatched portions of the curves in Fig. 10, $|\zeta_\nu| \lesssim 2$ so (6.9) should not be used. Indeed, as

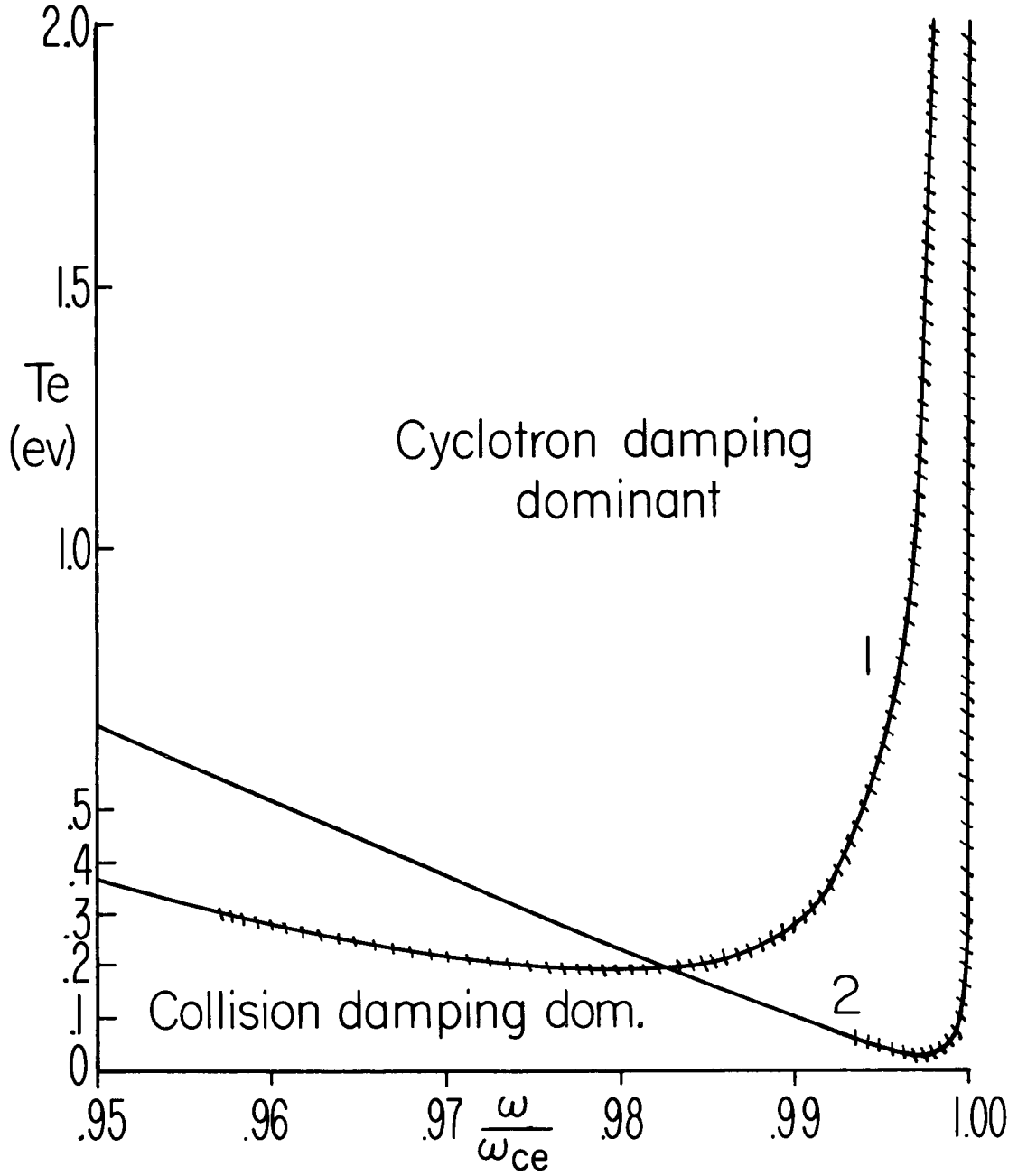

FIGURE 10. LOCUS OF POINTS WHERE HOT PLASMA CYCLOTRON DAMPING EQUALS COLD PLASMA COLLISIONAL DAMPING.

Locus of points, following Crawford et. al.[13], where Im k of the least-damped root of (6.7) equals Im k of the root of (6.9). CURVE 1: f_{ce}=2.25 GHz, ω_{pe}/ω_{ce}=4 (n_e=10^{12} cm^{-3}).
CURVE 2: f_{ce}=2.25 GHz, ω_{pe}/ω_{ce}=.4 (n_e=10^{10} cm^{-3}).
(Curve 1 corresponds to Crawford's parameters.)
These loci are meaningless however for those portions shown hatched (see text).

we shall now show, the true loci never turn upward (as $\omega/\omega_{ce} \to 1$) as the loci in Fig. 10 do.

To correctly compare cyclotron damping with collisional damping, it is apparent we should compare the roots of (6.7) with the roots of (6.8). Let

$$L = \text{Im } k \quad \text{of the root of (6.7)}$$

$$M = \text{Im } k \quad \text{of the root of (6.8)}$$

then L represents the effects of cyclotron damping whereas M represents the effects of cyclotron damping plus collisional damping. Thus roughly, L/M represents the fraction of the total damping due to cyclotron damping. Accordingly we have numerically calculated the locus of points where cyclotron damping accounts for 80%, 50%, 20% of the total damping (L/M = 0.8, 0.5, 0.2) with the results displayed in Fig. 11 as curves A, B, C, respectively. The curves of Fig. 11 were computed for the same parameters used to compute curve 2 in Fig. 10; in particular note that curve B in Fig. 11 does not turn upward as curve 2 in Fig. 10 does. Also note that to measure cyclotron damping we must be above the shaded region in Fig. 11 for collisional effects to be negligible. For $T_e = 0.2$ eV this means we should consider only frequencies in the range $0.988 \lesssim \omega/\omega_{ce} \leq 1$.

In the shaded region for $T_e \gtrsim 0.1$ eV in Fig. 11, the total damping is very small. Thus one should not interpret curve A of Fig. 11 to mean that collisional damping is becoming as large as cyclotron damping, but rather that cyclotron damping is becoming as small as collisional damping. This conclusion is apparent when one considers

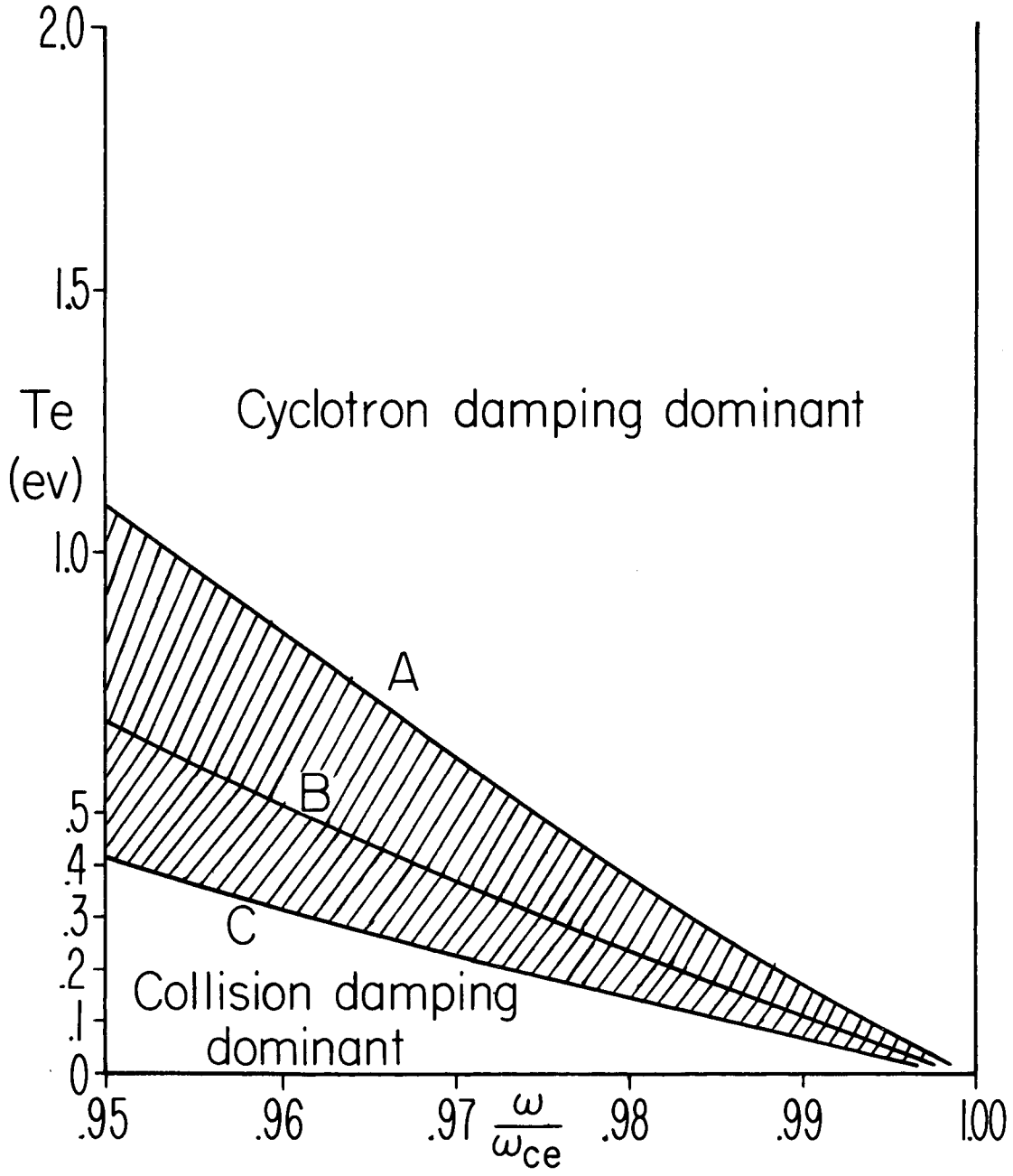

FIGURE 11. CYCLOTRON DAMPING AND COLLISIONAL DAMPING COMPARED CORRECTLY.

A. 20% collisional damping and 80% cyclotron damping.
B. 50% collisional damping and 50% cyclotron damping.
C. 80% collisional damping and 20% cyclotron damping.

(f_{ce}=2.25 GHz, ω_{pe}/ω_{ce}=.4 [$n_e=10^{10}$ cm^{-3}])

actual values of Im k of the roots of (6.7), (6.8) such as those displayed in Fig. 12 for $T_e = 0.204$ eV. Note that in Fig. 12 collisional damping is significant only when cyclotron damping is very small. Also note that a typical cyclotron damping length (for negligible collisional damping) is (for $\omega_1/\omega_{ce} = 0.99$)

$$\frac{1}{\mathrm{Im}\, k} = \frac{\frac{c}{\omega_{ce}}}{\frac{\mathrm{Im}\, kc}{\omega_{ce}}} \approx \frac{2\ \mathrm{cm.}}{.2} = 10\ \mathrm{cm.}$$

and damping lengths of this order should be easily observable experimentally. Thus for the parameters of Fig. 11 ($n_e = 10^{10}$ cm^{-3}, $\omega_{pe}/\omega_{ce} = 0.4$), experimentally, measurement of electron cyclotron damping rates would be feasible only for $T_e \gtrsim 0.1$ eV.

As the density n_e increases, collisional effects rapdily become more significant since $\nu \sim n_e$. For example consider values of Im k for $n_e = 10^{12}$ cm^{-3} as given in Fig. 13. We see that for $0.988 \leq \omega_1/\omega_{ce} \leq 1$,

$$\frac{\mathrm{Im}\ k_{\text{no collisions}}}{\mathrm{Im}\ k_{\text{with collisions}}} \geq 0.8 ,$$

but that at $\omega_1/\omega_{ce} = 0.998$, Im $kc/\omega_{ce} \approx 8$ which implies a damping length of $1/\mathrm{Im}\ k \approx 0.27$ cm, which is too small for accurate experimental measurement. Thus for "high" densities ($n_e > 10^{10}$ cm^{-3}) we must go to "high" temperatures ($T_e >> 0.2$ eV) if we wish to obtain a range of frequencies over which the cyclotron damping length is unhampered by collisional damping and also large enough to be easily measurable experimentally.

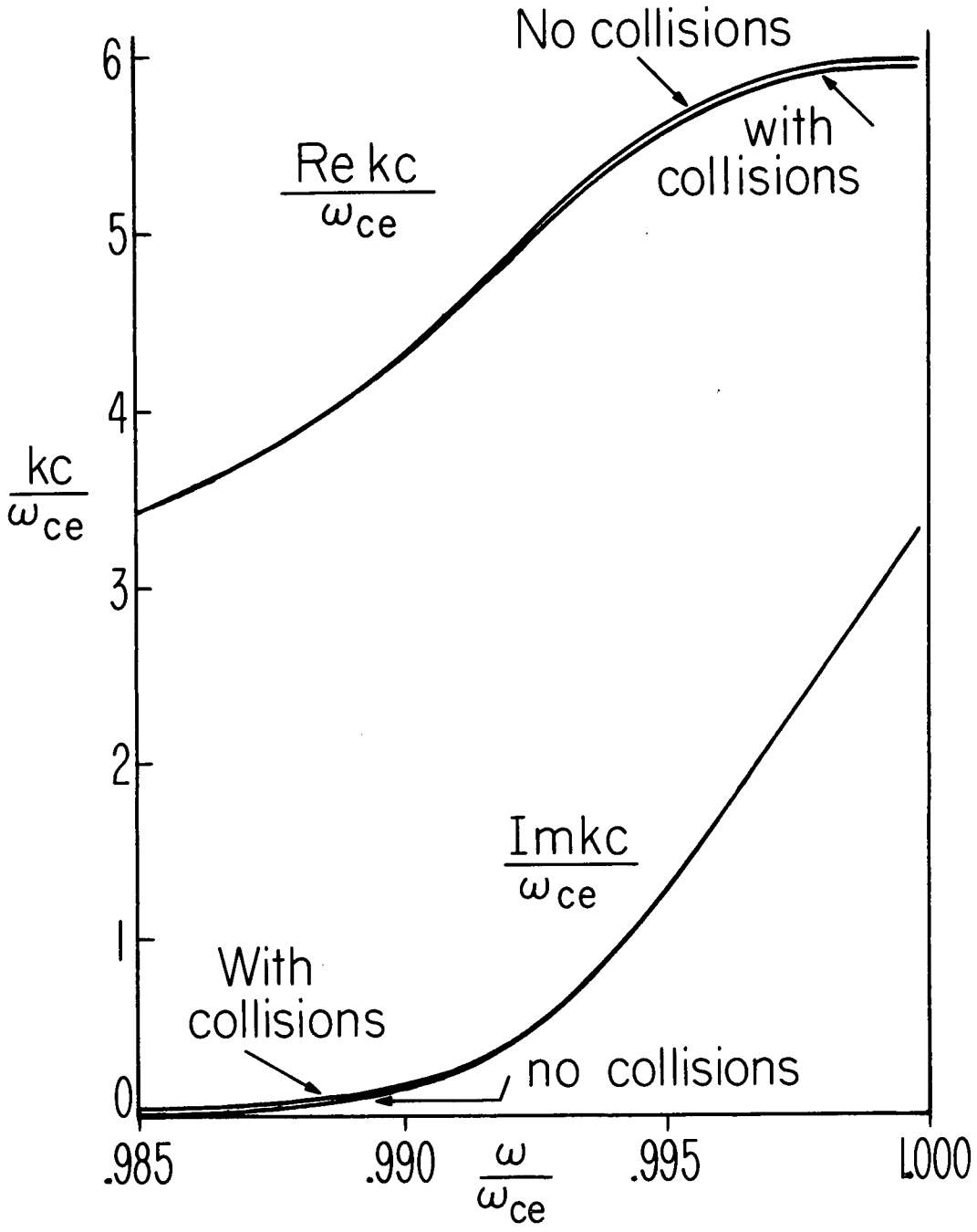

FIGURE 12. EFFECTS OF COLLISIONS ON THE CYCLOTRON-DAMPED ROOT.

f_{ce}=2.25 GHz, ω_{pe}/ω_{ce}=.4 (n_e=10^{10} cm^{-3})

c/a = 1120 (T_e=.204 ev.)

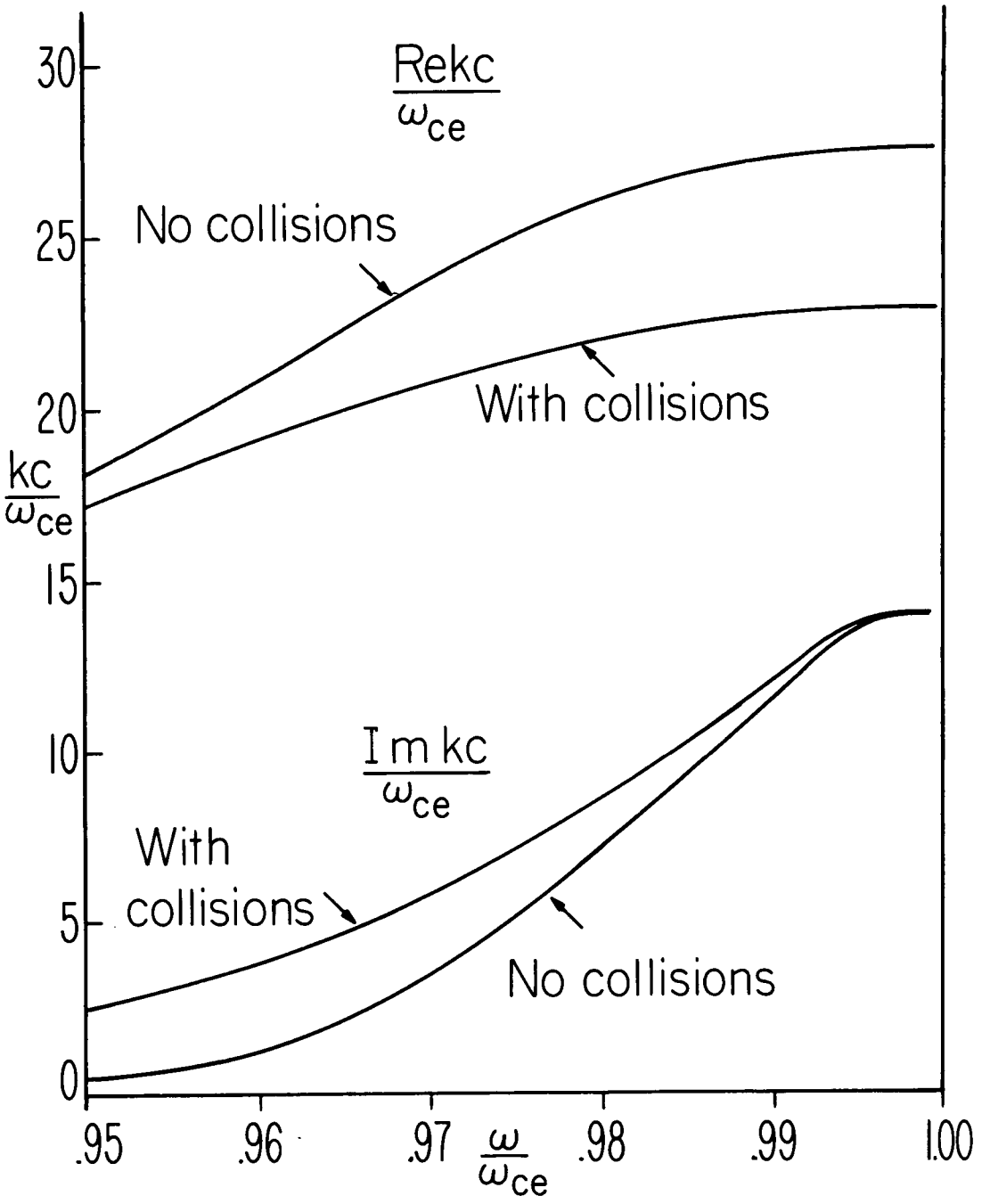

FIGURE 13. EFFECTS OF COLLISIONS ON THE CYCLOTRON-DAMPED ROOT.

f_{ce}=2.25 GHz, ω_{pe}/ω_{ce}=4 ($n_e=10^{12}$ cm^{-3})

c/a =1120 (T_e=.204 ev.)

Effects of collisions on the branch-cut and free-streaming terms.

In the regions where cyclotron damping rate measurements are feasible, the collisional damping rate is small; i.e., from the above considerations we find

$$\frac{\nu}{\omega_{ce}} \frac{c}{a} \lesssim 1 \tag{6.10}$$

Accordingly, in these regions, the free-streaming perturbations will eventually damp away by collisional damping (these perturbations are not affected by cyclotron damping) but phase mixing of these perturbations [as given by the free-streaming term in (2.85)] will occur long before the individual perturbations themselves are destroyed by collisions. Explicitly, when (6.10) holds, the free-streaming term in (6.4) differs only slightly from the corresponding term in (2.85); the analysis of Section 4 holds and the free-streaming term still diverges at $z = 0$. (As mentioned earlier in Section 5, Krook model collisions do not remove this divergence, whereas Fokker-Planck collisions do, as will be shown in the echo case of Part II.)

If (6.10) does not hold, i.e., if

$$\frac{\nu}{\omega_{ce}} \frac{c}{a} \gg 1 \tag{6.11}$$

then the analysis of Section 4 does not hold because the parameter Γ which is now

$$\Gamma = \left| \frac{\omega_1}{\omega_{ce}} + \frac{i\nu}{\omega_{ce}} - 1 \right| \frac{c}{a} \tag{6.12}$$

is never $\lesssim 1$ (even for $\omega_1 = \omega_{ce}$). Thus the shielding effect described

earlier for $\Gamma \lesssim 1$ never occurs in this case. On the other hand, the characteristic length λ_o which is now

$$\lambda_o = \frac{a}{|\omega_1 + i\nu - \omega_{ce}|} \tag{6.13}$$

no longer approaches infinity as ω_1 approaches ω_{ce}, and the exponential factor in the free-streaming term still damps this term away in a distance of a few λ_o.

Similar remarks apply to the branch-cut term. If (6.10) holds then the branch-cut term in (6.4) differs only slightly from the corresponding term in (2.85) and the analysis of Section 4 remains valid. If (6.11) nolds then the branch-cut term (like the free-streaming term) exhibits no shielding effect as ω_1 approaches ω_{ce} but it still damps away in a distance of a few λ_o where λ_o is given by (6.13).

7. Effects of a Finite-Width Excitation Mechanism on (2.85)

Up to now we have used the shape factor

$$E_1(z) = \phi_1 \delta(z) \tag{7.1}$$

in the transverse external exciting field

$$\underline{E}_{ext}(z,t) = E_1(z)\left\{\hat{e}_x \cos\omega_1 t + \hat{e}_y \sin\omega_1 t\right\} \tag{7.2}$$

(This form of excitation for transverse waves is the mathematical equivalent of the dipole-grid excitation mechanism for longitudinal waves.) The choice of a delta function in (7.1) is useful for computational purposes but unrealistic in that it is probably experimentally unattainable. Indeed it is difficult to conceive of a mechanism (or even a limiting case thereof) that would produce a field like (7.1), (7.2). On the other hand, these are conceivable mechanisms that would produce a field like (7.2) provided $E_1(z)$ had a finite z dependence. In this section we shall examine the effects of a square-shaped $E_1(z)$ and a Gaussian-shaped $E_1(z)$.

First note that in Section 2 we have already carried the general calculation for arbitrary $E_1(z)$ up to (2.76). Thus we only have to alter the derivation from (2.76) to the final result (2.85). Just glancing at (2.76), (2.78), (2.85) indicates that inclusion of a new $E_1(z)$ will simply produce new amplitude factors for the branch-cut and dielectric-pole terms while the free-streaming term will be affected in a more significant way.

Square-shaped $E_1(z)$.

Consider the square-shaped $E_1(z)$

$$E_1(z) = \frac{\Phi_1}{\Delta} \quad \text{for} \quad -\frac{\Delta}{2} \le z \le \frac{\Delta}{2}$$
$$0 \quad \text{for} \quad z < -\frac{\Delta}{2}\ ,\ z > \frac{\Delta}{2} \tag{7.3}$$

($\Delta > 0$) for which

$$E_1(k) = \frac{\sin(k\Delta)}{k\Delta} \tag{7.4}$$

Using (7.4), the pole term in (2.85) acquires an additional amplitude factor of $\sin(k_1\Delta)/k_1\Delta$. If $\Delta \ll \lambda_1$, $(\lambda_1 = 2\pi/k_1)$ then $E_1(k_1) \approx \Phi_1$ and the pole term is essentially unaltered. However, as Δ increases, the factor $\sin(k_1\Delta)/k_1\Delta$ oscillates and its magnitude decreases. If $k_1\Delta = n\pi$ $(n = 1,2,\ldots)$, i.e., if $\Delta = n(\lambda_1/2)$ then $E_1(k_1) = 0$ identically. Therefore if we want to avoid these zeros and maximize $E_1(k_1)$ we should have

$$\Delta \ll \frac{\lambda_1}{2} \tag{7.5}$$

Since λ_1 is typically a few centimeters, condition (7.5) should be easily attainable.

Both the branch-cut and free-streaming terms in (2.85) have (roughly) the characteristic wavenumber $k_o = 2\pi/\lambda_o$ $(\lambda_o = a/|\omega_1 - \omega_{ce}|)$, so from the above considerations we conclude that both of these terms will acquire additional amplitude factors of $\sin(k_o\Delta)/k_o\Delta$. Thus if

$$\Delta \ll \frac{\lambda_o}{2} \tag{7.6}$$

we shall have $E_1(k_o) \simeq \Phi_1$ and the amplitudes of both the branch-cut and free-streaming terms will be maximized.

In general, condition (7.6) is harder to attain than (7.5) because in general $\lambda_o << \lambda_1$. However, in studying cyclotron damping our interest lies in the pole term and in fact it would be to our advantage to have the branch-cut and free-streaming terms smaller than as given by (2.85). In that case it would be useful to have Δ such that

$$0 < \frac{\lambda_o}{2} << \Delta << \frac{\lambda_1}{2} \tag{7.7}$$

because this would help diminish the size of the "unwanted" branch-cut and free-streaming terms.

If we are explicitly concerned with the detailed behavior of the free-streaming term we must evaluate the free-streaming term integral in (2.76) more carefully, taking into full account the explicit v_z dependence of $E_1[(\omega_1-\omega_{ce})/v_z]$. Physically the integral in (2.76) is more complicated now because the particle trajectories are altered continuously over the region $-\frac{\Delta}{2} \leq z \leq \frac{\Delta}{2}$ rather than abruptly at $z = 0$. Using (7.4) for $E_1(k)$ the free-streaming term integral in (2.76) becomes

$$\frac{1}{\sqrt{\pi}a}\int_0^\infty \frac{\alpha v_z e^{-\frac{v_z^2}{a^2}}\left\{ e^{i\left(\frac{\omega_1-\omega_{ce}}{v_z}\right)(z+\Delta)} - e^{i\left(\frac{\omega_1-\omega_{ce}}{v_z}\right)(z-\Delta)}\right\}}{2i(\omega_1-\omega_{ce})\Delta\, \epsilon_{T\alpha}\left(\frac{\omega_1-\omega_{ce}}{v_z}, \omega_1\right)} \tag{7.8}$$

Evaluating (7.8) by the method of steepest descent we find the free-streaming term contained within the large brackets $\{\ \}$ in (2.85) should

be replaced by

$$\frac{e^{-i\omega_1 t}}{2\sqrt{3}i\left[\frac{(\omega_1-\omega_{ce})\Delta}{a}\right]}\left\{\frac{e^{-3\left[\frac{(\omega_1-\omega_{ce})\alpha(z+\Delta)}{2a}\right]^{2/3}\left[\frac{1}{2}+i\alpha\frac{\sqrt{3}}{2}\right]}}{\epsilon_{T_\alpha}\left(\frac{\omega_1-\omega_{ce}}{v_{s_+}},\omega_1\right)}\right.$$

$$\left.-\frac{e^{-3\left[\frac{(\omega_1-\omega_{ce})\alpha(z-\Delta)}{2a}\right]^{2/3}\left[\frac{1}{2}+i\alpha\frac{\sqrt{3}}{2}\right]}}{\epsilon_{T_\alpha}\left(\frac{\omega_1-\omega_{ce}}{v_{s_-}},\omega_1\right)}\right\} \tag{7.9}$$

where

$$\frac{v_{s\pm}}{a}=\left[\frac{(\omega_1-\omega_{ce})\alpha(z\pm\Delta)}{2a}\right]^{\frac{1}{3}}e^{-i\alpha\frac{\pi}{3}} \tag{7.10}$$

When $\Delta \to 0$ (7.9) reduces to the free-streaming term in (2.85). But for $\Delta \neq 0$ note that (7.7) does <u>not</u> diverge at $z = 0$ (since when $v_{s_\pm} \to 0$ we have $\epsilon_{T_\alpha}[(\omega_1-\omega_{ce}/v_{s_\pm}),\omega_1] \approx 1$. The $1/v_z$ factor in (2.76) which caused the $z = 0$ divergence earlier, was effectively removed in (7.8). Thus, as stated earlier, a finite-width excitation mechanism removes the $z = 0$ divergence of the free-streaming term in (2.85).

<u>Gaussian-shaped $E_1(z)$.</u>

In place of (7.3) we now consider a Gaussian-shaped $E_1(z)$

$$E_1(z)=\Phi_1\frac{e^{-\frac{z^2}{\Delta^2}}}{\sqrt{\pi}\,\Delta} \tag{7.11}$$

($\Delta > 0$) for which

$$E_1(k) = \Phi_1 \, e^{-\frac{k^2\Delta^2}{4}} \tag{7.12}$$

The field described by (7.11) is more realistic than that of (7.3) in that any excitation mechanism will be accompanied by a shielding sheath with an exponential dependence like that of (7.11). The consequences of (7.11) are very similar to the consequences of (7.3).

Thus when $E_1(z)$ is given by (7.11) we find the pole term in (2.85) acquires an additional amplitude factor of $\exp[-k_1^2\Delta^2/4]$ which is ≈ 1 for $k_1^2\Delta^2 \ll 4$, i.e., for

$$\Delta \ll \frac{2}{k_1} \approx \lambda_1 \tag{7.13}$$

Similarly the branch-cut and free-streaming terms in (2.85) each acquire (roughly) an additional amplitude factor of $\exp[-k_o^2\Delta^2/4]$ which is ≈ 1 for

$$\Delta \ll \frac{2}{|k_o|} \approx \lambda_o \tag{7.14}$$

Thus as earlier, if

$$0 < \lambda_o \ll \Delta \ll \lambda_1 \tag{7.15}$$

the sizes of the branch-cut and free-streaming terms will be diminished from those in (2.85) whereas the pole term in (2.85) will remain essentially unaltered.

Evaluating the free-streaming term more carefully, we find that the free-streaming term integral in (2.76) should be replaced by

$$\frac{1}{\sqrt{\pi}\,a}\int_0^\infty \frac{dv_z\, e^{-\frac{\Delta^2(\omega_1-\omega_{ce})^2}{4v_z^2}}\, e^{-\frac{v_z^2}{a^2}}\, e^{i\left(\frac{\omega_1-\omega_{ce}}{v_z}\right)z}}{v_z\, \epsilon_{T\alpha}\left(\frac{\omega_1-\omega_{ce}}{v_z},\omega_1\right)} \tag{7.16}$$

[Note that this integral, like (7.8), does not diverge at $z = 0$.] We shall evaluate (7.16) by the method of steepest descent for the two limits $|z| >> \Delta$ and $|z| << \Delta$ (the latter limit being of interest since from it we can obtain the size of the free-streaming term at $z = 0$).

(i) $\underline{|z| >> \Delta.}$ In this region we may consider the Δ^2 exponential factor in (7.16) as part of the slowly-varying portion of the integrand. Then evaluating (7.16) shows that the free-streaming term in (2.85) simply acquires an additional amplitude factor of $\exp\left(-[\Delta^2(\omega_1-\omega_{ce})^2]/[4v_s^2]\right)$ where v_s remains as given in (2.76).

(ii) $\underline{|z| << \Delta.}$ In this region we may consider the factor $\exp[i(\omega_1-\omega_{ce}/v_z)z]$ in (7.16) as part of the slowly-varying portion of the integrand. Then the free-streaming term contained with the large brackets $\{\ \}$ in (2.85) should be replaced by

$$\frac{e^{-\frac{\Delta(\omega_1-\omega_{ce})\alpha}{a}}\, e^{i\left(\frac{\omega_1-\omega_{ce}}{v_s}\right)z-i\omega_1 t}}{\sqrt{\frac{\pi}{2}}\,\frac{v_s}{a}\,\epsilon_{T\alpha}\left(\frac{\omega_1-\omega_{ce}}{v_s},\omega_1\right)} \tag{7.17}$$

where now

$$\frac{V_s}{a} = \sqrt{\frac{\Delta(\omega_i - \omega_{ce})\alpha}{2a}} \tag{7.18}$$

Expression (7.17) gives the amplitude of the free-streaming term at $z = 0$.

8. Conclusions

We have examined the linearized response of a Vlasov plasma to the steady-state excitation of transverse EM waves by an idealized delta-function excitation mechanism, (1.1) - (1.2). We summarize the main conclusions:

(1) The plasma response is given by (2.85) which is valid for any value of ω_1. (For use in the pole term, the roots of the transverse dispersion relation for real ω and complex k are discussed in Appendix C.)

(2) For cyclotron-damping measurements, the following points must be considered:

(a) The branch-cut and free-streaming terms in (2.85), in addition to the pole term, have significant amplitudes and penetration lengths (see Fig. 7).

(b) If $(\omega_{pe}^2/\omega_{ce}^2)(c/a) \gg 1$, then the branch-cut and free-streaming terms are shielded for $\Gamma = |(\omega_1/\omega_{ce}) - 1| \frac{c}{a} \lesssim 1$ and their penetration lengths go to zero as Γ goes to zero. If $(\omega_{pe}^2/\omega_{ce}^2)(c/a) \ll 1$, then no shielding effect occurs and both the branch-cut and free-streaming terms' penetration lengths go as $\lambda_o = a/|\omega_1-\omega_{ce}|$ which approaches infinity as Γ goes to zero.

(c) Use of only the "least-damped root" in the pole term was justified by showing that the remaining infinite number of roots of the transverse dispersion relation has a negligible effect except at distances very close to the place of excitation ($z = 0$).

(d) Collisional effects dominate the damping except when ω_1 is near ω_{ce} (see Fig. 11).

(e) For $\omega_1 \gtrsim \omega_{ce}$, the cyclotron-damped root is so heavily damped (see Appendix C) that it is probably not possible to measure it experimentally.

(f) A finite-width excitation mechanism removes the divergence at $z = 0$ of the free-streaming term, and selectively reduces the amplitude of the three terms in (2.85). Under special conditions [(7.7) or (7.15)] the branch-cut and free-streaming terms are reduced significantly while the pole term is left essentially unchanged.

From (d) and (e) we conclude that cyclotron-damping measurements should be performed in a narrow range of frequencies just below ω_{ce} (e.g., $0.998 \lesssim \omega_1/\omega_{ce} \lesssim 0.999$ for the parameters of Fig. 7). This range of frequencies can be deduced from graphs like Fig. 11. It was concluded that cyclotron damping measurements are barely feasible for $T_e = 0.2$ eV and $n_e = 10^{10}$ cm^{-3}. For higher densities ($n_e > 10^{10}$ cm^{-3}) one must go to much higher temperatures ($T_e \gg 0.2$ eV) because the Coulomb collision frequency, (6.3), goes as $\nu \sim n_e/T_e^{3/2}$.

(3) A special section on transverse free-streaming waves showed how these waves are created and explained many of their interesting properties (e.g., negative phase velocities for $0 < \omega_1 < \omega_{ce}$, absence of cyclotron damping, etc.). The free-streaming term in (2.85) was shown to be the result of the superposition of many such free-streaming waves, and explanations were given for some unusual properties of this

term (why there is no accompanying pole contribution for $0 < \omega_1 < \omega_{ce}$, why this term always diverges at $z = 0$, etc.). Since free-streaming waves are responsible for the production of echoes, all of the unique features of transverse free-streaming waves discussed above will be especially significant when considering transverse plasma wave echoes in Part II.

II. STEADY-STATE TRANSVERSE PLASMA WAVE ECHOES

1. Introduction and Physical Picture

The phenomenon of longitudinal plasma wave echoes, introduced by Gould and O'Neil[26] and subsequently observed experimentally,[27-29] may be described as follows. If in a hot collisionless plasma a wave with wavenumber k_1 is excited at some time which subsequently damps away; and if another wave with wavenumber k_2 is excited at a later time and it also damps away; then at a still later time an echo with wavenumber $|k_2-k_1|$ will appear and subsequently damp away: this is called a temporal echo process. The corresponding process for spatial echoes is also readily visualized: if an excitation at frequency ω_1 is made continuously at some point in a hot collisionless plasma and the response damps away in distance; and if further away another excitation at frequency ω_2 is made continuously whose response also damps away in distance; then still farther away an echo at frequency $|\omega_2-\omega_1|$ will appear and subsequently damp away in distance. In this work we focus our attention on spatial echoes since they are more readily experimentally attainable.

An echo results when the free-streaming perturbations produced by a first excitation are appropriately reordered by a second excitation. But since these perturbations are relatively sensitive to small angle Coulomb collisions, such collisions may destroy the formation of an echo. Alternatively though, the collision process can be investigated, as well as micro-turbulence, and also details of the particles' zero-order velocity distribution function by the appropriate use of echoes.[30]

Thus echoes may serve as an important diagnostic tool.

In this work the echo process described above for longitudinal plasma waves is generalized to the case of transverse plasma waves. This extension should greatly enlarge the potential importance of echoes as a diagnostic tool. Also we shall find transverse echoes offer a much richer variety of phenomenon to investigate than purely longitudinal echoes offer. In addition, a new use for echoes will be suggested and that is to excite instabilities in a well-controlled and localized manner.

We first present a physical picture of the echo process. We choose to have a transverse excitation with frequency ω_1 at $z = 0$ and a longitudinal excitation with frequency ω_2 at $z = L$ as shown in Fig. 1. Both excitations produce waves with vectors along an applied external magnetic field $\underline{B}_o = \hat{e}_z B_o$. Considering just those particles with cyclotron frequency Ω and velocity v_z, we see that the first excitation produces a free-streaming wave with wavehumber $[(\omega_1+\Omega)/v_z]$, as discussed in Section 5 of Part I. For $z \geq L$ the second excitation modulates the first's free-streaming wave to produce a wave with wavenumber $[(\omega_2+\omega_1+\Omega)/v_z]$. The net phase Φ of the wave for $z \geq L$ includes the phase for $0 \leq z \leq L$ and the phase for $z \geq L$, i.e.,

$$\Phi = \left(\frac{\omega_1+\Omega}{v_z}\right)L + \left(\frac{\omega_2+\omega_1+\Omega}{v_z}\right)(z-L)$$

$$= \left[(\omega_2+\omega_1+\Omega)z - \omega_2 L\right]\frac{1}{v_z} \qquad (1.1)$$

When we add the effects of many beams with different v_z's (to obtain the net current or electric field) we find that all their phases are

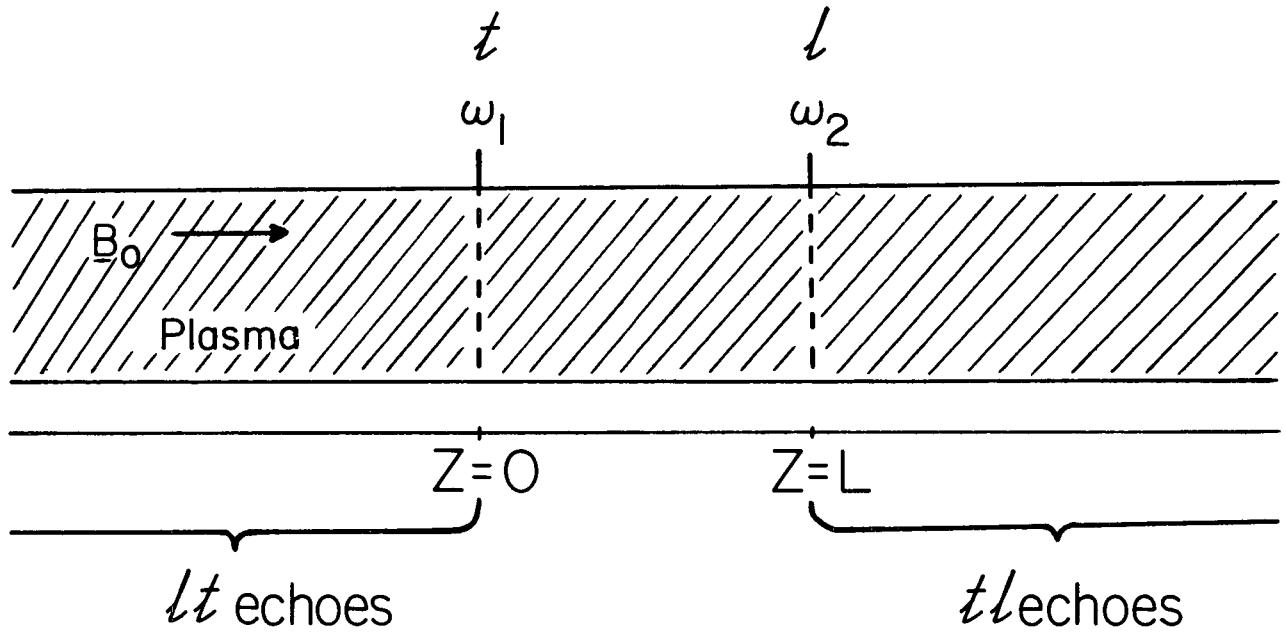

FIGURE 1. PRODUCTION OF TRANSVERSE PLASMA WAVE ECHOES FROM A TRANSVERSE (t) EXCITATION AND A SIMULTANEOUS LONGITUDINAL (l) EXCITATION.

different and therefore the net response phase mixes to zero everywhere except where

$$\left[(\omega_2 + \omega_1 + \Omega) z - \omega_2 L \right] = 0$$

i.e., at

$$z = z_0 \equiv \frac{\omega_2 L}{\omega_2 + \omega_1 + \Omega} \tag{1.2}$$

which defines the location of the echo peak.

The above physical picture is based on free-streaming particles that are non-interacting. If interactions are taken into account, then the possibility of exciting collective modes exists. The location of the echo peak remains unchanged (since it still depends only on the free-streaming terms) but the resultant echo shape may be appropriately enhanced. We shall study these effects via a full Maxwell-Vlasov equation analysis.

In the following we consider wave propagation exactly along the direction of an external magnetic field and we present a concise mathematical explanation of what type echo is produced, given the types of each of the two excitations (longitudinal or transverse). We find that a transverse echo is produced in lowest order only when one excitation is longitudinal and the other is transverse. For such excitations, or more specifically for

$$\underline{E}_{ext}(z,t) = E_1(z)\left[\hat{e}_x \cos \omega_1 t + \hat{e}_y \sin \omega_1 t\right] + E_2(z-L)\left[\hat{e}_z \cos \omega_2 t\right] \tag{1.3}$$

we then derive the second-order (nonlinear) echo response from the

Vlasov-Maxwell equations, up to an integral over the velocity variable, v_z.

We then discuss transverse echo characteristics, summarizing the results in Fig. 2. The final integral over v_z is evaluated by the method of steepest descent and numerical evaluation of the results for three specific cases are presented in Figs. 3-5.

Several important extensions are then considered: (1) effects of Fokker-Planck collisions and finite-width excitation mechanisms, (2) effects of temperature anisotropy ($T_\perp \neq T_z$), and (3) effects of propagation just off-axis ($k_\perp \neq 0$).

Lastly, transverse echoes for the case of no external magnetic field ($\underline{B}_o = 0$) are examined and their characteristics are summarized in Fig. 6.

In performing the above calculations, reference will be made to all five appendices. As stated in the Introduction of Part I, the appendices contain many useful analytical and numerical results. Of special significance for the present echo calculation are Appendix C (on the roots of the transverse dispersion relation for real ω and complex k), Appendix D (on the roots of the longitudinal dispersion relation for real ω and complex k), and Appendix E (on the method of steepest descent as used in evaluating phase-mixing integrals).

2. Derivation of the Second-Order (Nonlinear) Echo Response from the Vlasov-Maxwell Equations

2.1 Formulation of the problem.

The Vlasov equation for a plasma in an external magnetic field has already been discussed in (2.1) - (2.7) of Part I for the perturbation expansion

$$\begin{aligned} f(\underline{x},\underline{v},t) &= f_0(\underline{v}) + f_1(\underline{x},\underline{v},t) + f_2(\underline{x},\underline{v},t) + \cdots \\ E_p(\underline{x},t) &= E_1(\underline{x},t) + \underline{E}_2(\underline{x},t) + \cdots \\ B_p(\underline{x},t) &= B_1(\underline{x},t) + B_2(\underline{x},t) + \cdots \end{aligned} \tag{2.1}$$

In the notation used there, the Vlasov equation is in zero order,

$$-\Omega \frac{\partial f_0}{\partial \phi} = 0 \quad ; \tag{2.2}$$

in first order,

$$\frac{\partial f_1}{\partial t} + \underline{v}\cdot\frac{\partial f_1}{\partial \underline{x}} - \Omega \frac{\partial f_1}{\partial \phi} + \frac{q}{m}\left[(\underline{E}_1 + \underline{E}_{ext}) + \frac{1}{c}\underline{v}\times(\underline{B}_1 + \underline{B}_{ext})\right]\cdot\frac{\partial f_0}{\partial \underline{v}} = 0 \tag{2.3}$$

and in second order,

$$\begin{aligned} &\frac{\partial f_2}{\partial t} + \underline{v}\cdot\frac{\partial f_2}{\partial \underline{x}} - \Omega \frac{\partial f_2}{\partial \phi} + \frac{q}{m}\left[\underline{E}_2 + \frac{1}{c}\underline{v}\times\underline{B}_2\right]\cdot\frac{\partial f_0}{\partial \underline{v}} \\ &\qquad = -\frac{q}{m}\left[(\underline{E}_1 + \underline{E}_{ext}) + \frac{1}{c}\underline{v}\times(\underline{B}_1 + \underline{B}_{ext})\right]\cdot\frac{\partial f_1}{\partial \underline{v}} \end{aligned} \tag{2.4}$$

The nonlinear term (the right-hand side) of the second-order equation, (2.4), is the term that will produce an echo. Given two excitations, we will solve (2.4) to obtain the echo response.

30

Note that the right-hand side of (2.4) serves as an effective driving term (effective external source) for the full equation. It follows, as we shall find shortly, that in Fourier-Laplace transform space,

$$f_2 \propto \left[(\underline{E}_1 + \underline{E}_{ext}) + \frac{1}{c}\underline{v} \times (\underline{B}_1 + \underline{B}_{ext})\right] \cdot \frac{\partial f_1}{\partial \underline{v}} \tag{2.5}$$

Let $\underline{E}$ represent $[(\underline{E}_1 + \underline{E}_{ext}) + \frac{1}{c}\underline{v} \times (\underline{B}_1 + \underline{B}_{ext})]$ for the transverse case or $[\underline{E}_1 + \underline{E}_{ext}]$ for the longitudinal case. Then in general, if two spatial excitations are made as shown in Fig. 1, we will have

$$\underline{E} = \underline{E}(\omega_1) + \underline{E}(\omega_2) \tag{2.6}$$

and

$$f_1 = f_1(\omega_1) + f_1(\omega_2) \tag{2.7}$$

so the product $\underline{E} \cdot \frac{\partial}{\partial \underline{v}} f_1$ contains four terms. Each term produces a response at the sum or difference of the frequencies involved, as follows:

$$\left[\underline{E}(\omega_1) \cdot \frac{\partial}{\partial \underline{v}}\right] f_1(\omega_1) \qquad 0, 2\omega_1 \tag{2.8a}$$

$$\left[\underline{E}(\omega_2) \cdot \frac{\partial}{\partial \underline{v}}\right] f_1(\omega_2) \qquad 0, 2\omega_2 \tag{2.8b}$$

$$\left[\underline{E}(\omega_1) \cdot \frac{\partial}{\partial \underline{v}}\right] f_1(\omega_2) \qquad \omega_1 \pm \omega_2 \tag{2.8c}$$

$$\left[\underline{E}(\omega_2) \cdot \frac{\partial}{\partial \underline{v}}\right] f_1(\omega_1) \qquad \omega_1 \pm \omega_2 \tag{2.8d}$$

The first two terms are second-order corrections to the individual excitations (at zero frequency and the second harmonic) and these would

characteristically damp away in a few Landau damping lengths from the position of the individual excitations. The last two terms represent the nonlinear interaction between the two excitations and these are what drive the echo. Typically the fields ($\underline{E}$'s), and the branch-cut and dielectric-pole portions of f_1 damp away in a distance $\delta << L$ whereas the free-streaming part of f_1 persists indefinitely (if there are no collisions). Thus if we are interested in echoes only for $z > L$, we know $\underline{E}(\omega_1)$ will be essentially zero at $z = L$, and therefore the only term we need consider in calculating the echo is (2.8d). Similarly for echoes at $z < 0$, we need consider only (2.8c).

2.2 Possible echo types.

We now give a concise explanation as to what type of echo will be produced, given the types of excitations (transverse or longitudinal) that are made. Consider just the ϕ dependence of f_2 in (2.5) (the angle ϕ is defined in Fig. 1 of Part I). For a transverse excitation, we know that $\underline{E} \cdot \frac{\partial}{\partial \underline{v}} \sim e^{\pm i\phi}$ and $f_1 \sim e^{\pm i\phi}$ [see (2.30) and (2.73) of Part I]. Similarly we shall find that for a longitudinal excitation both $\underline{E} \cdot \frac{\partial}{\partial \underline{v}}$ and f_1 have no ϕ dependence. The current response is

$$\underline{J}_2 = nq \int f_2 \underline{v}\, d^3v$$
$$\sim \int_0^{2\pi} f_2 \left[\hat{e}_+ \frac{v_\perp}{\sqrt{2}} e^{-i\phi} + \hat{e}_- \frac{v_\perp}{\sqrt{2}} e^{+i\phi} + \hat{e}_z v_z \right] d\phi \tag{2.9}$$

using the circular polarization representation of Part I [see (2.33) of Part I], and where we have indicated only the ϕ integration. If f_2 has no ϕ dependence then the only term of (2.9) that survives the ϕ

integration is the $\hat{e}_z$ term so the resultant $\underline{J}_2$ will be a longitudinal wave. If $f_2 \sim e^{\pm i\phi}$ then the only term of (2.9) that survives the ϕ integration is the $\hat{e}_\pm$ term so the resultant $\underline{J}_2$ will be a transverse wave. Recall that $f_2 \propto \left[\underline{E} \cdot \frac{\partial}{\partial \underline{v}}\right] f_1$ and that for an echo calculation f_1 comes from the first excitation and $\left[\underline{E} \cdot \frac{\partial}{\partial \underline{v}}\right]$ comes from the second excitation. Let t represent a transverse excitation and ℓ represent a longitudinal excitation. Then for excitations in the sequence listed, we will obtain the following echo types:

$$\begin{aligned} \ell\ell &\longrightarrow \ell \\ t\ell &\longrightarrow t \\ \ell t &\longrightarrow t \\ tt &\longrightarrow \ell \end{aligned} \tag{2.10}$$

These results are for the lowest-order echoes that will occur when all waves considered propagate along the direction of the external magnetic field $\underline{B}_o$. Later we shall consider the effects of having propagation just off-axis.

The strictly longitudinal case ($\ell\ell \rightarrow \ell$) is the original echo case investigated by Gould and O'Neil, et al.,[26] and subsequently verified experimentally.[27-29] The production of a longitudinal echo by two transverse excitations ($tt \rightarrow \ell$) has been investigated in theory only.[20] We shall be concerned only with the combinations that produce transverse echoes, i.e., $t\ell \rightarrow t$ and $\ell t \rightarrow t$. These cases have not been investigated previously.

2.3 Transverse plasma wave echoes.

We choose to make a t excitation with frequency ω_1 at $z = 0$

and an ℓ excitation with frequency ω_2 at $z = L$ as shown in Fig. 1. Explicitly we choose

$$\underline{E}_{ext}(z,t) = \mathcal{E}_1(z)\left[\hat{e}_x \cos(\omega_1 t) + \hat{e}_y \sin(\omega_1 t)\right] + E_2(z-L)\left[\hat{e}_z \cos(\omega_2 t)\right] \quad (2.11)$$

where the $E_1(z)$ term is the same transverse excitation used in Part I, and the $E_2(z-L)$ term is the longitudinal excitation at $z = L$. By considering echoes at both $z > L$ and $z < 0$ we can investigate both the $t\ell$ case (for which the echo is at $z > L$) and the ℓt case (for which the echo is at $z < 0$). For the transverse excitation we already have an expression for $f_1(z,v_z,t)$ [i.e., (2.73) of Part I] and we can easily obtain an expression for $\underline{E}(z,t)$ [by taking the inverse Fourier-Laplace transform of (2.48) of Part I]. We shall need analogous expressions for the longitudinal excitation and we now give a brief summary of them.

In first order the Vlasov equation (2.3) is linear in $\underline{E}$, $\underline{B}$, and f_1 and therefore the effects of the longitudinal excitation may be considered independently of the effects of the transverse excitation. We assume that the longitudinal wave propagates exactly along the direction of the external magnetic field $\underline{B}_0$ so $\underline{k}$, $\underline{E}$, and $\underline{B}_0$ all lie along the same direction and f_1 has no ϕ dependence. There is no induced magnetic field so $\nabla \times \underline{E} = 0$ (this is the well known electrostatic case). The appropriate form of the Vlasov equation is then

$$\frac{\partial f_1}{\partial t} + \underline{v} \cdot \frac{\partial f_1}{\partial \underline{x}} + \frac{q}{m} \underline{E}_1 \cdot \frac{\partial f_0}{\partial \underline{v}} = 0 \quad (2.12)$$

which combines with Poisson's equation (the appropriate Maxwell equation)

to give[7]

$$\underline{E}_{TOTAL}(k,\omega) = \frac{\underline{E}_{ext}(k,\omega)}{\epsilon_\ell(k,\omega)} \tag{2.13}$$

where

$$\epsilon_\ell(k,\omega) = 1 - \frac{\omega_{pe}^2}{k^2a^2} Z_1'\left(\frac{\omega}{ka}\right) - \frac{\omega_{pi}^2}{k^2A^2} Z_1'\left(\frac{\omega}{kA}\right) \tag{2.14}$$

for which we assumed $f_o(v_z)$ is Maxwellian. Symmetry properties of the longitudinal dielectric function $\epsilon_\ell(k,\omega)$ are discussed in Appendix B and a brief summary of what is known about the roots of $\epsilon_\ell(k,\omega) = 0$ for real ω and complex k is given in Appendix D.

The longitudinal part of the external excitation is from (2.11), where for definiteness we require $\omega_2 \geq 0$,

$$\begin{aligned} \underline{E}_{ext}(z,t) &= E_z(z-L)\,\hat{e}_z \cos(\omega_2 t) \\ &= \hat{e}_z \sum_{s=\pm 1} \frac{1}{2} E_z(z-L)\, e^{is\omega_2 t} \end{aligned} \tag{2.15}$$

which has the Fourier-Laplace transform

$$\underline{E}_{ext}(k,\omega) = \hat{e}_z \sum_{s=\pm 1} \frac{i}{2} \frac{E_z(k)\, e^{-ikL}}{(\omega + s\omega_2)} \tag{2.16}$$

Henceforth we shall drop the summation symbol, although summation over $s = \pm 1$ will still be implied. Then from (2.13) and (2.16) we have

$$\underline{E}_{TOTAL}(k,\omega) = \hat{e}_z \frac{i}{2} \frac{E_z(k)\, e^{-ikL}}{(\omega + s\omega_2)\,\epsilon_\ell(k,\omega)} \tag{2.17}$$

whose inverse transform is

$$\underline{E}_{TOTAL}(z,t) = \hat{e}_z \frac{i}{2} \int_{-\infty}^{+\infty} \frac{dk}{2\pi} e^{ik(z-L)} \int_{-\infty+ib}^{+\infty+ib} \frac{d\omega}{2\pi} \frac{e^{-i\omega\tau}}{(\omega+s\omega_z)\,\epsilon_\ell(k,\omega)} \tag{2.18}$$

Noting that for real k and complex ω the function $\epsilon_\ell(k,\omega)$ has no zeros in the upper-half ω plane,[7] we lower the ω contour (as shown in Fig. 2 of Part I) and obtain

$$\underline{E}_{TOTAL}(z,t) = \hat{e}_z \frac{1}{2} e^{is\omega_z t} \int_{-\infty}^{+\infty} \frac{dk\, E_z(k)\, e^{ik(z-L)}}{2\pi\, \epsilon_\ell(k, s\omega_z)} \tag{2.19}$$

We proceed to calculate the echo response for the $t\ell$ case and then the ℓt case.

2.3.1 $t\ell$ Case

We may rewrite the second-order Vlasov equation (2.4) as

$$\frac{\partial f_2}{\partial \tau} + \underline{v} \cdot \frac{\partial f_2}{\partial \underline{x}} - \Omega \frac{\partial f_2}{\partial \phi} = -g_1(\phi) - g_2(\phi) \tag{2.20}$$

where

$$g_1(\phi) = \frac{q}{m}\left[\underline{E}_2 + \frac{1}{c}\underline{v}\times\underline{B}_2\right] \cdot \frac{\partial f_0}{\partial \underline{v}}$$

$$g_2(\phi) = \frac{q}{m}\left[(\underline{E}_1 + \underline{E}_{ext}) + \frac{1}{c}\underline{v}\times(\underline{B}_1 + \underline{B}_{ext})\right] \cdot \frac{\partial f_1}{\partial \underline{v}} \tag{2.21}$$

Equation (2.20) is of the same form as the first-order equation and thus has the solution (as shown in Appendix A)

$$f_2(\phi) = \frac{\frac{1}{\Omega}}{e^{2\pi i \nu} - 1} \int_0^{2\pi} d\phi' \left\{ g_1(\phi + \phi') + g_2(\phi + \phi') \right\} e^{i\nu\phi'} \tag{2.22}$$

The Maxwell curl equations combine to give [in analogy to (2.16) of Part I]

$$E_{2\sigma}(k^2c^2 - \omega^2) = 4\pi i \omega J_{2\sigma} \tag{2.23}$$

where

$$\underline{J}_2 = nq \int f_2 \underline{v}\, d^3v \tag{2.24}$$

The g_1 term in (2.22) contributes to $\underline{J}_2$ exactly as the g term contributed to $\underline{J}_1$ in the single transverse excitation case examined in Part I. The g_2 term in (2.22) produces what may be considered an external current and which we shall designate as $\underline{J}_{2\ \mathrm{ext}}$ where

$$\underline{J}_{2\ ext} = nq \int \left[\begin{array}{c} \text{The part of } f_2 \text{ that} \\ \text{depends on } g_2 \end{array} \right] \underline{v}\, d^3v \tag{2.25}$$

Then in analogy to (2.43) of Part I we find

$$J_{2\ TOTAL\ \sigma}(k,\omega) = \frac{J_{2\ ext\ \sigma}(k,\omega)}{\epsilon_T(k,\omega,\sigma)} \tag{2.26}$$

We proceed to calculate $\underline{J}_{2\ \mathrm{ext}}$.

For this, the $\mathcal{TL}$ case, we have

$$g_2(\phi) = \underbrace{\frac{\mathcal{I}}{m} \underline{E}_{TOTAL}(\underline{x}, t)}_{\text{from } \mathcal{L} \text{ excitation at } z = L} \cdot \underbrace{\frac{\partial}{\partial \underline{v}} f(z, \underline{v}, t)}_{\text{from } \mathcal{T} \text{ excitation at } z = 0} \tag{2.27}$$

Combining (2.19) with the free-streaming part of (2.73) of Part I, and then Fourier-Laplace transforming, we obtain

$$g_z(\phi) = \iint dz\, dt\, e^{-ikz+i\omega t} \frac{q}{m}\left[\frac{e^{is\omega_z t}}{2}\int_{-\infty}^{+\infty}\frac{dk\, E_z(k)\, e^{ik(z-L)}}{2\pi\ \ \epsilon_l(k, s\omega_z)}\right]\cdot$$

$$\frac{\partial}{\partial v_z}\left\{\left[\frac{q e^{-i\sigma\phi}}{m\sqrt{2}\,(-v_z)}\,\frac{\partial f_0}{\partial v_\perp}\,\theta(v_z)\right]\frac{E_1(k_1)\, e^{ik_1 z + i\sigma\omega_1 t}}{\epsilon_T(k_1, -\sigma\omega_1)}\right\} \tag{2.28}$$

where

$$k_1 = \frac{-\sigma(\omega_1+\Omega)}{v_z} \tag{2.29}$$

Moving the $\partial/\partial v_z$ operator to the far left and interchanging orders of integration gives

$$g_z(\phi) = \frac{\partial}{\partial v_z}\left\{\left(\frac{q}{m}\right)^2\frac{(-)}{2\sqrt{2}}\,\frac{\theta(v_z)}{v_z}\,e^{-i\sigma\phi}\,\frac{\partial f_0}{\partial v_\perp}\,\frac{E_1(k_1)}{\epsilon_T(k_1, -\sigma\omega_1)}\cdot\right.$$

$$\left.\int_0^\infty dt\, e^{i(\omega+s\omega_z+i\sigma\omega_1)t}\int_{-\infty}^{+\infty}\frac{dk' E_z(k') e^{-ik'L}}{2\pi\,\epsilon_l(k', s\omega_z)}\int_{-\infty}^{+\infty} dz\, e^{iz(-k+k'+k_1)}\right\} \tag{2.30}$$

The integral over z equals $2\pi\delta(k'-k+k_1)$. Performing the remaining two integrals, we obtain

$$g_z(\phi) = \frac{\partial}{\partial v_z}\left\{\left[\left(\frac{q}{m}\right)^2\frac{\theta(v_z)}{2\sqrt{2}\,v_z}\,e^{-i\sigma\phi}\,\frac{\partial f_0}{\partial v_\perp}\right]\cdot\right.$$

$$\left.\frac{E_1(k_1)\, E_z(k-k_1)\, e^{-i(k-k_1)L}}{(\omega-\omega_3)\ \ \epsilon_T(k_1, -\sigma\omega_1)\,\epsilon_l(k-k_1, s\omega_z)}\right\} \tag{2.31}$$

where

$$\omega_3 = -s\omega_2 - \sigma\omega_1 \tag{2.32}$$

Since $g_2(\phi) \sim e^{-i\sigma\phi}$, the part of f_2 associated with g_2 is, after performing the ϕ' integration in (2.22),

$$f_2(\phi) = \frac{1}{i(\omega - kv_z - \sigma\Omega)}\, g_2(\phi) \tag{2.33}$$

where $g_2(\phi)$ is still given by (2.31).

The "external current" that drives the echo is given by (2.25). Performing the integrations over ϕ and $v_\perp$, we obtain

$$\underline{J}_{2ext} = \hat{e}_{-\sigma} C \int_0^\infty \frac{\alpha v_z}{(\omega - kv_z - \sigma\Omega)} \frac{\partial}{\partial v_z} \left\{ \quad \right\} \tag{2.34}$$

where

$$C = \frac{i}{2\sqrt{2}} \frac{q}{m} \omega_p^2$$

$$\left\{ \quad \right\} = \left\{ \frac{f_0(v_z)\, E_1(k_1)\, E_2(k-k_1)\, e^{-i(k-k_1)L}}{v_z(\omega-\omega_3)\, \epsilon_T(k_1, -\sigma\omega_1)\, \epsilon_\ell(k-k_1, s\omega_2)} \right\}$$

Integrating (2.34) by parts then gives

$$\underline{J}_{2ext} = \hat{e}_{-\sigma}(-) C \int_0^\infty \frac{k\alpha v_z}{(\omega - kv_z - \sigma\Omega)^2} \left\{ \quad \right\} \tag{2.35}$$

Using (2.35) in (2.26) we find

$$\underset{-z\,TOTAL}{\mathcal{J}}(k,\omega) =$$

$$\hat{e}_{-\sigma}(-)C\int_0^\infty \frac{dv_z\, k f_0(v_z) E_1(k_1) E_2(k-k_1) e^{-i(k-k_1)L}}{v_z(\omega-\omega_3)(\omega-kv_z-\sigma\Omega)^2 \epsilon_T(k_1,-\sigma\omega_1)\epsilon_\ell(k-k_1,s\omega_2)\epsilon_T(k,\omega)} \tag{2.36}$$

The actual response is the Fourier-Laplace transform of (2.36), i.e.,

$$\underset{-z\,TOTAL}{\mathcal{J}}(z,t) = \iint \frac{dk\,d\omega}{(2\pi)^2} \underset{-z\,TOTAL}{\mathcal{J}}(k,\omega) e^{ikz-i\omega t} \tag{2.37}$$

The primitive contours in the ω and k planes are the same as given earlier (in Figs. 2a and 3a of Part I). We perform the k integral first. Branch-cut integrals arise from proper consideration of $\epsilon_\ell(k-k_1,s\omega_2)$ and $\epsilon_t(k,\omega)$ in the denominator of (2.37) but these give a damped response at $z = L$ whereas the echo response occurs typically a good distance away from $z = L$. The dielectric poles in the k plane of $\epsilon_\ell(k-k_1,s\omega_2)$ and $\epsilon_t(k,\omega)$ also produce damped responses near $z = L$. Thus to obtain the echo response we need consider only the double pole at $k = (\omega-\sigma\Omega)/v_z$. Since the integrand of (2.37) contains the factor $e^{ik(z-L)}$, we pull the primitive k contour above for $z > L$ and below for $z < L$. Then since we have $\mathrm{Im}\,\omega > 0$, we obtain a contribution only for $z > L$, i.e.,

$$\underset{-z\,TOTAL}{\mathcal{J}}(z,t) = \hat{e}_{-\sigma} iC\int_0^\infty dv_z \left[\frac{f_0(v_z) E_1(k_1)}{v_z^3 \epsilon_T(k_1,-\sigma\omega_1)}\right]\theta(z-L)\,.$$

$$\int \frac{d\omega\, e^{-i\omega t}}{2\pi(\omega-\omega_3)} \frac{\partial}{\partial k}\left\{ \frac{k E_2(k-k_1)\, e^{-i(k-k_1)L + ikz}}{\epsilon_\ell(k-k_1, s\omega_2)\,\epsilon_T(k,\omega)} \right\}\Bigg|_{k=\frac{\omega-\sigma\Omega}{V_z}} \tag{2.38}$$

Lowering the ω contour we obtain a residue contribution at $\omega = \omega_3$,

$$\underline{J}_{z\,TOTAL}(z,t) =$$

$$\hat{e}_{-\sigma} C\, \theta(z-L) \int_0^\infty \frac{d V_z\, f_0(V_z)\, E_1(k_1)\, E_2(k_2)\, k_3\, A(V_z)\, e^{ik_3(z-z_0) - i\omega_3 t}}{V_z^3\, \epsilon_T(k_1, -\sigma\omega_1)\, \epsilon_\ell(k_2, s\omega_2)\, \epsilon_T(k_3, \omega_3)} \tag{2.39}$$

where

$$\left.\begin{aligned} A(V_z) &= \frac{\partial}{\partial k}\, \ell n\left\{ \frac{k E_2(k-k_1)\, e^{ik(z-L)}}{\epsilon_\ell(k-k_1, s\omega_2)\,\epsilon_T(k,\omega)} \right\}\Bigg|_{k=k_3} \\ k_1 &= \frac{-\sigma(\omega+\Omega)}{V_z} \\ k_2 &= \frac{s\omega_2}{V_z} \\ k_3 &= \frac{-\sigma(\omega_3+\Omega)}{V_z} \\ z_0 &= \frac{k_z L}{k_3} = \frac{s\omega_2 L}{-\sigma(\omega_3+\Omega)} \end{aligned}\right\} \tag{2.40}$$

Recall that we are still supposed to sum over $s = \pm 1$ and $\sigma = \pm 1$. When this is done we find [using symmetry properties (B.6) and (B.8) from Appendix B] that the $s = +1$, $\sigma = +1$ term is the complex conjugate of the $s = -1$, $\sigma = -1$ term so the response is just twice the real part of either term. Similarly the $s = -1$, $\sigma = +1$ term is the complex conjugate of the $s = +1$, $\sigma = -1$ term. Thus with a new dummy index s, we have (arbitrarily using $\sigma = -1$),

$$\underset{-z\ TOTAL}{\mathcal{J}}(z,t) = \sum_{s=\pm 1} z\, \mathcal{R}e\left\{ \hat{e}_+ C\, \theta(z-L) \cdot \int_0^\infty \frac{dv_z\, f_0(v_z)\, E_1(k_1)\, E_2(k_2)\, A_1(v_z)\, e^{ik_3(z-z_0)-i\omega_3 \tau}}{v_z^3\, \epsilon_{T_\alpha}(k_1,\omega_1)\, \epsilon_{\ell_s}(k_2,s\omega_2)\, \epsilon_{T_\beta}(k_3,\omega_3)} \right\} \tag{2.41}$$

where

$$\left.\begin{aligned} C &= \frac{i}{2\sqrt{2}}\,\frac{q}{m}\,\omega_p^2 \\ A_1(v_z) &= k_3 \frac{\partial}{\partial k} \ln\left\{ \frac{k E_2(k-k_1)\, e^{ik(z-L)}}{\epsilon_{\ell_s}(k-k_1,s\omega_2)\, \epsilon_{T_\beta}(k,\omega_3)} \right\}\Bigg|_{k=k_3} \\ \omega_3 &= \omega_1 + s\omega_2 \\ z_0 &= \frac{\omega_2 L}{\omega_2 + s(\omega_1+\Omega)} \\ k_1 &= \frac{\omega_1+\Omega}{v_z} \qquad k_2 = \frac{s\omega_2}{v_z} \qquad k_3 = \frac{\omega_3+\Omega}{v_z} \\ \alpha &= SGN(\omega_1+\Omega) \qquad \beta = SGN(\omega_3+\Omega) \end{aligned}\right\} \tag{2.42}$$

In (2.41) - (2.42) we have explicitly specified which branches of the dielectric functions are to be used.

Equation (2.41) gives the transverse echo response for $t\ell$ excitations. Note that since k_3 depends on v_z there will be phase mixing everywhere except near $z = z_0$, the position of the echo peak. We defer calculation of the integral over v_z in (2.41) and further discussion of this, the $t\ell$ case, until after we have investigated the ℓt case, which we now do. [Numerical results concerning (2.41) for some specific cases will be given in Figs. 3-5.]

2.3.2 ℓt Case

The derivation proceeds exactly as in (2.20) - (2.26) but then instead of (2.27) we have

$$g_2(\phi) = \frac{q}{m}\underbrace{\left[\underline{E}_{TOTAL}(z,t) + \frac{1}{c}\underline{v}\times\underline{B}_{TOTAL}(z,t)\right]}_{\text{from } t \text{ excitation at } z=0}\cdot\frac{\partial}{\partial\underline{v}}\underbrace{f_1(z,\underline{v},t)}_{\text{from } \ell \text{ excitation at } z=L} \tag{2.43}$$

The expression $\frac{q}{m}\left[\underline{E}_{TOTAL}(k,\omega) + \frac{1}{c}\underline{v}\times\underline{B}_{TOTAL}(k,\omega)\right]\cdot\frac{\partial}{\partial\underline{v}}$ for a transverse excitation was calculated earlier to be [see (2.31) and (2.39) of Part I]

$$\frac{q}{m}\left[\underline{E}_{TOTAL}(k,\omega) + \frac{1}{c}\underline{v}\times\underline{B}_{TOTAL}(k,\omega)\right]\cdot\frac{\partial}{\partial\underline{v}}$$

$$= \frac{q}{m\sqrt{2}}\,\frac{E_{ext}(k,\omega)}{\epsilon_T(k,\omega)}\,e^{-i\sigma\phi}\left\{\left(1-\frac{kv_z}{\omega}\right)\frac{\partial}{\partial v_\perp} + \frac{kv_\perp}{\omega}\,\frac{\partial}{\partial v_z}\right\} \tag{2.44}$$

Using (2.48) of Part I for $\underline{E}_{ext}(k,\omega)$, the inverse transform of (2.44) is

$$\frac{q}{m}\left[\underline{E}_{TOTAL}(z,t) + \frac{1}{c}\underline{v}\times\underline{B}_{TOTAL}(z,t)\right]\cdot\frac{\partial}{\partial\underline{v}}$$

$$= \frac{q}{m\sqrt{2}}\, e^{-i\sigma\phi} e^{+i\sigma\omega_1 t}\int_{-\infty}^{+\infty}\frac{dk\, E_1(k)\, e^{ikz}}{2\pi\,\epsilon_T(k,-\sigma\omega_1)}\left\{\left(1+\frac{kv_z}{\sigma\omega_1}\right)\frac{\partial}{\partial v_\perp} - \frac{kv_\perp}{\sigma\omega_1}\frac{\partial}{\partial v_z}\right\} \tag{2.45}$$

The expression for $f_1(k,\underline{v},\omega)$ for a longitudinal excitation is

$$f_1(k,\underline{v},\omega) = \frac{q}{m}\,\frac{E_{ext}(k,\omega)\,\frac{\partial f_0}{\partial v_z}}{\epsilon_\ell(k,\omega)\; i\,(\omega - kv_z)} \tag{2.46}$$

which follows directly from (2.12) and (2.13). Using (2.16) for $\underline{E}_{ext}(k,\omega)$ and then taking the inverse transform of (2.46), we find the free-streaming part of $f_1(z,\underline{v},t)$ is, for $z < 0$,

$$f_1(z,\underline{v},t) = \frac{q\,\theta(-v_z)\,E_2(k_2)\,\frac{\partial f_0}{\partial v_z}\, e^{ik_2(z-L)+is\omega_2 t}}{m\,2\,v_z \qquad \epsilon_\ell\left(k_2,-s\omega_2\right)} \tag{2.47}$$

where $k_2 = -s\omega_2/v_z$. Equations (2.43), (2.45), (2.47) combine to give

$$g_2(\phi) = \left(\frac{q}{m}\right)^2 \frac{e^{-i\sigma\phi}}{2\sqrt{2}}\; e^{i\sigma\omega_1 t + is\omega_2 t}\int_{-\infty}^{+\infty}\frac{dk'\,E_1(k')\,e^{ik'z}}{2\pi\,\epsilon_T\left(k',-\sigma\omega_1\right)}\cdot\Bigg\{$$

$$\left[\left(1+\frac{k'v_z}{\sigma\omega_1}\right)\frac{\partial}{\partial v_\perp} - \frac{k'v_\perp}{\sigma\omega_1}\frac{\partial}{\partial v_z}\right]\left[\frac{\theta(-v_z)\,E_2(k_2)\,\frac{\partial f_0}{\partial v_z}\, e^{ik_2(z-L)}}{v_z \quad \epsilon_\ell\left(k_2,-s\omega_2\right)}\right]\Bigg\} \tag{2.48}$$

This expression is more complicated than the corresponding expression for the $t\ell$ case, (2.28), mainly because of the factor

$$\left\{ \left(1 + \frac{k' v_z}{\sigma \omega_1} \right) \frac{\partial}{\partial v_\perp} - \frac{k' v_\perp}{\sigma \omega_1} \frac{\partial}{\partial v_z} \right\}$$

which in the $t\ell$ case was just $\partial / \partial v_z$.

We proceed to calculate $\underline{J}_{2\ \mathrm{TOTAL}}(z,t)$ in the same manner as used for the $t\ell$ case in (2.28) - (2.42). This computation is more involved than that of the $t\ell$ case but the final result is similar to the final result of the $t\ell$ case. Omitting the details of this calculation, we find:

$$\underline{J}_{2\ \mathrm{TOTAL}}(z,t) = \sum_{s=\pm 1} 2\, \mathcal{R}e \left[\hat{e}_+ C\, \theta(-z) \cdot \int_{-\infty}^{0} \frac{dv_z\, f_0(v_z)\, E_1(k_1)\, E_2(k_2)\, k_3\, A_2(v_z)\, e^{i k_3 (z - z_0) - i \omega_3 t}}{v_z^3\, \epsilon_{T-\alpha}(k_1, \omega_1)\, \epsilon_{\ell - s}(k_2, s\omega_2)\, \epsilon_{T-\beta}(k_3, \omega_3)} \right] \tag{2.49}$$

where

$$A_2(v_z) = \frac{v_z \Omega}{\omega_1 k_3} \frac{1}{f_0} \frac{\partial f_0}{\partial v_z} + \frac{k_1}{\omega_1} \langle v_\perp^2 \rangle \frac{1}{f_0} \frac{\partial f_0}{\partial v_z} \frac{\partial}{\partial k} \ln \left\{ \frac{k(k-k_2) E_1(k-k_2) e^{ikz}}{\epsilon_{T-\alpha}(k-k_2, \omega_1)\, \epsilon_{T-\beta}(k, \omega_3)} \right\} \Bigg|_{k=k_3} \tag{2.50}$$

$$\langle v_\perp^2 \rangle = \int v_\perp^2 f_0(v_\perp)\, dv_\perp$$

and the k's, C, ω_3, and z_o are as defined in (2.42). Equation (2.49) gives the transverse echo response for ℓt excitations. Note that only particles with $v_z < 0$ contribute to the echo [i.e., note $\int_{-\infty}^{0} dv_z$ in (2.49)] and that there is a response only for $z < 0$ [i.e., note $\theta(-v_z)$ factor in (2.49)]. Note, however, that particles with all values of v_z contribute to the ε's in (2.49) and thus particles with $v_z > 0$ may affect the echo shape.

Having obtained the transverse echo response for both the $t\ell$ and ℓt cases we continue by investigating the consequences of these results, (2.41) and (2.49), and then actually performing the integrals over v_z to obtain echo shapes for some specific cases.

3. Transverse Echo Characteristics

Equations (2.41) and (2.49) represent the transverse echo response for the species of particles that has cyclotron frequency Ω and zero-order distribution function $f_o(v_z)$. Thus there is an electron echo and an ion echo and since z_o depends on Ω, i.e., from (2.42)

$$z_o = \frac{\omega_2 L}{\omega_2 + s(\omega_1 + \Omega)} \tag{3.1}$$

it follows that in general the electron and ion echo peaks will occur at different locations. Also note that since

$$\omega_3 = \omega_1 + s\omega_2 \tag{3.2}$$

it is possible to have echoes at the sum (s = +1) or difference (s = -1) of the excitation frequencies.

Recall that ω_2 is always positive and that ω_1 may have either sign, $\omega_1 < 0$ corresponding to a left-hand (LH) excitation and $\omega_1 > 0$ corresponding to a right-hand (RH) excitation. We adopt the convention that RH polarization of a wave means that the $\underline{J}$ (or $\underline{E}$) associated with the wave rotates in the same direction as electrons gyrate in the zero-order magnetic field $\underline{B}_o$. (N.B. This differs from the usual convention in optics where polarization is referred to the direction of propagation of the wave.)

Now consider just $t\ell$ echoes, which exist only for $z_o > L$. From (3.1) this places restrictions on the allowed values of ω_1 and ω_2. Thus to obtain a $t\ell$ echo for electrons ($\Omega = -\omega_{ce}$) at the difference frequency (s = -1) we must have

$$\frac{\omega_2 L}{\omega_2 - (\omega_1 - \omega_{ce})} > L$$

or

$$\omega_2 > (\omega_1 - \omega_{ce}) > 0 \tag{3.3}$$

Furthermore, since from (2.41) $\underline{J}_2 \sim \mathrm{Re}\,\{\hat{e}_+ \exp[i(\omega_1-\omega_2)t]\}$, the region of ω_1, ω_2 space defined by (3.3) will be divided into two regions; for $\omega_1 > \omega_2$ the echo will have LH polarization, for $\omega_1 < \omega_2$ the echo will have RH polarization. These two regions are shown in Fig. 2 as regions IV and V respectively. In Fig. 2, each region shown has distinct echo characteristics; i.e., type (tl or lt), polarization, frequency, and direction of propagation (→ or ←) of the waves comprising the echo are all indicated. The boundaries of each region are obtained in the manner used to define regions IV and V above. As shown, Fig. 2 applies to electron echoes but it can be used for ion echoes by interchanging RH and LH everywhere, including along the ω_1 axis, where then $\omega_1 > 0$ would mean a LH excitation.

The transverse echoes we have been considering offer a much more abundant variety of phenomena than those which occur for purely longitudinal echoes ($ll \to l$). We summarize the basic differences and new features:

1.) Echoes can occur at the sum or difference frequency whereas in the longitudinal case the echo occurs only at the difference frequency.

2.) The echo location (z_o) and frequency (ω_3) depend on the

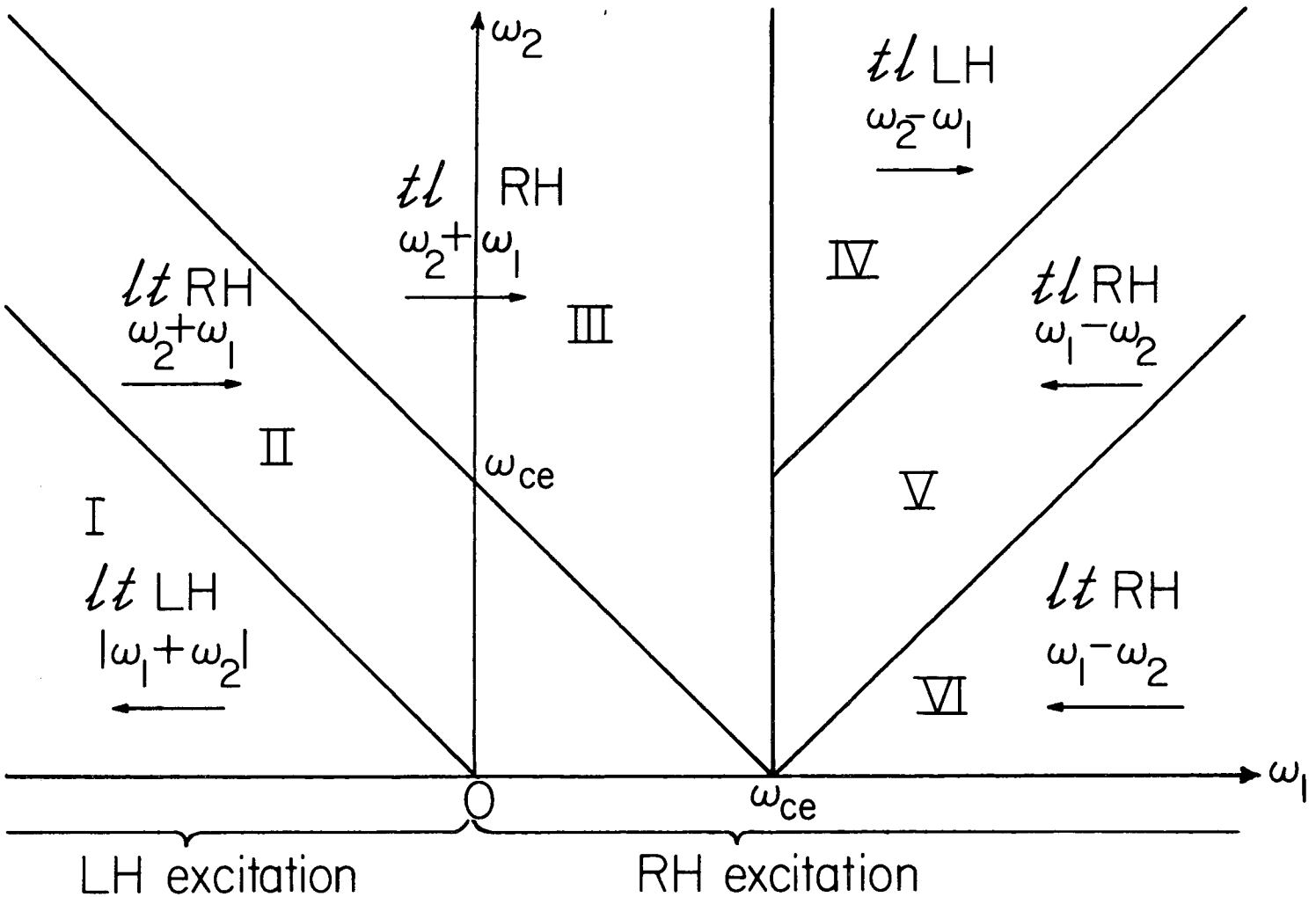

FIGURE 2. TRANSVERSE ECHO CHARACTERISTICS.

This figure applies for electron echoes; for ion echoes interchange RH and LH everywhere.

species, whereas in the longitudinal case both the electron and ion echoes occur at the same position and at the same frequency. By saying ω_3 depends on species we mean that it is possible to have the electron echo at the sum frequency while the ion echo is at the difference frequency. We emphasize though that given ω_1, ω_2 there is only one electron echo (with $z_o > L$ or $z_o < 0$) and similarly only one ion echo.

3.) The polarization of the echo may be different than that of the initial ω_1 excitation. For example, in region IV, the excitation has RH polarization while the echo has LH polarization.

4.) The propagation direction of the waves comprising the echo may be away from or <u>toward</u> the excitation region whereas in the longitudinal case, the propagation direction is always away from the excitation region. The cases where the waves propagate toward the excitation region are those which have $0 < \omega_3 < \omega_{ce}$ and the phenomenon involved is the same as that of the negative phase velocity free-streaming waves that occur for a single transverse excitation if $0 < \omega_1 < \omega_{ce}$, as was discussed in Part I.

5.) There is a unique echo for every value of ω_1, ω_2 whereas in the longitudinal case $-\omega_1$, ω_2 represented the same echo phenomenon as $+\omega_1$, ω_2 ; the only difference being that the echo appeared on the opposite side of the excitation region.

We now comment on a few of the many interesting experiments suggested by Fig. 2.

1.) Consider echoes in region IV. With an initial high frequency ($\omega_1 > \omega_{ce}$) RH polarized excitation and with $\omega_2 \gtrsim \omega_1$ we may generate

an echo that is a low frequency LH polarized Alfven wave.

2.) We may examine the consequences of echoes comprised of waves which have negative phase velocities by considering echoes in regions II and V, since in both of these regions we have $0 < \omega_3 < \omega_{ce}$.

3.) Note that an echo occurs even if $\omega_1 = 0$. This means that if the first excitation is simply a fixed transverse electric field, i.e., like

$$\underline{E}_{ext}(z,t) = \hat{e}_x E(z) \tag{3.4}$$

and if a longitudinal excitation is made at frequency ω_2 , then a transverse echo with RH polarization will occur at the same frequency ω_2 , at the location

$$z_o = \frac{\omega_2 L}{\omega_2 - \omega_{ce}} \tag{3.5}$$

Thus a longitudinal wave may be "converted" into a transverse wave (of the same frequency) which is localzied about a specific position (z_o) in the plasma. This novel feature occurs in both regions II and III.

4. Evaluation of Transverse Echo Shapes

4.1 Use of the method of steepest descent.

We proceed to evaluate the integral over v_z that occurs in (2.41) for the tl echo case. [The integral in (2.49) for the lt echo case can be evaluated in the same manner.] Using a Maxwellian distribution,

$$f_o(v_z) = \frac{1}{\sqrt{\pi}a} e^{-\frac{v_z^2}{a^2}} \tag{4.1}$$

assuming delta function sources [as in (2.77)-(2.78) of Part I] so

$$E_1(k_1) = \mathcal{I}_1 \qquad E_2(k_2) = \mathcal{I}_2 \tag{4.2}$$

and considering just electron echoes ($\Omega = -\omega_{ce}$), we find (2.41) becomes

$$\underline{J}_{2\,TOTAL}(z,t) = \sum_{s=\pm 1} 2\,\mathcal{R}e\left\{\hat{e}_+\left[\frac{c\mathcal{I}_1\mathcal{I}_2}{a^3}\right] I\, e^{-i\omega_3 t}\right\}\theta(z-L) \tag{4.3}$$

where the integral we must evaluate is

$$I = \int_0^\infty \frac{\frac{dv_z}{a} A_1(v_z)\, e^{i\frac{(\omega_3-\omega_{ce})(z-z_o)}{v_z} - \left(\frac{v_z}{a}\right)^2}}{\sqrt{\pi}\left(\frac{v_z}{a}\right)^3 \epsilon_{T_\alpha}\left(\frac{\omega_1-\omega_{ce}}{v_z}, \omega_1\right)\epsilon_{\ell_s}\left(\frac{s\omega_2}{v_z}, s\omega_2\right)\epsilon_{T_\beta}\left(\frac{\omega_3-\omega_{ce}}{v_z}, \omega_3\right)} \tag{4.4}$$

in which

$$A_1(v_z) = 1 + ik_3(z-L) - \frac{k_3 \left.\frac{\partial \epsilon_{\ell_s}(k-k_1, s\omega_2)}{\partial k}\right|_{k=k_1}}{\epsilon_{\ell_s}(k_2, s\omega_2)} - \frac{k_3 \left.\frac{\partial \epsilon_{T_\beta}(k,\omega_3)}{\partial k}\right|_{k=k_3}}{\epsilon_{T_\beta}(k,\omega_3)} \tag{4.5}$$

In (4.4) we have explicitly indicated the v_z dependence of the k arguments of the ε's.

We evaluate (4.4) by the method of steepest descent as discussed in Appendix E. The appropriate saddle point of the integrand of (4.4) is

$$\frac{v_s}{a} = \left[\frac{\delta(\omega_3-\omega_{ce})(z-z_0)}{2a}\right]^{\frac{1}{3}} e^{-i\delta\frac{\pi}{6}} \tag{4.6}$$

where $\delta = \pm 1$ for $[(\omega_3-\omega_{ce})(z-z_0)] \gtrless 0$. The primitive contour $(0 \leq v_z/a \leq \infty)$ in the complex v_z/a plane is deformed through the appropriate saddle point along the path of steepest descent, care being taken to indent the contour around any poles caused by the ε's in (4.4). The three possible pole terms arising from the dielectric functions involving ω_1, ω_2, ω_3 in (4.4) will be referred to as the pole 1, pole 2, pole 3 terms, respectively. Thus we find

$$I = I_{\substack{SADDLE\\POINT}} + \sum_{i=1}^{3} I_{POLE\ i} \tag{4.7}$$

The saddle point contribution is

$$I_{\substack{SADDLE\\POINT}} = \frac{A_1(v_s)\, e^{-3\left[\frac{\delta(\omega_3-\omega_{ce})(z-z_0)}{2a}\right]^{2/3}\left[\frac{1}{2}-i\delta\frac{\sqrt{3}}{2}\right]}}{\sqrt{3}\left(\frac{v_s}{a}\right)^3 \epsilon_{T_\alpha}\left(\frac{\omega_1-\omega_{ce}}{v_s},\omega_1\right)\epsilon_{l_s}\left(\frac{s\omega_2}{v_s},s\omega_2\right)\epsilon_{T_\beta}\left(\frac{\omega_3-\omega_{ce}}{v_s},\omega_3\right)} \tag{4.8}$$

[which is valid for $|(z-z_0)(\omega_3-\omega_{ce})/a| \gtrsim 0.12$ as discussed in Appendix E]. Assuming simple first-order poles in each case, the three pole terms are:

$$I_{POLE\,1} = \gamma_1 \frac{i2\sqrt{\pi}\, A_1(v_1)\, e^{i\left(\frac{\omega_3-\omega_{ce}}{v_1}\right)(\bar{z}-\bar{z}_0) - \frac{v_1^2}{a^2}}}{-\frac{v_1^2}{a^2}\left[k\frac{\partial \epsilon_{T_\alpha}(k,\omega_1)}{\partial k}\right]\Big|_{k=\frac{\omega_1-\omega_{ce}}{v_1}} \epsilon_{\ell_s}\left(\frac{s\omega_2}{v_1}, s\omega_2\right)\epsilon_{T_\beta}\left(\frac{\omega_3-\omega_{ce}}{v_1}, \omega_3\right)}$$

$$I_{POLE\,2} = \gamma_2 \frac{i2\sqrt{\pi}\, A_1(v_2)\, e^{i\left(\frac{\omega_3-\omega_{ce}}{v_2}\right)(\bar{z}-\bar{z}_0) - \frac{v_2^2}{a^2}}}{-\frac{v_2^2}{a^2}\epsilon_{T_\alpha}\left(\frac{\omega_1-\omega_{ce}}{v_2}, \omega_1\right)\left[k\frac{\partial \epsilon_{\ell_s}(k, s\omega_2)}{\partial k}\right]\Big|_{k=\frac{s\omega_2}{v_2}} \epsilon_{T_\beta}\left(\frac{\omega_3-\omega_{ce}}{v_2}, \omega_3\right)} \qquad (4.9)$$

$$I_{POLE\,3} = \gamma_3 \frac{i2\sqrt{\pi}\, A_1(v_3)\, e^{i\left(\frac{\omega_3-\omega_{ce}}{v_3}\right)(\bar{z}-\bar{z}_0) - \frac{v_3^2}{a^2}}}{-\frac{v_3^2}{a^2}\epsilon_{T_\alpha}\left(\frac{\omega_1-\omega_{ce}}{v_3}, \omega_1\right)\epsilon_{\ell_s}\left(\frac{s\omega_2}{v_3}, s\omega_2\right)\left[k\frac{\partial \epsilon_{T_\beta}(k,\omega_3)}{\partial k}\right]\Big|_{k=\frac{\omega_3-\omega_{ce}}{v_3}}}$$

where v_1, v_2, v_3 are defined by

$$\epsilon_{T_\alpha}\left(\frac{\omega_1-\omega_{ce}}{v_1}, \omega_1\right) = 0$$

$$\epsilon_{\ell_s}\left(\frac{s\omega_2}{v_2}, \omega_2\right) = 0 \qquad (4.10)$$

$$\epsilon_{T_\beta}\left(\frac{\omega_3-\omega_{ce}}{v_3}, \omega_3\right) = 0$$

and

$$A_1(v_1) = \left\{ 1 + \underline{i k_3 (z - L)} - \frac{k_3 \epsilon'_{\ell_s}(k - k_1, s\omega_2)_{k=k_3}}{\epsilon_{\ell_s}(k_2, s\omega_2)} - \frac{k_3 \epsilon'_{T_\beta}(k, \omega_3)_{k=k_3}}{\epsilon_{T_\beta}(k_3, \omega_3)} \right\}_{v=v_1}$$

$$A_1(v_2) = \left\{ 1 + \underline{i k_3 (z_0 - L)} - 4\frac{k_3}{k_1} - 2\frac{k_3}{k_2}\left(\frac{v_3}{a}\right)^2 - \frac{k_3}{k_2}\left[\frac{k^2 \epsilon''_{\ell_s}(k, s\omega_2)}{k \epsilon'_{\ell_s}(k, s\omega_2)}\right]_{k=k_2} \right.$$

$$\left. + \frac{k_3}{k_2}\left[\frac{k \epsilon'_{T_\alpha}(k, \omega_1)}{\epsilon_{T_\alpha}(k, \omega_1)}\right]_{k=k_1} + \frac{k_1}{k_2}\left[\frac{k \epsilon'_{T_\beta}(k, \omega_3)}{\epsilon_{T_\beta}(k, \omega_3)}\right]_{k=k_3} \right\}_{v=v_2} \qquad (4.11)$$

$$A_1(v_3) = \left\{ -3 + \underline{i k_3 (z_0 - L)} - 2\left(\frac{v_3}{a}\right)^2 - \left[\frac{k^2 \epsilon'_{T_\beta}(k, \omega_3)}{k \epsilon'_{T_\beta}(k, \omega_3)}\right]_{k=k_3} \right.$$

$$\left. + \left[\frac{k \epsilon'_{T_\alpha}(k, \omega_1)}{\epsilon_{T_\alpha}(k, \omega_1)}\right]_{k=k_1} - \frac{k_1}{k_2}\left[\frac{k \epsilon'_{\ell_s}(k, s\omega_2)}{\epsilon_{\ell_s}(k, s\omega_2)}\right]_{k=k_2} \right\}_{v=v_3}$$

A prime (') denotes differentiation with respect to k , and

$$k_1 = \frac{\omega_1 - \omega_{ce}}{v_i} \qquad k_2 = \frac{s\omega_2}{v_i} \qquad k_3 = \frac{\omega_3 - \omega_{ce}}{v_i} \qquad (4.12)$$

where i = 1, 2, 3. The factor γ_i equals ± 1 depending on which direction the contour encircles the pole in question, and if there is

no pole $\gamma_i = 0$.

In (4.11), note the abundance of terms in $A_1(v_2)$ and $A_1(v_3)$ as compared to $A_1(v_1)$. These terms occur because when the third and fourth terms of $A_1(v_z)$, as given in (4.5), are evaluated at pole 2 and pole 3 respectively, second-order poles are produced. The new terms in $A_1(v_2)$ and $A_1(v_3)$ come from the rather complicated residue expressions that result from these second-order poles.

Concerning the sizes of the various terms in the $A_1(v_i)$ factors in (4.11), we find that all terms that contain an ε, ε', or ε'' are typically of order one. Noting that

$$\left| k_3(z_o-L) \right| = \left| k_1 L \right| = \left| \frac{L}{\left(\frac{a}{\omega_1-\omega_{ce}}\right)\frac{v_i}{a}} \right| \tag{4.13}$$

and that the pole terms are important only if $|v_i/a| \lesssim 3$ [because of the exponential factors $\exp(-v_i^2/a^2)$ in (4.9)], we find $|k_3(z_o-L)|$ >> 1 provided

$$\left| \frac{L}{\frac{a}{\omega_1-\omega_{ce}}} \right| = \frac{L\omega_{ce}}{c}\left| \left(\frac{\omega_1}{\omega_{ce}}-1\right)\frac{c}{a} \right| \gg 1 \tag{4.14}$$

Since typically $L\omega_{ce}/c$ is >> 1, we find (4.14) holds if ω_1 is not extremely close to ω_{ce} ($|\omega_1/\omega_{ce} - 1|\,\frac{c}{a} >> 1$) in which case the underlined term in each $A(v_i)$ in (4.11) is the dominant term. If ω_1 is extremely close to ω_{ce} ($|\omega_1/\omega_{ce} - 1|\,\frac{c}{a} << 1$) then the $A_1(v_i)$'s must be evaluated in full. In any case, the $A_1(v_i)$'s are only amplitude factors for the various pole terms. More specifically, the $A_1(v_i)$'s have no z dependence [except for the slight z dependence in the

underlined terms in (4.11)] and, therefore, they can affect the echo shape only by affecting the size, but not the shape, of the pole terms.

4.2 Numerical examples of transverse echo shapes.

First we explain why we should not evaluate (4.8), (4.9) analytically by using asymptotic exmapsions for the Z functions involved. In the saddle-point term (4.8), the arguments of the Z functions contained in the three ε's are all identically equal to v_s/a, which is defined by (4.6). Typically we shall want to compute the echo shape for $0 < |(z-z_o)(\omega_3-\omega_{ce})/a| \lesssim 10$ say, over which range we have $0 < |v_s|/a \lesssim 1.8$, for which $Z(v_s/a)$ is clearly not in its asymptotic limit. Similarly for the i^{th} pole term in (4.9), the arguments of the Z functions contained in the three ε's are all identically equal to v_i/a, which is defined by (4.10). As mentioned earlier, the i^{th} pole term is significant only if $|v_i|/a \lesssim 3$ [because of the exponential factor $\exp(-v_i^2/a^2)$ in (4.9)], in which case $Z(v_i/a)$ is clearly not in its asymptotic limit. Thus, when the saddle point and pole terms are significant, the Z functions involved are clearly not in their asymptotic limits. Hence it is rather pointless to rewrite (4.8) and (4.9) using asymptotic expansions for the Z functions involved because the resultant expressions would not be valid at the very places we would like to use them. (These remarks apply also to the purely longitudinal echo case. In particular, the final expression for the spatial longitudinal echo case of Gould and O'Neil[26] was computed using the asymptotic expansion of the Z function and accordingly their result is essentially of little value since it does not apply to any cases wherein the saddle point and pole terms are significant.)

Thus we have numerically evaluated (4.8), (4.9) for three cases of the $t\ell$ echoes with the results presented in Figs. 3, 4, 5. (As in Part I, we chose $\omega_{pe}/\omega_{ce} = 0.4$ and $c/a = 1120$, these being typical values for the UCLA Q machine.) Choices of ω_1, ω_2 for each case are given in Fig. 3, which may be compared with Fig. 2 to obtain the echo characteristics. (The hatched regions in Fig. 3 will be shown to be the regions wherein the pole 1 or pole 3 terms are significant.) Values of the poles v_i/a were obtained from Appendices C and D. Note that cases 1 and 2 are echoes at the sum frequency $(\omega_1 + \omega_2)$ whereas case 3 is an echo at the difference frequency $(\omega_1 - \omega_2)$.

In Fig. 4 we have drawn the appropriate saddle point contour for each case. Recall from Part I that for $0 < \omega_1 < \omega_{ce}$ the free-streaming pole appeared on the "wrong" side of the contour and therefore never contributed to the final response (see Fig. 5 of Part I). For the echo calculation, poles 1 and 3 also appear on the "wrong" side of the contour for $0 < \omega_1 < \omega_{ce}$ and $0 < \omega_3 < \omega_{ce}$, respectively; the "right" side of the contour being that for which the pole 1 term contributes for $z < z_o$ and the pole 3 term contributes for $z > z_o$. However, in the echo case the primitive v_z contour is deformed upward, say, for $z < z_o$, and downward for $z > z_o$, so a pole will always be enclosed somewhere, even if it is on the "wrong" side. In those cases where pole 1 or pole 3 is past the end of the contour in Fig. 4 we mean that the pole occurs at some v_i where $|v_i| \simeq c$ and therefore the corresponding pole term is insignificant because the exponential factor $\exp(-v_i^2/a^2)$ [in (4.9)] is zero for all practical purposes. Note that any pure imaginary poles (as in case 1) never come near the saddle

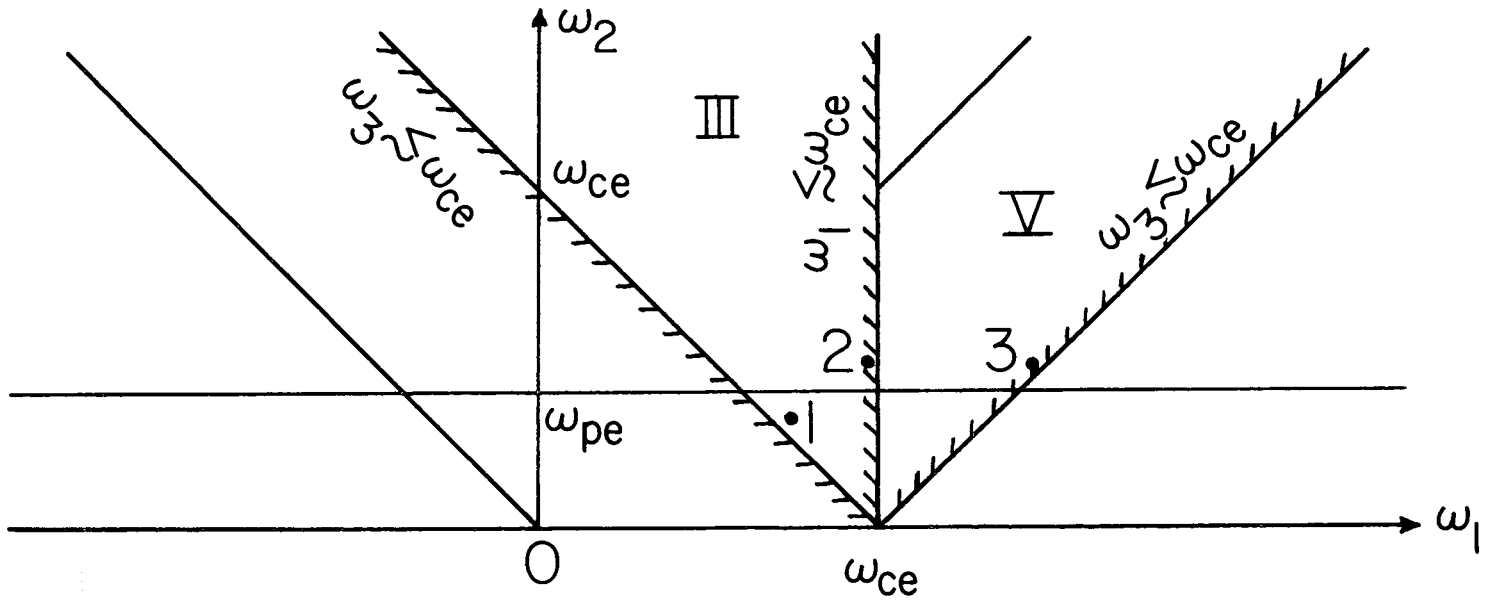

FIGURE 3. PARAMETER VALUES FOR THREE CASES OF $t\ell$ ECHOES.

(ω_{pe}/ω_{ce} = .4, c/a = 1120)

	ω_1/ω_{ce}	V_1/a	ω_2/ω_{pe}	V_2/a	S	ω_3/ω_{ce}	V_3/a
CASE 1	.75	274-iδ	.8	i2.04	+	1.07	i68.7
CASE 2	.994	1.21-i.205	1.2	2.59-i.142	+	1.474	410-iδ
CASE 3	1.474	410-iδ	1.2	2.59+i.142	-	.994	1.21-i.205

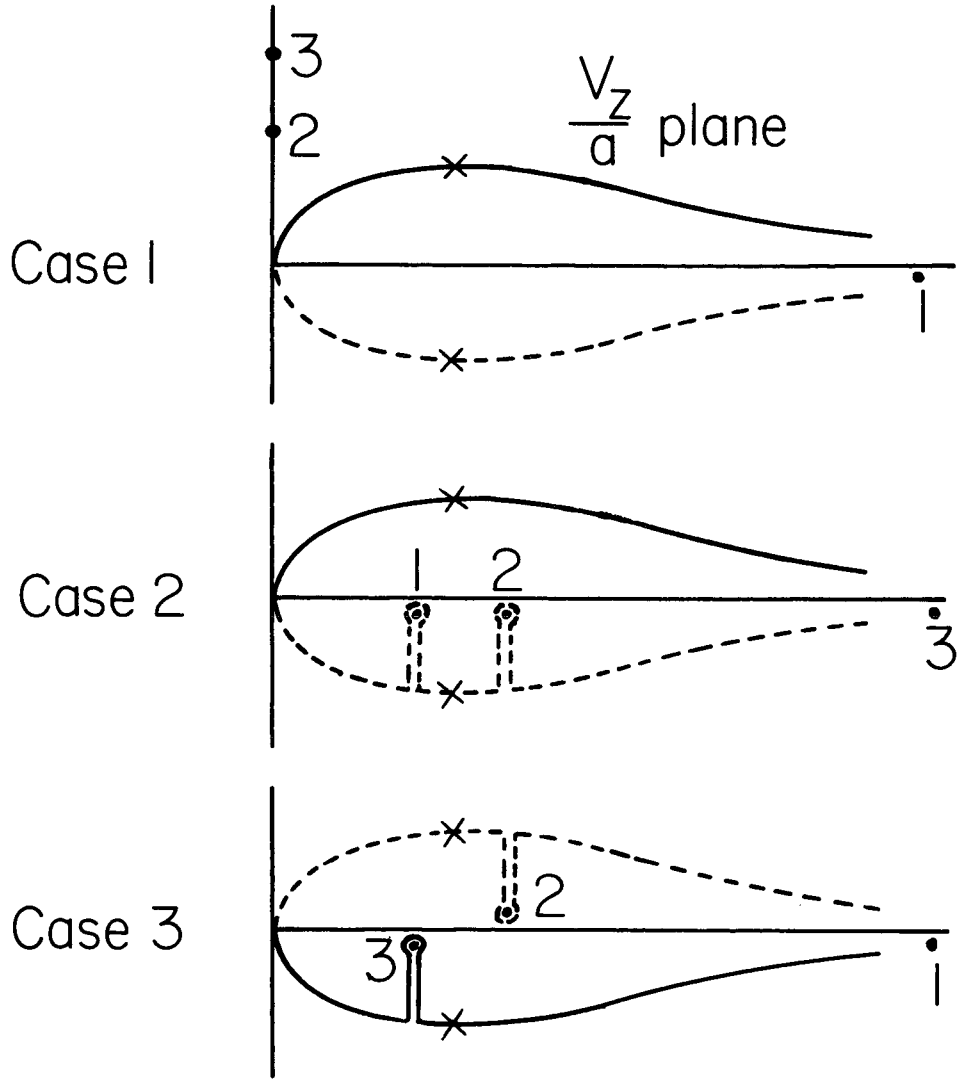

FIGURE 4. SADDLE-POINT CONTOURS FOR THE THREE ECHO CASES OF FIGURE 3.

In each case the primitive contour in the complex v_z/a plane (the real axis for $0 \leq \text{Re } v_z \leq c$) has been deformed to the appropriate saddle-point contour for $z \leq z_o$ (solid line) and $z \geq z_o$ (dashed line). The saddle points are indicated by X's and the three poles by dots.

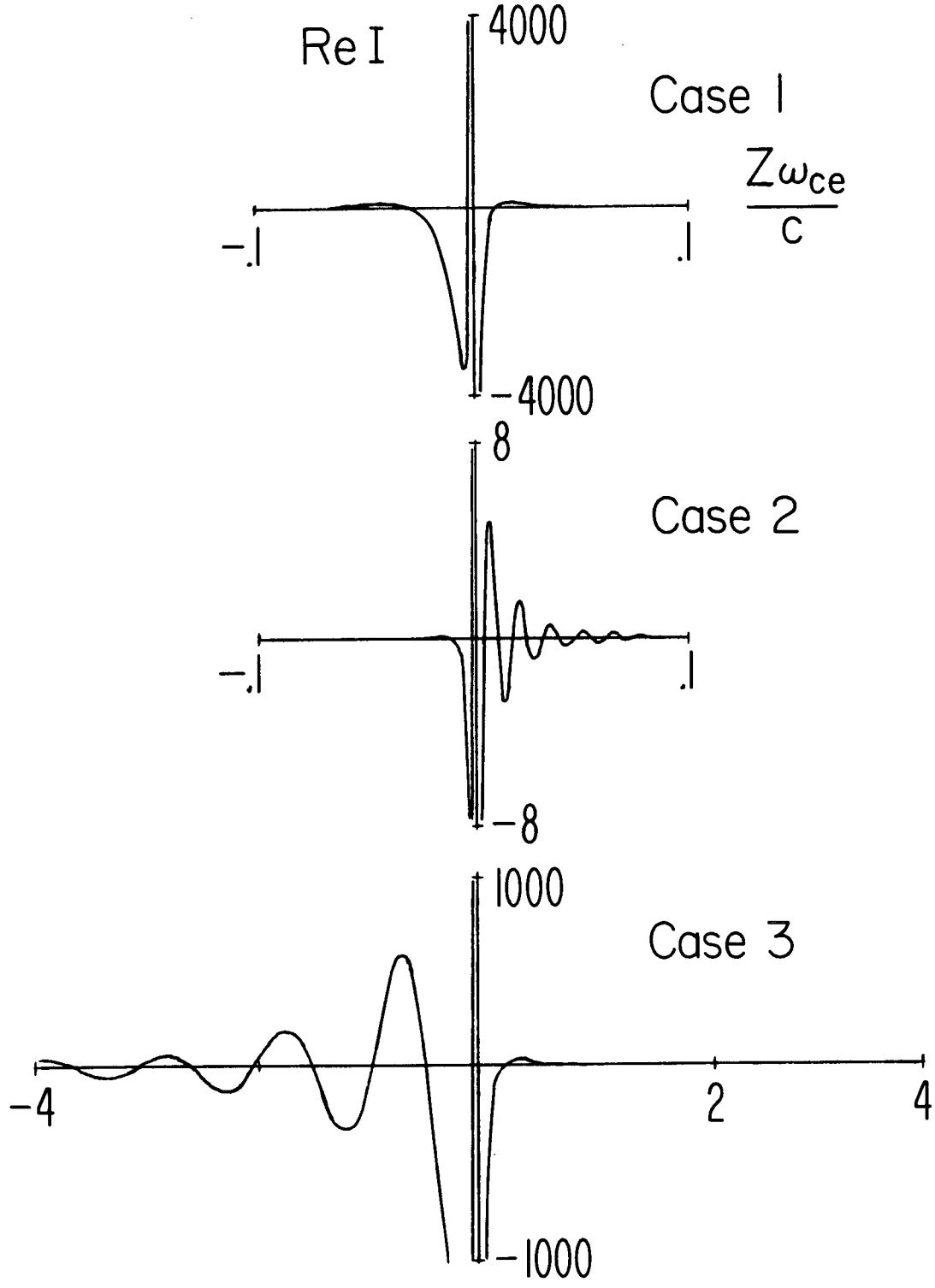

FIGURE 5. TRANSVERSE ECHO SHAPES FOR THE THREE CASES OBTAINED BY EVALUATING (4.8),(4.9) NUMERICALLY. ($L\omega_{ce}/c = 10$)

point contours.

In Fig. 5 we display numerical results of echo shapes for the three cases. From (4.3) we see that $J_x \sim \mathrm{Re}\ I$ and in Fig. 5 we have plotted

$$\mathrm{Re}\, I = \mathrm{Re}\left[I_{\substack{SADDLE \\ POINT}} + \sum_{i=1}^{3} I_{POLE\ i} \right] \tag{4.15}$$

against zc/ω_{ce} using (4.8), (4.9). For these calculations we chose $Lc/\omega_{ce} = 10$. (For the typical value $\omega_{ce}/2\pi = 2.25$ GHz, $c/\omega_{ce} \simeq 2$ cm, and $L \simeq 20$ cm.) We note the following results:

CASE 1. There are no pole contributions so the echo shape is determined entirely by the saddle point contribution. The echo width is large (compared to a/ω_{ce}) because the saddle point term's characteristic length $|a/\omega_3 - \omega_{ce}|$ is relatively large (because $\omega_3 \simeq \omega_{ce}$). Also the amplitude is relatively large because the dominant term in $A_1(v_s)$, i.e.,

$$\left| ik_3(z_0 - L) \right| = \frac{\frac{Lc}{\omega_{ce}}}{\frac{v_i}{a}} \left| \left(\frac{\omega_1}{\omega_{ce}} - 1 \right) \frac{c}{a} \right| \tag{4.16}$$

[see (4.13), (4.14)] is $\simeq c/a$ (because $\omega_1 \neq \omega_{ce}$).

CASE 2. There are contributions from the saddle-point, pole 1, and pole 2 terms. The saddle-point term exhibits a very narrow peak because $|a/\omega_3 - \omega_{ce}| \simeq a/\omega_{ce}$ (because $\omega_3 \neq \omega_{ce}$). Also the amplitude of the saddle-point term is relatively small because the dominant term in $A_1(v_s)$, i.e., (4.16), is relatively small (because $\omega_1 \simeq \omega_{ce}$). Both the pole 1 and pole 2 terms occur on the $z > z_0$ side of the echo

but since the pole 2 term is much smaller than the pole 1 term (primarily because $\exp[-v_2^2/a^2] \ll \exp[-v_1^2/a^2]$), only the pole 1 term makes a visible contribution in Fig. 2. The amplitudes of both pole terms are also governed by the dominant term of $A_1(v_i)$, i.e., (4.16), which for this case is relatively small (because $\omega_1 \simeq \omega_{ce}$).

CASE 3. There are contributions from the saddle-point, pole 2, and pole 3 terms. The echo frequency ω_3 is just below the cyclotron frequency and the resultant echo has a large amplitude and an extensive width. Both the amplitude and width of the saddle-point term are large because both $|a/\omega_3-\omega_{ce}|$ and $|ik_3(z-L)|$ [i.e., (4.16)] are relatively large. Similarly the pole 3 term has a large amplitude and penetration length. The pole 2 term occurs on the $z > z_o$ side of the echo, but it is not visible in Fig. 5 because it is much smaller than the pole 3 term (since $\exp[-v_2^2/a^2] \ll \exp[-v_3^2/a^2]$).

4.3 Physical meaning of the echo terms and where they are important.

The saddle-point term (4.8) represents phase mixing of the free-streaming waves that comprise the echo. This term is always significant in the echo peak region, which is centered at $z = z_o$ and which has a characteristic width or order $|a/\omega_3-\omega_{ce}|$.

The pole 1, 2, 3 terms in (4.9) represent the collective effects of the plasma in response to the free-streaming terms that result respectively from the ω_1 excitation, the ω_2 excitation, and the effective ω_3 excitation. We emphasize that only the free-streaming terms enter the echo calculation; i.e., velocity-dependent free-

streaming terms [in $f_1(z,\underline{v},t)$ and $E_1(z,t)$] of the form $\exp[i(\omega/v_z)z]$ contribute to the echo whereas collective oscillations of the form $\exp[ik_1 z]$ (where k_1 is a fixed complex number) do not. An important consequence of this is that the collective oscillations of f_1 for the first excitation at ω_1 [as given in (2.73) of Part I] may persist past the echo position since they do not interfere with the established echo at ω_3 or produce any new echoes.

We now determine for what values of ω_1, ω_2, ω_3 the corresponding pole terms are significant in comparison to the saddle-point term. The size of a pole term is determined predominantly by the size of the factor $\exp[-v_i^2/a^2]$ which (for $|\text{Re } v_i| >> |\text{Im } v_i|$) is very small for $|v_i|/a \gtrsim 3$ say, and therefore the pole terms are significant only for $|v_i|/a \lesssim 3$. For the pole 2 term we consider the least-damped root of $\varepsilon_\ell(k,\omega) = 0$ as discussed in Appendix D. For $|\omega_2| < \omega_{pe}$ the root is pure imaginary and no pole term results. For $|\omega_2| > \omega_{pe}$ the root is complex, but only for $|\omega_2| \gtrsim 1.08\ \omega_{pe}$ is $|\omega/''k''a| = |v_2/a| \lesssim 3$ (see Fig. D-1). Thus only for $|\omega_2| \gtrsim 1.08\ \omega_{pe}$ is the pole 2 term significant . Similarly for the pole 1 and pole 3 terms we consider the least-damped roots of $\varepsilon_T(k,\omega) = 0$ as discussed in Appendix C. From Fig. C-2, we note that $|\omega-\omega_{ce}/''k''a| = |v_i/a| \lesssim 3$ only if $\omega \approx \omega_{ce}$. Thus the pole 1 and pole 3 terms are significant only if ω_1 or ω_3 is very close to ω_{ce} (as shown by the hatched regions in Fig. 3).

Finally, in evaluating (4.4) we consider the $1/v_z^3$ factor which causes the echo amplitude to diverge at $z = z_o$. This behavior also appears in the saddle point term (4.5) because, as given by (4.6),

$v_s \to 0$ as $z \to z_o$. The $1/v_z^3$ factor in (4.4) is presumably due to three factors of $1/v_z$: one for the excitation at ω_1 [see the free-streaming part of (2.73) in Part I], one for the excitation at ω_2 [see (2.47)], and one for the echo response at ω_3. Recall that for the single transverse excitation in Part I, the free-streaming term diverged at $z = 0$ (as explained in Section 5.2 of Part I). For similar reasons the echo diverges at $z = z_o$. In the next section we shall show that Fokker-Planck collisions and/or finite-width excitation mechanisms remove this divergence at $z = z_o$.

5. Effects of Fokker-Planck Collisions and Finite-Width Excitation Mechanisms.

We first discuss the effects of collisions and finite widths in the excitation mechanisms from a physical point of view. Recall from Part I that for a single transverse excitation, the inclusion of a finite z dependence in $\underline{E}_{ext}(z,t)$ reduced the amplitude of the free-streaming term and also removed its divergence at $z = 0$. Physical reasons for the removal of this divergence were given in Section 5.2 of Part I. For similar reasons we shall find in the echo case that inclusion of finite z dependence for the $\mathcal{T}$ excitation and/or the $\mathcal{L}$ excitation effectively removes the divergence of the echo response at its peak $z = z_o$.

When velocity-dependent collisions are taken into account, we can make the following physical picture. We consider delta-function excitation mechanisms. Then we note the echo problem as derived above reduced essentially to the consideration of free-streaming waves that propagate in one direction (the z direction). Since $\underline{B}_o = B_o \hat{e}_z$, the particles that comprise these waves have helical orbits that are confined to lie along the z direction. Each free-streaming wave has a definite wavelength and is characterized by the velocity v_z of the particles that comprise the wave. The effect of long-range collisions (such as Coulomb collisions) is principally to "slide" the particles along the field lines. Thus collisions can effectively spatially reorient the particles in a particular free-streaming wave. And those particles that suffer collisions may no longer be in phase with the wave. In the limit of many collisions there results a mixture of free-

streaming particles with uncorrelated phases so no net wave is discernible.

The Fokker-Planck collision term, when Coulomb collisions are considered, is particularly effective in destroying those free-streaming waves whose particles have velocities near $v_z = 0$. Since these are the particles that cause the divergence of the echo at its peak, we find that the aforementioned collisions are effective in eliminating this divergence.

We now compute these collisional effects using the Fokker-Planck equation

$$\frac{\partial f_1}{\partial t} + \underline{v}\cdot\frac{\partial f_1}{\partial \underline{x}} - \Omega\frac{\partial f_1}{\partial \phi} + \frac{q}{m}\left[\underline{E}_{1,TOTAL} + \frac{1}{c}\underline{v}\times\underline{B}_{1,TOTAL}\right]\cdot\frac{\partial f_0}{\partial \underline{v}} = F.P.\{f_1\}$$

$$F.P.\{f_1\} = -\frac{\partial}{\partial v}\{D_1 f\} + \frac{\partial^2}{\partial v^2}\{D_2 f_1\} \tag{5.1}$$

where D_1 and D_2 are the frictional force and diffusion coefficients respectively. Considering a single transverse excitation, we recall that the free-streaming part of f_1 goes like

$$f_1(z, v_z, t) \sim e^{i\left(\frac{\omega_1 - \omega_{ce}}{v_z}\right)z - i\omega_1 t} \tag{5.2}$$

[see (2.73) of Part I]. When the Fokker-Planck operator acts on this f_1 we find

$$\frac{\partial}{\partial v_z}\{D_1 f_1\} = \frac{\partial D_1}{\partial v_z} f_1 + D_1 f_1\left\{\frac{-i(\omega_1 - \omega_{ce})z}{v_z^2}\right\}$$

$$\frac{\partial^2}{\partial v_z^2}\left\{D_2 f_1\right\} = \frac{\partial^2 D_2}{\partial v_z^2} f_1 + \frac{\partial D_2}{\partial v_z} f_1 \left\{\frac{-2i(\omega_1-\omega_{ce})Z}{v_z^2}\right\}$$

$$+D_2 f_1\left\{\frac{2i(\omega_1-\omega_{ce})Z}{v_z^3}\right\} \underline{- D_2 f_1\left\{\frac{(\omega_1-\omega_{ce})^2 Z^2}{v_z^4}\right\}} \qquad (5.3)$$

Since generally

$$\left|\frac{\partial D_i}{\partial v}\right| \leq \left|\frac{D_i}{v}\right| \qquad \left|\frac{\partial^2 D_i}{\partial v^2}\right| \leq \left|\frac{D_i}{v^2}\right| \qquad (5.4)$$

(i = 1,2) we conclude that the underlined term in (5.3) is the dominant term in F.P. $\{f_1\}$ provided

$$\left|\frac{(\omega_1-\omega_{ce})Z}{v_z}\right| \gg 1 \qquad (5.5)$$

Thus we may write

$$F.P.\left\{f_1\right\} = -\nu_{eff} f_1$$

$$\nu_{eff} = \left[\frac{D_2(\omega_1-\omega_{ce})^2}{v_z^4}\right] Z^2 \qquad (5.6)$$

provided (5.5) holds.

Now assume that $\underline{E}_{1\ \mathrm{TOTAL}}$ and $\underline{B}_{1\ \mathrm{TOTAL}}$ damp away in a small distance d . Then for z > d and $z \gg |a/\omega_1-\omega_{ce}|$ [so (5.5) holds] we may rewrite the Fokker-Planck equation (5.1) as

$$\frac{\partial f_1}{\partial t} + v_z \frac{\partial f_1}{\partial z} - \Omega \frac{\partial f_1}{\partial \phi} = - \nu_{eff} f_1 \tag{5.7}$$

Recalling that $f_1 \sim e^{i\phi}$ and Laplace transforming (5.7), we find

$$\frac{\partial f_1}{\partial z} = i\left(\frac{\omega_1 - \omega_{ce}}{v_z}\right) f_1 - \left(\frac{\nu_{eff}}{v_z}\right) f_1 \tag{5.8}$$

where we have assumed $f_1(t=0) = 0$. Equation (5.8) has the solution

$$f_1(z) = f_1(z=0)\, e^{i\left(\frac{\omega_1 - \omega_{ce}}{v_z}\right) z - \int_0^z \frac{\nu_{eff}(z')}{v_z} dz'} \tag{5.9}$$

Thus we have derived an equation which gives $f_1(z)$ in terms of the initial spatial value $f_1(z=0)$. This derivation [(5.7) - (5.9)] parallels that of O'Neil[30] for the temporal longitudinal case.

Thus in the echo calculation (specifically for ℓ echoes), the free-streaming term f_1 acquires the factor

$$e^{-\int_0^z \left[\frac{D_z (\omega_1 - \omega_{ce})^2}{v_z^5}\right] z'^2 dz'}$$

over the range $0 \leq z \leq L$. For $z > L$ we have, in place of (5.2),

$$f_1 \sim e^{i\left(\frac{\omega_1 - \omega_{ce}}{v_z}\right) L + i\left(\frac{\omega_3 - \omega_{ce}}{v_z}\right)(z - L)} \tag{5.10}$$

and therefore, in place of (5.6),

$$\nu_{eff} = D_z \left[\frac{(\omega_1 - \omega_{ce}) L}{v_z^2} + \frac{(\omega_3 - \omega_{ce})}{v_z^2}(z - L)\right]^2 \tag{5.11}$$

Thus for $\mathcal{TL}$ echoes, the integrand of (4.4) should include the factor

$$e^{-\int_0^L \left[\frac{D_2(\omega_1-\omega_{ce})^2}{V_z^5}\right] z'^2 dz' - \int_L^z \left[\frac{D_2\{(\omega_1-\omega_{ce})L + (\omega_3-\omega_{ce})(z'-L)\}^2}{V_z^3}\right] dz'} \tag{5.12}$$

If D_2 does not depend on z we may perform the integrals in (5.12) to obtain the factor

$$e^{-D_2\left[\frac{(\omega_1-\omega_{ce})^2 5\omega_2}{3V_z^5(\omega_3-\omega_{ce})}\right]L^3} \tag{5.13}$$

in the neighborhood of the echo peak. In obtaining (5.13) we used

$$(z-L) \approx (z_0-L) = -\frac{k_1}{k_3}L = -\frac{(\omega_1-\omega_{ce})}{(\omega_3-\omega_{ce})}L$$

The factor (5.13) represents the effects of Fokker-Planck collisions. (Numerical examples will be given later.)

To investigate the effects of finite-width excitation mechanisms we assume the excitation fields are given by (2.11) with

$$E_i(z) = \Phi_i \frac{e^{-\frac{z^2}{\Delta_i^2}}}{\sqrt{\pi}\,\Delta_i} \tag{5.14}$$

(i = 1,2) so

$$E_i(k) = \Phi_i\, e^{-\frac{k^2\Delta_i^2}{4}} \tag{5.15}$$

Thus the integrand of (4.4) should include the factor

$$e^{-\frac{(\omega_1-\omega_{ce})^2\Delta_1^2}{4v_z^2}-\frac{(s\omega_2)^2\Delta_2^2}{4v_z^2}} \tag{5.16}$$

Combining the above results we find that when both Fokker-Planck collisions and finite-width excitation mechanisms are taken into account, (4.4) should be replaced by

$$I=\int_0^\infty \frac{\frac{dv_z}{a}A_1(v_z)e^{i\frac{(\omega_3-\omega_{ce})(z-z_0)}{v_z}-\frac{\Delta^2}{v_z^2}-\frac{\gamma D_z(v_z)}{v_z^5}-\frac{v_z^2}{a^2}}}{\sqrt{\pi}\left(\frac{v_z}{a}\right)^3\epsilon_{T_\alpha}\left(\frac{\omega_1-\omega_{ce}}{v_z},\omega_1\right)\epsilon_{l_s}\left(\frac{s\omega_2}{v_z},s\omega_2\right)\epsilon_{T_\beta}\left(\frac{\omega_3-\omega_{ce}}{v_z},\omega_3\right)} \tag{5.17}$$

where

$$\Delta^2=\left[\frac{(\omega_1-\omega_{ce})^2\Delta_1^2}{4}+\frac{\omega_2^2\Delta_2^2}{4}\right]$$

$$\gamma=\left[\frac{(\omega_1-\omega_c)^2 s\omega_2 L^3}{3(\omega_3-\omega_{ce})}\right] \tag{5.18}$$

For Coulomb collisions the Fokker-Planck diffusion coefficient as derived by Thompson[31] may be put in the form

$$D_z(v_z)=-\frac{4\pi n q^4 a^2}{m^2}\ln\Lambda\,\frac{1}{v_z}\frac{\partial}{\partial v_z}\left[\frac{1}{v_z}\,erf\left(\frac{v_z}{a}\right)\right] \tag{5.19}$$

Using the series representation[32]

$$erf(z)=\frac{2}{\sqrt{\pi}}\left\{z-\frac{z^3}{3}+\cdots\right\} \qquad |z|\ll 1$$

and the asymptotic series[32]

$$erf(z) = 1 - \frac{e^{-z^2}}{\sqrt{\pi}\, z} + \cdots \qquad |z| \gg 1$$

we find

$$D_2(v_z) \approx \left[\frac{4\pi n q^4 \ln\Lambda}{m^2 a}\right]\frac{4}{3\sqrt{\pi}} \qquad \frac{|v_z|}{a} \ll 1 \tag{5.20a}$$

$$D_2(v_z) \approx \left[\frac{4\pi n q^4 \ln\Lambda}{m^2 a}\right]\left(\frac{a}{v_z}\right)^3 \qquad \frac{|v_z|}{a} \gg 1 \tag{5.20b}$$

The integrand of (5.17) is now so complicated that in general it is only feasible to evaluate the integral by numerically integrating along the real axis in the complex v_z/a plane. However, we can make the following useful comments.

Evaluation of (5.17).

If (5.17) is evaluated by the saddle-point method, then the pole terms that occur are no more difficult to evaluate than earlier. Since each pole occurs at a single fixed point in the complex v_z/a plane, we note that the i^{th} pole term in (4.9) simply acquires an additional factor of

$$e^{-\frac{\Delta^2}{v_i^2} - \frac{\gamma D_2(v_i)}{v_i^5}} \tag{5.21}$$

To obtain a usable result, we assume $|v_z| >> a$ so we may use (5.20b). Then the factor (5.21) is

$$e^{-\frac{\Delta^2}{v_i^2} - \frac{F}{(v_i/a)^8}} \tag{5.22}$$

where

$$F = \left[\frac{4\pi n q^4 \ln\Lambda}{m^2 a^6}\right]\left[\frac{(\omega_1-\omega_{ce})^2 5\omega_2 L^3}{3(\omega_3-\omega_{ce})}\right] \tag{5.23}$$

We shall evaluate F for a numerical example, but first we consider the saddle points of $e^{\phi(z)}$ where

$$\phi(v_z) = i\frac{(\omega_3-\omega_{ce})(z-z_o)}{v_z} - \frac{\Delta^2}{v_z^2} - \frac{\gamma D_2(v_z)}{v_z^5} - \frac{v_z^2}{a^2} \tag{5.24}$$

We note immediately that even when the v_z dependence of D_2 is neglected, the equation that defines the saddle points, $\frac{\partial}{\partial v_z}\{\phi(v_z)\} = 0$, is a seventh degree polynomial. It is apparent that it is worthwhile to use the method of steepest descent now only in special limiting cases. For example, it would be useful to know the height of the echo peak. Thus setting $z = z_o$ we shall investigate the limits when (i) collisions effects are dominant, and (ii) when finite-width effects are dominant.

(i) Collisional effects dominant.

If we have

$$\left|\frac{\Delta^2}{v_s^2}\right| \ll \left|\frac{v_s^2}{a^2}\right| \tag{5.25}$$

where v_s is a saddle point to be chosen, then

$$\phi(v_s) \approx -\frac{\gamma D_2(v_z)}{v_z^5} - \frac{v_z^2}{a^2} \tag{5.26}$$

To proceed we assume $|v_z| >> a$, then using (5.20b), we find the appropriate saddle point to be

$$\frac{v_s}{a} = (4F)^{\frac{1}{10}} \tag{5.27}$$

where F is defined by (5.23). Accordingly we obtain

$$I(z=z_0) \approx \frac{A_1(v_s)\, e^{-1.65 F^{\frac{1}{5}}}}{\sqrt{9}\left(\frac{v_s}{a}\right)^3 \epsilon_{T_\alpha}\left(\frac{\omega_1-\omega_{ce}}{v_s}, \omega_1\right) \epsilon_{\ell_s}\left(\frac{s\omega_2}{v_s}, s\omega_2\right) \epsilon_{T_\beta}\left(\frac{\omega_3-\omega_{ce}}{v_s}, \omega_3\right)} \tag{5.28}$$

where we have evaluated the constant $5/4^{4/5} \approx 1.65$. If instead $|v_z| << a$, then using (5.20b) we find the appropriate saddle point to be

$$\frac{v_s'}{a} = \left(\frac{10}{3\sqrt{\pi}} F\right)^{\frac{1}{7}} \tag{5.29}$$

and

$$I(z=z_0) \approx \frac{A_1(v_s)\, e^{-1.82 F^{\frac{2}{7}}}}{\sqrt{7}\left(\frac{v_s'}{a}\right)^3 \epsilon_{T_\alpha}\left(\frac{\omega_1-\omega_{ce}}{v_s'}, \omega_1\right) \epsilon_{\ell_s}\left(\frac{s\omega_2}{v_s'}, s\omega_2\right) \epsilon_{T_\beta}\left(\frac{\omega_3-\omega_{ce}}{v_s'}, \omega_3\right)} \tag{5.30}$$

where we have evaluated the constant $\frac{7}{5}\,(10/3\sqrt{\pi})^{2/7} \approx 1.82$.

Summarizing these results, we find from (5.22), (5.28), and (5.30) that Coulomb collisions decrease the size of the pole terms and the saddle point term (at the echo peak) according to the factors, roughly

$$\text{POLE TERMS} \qquad e^{-\frac{F}{(v_i/a)^8}} \tag{5.31a}$$

$$\text{ECHO PEAK} \begin{cases} e^{-F^{\frac{1}{5}}} & (4F)^{\frac{1}{10}} \gtrsim 2 \qquad (5.31b) \\ e^{-F^{\frac{2}{7}}} & \left(\frac{10}{3\sqrt{7}}F\right)^{\frac{1}{7}} \ll 1 \qquad (5.31c) \end{cases}$$

For the parameter values used earlier ($\omega_{pe}/\omega_{ce} = 0.4$, $c/a = 1120$, $n = 10^{10}\ cm^{-3}$), we calculate F from (5.23) to be

$$F = 3\cdot 10^{4}\left[\frac{\left(\frac{\omega_1}{\omega_{ce}}-1\right)\frac{\omega_{pe}}{\omega_{ce}}}{\left|\frac{\omega_3}{\omega_{ce}}-1\right|}\right]\left(\frac{L\omega_{ce}}{c}\right)^{3} \qquad (5.32)$$

Then using values of ω_1, ω_2, ω_3 as given in Fig. 3, we find

$$F = (2\cdot 10^{4})\left(\frac{L\omega_{ce}}{c}\right)^{3} \qquad \text{CASE 1}$$

$$(3)\left(\frac{L\omega_{ce}}{c}\right)^{3} \qquad \text{CASE 2}$$

$$(1.3\times 10^{6})\left(\frac{L\omega_{ce}}{c}\right)^{3} \qquad \text{CASE 3}$$

Thus if $(L\omega_{ce}/c) = 10$ the echo will be essentially destroyed in all three cases. However, if $(L\omega_{ce}/c) = 1$, the case 2 echo would be clearly visible. Thus for the parameters under consideration, transverse echoes could be seen, but only for small values of $(L\omega_{ce}/c)$. Of course, since $F \sim n/T_e^{3}$, collisional effects could be reduced substantially by going to higher temperatures or lower densities.

(ii) Finite-width effects dominant.

We return to our consideration of (5.24). If

$$\left| \frac{\gamma D_2(v_s)}{v_s^5} \right| \ll \left| \frac{v_s^2}{a^2} \right| \tag{5.33}$$

where v_s is a new saddle point to be determined, then

$$\phi(v_z) \approx -\frac{\Delta^2}{v_z^2} - \frac{v_z^2}{a^2} \tag{5.34}$$

and the appropriate saddle point is

$$\frac{v_s}{a} = \sqrt{\frac{\Delta}{a}} \tag{5.35}$$

and

$$I(z=z_0) \approx \frac{A_1(v_s)\, e^{-\left[\frac{(\omega_1-\omega_{ce})^2\Delta_1^2}{a^2} + \frac{\omega_2^2\Delta_2^2}{a^2}\right]^{\frac{1}{2}}}}{\sqrt{\frac{\pi}{2}}\left(\frac{v_s}{a}\right)^3 \epsilon_{T_\alpha}\left(\frac{\omega_1-\omega_{ce}}{v_s}, \omega_1\right) \epsilon_{l_s}\left(\frac{s\omega_2}{v_s}, s\omega_2\right) \epsilon_{T_\beta}\left(\frac{\omega_3-\omega_{ce}}{v_s}, \omega_3\right)} \tag{5.36}$$

which may be compared with (7.17) of Part I for the single transverse excitation. Note that even if Δ_1 or Δ_2 is zero, the result (5.36) still holds.

6. Effects of Temperature Anisotropy ($T_\perp \neq T_z$)

We return to the collisionless transverse echo case and investigate the consequences of having $T_\perp \neq T_z$. Assuming an anisotropic Maxwellian distribution

$$f_o(\underline{v}) = f_o(v_z) f_o(v_\perp) = \left[\frac{e^{-\frac{v_z^2}{a^2}}}{\sqrt{\pi}\, a}\right]\left[\frac{e^{-\frac{v_\perp^2}{b^2}}}{\pi b^2}\right] \tag{6.1}$$

(where $a = \sqrt{2\kappa T_z/m}$, $b = \sqrt{2\kappa T_\perp/m}$), and carefully reviewing the derivation for tl and lt echoes, we find that only the following modifications are required:

(i) tl CASE: replace $f_o(v_z)$ in (2.41) by

$$f_o(v_z)\left[1 - \frac{k_1 v_z}{\omega}\left(1 - \frac{T_\perp}{T_z}\right)\right]$$

(ii) lt CASE: no change.

(iii) $\varepsilon_l(k,\omega)$: no change.

(iv) $\varepsilon_T(k,\omega)$: has already been given for $T_\perp \neq T_z$ in (2.40) of Part I. The roots of $\varepsilon_{T_+}(k,\omega) = 0$ for real ω, complex k, and $T_\perp \neq T_z$ are discussed in Appendix C in (C.45) - (C.54).

Thus for electron echoes in the tl case, there is an additional amplitude factor of

$$\left[1 - \left(\frac{\omega_1 - \omega_{ce}}{\omega_1}\right)\left(1 - \frac{T_\perp}{T_z}\right)\right] \tag{6.2}$$

and for the lt case, there is no change.

The only significant difference from the previous echo results

comes from the possibility of having different dispersion characteristics for the transverse waves. In Appendix C, we conclude that for $\omega \neq 0$ there is no appreciable change in the positions of the roots of $\varepsilon_{T_+}(k,\omega) = 0$ from their positions in the isotropic case. Thus for $\omega \neq 0$, there is essentially no change in the echo results given earlier. On the other hand, if $\omega \approx 0$ and there is a temperature anisotropy, then the fire-hose instability may occur. [We obtain the usual criterion for the onset of this instability in (C.53).]

Thus a novel use of echoes is suggested and that is to choose ω_1 to be in a stable region and ω_3 to be in an unstable region so only the echo would excite the instability. Use of an echo to examine instabilities has the advantage that at the position at which the instability is excited, i.e., the echo position, there is no external excitation mechanism (grids or current loops, etc.) to be considered.

7. Effects of Propagation Just Off-Axis ($k_\perp \neq 0$)

Up to now, we have considered all waves to be propagating exactly along the direction of $\underline{B}_o$. In an actual experiment, this may be difficult to attain and undoubtedly the excitations will produce waves that propagate slightly off-axis so $k_\perp$ would be small but non-zero. We now investigate the consequences of having such slightly-off-axis wave excitations.

Consider the longitudinal excitation first. If the excitation is made slightly off-axis, then the $\underline{E}_{TOTAL}$ field of the wave it produces will have mainly a z component, but also small x and y components. Thus

$$\underline{E}_{TOTAL} = \hat{e}_x \delta_x + \hat{e}_y \delta_y + e_z E \tag{7.1}$$

where δ represents the small transverse electric field ($|\delta| \ll |E|$). As shown in Appendix A, the corresponding driving term for the first order Vlasov equation is [for isotropic $f_o(\underline{v})$]

$$g(\phi+\phi') = \frac{q}{m}\left\{ \delta_x \frac{\partial f_o}{\partial v_\perp} \cos(\phi+\phi') - \delta_y \frac{\partial f_o}{\partial v_\perp} \sin(\phi+\phi') + E \frac{\partial f_o}{\partial v_z} \right\} \tag{7.2}$$

which is to be used in (A.5), i.e.,

$$f_1(v_z, v_\perp, \phi) = \frac{e^{i\lambda \sin\phi}}{\left(e^{i2\pi\nu} - 1\right)\Omega_z} \int_0^{2\pi} d\phi'\, g(\phi+\phi')\, e^{i\nu\phi' - i\lambda \sin(\phi+\phi')} \tag{7.3}$$

where

$$\lambda = \frac{k_\perp v_\perp}{\Omega_z}$$

$$\nu = \frac{\omega - k_z v_z}{\Omega_z} \tag{7.4}$$

Thus

$$f_1(v_z, v_\perp, \phi) = \frac{g}{m} \frac{e^{i\lambda \sin\phi}}{\left(e^{i2\pi\nu} - 1\right)} \left\{ \delta_x \frac{\partial f_0}{\partial v_\perp} \frac{i}{\lambda} \frac{\partial}{\partial \phi} I + \delta_y \frac{\partial f_0}{\partial v_\perp} \frac{\partial}{\partial \lambda} I + E \frac{\partial f_0}{\partial v_z} I \right\} \tag{7.5}$$

where

$$I = \int_0^{2\pi} d\phi' e^{i\nu\phi' - i\lambda \sin(\phi + \phi')} \tag{7.6}$$

Using the Bessel function identity[32]

$$e^{-i\lambda \sin\phi} = \sum_{m=-\infty}^{+\infty} e^{-im\phi} J_m(\lambda) \tag{7.7}$$

together with

$$J_{-m}(x) = (-1)^m J_m(x) \qquad \text{n integer} \tag{7.8}$$

we find

$$I = \sum_{m=-\infty}^{+\infty} e^{-im\phi} J_m(\lambda) \frac{e^{i(\nu - m)2\pi} - 1}{i(\nu - m)} \tag{7.9}$$

Then using the series expansion

$$J_n(x) = \frac{x^n}{2^n n!}\left\{1 - \frac{x^2}{4(n+1)} + \cdots\right\} \qquad \begin{matrix} \text{n integer} \\ \text{x real} \end{matrix} \tag{7.10}$$

we find that for $|\lambda| << 1$ (i.e., $|k_\perp|$ much less than the reciprocal of the gyroradius, $|v_\perp/\Omega_z|$)

$$f_1(\phi) \equiv f_1(v_z, v_\perp, \phi)$$

$$= \frac{q}{m\Omega i}\left\{\frac{1}{\nu}\left[\delta_y \frac{\partial f_0}{\partial v_\perp} i\left(-\frac{\lambda}{2}\right) + E\frac{\partial f_0}{\partial v_z}\left(1 - \frac{\lambda^2}{2}\right)\right]\right.$$

$$+\left(\frac{1}{\nu-1} + \frac{1}{\nu+1}\right)\left[\delta_x \frac{\partial f_0}{\partial v_\perp}\left(\frac{\lambda}{4}\right) + \delta_y \frac{\partial f_0}{\partial v_\perp} i\left(\frac{\lambda}{4}\right) + E\frac{\partial f_0}{\partial v_z}\left(\frac{\lambda^2}{4}\right)\right]$$

$$+\left(\frac{e^{i\phi}}{\nu} - \frac{e^{-i\phi}}{\nu}\right)\left[\delta_y \frac{\partial f_0}{\partial v_\perp} i\left(\frac{-\lambda^2}{4}\right) + E\frac{\partial f_0}{\partial v_z}\left(\frac{\lambda}{2}\right)\right]$$

$$+\left(\frac{e^{-i\phi}}{\nu-1} - \frac{e^{+i\phi}}{\nu+1}\right)\left[\delta_x \frac{\partial f_0}{\partial v_\perp}\left(\frac{1}{2} - \frac{3\lambda^2}{16}\right) + \delta_y \frac{\partial f_0}{\partial v_\perp} i\left(\frac{1}{2} - \frac{5\lambda^2}{16}\right) + E\frac{\partial f_0}{\partial v_z}\left(\frac{\lambda}{2}\right)\right]$$

$$+\left(\frac{e^{-i\phi}}{\nu-2} + \frac{e^{+i\phi}}{\nu+2}\right)\left[\delta_x \frac{\partial f_0}{\partial v_\perp}\left(\frac{\lambda^2}{3}\right) + \delta_y \frac{\partial f_0}{\partial v_\perp} i\left(\frac{\lambda^2}{8}\right)\right]$$

$$+\left(\frac{e^{i2\phi}}{\nu} - \frac{e^{-i2\phi}}{\nu}\right)\left[E\frac{\partial f_0}{\partial v_z}\left(\frac{\lambda^2}{8}\right)\right]$$

$$-\left(\frac{e^{-i2\phi}}{\nu-1} + \frac{e^{+i2\phi}}{\nu+1}\right)\left[\delta_x \frac{\partial f_0}{\partial v_\perp}\left(\frac{\lambda}{4}\right) + \delta_y \frac{\partial f_0}{\partial v_\perp} i\left(\frac{\lambda}{4}\right) + E\frac{\partial f_0}{\partial v_z}\left(\frac{\lambda^2}{4}\right)\right]$$

$$+\left(\frac{e^{-i2\phi}}{\nu-2} - \frac{e^{+i2\phi}}{\nu+2}\right)\left[\delta_x \frac{\partial f_0}{\partial v_\perp}\left(\frac{\lambda}{4}\right) + \delta_y \frac{\partial f_0}{\partial v_\perp} i\left(\frac{\lambda}{4}\right) + E\frac{\partial f_0}{\partial v_z}\left(\frac{\lambda^2}{8}\right)\right]$$

$$
-\left(\frac{e^{-i3\phi}}{\nu-1}-\frac{e^{+i3\phi}}{\nu+1}\right)\left[\delta_x\frac{\partial f_o}{\partial v_\perp}\left(\frac{\lambda^2}{16}\right)+\delta_y\frac{\partial f_o}{\partial v_\perp}i\left(\frac{\lambda^2}{16}\right)\right]
$$

$$
-\left(\frac{e^{-i3\phi}}{\nu-2}-\frac{e^{+i3\phi}}{\nu+2}\right)\left[\delta_x\frac{\partial f_o}{\partial v_\perp}\left(\frac{\lambda^2}{8}\right)+\delta_y\frac{\partial f_o}{\partial v_\perp}i\left(\frac{\lambda^2}{8}\right)\right]
$$

$$
+\left(\frac{e^{-i3\phi}}{\nu-3}-\frac{e^{+i3\phi}}{\nu+3}\right)\left[\delta_x\frac{\partial f_o}{\partial v_\perp}\left(\frac{\lambda^2}{16}\right)+\delta_y\frac{\partial f_o}{\partial v_\perp}i\left(\frac{\lambda^2}{16}\right)\right]\Bigg\} \qquad (7.11)
$$

which is correct through terms of order λ^2 .

To zero order in λ we retain only the three underlined terms. If in addition $\delta = 0$, then only the double-underlined term remains

$$
f_1(\phi) = \frac{qE\,\frac{\partial f_o}{\partial v_z}}{mi(\omega - k_z v_z)} \qquad (7.12)
$$

in agreement with (2.46) obtained earlier. For $\delta \neq 0$ we include the single underlined terms

$$
f_1(\phi) = \frac{q}{m}\frac{1}{2i}\left(\frac{e^{-i\phi}}{\omega - k_z v_z - \Omega} - \frac{e^{+i\phi}}{\omega - k_z v_z + \Omega}\right)\frac{\partial f_o}{\partial v_\perp}\left(\delta_x + i\delta_y\right) \qquad (7.13)
$$

To first and second order in λ , we obtain the additional myriad of terms in (7.11). Considering the $e^{\pm in\phi}$ factors (where n is an integer), we note that as n increases, the terms become higher order in λ and therefore have smaller magnitudes (since $|\lambda| << 1$).

Knowing the ϕ dependence of f_1 , we proceed to find the ϕ dependence of $\underline{E}_{TOTAL}$. We need to know the ϕ dependence of both f_1 and

$\underline{E}_{TOTAL}$ to establish what types of echoes and other miscellaneous responses are generated by the new terms created by the off-axis excitation.

If we compute

$$\underline{J}_1 = nq \int f_1 \, \underline{v} \, d^3v \tag{7.14}$$

we find that $\underline{J}_1$ and $\underline{E}_{TOTAL}$ no longer obey a simple scalar relation but instead they obey

$$\underline{J}_1 = \underset{\sim}{\sigma} \cdot \underline{E}_{TOTAL} \tag{7.15}$$

where the elements of the conductivity tensor $\underset{\sim}{\sigma}$ could be extracted from (7.11) but this information is not needed for our present purposes. Noting that Maxwell's equations for the plasma fields give

$$\underline{E}_{PLASMA} (\omega^2 - k^2c^2) = -4\pi i \omega \underline{J}_1 \tag{7.16}$$

[as in (2.38) of Part I] and that $\underline{E}_{TOTAL} = \underline{E}_{PLASMA} + \underline{E}_{EXT}$, we find

$$\underset{\sim}{\epsilon} \cdot \underline{E} = \underline{E}_{ext} \tag{7.17}$$

where the dielectric tensor $\underset{\sim}{\epsilon}$ is

$$\underset{\sim}{\epsilon} = 1 + \frac{4\pi i \omega}{\omega^2 - k^2c^2} \underset{\sim}{\sigma} \tag{7.18}$$

Thus

$$\underline{E}_{TOTAL} = \underset{\sim}{\epsilon}^{-1} \cdot \underline{E}_{ext} \tag{7.19}$$

and it follows that in general $\underline{E}_{TOTAL}$ and $\underline{E}_{EXT}$ are not necessarily

parallel. Nonetheless, if the excitation is made just slightly off-axis, both $\underline{E}_{TOTAL}$ and $\underline{E}_{EXT}$ will be directed almost along the z direction.

Since [from (2.33) of Part I]

$$\underline{v}\, d^3v = \left[\hat{e}_+ \frac{v_\perp}{\sqrt{2}} e^{-i\phi} + \hat{e}_- \frac{v_\perp}{\sqrt{2}} e^{+i\phi} + \hat{e}_z v_z\right] v_\perp\, dv_\phi\, dv_z\, dv_\perp \tag{7.20}$$

the only terms of $f_1(\phi)$ that survive the ϕ integration in (7.14) are those with a ϕ dependence of $e^{\pm i\phi}$ or those with no ϕ dependence. Accordingly $\underline{J}_1$ has terms of the form

$$\hat{e}_\pm \left[\begin{array}{l}\text{terms of } f_1(\phi) \text{ that went as } e^{\pm i\phi}, \\ \qquad\qquad\qquad \text{such as (7.13)}\end{array}\right]$$

and

$$\hat{e}_z \left[\begin{array}{l}\text{terms of } f_1(\phi) \text{ that had no } \phi \text{ dependence}, \\ \qquad\qquad\qquad \text{such as (7.12)}\end{array}\right]$$

This spatial behavior of $\underline{J}_1$ eventually becomes the spatial behavior of $\underline{E}_{TOTAL}$ [via (7.16) - (7.19)] and we finally obtain [using (2.26) - (2.27) of Part I]

$$\underline{E}_{TOTAL} \cdot \frac{\partial}{\partial \underline{v}} \sim \left[\text{terms of } f_1(\phi) \text{ that had no } \phi \text{ dependence}\right] + e^{\pm i\phi}\left[\text{terms of } f_1(\phi) \text{ that went as } e^{\pm i\phi}\right] \tag{7.21}$$

In the right half of Table I, we have summarized the above results concerning the ϕ dependence of $f_1(\phi)$ and $\underline{E}_{TOTAL} \cdot \frac{\partial}{\partial \underline{v}}$ for a longitudinal excitation made slightly off-axis. If we repeat the derivation

	$\mathcal{T}$ EXCITATION	$\mathcal{L}$ EXCITATION
$f_1(\phi) \sim$	$1 \cdot (\delta + E\lambda + \ldots)$	$\underline{1 \cdot (E} + \delta\lambda + \ldots)$
	$\underline{e^{\pm i\phi} \cdot (E} + \delta\lambda + \ldots)$	$e^{\pm i\phi} \cdot (\delta + E\lambda + \ldots)$
	$e^{\pm i2\phi} \cdot (E\lambda + \delta\lambda^2 + \ldots)$	$e^{\pm i2\phi} \cdot (\delta\lambda + E\lambda^2 + \ldots)$
	$e^{\pm i3\phi} \cdot (E\lambda^2 + \ldots)$	$e^{\pm i3\phi} \cdot (\delta\lambda^2 + \ldots)$
	$\vdots$	$\vdots$
$\underline{E}_{total} \cdot \frac{\partial}{\partial \underline{v}} \sim$	$1 \cdot (\delta + E\lambda + \ldots)$	$\underline{1 \cdot (E} + \delta\lambda + \ldots)$
	$\underline{e^{\pm i\phi} \cdot (E} + \delta\lambda + \ldots)$	$e^{\pm i\phi} \cdot (\delta + E\lambda + \ldots)$

TABLE 1. THE ϕ DEPENDENCE OF $f_1(\phi)$ AND $\underline{E}_{total} \cdot \frac{\partial}{\partial \underline{v}}$ FOR SLIGHTLY OFF-AXIS $\mathcal{T}$ AND $\mathcal{L}$ EXCITATIONS.

For the $\mathcal{T}$ excitation $E = |(\underline{E}_{total})_\perp|$ and $\delta = |(\underline{E}_{total})_z|$. For the $\mathcal{L}$ excitation $\delta = |(\underline{E}_{total})_\perp|$ and $E = |(\underline{E}_{total})_z|$. In all cases $\lambda = k_\perp v_\perp / \Omega_z$. If the excitations are made just slightly off-axis, then $|\lambda| << 1$ and $|\delta| << |\underline{E}_{total}|$ and the dominant terms are the underlined terms.

in (7.1) - (7.21) for a transverse excitation made slightly off-axis, we note we would begin by assuming

$$\underline{E}_{TOTAL} = \hat{e}_x E_x + \hat{e}_y E_y + \hat{e}_z \delta \tag{7.22}$$

where $E = (\underline{E}_{TOTAL})$ and $|\delta| << |\underline{E}_{TOTAL}|$. But since (7.22) is the same as (7.1) with δ and E interchanged, it follows from (7.1) - (7.21) that we can obtain the results for a $\mathcal{T}$ excitation simply by interchanging δ and E in the results of the $\mathcal{L}$ excitation. We thus obtain the left-hand side of Table I. The dominant terms for both types of excitations are shown underlined. We have not shown the resonant denominators that are associated with most terms but these can be readily deduced from (7.11).

We may now easily deduce the new types of echoes that are produced by the off-axis terms in $f_1(\phi)$ and $\underline{E}_{TOTAL} \cdot \frac{\partial}{\partial \underline{v}}$. We know from the argument used to obtain (2.10) that if $g_2(\phi) \sim e^{\mp i\phi}$ where

$$\mathcal{G}_2(\phi) \sim \underbrace{\left[\underline{E}_{TOTAL} \cdot \frac{\partial}{\partial \underline{v}} \right]}_{\text{one excitation}} \underbrace{\left[f_1(\phi) \right]}_{\text{the other excitation}} \tag{7.23}$$

there will be a transverse echo and if $g_2(\phi)$ has no ϕ dependence, there will be a longitudinal echo. From Table I, we can easily obtain the ϕ dependence of $g_2(\phi)$ for all possible combinations of excitations. We can then construct Table II which gives the echo type and amplitude for the various possible excitations. We note that the dominant echo (which is underlined in Table II) has corrections of order $\frac{\delta}{E}\lambda$ and that there is always an echo of the opposite type of order $\frac{\delta}{E}$.

To demonstrate the wide variety of echo locations involved, we

$$\ell\ell \longrightarrow \begin{cases} \underline{\ell(\,E^2 + E\delta\lambda + \ldots)} \\ \nu(\,E\delta + E^2\lambda + \ldots) \end{cases}$$

$$\nu\ell \longrightarrow \begin{cases} \ell(\,E\delta + E^2\lambda + \ldots) \\ \underline{\nu(\,E^2 + E\delta\lambda + \ldots)} \end{cases}$$

$$\ell\nu \longrightarrow \begin{cases} \ell(\,E\delta + E^2\lambda + \ldots) \\ \underline{\nu(\,E^2 + E\delta\lambda + \ldots)} \end{cases}$$

$$\nu\nu \longrightarrow \begin{cases} \underline{\ell(\,E^2 + E\delta\lambda + \ldots)} \\ \nu(\,E\delta + E^2\lambda + \ldots) \end{cases}$$

TABLE 2. ECHO TYPES FOR SLIGHTLY OFF-AXIS EXCITATIONS.

Shown are the echo types and their amplitudes. Here E and δ refer to either the ℓ or the ν excitations. The dominant echo types are underlined.

note that for $\mathcal{T}\ell$ excitations we may have terms like

$$\frac{e^{im\phi}}{r-m} E\lambda^{|m|-1|} \quad \text{and} \quad \frac{e^{ir\phi}}{r-t} E\lambda^{|r|} \tag{7.24}$$

where m, n, r, t are all integers. An echo will occur only if (m+r) equals ± 1 (which gives a $\mathcal{T}$ echo) or zero (which gives an ℓ echo). We may easily deduce that the echo will have frequency

$$\omega_3 = \omega_1 + s\omega_2 \qquad s = \pm 1 \tag{7.25}$$

occur at location

$$z_0 = \frac{(\omega_2 + t\Omega) L}{(\omega_2 + r\Omega) + s(\omega_1 + m\Omega)} \tag{7.26}$$

with an amplitude factor of

$$E^2\lambda^{|m|-1| + |r|} \tag{7.27}$$

In summary, we note that if the $\mathcal{T}$ and ℓ excitations are made slightly off-axis, the lowest-order echoes for on-axis excitations as given in (2.10) will be the dominant echoes, but there will be correction terms of order $\frac{\delta}{E}\lambda$ also present. In addition, there will be an echo of the opposite type (ℓ if the dominant echo is $\mathcal{T}$, or $\mathcal{T}$ if the dominant echo is ℓ) of order $\frac{\delta}{E}$, as well as many other echoes that are higher order in $\frac{\delta}{E}$ and λ, and that involve interactions between harmonics of the cyclotron frequency [as in (7.24) - (7.27)].

However, typically we may have

$$\left| \frac{k_\perp a}{\Omega} \right| \ll 1 \tag{7.28}$$

and then all terms involving λ may be neglected. In this case we find that only the dominant echo and the echo of the opposite type (which is of order $\frac{\delta}{E}$) occur. And for any of the four possible types of echo excitation in Table II, we note that the echo of the opposite type always occurs at a location different from that of the dominant echo. Thus the dominant echo should always be clearly distinguishable.

40

8. Transverse Echoes for $\underline{B}_o = 0$

For the limit of no external magnetic field, we set ω_{ce}, ω_{ci} equal to zero wherever they occur in the above calculations. Thus the final results for the tl case and the lt case derived above for an external magnetic field, i.e., (2.41) and (2.49), carry over directly by simply setting ω_{ce}, $\omega_{ci} = 0$ in them. Thus echoes with frequency

$$\omega_3 = \omega_1 + s\omega_2 \tag{8.1}$$

occur at location

$$z_o = \frac{\omega_2 L}{\omega_2 + s\omega_1} \tag{8.2}$$

The appropriate echo type diagram in ω_1, ω_2 space is shown in Fig. 6 (compare to Fig. 2). Note that many of the interesting features of transverse echoes in an external magnetic field have disappeared: (1) there is no echo at the sum frequency $(|\omega_1| + |\omega_2|)$; (2) there are no negative phase velocity waves (as occurred earlier for $0 < \omega_1 < \omega_{ce}$ or $0 < \omega_3 < \omega_{ce}$); and (3) the ion and electron echoes occur with the same frequency at the same location. Furthermore, echoes in regions 1, 2 represent the same phenomena as echoes in regions 3, 4. The only interesting feature that remains is the polarization change that occurs for $|\omega_2| > |\omega_1|$, i.e., for tl echoes in regions 2, 3.

The transverse dielectric function $\varepsilon_{T_+}(k,\omega)$ for $\underline{B}_o = 0$ is examined in Appendix C, in Eqs. (C.55)-(C.58). The basic dispersion relation is shown in Fig. C-14a where we note there is an evanescent region for $|\omega| < \omega_{pe}$ and a propagation region for $|\omega| > \omega_{pe}$. In

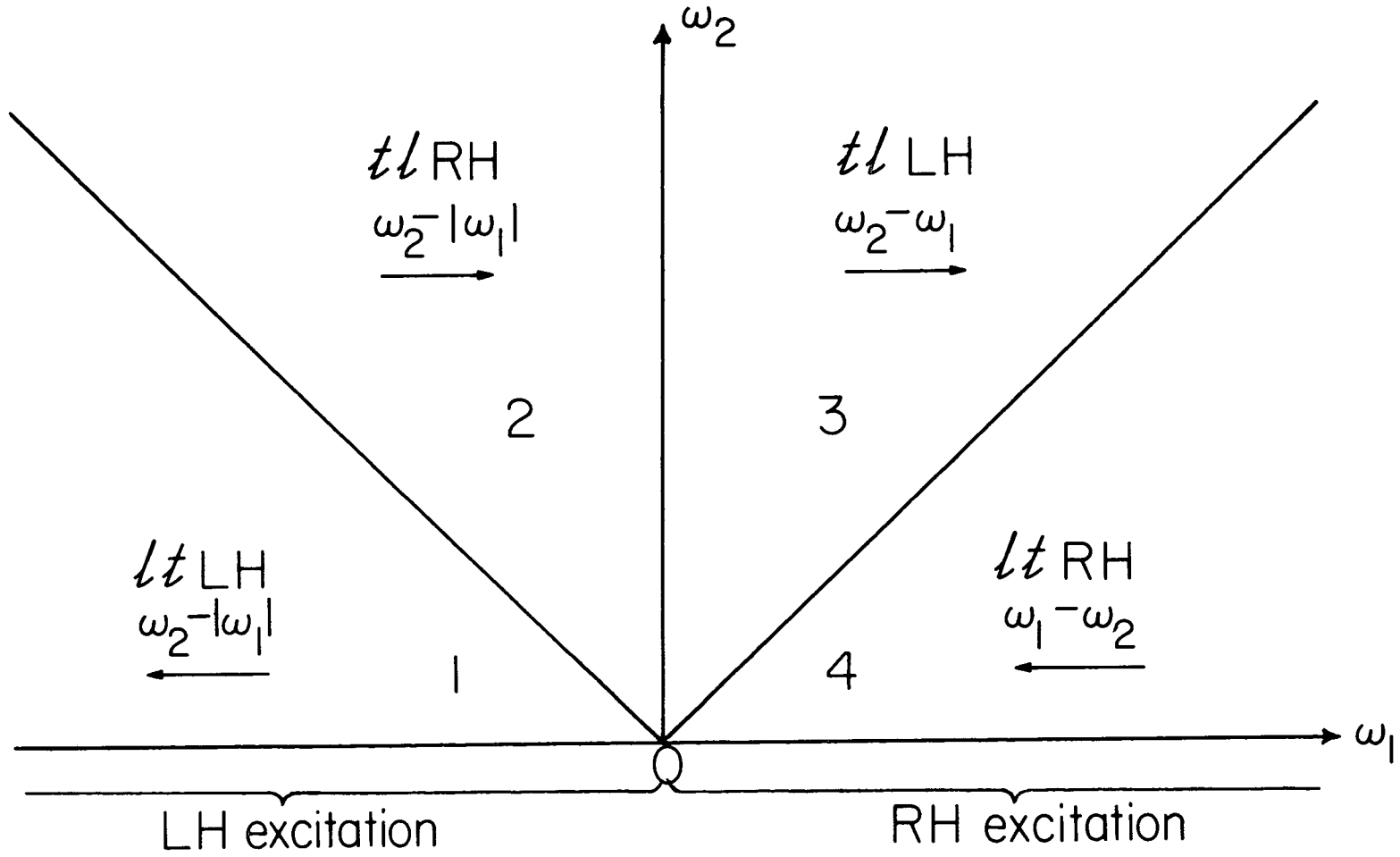

FIGURE 6. TRANSVERSE ECHO CHARACTERISTICS FOR $\underline{B}_o = 0$.

Fig. C-14b, we have plotted $|\omega/ka|$ vs. ω/ω_{pe}. Considering the roots of $\varepsilon_{T_+}[(\omega/v_z),\omega] = 0$, we note that $\omega/"k"a = v_z/a$ and since $|\omega/ka| \sim c/a$ (from Fig. C-14b), any echo pole terms [as in (4.9)] will be insignificant since they contain the factor $\exp[-v_i^2/a^2] \approx \exp[-c^2/a^2]$ which is essentially zero. (Rigorously the distribution function should be zero for $|v_z| \geq c$ so there should be no pole contribution whatsoever for $|\omega/ka| \geq c/a$.) Thus the pole 1 and pole 3 terms will never contribute to the echo shape. The only possibility of echo shape enhancement is a pole 2 term on the side of the echo furthest away from the excitation region (i.e., $z > z_o$ for tl echoes and $z < z_o$ for lt echoes).

9. Summary

We have examined the second-order (nonlinear) echo response that follows from the Vlasov-Maxwell equations when two spatially separated steady-state excitations are made. We found that given the types of excitations, the lowest-order echo is given by (2.10). Assuming the excitation (2.11), we then derived the transverse echo response up to an integral over v_z for both the tl case [i.e., (2.41)] and the lt case [i.e., (2.49)]. The various characteristics of transverse echoes were discussed and summarized in Fig. 2, after which several possible experiments were suggested.

Evaluating the integral over v_z by the method of steepest descent, we obtained the saddle-point contribution (4.8) and the three pole contributions (4.9) for the tl echo case. Results of numerical evaluation of these terms for three specific cases were given in Figs. 3-5. The physical meanings of these terms were discussed, and it was determined that (i) the saddle-point term is always significant, (ii) the pole 1 (pole 3) term is significant only if $\omega_1 \approx \omega_{ce}$ ($\omega_3 \approx \omega_{ce}$), and (iii) the pole 2 term is significant only if $|\omega_2| \gtrsim 1.08\, \omega_{pe}$.

We continued by examining several additional effects, some of which occur only for transverse echoes in an external magnetic field (as we have been considering). First, in examining the effects of Fokker-Planck collisions and finite-width excitation mechanisms, we found that the resultant integral over v_z, (5.17) was very complicated but that it could be evaluated by the method of steepest descent in special limiting cases; we obtained approximate solutions in the limits when collisional effects dominate and when finite-width effects

dominate. We concluded that for the parameter values of Figs. 3-5 (i.e., $\omega_{pe}/\omega_{ce} = 0.4$, $c/a = 1120$, $n_e = 10^{10}$ cm^{-3}), transverse plasma wave echoes could be seen but only for $L\omega_{ce}/c \lesssim 1$. In general, to reduce collisional effects, it would be more feasible to observe transverse echo phenomena at higher temperatures or lower densities.

Next we investigated the effects of temperature anisotropy ($T_\perp \neq T_z$) in the zero-order particle distribution function. We concluded that the only interesting effect was if $\omega_1 \approx 0$ or $\omega_3 \approx 0$ in which case the firehose instability may be initiated. A novel use of transverse echoes was then suggested and that was to have ω_1 in a stable region and ω_3 in an unstable region so that the instability would be excited only at the position of the echo.

Then we examined the consequences of having propagation just off-axis ($k_\perp \neq 0$). We found that if finite Larmor radius corrections were neglected, then the usual first-order echo would occur and this would be the dominant echo; but in addition, an echo of the opposite type would also occur (but at a different location and with a smaller amplitude). It was also shown that if finite Larmor radius effects are included, then a myriad of associated higher-order echoes appear.

Lastly we considered transverse plasma wave echoes when $\underline{B}_o = 0$. The resultant echo characteristics were summarized in Fig. 6. It was concluded that this case was much less interesting than the case for $\underline{B}_o \neq 0$ and also that for $\underline{B}_o = 0$ the transverse echo would never be enhanced by collective oscillations at frequencies ω_1 and ω_3.

APPENDIX A

SOLUTION OF THE LINEARIZED VLASOV EQUATION FOR $\underline{B}_0$, $k_\perp$, k_z, ALL NON-ZERO

We consider the linearized Vlasov equation in k, ω space as used in (2.17) of Part I, i.e.,

$$i(\underline{k}\cdot\underline{v}-\omega) f_1 - \Omega \frac{\partial f_1}{\partial \phi} = - g_1(\phi) \tag{A.1}$$

where

$$g_1(\phi) = \frac{q}{m}\left[\underline{E}_{TOTAL} + \frac{1}{\omega}\underline{v}\times\underline{k}\times\underline{E}_{TOTAL}\right]\cdot\frac{\partial f_0}{\partial \underline{v}} \tag{A.2}$$

Equation (A.1) has been solved in a particularly convenient form by Fried and Hedrick,[33] and we give here a brief summary of their method. We may write (A.1) as

$$i(\tilde{\omega} - k_\perp v_\perp \cos\phi) f_1 + \Omega \frac{\partial f_1}{\partial \phi} = g(\phi)$$

or

$$-i\frac{\partial H}{\partial \phi} f_1 + \frac{\partial f_1}{\partial \phi} = \frac{g(\phi)}{\Omega}$$

or

$$\frac{\partial}{\partial \phi}\left\{ f e^{-iH}\right\} = \frac{g(\phi)}{\Omega} e^{-iH} \tag{A.3}$$

where

$$\left.\begin{aligned} \tilde{\omega} &= \omega - k_z v_z \\ \lambda &= \frac{k_\perp v_\perp}{\Omega} \\ \nu &= \frac{\tilde{\omega}}{\Omega} \\ H &= \lambda \sin\phi - \nu\phi \end{aligned}\right\} \tag{A.4}$$

Then integrating (A.3) from ϕ to $\phi + 2\pi$ gives

$$f_1(\phi)\left\{ e^{-i H(\phi+2\pi)} - e^{-i H(\phi)} \right\} = \int_{\phi}^{\phi+2\pi} d\phi' \, \frac{g(\phi')}{\Omega} \, e^{-i H(\phi')}$$

or using the change of variable $\phi' \to \phi' + 2\pi$ and explicitly evaluating the H's we obtain

$$f_1(\phi) = \frac{e^{+i\lambda \sin\phi}}{\left(e^{i2\pi\nu} - 1\right)} \int_0^{2\pi} d\phi' \, g(\phi+\phi') \, e^{i\nu\phi' - i\lambda \sin(\phi+\phi')} \tag{A.5}$$

To express g_1 in terms of ϕ explicitly we let

$$\underline{E}_{TOTAL} = \hat{e}_x E_x + \hat{e}_y E_y + \hat{e}_z E_z \tag{A.6}$$

and take $\underline{k}$ to be in the xy plane ($\underline{B}_o = \hat{e}_z B_o$). Then (A.2) is

$$\begin{aligned} g_1(\phi) = \frac{q}{m}\Bigg[& E_x \frac{\partial f_o}{\partial v_x} + E_y \frac{\partial f_o}{\partial v_y} + E_z \frac{\partial f_o}{\partial v_z} \\ & + \frac{1}{\omega}\Bigg\{ E_x k_z \left(v_x \frac{\partial f_o}{\partial v_z} - v_z \frac{\partial f_o}{\partial v_x} \right) \\ & + E_y k_x \left(v_y \frac{\partial f_o}{\partial v_x} - v_x \frac{\partial f_o}{\partial v_y} \right) \\ & + E_y k_z \left(v_x \frac{\partial f_o}{\partial v_z} - v_z \frac{\partial f_o}{\partial v_y} \right) \\ & + E_z k_x \left(v_z \frac{\partial f_o}{\partial v_x} - v_x \frac{\partial f_o}{\partial v_z} \right) \Bigg\} \Bigg] \end{aligned} \tag{A.7}$$

Since

$$\begin{aligned} v_x &= v_\perp \cos\phi \\ v_y &= v_\perp \sin\phi \end{aligned} \tag{A.8}$$

we find

$$\frac{\partial}{\partial v_x} = \cos\phi \frac{\partial}{\partial v_\perp} - \frac{\sin\phi}{v_\perp} \frac{\partial}{\partial \phi}$$

$$\frac{\partial}{\partial v_y} = \sin\phi \frac{\partial}{\partial v_\perp} + \frac{\cos\phi}{v_\perp} \frac{\partial}{\partial \phi} \tag{A.9}$$

but we may ignore the $\partial/\partial\phi$ operators when they occur in (A.7) because $\partial f_o/\partial\phi = 0$ from (2.4) of Part I. Thus

$$g_1(\phi) = \frac{q}{m}\left[E_x \cos\phi \left\{ \frac{\partial f_o}{\partial v_\perp} + \frac{k_z}{\omega} G \right\} \right.$$

$$+ E_y \sin\phi \left\{ \frac{\partial f_o}{\partial v_\perp} + \frac{k_z}{\omega} G \right\} \tag{A.10}$$

$$\left. + E_z \left\{ \frac{\partial f_o}{\partial v_z} - \frac{k_x}{\omega} \cos\phi\, G \right\} \right]$$

where

$$G = v_\perp \frac{\partial f_o}{\partial v_z} - v_z \frac{\partial f_o}{\partial v_\perp} \tag{A.11}$$

which vanishes for an isotropic f_o .

APPENDIX B

SYMMETRY PROPERTIES OF THE TRANSVERSE AND LONGITUDINAL DIELECTRIC FUNCTIONS

From the definition of the plasma dispersion function as given in (2.45), (2.51) of Part I we can derive the identities

$$Z_{\pm}(\zeta^*) = -\left[Z_{\pm}(-\zeta)\right]^* \tag{B.1}$$

$$\left[Z_{\pm}(\zeta)\right]^* = Z_{\mp}(\zeta^*) \tag{B.2}$$

(where * means complex conjugate).

We first discuss the symmetry properties of the transverse dielectric function [as given in (2.44) of Part I] for $\omega = -\sigma\omega_1$ as occurs in (2.70) of Part I,

$$\epsilon_{T_{\pm}}(k_1, -\sigma\omega_1, \sigma) =$$

$$1 - \frac{1}{(k^2c^2-\omega_1^2)}\left\{\frac{\omega_{pe}^2(-\sigma\omega_1)}{ka} Z_{\pm}\left[\frac{-\sigma(\omega_1-\omega_{ce})}{ka}\right] + \frac{\omega_{pi}^2(-\sigma\omega_1)}{kA} Z_{\pm}\left[\frac{-\sigma(\omega_1-\omega_{ce})}{kA}\right]\right\} \tag{B.3}$$

We may write

$$\epsilon_{T_{\pm}}(-\sigma k_1, -\sigma\omega_1, \sigma) = F\left[k^2, \omega_1^2, \frac{\omega_1}{k} Z_{\pm}\left(\frac{\omega_1-\omega_{ce}}{ka}\right), \frac{\omega_1}{k} Z_{\pm}\left(\frac{\omega_1+\omega_{ci}}{kA}\right)\right] \tag{B.4}$$

and then it follows trivially that

$$\epsilon_{T_{\pm}}(-\sigma k, -\sigma\omega_1, \sigma)\Big|_{\sigma=+1} = \epsilon_{T_{\pm}}(-\sigma k, -\sigma\omega_1, \sigma)\Big|_{\sigma=-1} \tag{B.5}$$

Also, from (B.4) and (B.2), we have

$$\left[\epsilon_{T_\pm}(-\sigma k_1, -\sigma\omega_1, \sigma)\right]^* = F\left[k_1^{*2}\omega_1^2,\ \frac{\omega_1}{k^*}\left\{Z_\pm\left(\frac{\omega_1-\omega_{ce}}{ka}\right)\right\}^*,\ \frac{\omega_1}{k^*}\left\{Z_\pm\left(\frac{\omega_1+\omega_{ci}}{kA}\right)\right\}^*\right]$$

$$= F\left[k_1^{*2}\omega_1^2,\ \frac{\omega_1}{k^*}Z_\mp\left(\frac{\omega_1-\omega_{ce}}{k^*a}\right),\ \frac{\omega_1}{k^*}Z_\mp\left(\frac{\omega_1+\omega_{ci}}{k^*A}\right)\right] \quad (B.6)$$

$$= \epsilon_{T_\mp}(-\sigma k^*, -\sigma\omega_1, \sigma)$$

And since

$$\frac{\partial}{\partial k^*} = -\frac{\partial}{\partial(-k^*)} \quad (B.7)$$

we find

$$\left[\frac{\partial\epsilon_{T_\pm}(\sigma k, \sigma\omega_1, -\sigma)}{\partial k}\right]^* = -\frac{\partial\epsilon_{T_\mp}(-\sigma k^*, -\sigma\omega_1, \sigma)}{\partial(-k^*)} \quad (B.8)$$

where we have used (B.5) on the left side of (B.8).

The longitudinal dielectric function, as introduced in (2.14) of Part II,

$$\epsilon_{\ell_\pm}(k,\omega) = 1 - \frac{\omega_{pe}^2}{k^2a^2}Z_\pm\left(\frac{\omega}{ka}\right) - \frac{\omega_{pi}^2}{k^2A^2}Z_\pm\left(\frac{\omega}{kA}\right) \quad (B.9)$$

may be written

$$\epsilon_{\ell_\pm}(k,\omega) = F\left[k^2, \omega^2, \frac{\omega}{k}Z_\pm\left(\frac{\omega}{ka}\right), \frac{\omega}{k}Z_\pm\left(\frac{\omega}{kA}\right)\right] \quad (B.10)$$

since

$$Z_\pm'(\zeta) = -2 - 2\zeta Z_\pm(\zeta) \quad (B.11)$$

Similarly, the transverse dielectric function as used in (2.73) of Part I and thereafter

$$\epsilon_{T_\pm}(k,\omega) = 1 - \frac{1}{(k^2c^2-\omega^2)}\left\{\frac{\omega_{pe}^2\omega}{ka} Z_\pm\left(\frac{\omega-\omega_{ce}}{ka}\right) + \frac{\omega_{pi}^2\omega}{kA} Z_\pm\left(\frac{\omega+\omega_{ci}}{kA}\right)\right\} \tag{B.12}$$

may be written

$$\epsilon_{T_\pm}(k,\omega) = F\left[k^2, \omega^2, \frac{\omega}{k} Z_\pm\left(\frac{\omega-\omega_{ce}}{ka}\right), \frac{\omega}{k} Z_\pm\left(\frac{\omega+\omega_{ci}}{kA}\right)\right] \tag{B.13}$$

Let $\epsilon_\pm(k,\omega)$ represent $\epsilon_{T_\pm}(k,\omega)$ or $\epsilon_{\ell_\pm}(k,\omega)$ and let W represent ω/a, ω/A, $\omega-\omega_{ce}/a$, or $\omega+\omega_{ci}/A$. Then in this general notation we have

$$\epsilon_\pm(k,\omega) = F\left[k^2, \omega^2, \frac{\omega}{k} Z_\pm\left(\frac{W}{k}\right)\right] \tag{B.14}$$

Now let ω be real and consider the roots of

$$\epsilon_\pm(k,\omega) = 0 \tag{B.15}$$

in the complex k plane. From (B.14) we have identically

$$F\left[k^2, \omega^2, \frac{\omega}{k} Z_\pm\left(\frac{W}{k}\right)\right] = 0 \tag{B.16}$$

Taking complex conjugates gives

$$F\left[k^{*2}, \omega^2, \frac{\omega}{k^*}\left\{Z_\pm\left(\frac{\omega}{k}\right)\right\}^*\right] = 0 \tag{B.17}$$

or using (B.1)

$$F\left[(-k^*)^2, \omega^2, \frac{\omega}{(-k^*)} Z_\pm\left(\frac{W}{-k^*}\right)\right] = 0 \tag{B.18}$$

which is just

$$\epsilon_{\pm}(-k^*, \omega) = 0 \tag{B.19}$$

Now consider (B.17) again and use (B.2) to obtain

$$F\left[k^{*2}, \omega^2, \frac{\omega}{k^*} Z_{\mp}\left(\frac{W}{k^*}\right)\right] = 0 \tag{B.20}$$

which is just

$$\epsilon_{\mp}(k^*, \omega) = 0 \tag{B.21}$$

Thus if k is a root of $\epsilon_{\pm}(k,\omega) = 0$ it follows from (B.19) that $-k^*$ is a root of the same equation, and from (B.21) that k^* is a root of $\epsilon_{\mp}(k,\omega) = 0$. Hence if $k + i\gamma$ (k, γ real and positive) is a root of $\epsilon_{+}(k,\omega) = 0$, then the other related roots would be located as shown in Fig. B-1.

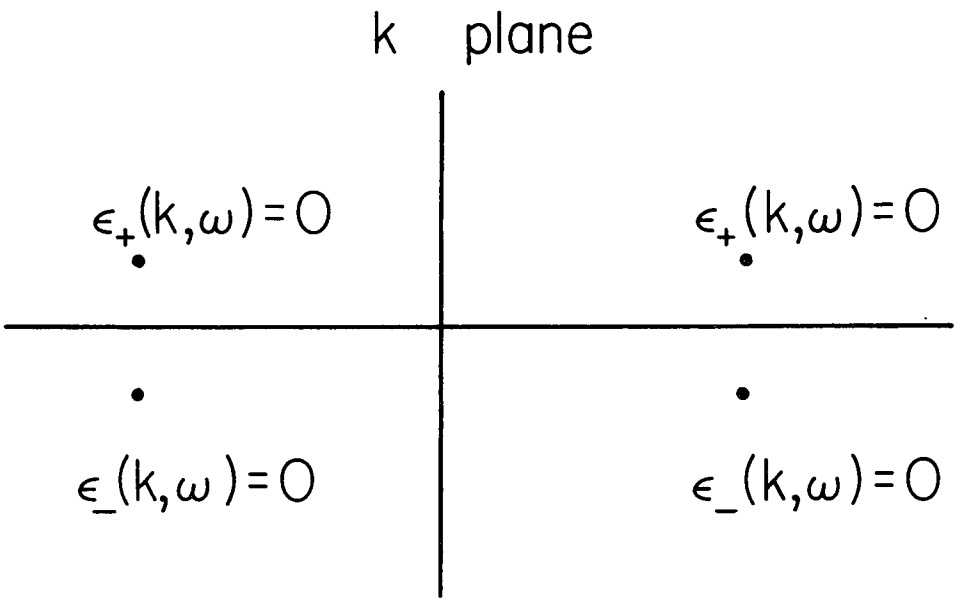

FIGURE B-1. SYMMETRY PROPERTIES OF ROOTS OF THE TRANSVERSE AND LONGITUDINAL DISPERSION RELATIONS FOR REAL ω AND COMPLEX k.

Roots of $\epsilon_\pm(k,\omega)=0$ in the complex k plane for real ω [showing that $\epsilon_+(k,\omega)=0$ implies that $\epsilon_+(-k^*,\omega)=0$, $\epsilon_-(k^*,\omega)=0$, and $\epsilon_-(-k,\omega)=0$]. Both the transverse and longitudinal dispersion relations obey this symmetry.

APPENDIX C

ROOTS OF THE TRANSVERSE DISPERSION RELATION FOR REAL ω AND COMPLEX k

1. Summary

In this appendix we examine the roots of the transverse dispersion relation for real ω and complex k. The major results obtained are:

1. The cold plasma dispersion relation with negligible warm plasma damping (C.9), (C.10) is valid for all ω except $\omega \approx \omega_{ce}$. For $\omega \leq \omega_L$ and $\omega \geq \omega_R$, Im k is essentially zero. For $0 \leq \omega \leq \omega_{ce}$ it is shown that no simple expression for Im k can be derived, and it is concluded that the root comes from the algebraic terms of the Z function involved. The basic dispersion properties are given in Fig. C-1.

2. The locus of roots in the complex ζ_e plane of the hot plasma dispersion relation is given in Fig. C-3. The loci are classified [least-damped or cyclotron-damped (for $\omega \approx \omega_{ce}$) root; infinite sequence of roots; pure imaginary roots] and the corresponding roots in the k plane are then investigated.

3. Numerical results concerning the cyclotron-damped root for ω slightly below ω_{ce} (Figs. C-4a,b,c, C-5) and for ω slightly above ω_{ce} (Fig. C-6) are presented. An expression for the value of this root at $\omega = \omega_{ce}$ is given by (C.30). It is noted that for $\omega_{ce} \leq \omega \leq \omega_R$ both the hot plasma cyclotron-damped root and the "cold plasma" pure imaginary root contribute to the response of a single transverse excitation.

4. The infinite sequence of roots is examined both numerically (Figs. C-7, C-8) and analytically. It is shown that these roots are caused by the term $2\sqrt{\pi}i\, e^{-\zeta^2}$ that occurs in the asymptotic expansion of the Z function involved. Expressions are given for the approximate

values of these roots (C.35) and the value of the term $2\sqrt{\pi}i\ e^{-\zeta^2}$ at these roots (C.32).

5. Pure imaginary roots are found to occur for $\omega_L \leq \omega \leq \omega_R$. For $\omega_L \leq \omega \leq 0$ and $\omega_{ce} \leq \omega \leq \omega_R$ the pure imaginary roots are just the cold plasma evanescent roots (C.36), but it is shown that these roots occur only in one-half of the k plane. For $0 \leq \omega \leq \omega_{ce}$ the pure imaginary root must be calculated numerically.

6. For reference, the locations of all the roots of $\varepsilon_{T_\pm}(k,\omega) = 0$ are summarized in Figs. C-9, C-10.

In addition, several investigations involving the transverse dispersion relation are made:

7. A physical explanation of the cyclotron-damped root results is given using Figs. C-11, C-12.

8. The cyclotron-damped root may be computed to very good approximation by using the two-pole approximation[34] for the Z function involved, but only for $\omega \leq \omega_{ce}$. For $\omega \geq \omega_{ce}$ the cyclotron-damped root passes through the region defined by $\text{Im}\ \zeta < 0$ and $|\zeta| \lesssim 3$ wherein the two-pole approximation should not be used (see Fig. 13).

9. Effects of anisotropic temperature are examined ($T_\perp \neq T_z$). The usual criterion for the firehose instability is obtained. In general it is concluded that the roots for the anisotropic case are essentially the same as the roots for the isotropic case, except if $\omega \approx 0$.

10. The transverse dispersion relation in the limit $B_o \to 0$ is investigated. Using Fig. C-14 it is shown that Im k of the least-damped root is always essentially zero.

11. Lastly, in Fig. C-15, it is shown that the roots of

$\varepsilon_{T_+}[(\omega-\omega_{ce}/v_z),\omega] = 0$ (v_z real) in the complex ω plane are centered about $\omega = \omega_{ce}$ while the roots of $\varepsilon_{T_+}(k,kv_z+\omega_{ce}) = 0$ (v_z real) in the complex k plane are centered about $k = 0$.

2. Warm Plasma Results

2.1 Use of the asymptotic expansion of $Z(\zeta_e)$.

From the symmetry properties discussed in Appendix B we find it is sufficient to obtain only the roots of

$$\epsilon_{T_+}(k,\omega) = 1 - \frac{\omega}{(k^2c^2-\omega^2)}\left\{\frac{\omega_{pe}^2}{ka} Z_+\left(\frac{\omega-\omega_{ce}}{ka}\right) + \frac{\omega_{pi}^2}{kA} Z_+\left(\frac{\omega-\omega_{ci}}{kA}\right)\right\} = 0 \qquad (C.1)$$

For Maxwellian distributions, the Z functions in (C.1) have the asymptotic expansion

$$Z_+(\zeta) = -\frac{1}{\zeta} - \frac{1}{2\zeta^3} - \frac{3}{4\zeta^5} - \cdots + i\sqrt{\pi}\,\sigma_+(\zeta)\, e^{-\zeta^2}$$

where

$$\sigma_+(\zeta) = \begin{cases} 0 & \text{for } Im\,\zeta > 0 \\ 1 & = 0 \\ 2 & < 0 \end{cases} \qquad (C.2)$$

To good approximation we may use

$$Z_+(\zeta) = -\frac{1}{\zeta} + i\sqrt{\pi}\,\sigma_+(\zeta)\, e^{-\zeta^2} \qquad (C.3)$$

for $|\zeta| \gtrsim 3$. Using (C.3) in (C.1) we obtain

$$k^2 = \frac{\omega^2}{c^2}\left[1 - \frac{\omega_{pe}^2}{\omega(\omega-\omega_{ce})} - \frac{\omega_{pi}^2}{\omega(\omega+\omega_{ci})}\right]$$

$$+ i\frac{\sqrt{\pi}\omega}{c^2 k}\left[\sigma_+(\zeta_e)\frac{\omega_{pe}^2}{a}e^{-\zeta_e^2} + \sigma_+(\zeta_i)\frac{\omega_{pi}^2}{A}e^{-\zeta_i^2}\right] \qquad \text{(C.4)}$$

where

$$\zeta_e \equiv \frac{\omega-\omega_{ce}}{ka} \qquad \zeta_i \equiv \frac{\omega+\omega_{ci}}{kA} \qquad \text{(C.5)}$$

Then assuming $|\mathrm{Re}\ k| >> |\mathrm{Im}\ k|$ so

$$k^2 \approx (\mathrm{Re}\,k)^2 + 2i(\mathrm{Re}\,k)(\mathrm{Im}\,k)$$

and equating real and imaginary parts in (C.4), we find

$$\mathrm{Re}\,k = \pm\frac{\omega}{c}\left[1 - \frac{\omega_{pe}^2}{\omega(\omega-\omega_{ce})} - \frac{\omega_{pi}^2}{\omega(\omega+\omega_{ci})}\right]^{\frac{1}{2}} \qquad \text{(C.6)}$$

$$\mathrm{Im}\,k = \frac{\sqrt{\pi}\omega}{2c^2(\mathrm{Re}\,k)^2}\left[\sigma_+(\zeta_e)\frac{\omega_{pe}^2}{a}e^{-\zeta_e^2} + \sigma_+(\zeta_i)\frac{\omega_{pi}^2}{A}e^{-\zeta_i^2}\right] \qquad \text{(C.7)}$$

Equation (C.6) gives just the cold plasma dispersion relation while (C.7) gives the damping associated with a finite temperature.

2.2 Problem of $\sigma_+(\zeta_e)$.

Evaluation of the σ's in (C.7) produces some unexpected results. From (C.2) we know $\sigma_+(\zeta_e)$ and $\sigma_+(\zeta_i)$ are each positive or zero. Thus for ω positive it follows from (C.7) that Im k is positive or zero. Accordingly in (C.5), if $\omega > \omega_{ce}$ we have $\mathrm{Im}\,\zeta_e > 0$,

Im $\zeta_i > 0$ so $\sigma_+(\zeta_e) = \sigma_+(\zeta_i) = 2$. However, for $0 < \omega < \omega_{ce}$ we have Im $\zeta_e < 0$, Im $\zeta_i > 0$ so $\sigma_+(\zeta_e) = 0$, $\sigma_+(\zeta_i) = 2$. This last result is surprising since it claims all the damping is due to the ion term in (C.7).

Thus we are faced with the following dilemma. If we neglect the ion term in (C.1) and use (C.3) for $Z_+(\zeta_e)$ then for $0 < \omega < \omega_{ce}$ we cannot legitimately find <u>any</u> root, not even the cold plasma root (C.6). This occurs because if we assume Im $k > 0$ we find $\sigma_+(\zeta_e) = 0$ so Im $k = 0$; if we assume Im $k = 0$, then we find $\sigma_+(\zeta_e) = 1$ so Im $k > 0$.

The solution to this dilemma must be that, for $0 < \omega < \omega_{ce}$, Im k is caused by the algebraic terms of $Z_+(\zeta_e)$. Indeed we shall find shortly from numerical considerations that the least-damped root, for ω slightly below ω_{ce} , occurs in the half of the ζ_e plane wherein $\sigma_+(\zeta_e) = 0$. The point is that for $0 < \omega < \omega_{ce}$ and $|\zeta| \gtrsim 3$ there is no simple expression for Im k like (C.7).

However, we shall find that Im k for the least-damped root is negligible except for $|\zeta_e| \lesssim 3$ which occurs only when ω is very near ω_{ce} . Thus the cold plasma dispersion relation (C.6) with Im $k = 0$ is a valid approximation for $0 < \omega < \omega_{ce}$ except for ω very near ω_{ce}.

2.3 <u>Basic dispersion properties.</u>

Henceforth we shall ignore the ions in (C.1) and investigate the electron dispersion relation

$$1 - \frac{\omega}{(k^2c^2 - \omega^2)} \frac{\omega_{pe}^2}{ka} Z_+\left(\frac{\omega - \omega_{ce}}{ka}\right) = 0 \qquad \text{(C.8)}$$

Then (C.6), (C.7) become

$$\mathrm{Re}\, k = \pm \frac{\omega}{c}\left[1 - \frac{\omega_{pe}^2}{\omega(\omega-\omega_{ce})}\right]^{\frac{1}{2}} \tag{C.9}$$

$$\mathrm{Im}\, k = \frac{\sqrt{\pi}\,\omega\omega_{pe}^2}{2c^2(\mathrm{Re}\, k)^2 a}\,\sigma_+(\zeta_e)\,e^{-\zeta_e^2} \tag{C.10}$$

We understand that (C.10) is valid only if $(\mathrm{Re}\ k)^2$ as given by (C.9) is positive. In addition (C.10) is to be used only for $\omega_1 \leq 0$ or $\omega \geq \omega_{ce}$, in which case we shall soon see that $|\zeta_e|$ is so large that we may simply set $\mathrm{Im}\ k = 0$. According to the above discussion, for $0 < \omega < \omega_{ce}$ and $|\zeta_e| \gtrsim 3$ we may also set $\mathrm{Im}\ k = 0$.

We have plotted the cold plasma dispersion relation (C.9) in Fig. C-1 for $\omega_{pe}/\omega_{ce} = 0.4$. Note that k goes to zero at $\omega = 0$ and at the right- and left-hand cutoffs defined by

$$\omega_{R,L} = \frac{1}{2}\left[\omega_{ce} \pm \sqrt{\omega_{ce}^2 + 4\omega_{pe}^2}\,\right] \tag{C.11}$$

In the propagating regions ($\omega < \omega_L$, $0 < \omega < \omega_{ce}$, $\omega > \omega_R$) k is real, whereas in the evanescent regions ($\omega_L < \omega < 0$, $\omega_{ce} < \omega < \omega_R$) k is pure imaginary.

In Fig. C-2 we have plotted $\log_{10}|\zeta_e|$ vs. ω (for $\omega_{pe}/\omega_{ce} = 0.4$, $c/a = 1120$) where $\zeta_e = (\omega-\omega_{ce})/ka$ and k is given by (C.9). Note that $|\zeta_e|$ is extremely large everywhere ($|\zeta_e| \gg 3$) except for $\omega \approx \omega_{ce}$, in which case (C.9) is not valid and we must solve (C.8) numerically to obtain the desired root.

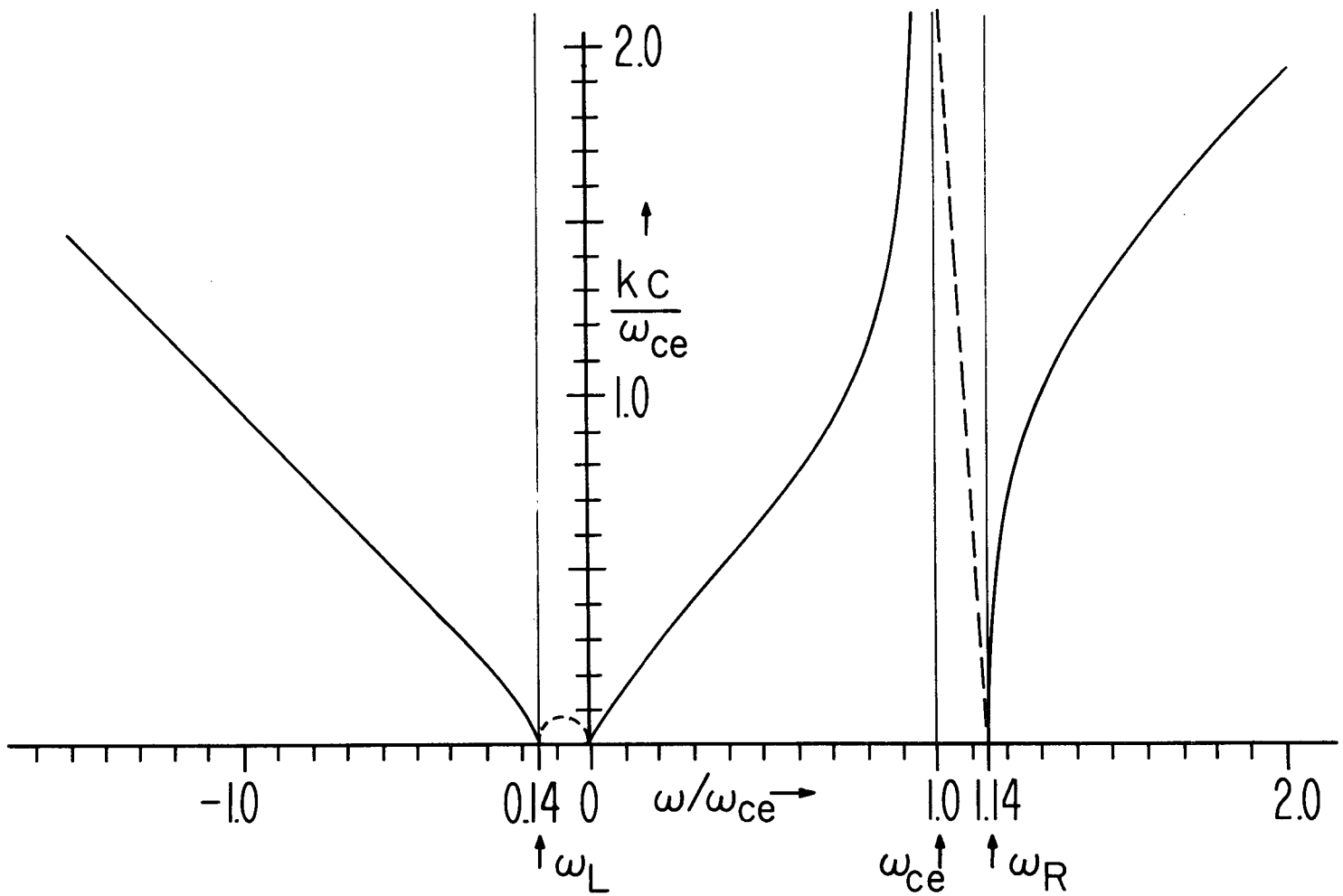

FIGURE C-1. THE COLD PLASMA TRANSVERSE DISPERSION RELATION (ω_{pe}/ω_{ce} = .4).
Equation (C.9) is plotted for $(\mathrm{Re}\ k)^2 > 0$ [solid line] and for $(\mathrm{Re}\ k)^2 < 0$ [dashed line].

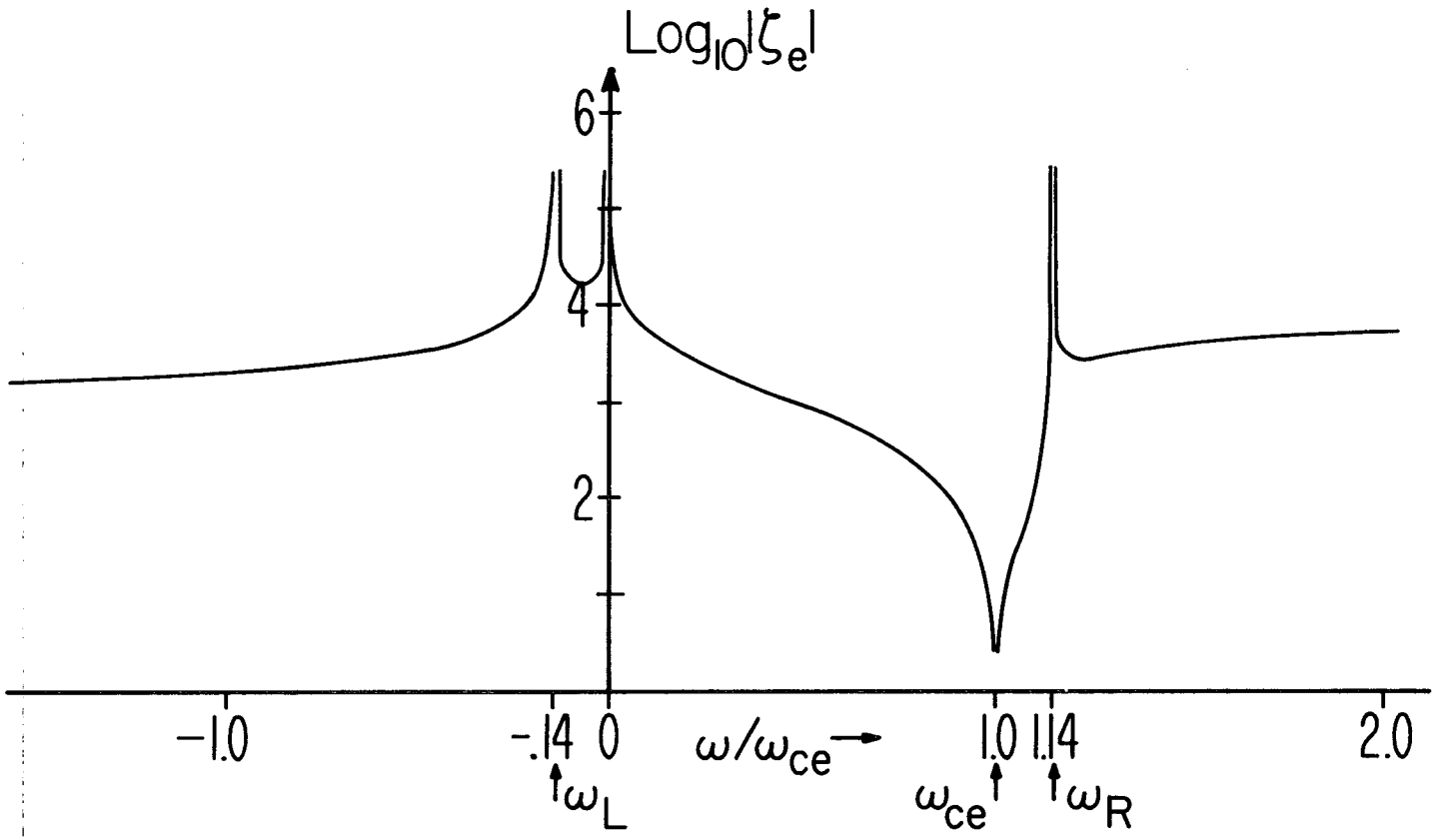

FIGURE C-2. $LOG_{10}\ |\zeta_e|$ VS. ω_1/ω_{ce} (ω_{pe}/ω_{ce} = .4 , c/a = 1120).

Plotted is $\log_{10}\ |\zeta_e|$ where $\zeta_e=(\omega-\omega_{ce})/([\text{Re } k]a)$ and Re k is given by (C.9).

3. Hot Plasma Results

3.1 Locus of roots in the ζ_e plane.

We proceed to investigate the hot plasma results obtained by solving (C.8) numerically. We first examine the locus of roots of (C.8) in the complex ζ_e plane. Later we shall consider specific types of roots and compute their actual values in the complex k plane.

In terms of $\zeta_e = (\omega-\omega_{ce})/ka$, the transverse dispersion relation (C.8) may be written

$$\zeta_e^3 Z_+(\zeta_e) = \left[\frac{(\omega-\omega_{ce})^3 c^2}{\omega\,\omega_{pe}^2\, a^2}\right] - \left[\frac{\omega(\omega-\omega_{ce})}{\omega_{pe}^2}\right]\zeta_e^2 \qquad (C.12)$$

For now we assume the ζ_e^2 term on the right-hand side of (C.12) may be neglected, i.e., we consider

$$\zeta_e^3 Z_+(\zeta_e) = \left[\frac{(\omega-\omega_{ce})^3 c^2}{\omega\,\omega_{pe}^2\, a^2}\right] \qquad (C.13)$$

Then in the spirit of Fried and Gould[7] who examined the roots of the longitudinal dispersion relation for real k and complex ω) followed by Kuehl, Stewart, and Yeh[8] (who examined the roots of the longitudinal dispersion relation for real ω and complex k), we note that we can find the locus of roots of (C.13) in the complex ζ_e plane by plotting solutions of

$$Im\left[\zeta_e^3 Z_+(\zeta_e)\right] = 0 \qquad (C.14)$$

Then a true solution to (C.13) exists if for a point on the locus given

by (C.14) we have

$$\mathrm{Re}\left[\zeta_e^3 Z_+(\zeta_e)\right] = \left[\frac{(\omega-\omega_{ce})^3 c^2}{\omega \omega_{pe}^2 a^2}\right] \tag{C.15}$$

We have calculated the first several branches of the loci of roots given by (C.14) and these are shown in Fig. C-3, where for points on the solid (dashed) lines we have $\mathrm{Re}[\zeta_e^3 Z_+(\zeta_e)] > 0$ (< 0). Noting

$$\left[\frac{(\omega-\omega_{ce})^3 c^2}{\omega \omega_{pe}^2 a^2}\right] \quad \begin{array}{ll} > 0 & \text{for} \quad \omega < 0, \ \omega > \omega_{ce} \\ < 0 & \text{for} \quad 0 < \omega < \omega_{ce} \end{array} \tag{C.16}$$

we conclude that in Fig. C-3 the solid lines are valid loci for $\omega < 0$ or $\omega > \omega_{ce}$ while the dashed lines are valid loci for $0 < \omega < \omega_{ce}$.

The various loci in Fig. C-3 may be classified according to the types of roots they represent:

(a) <u>The least-damped root</u> in the ζ_e plane. (For ω near ω_{ce} we shall refer to this root as the cyclotron-damped root.) In Fig. C-3, for ω slightly below ω_{ce} the cyclotron-damped root is on the dashed loci just above the real axis; as ω approaches ω_{ce}, the root approaches $\zeta_e = 0$. For $\omega = \omega_{ce}$ the root is at $\zeta_e = 0$; for ω slightly above ω_{ce} the root is on the curved solid loci that begins at $\zeta_e = 0$ and progresses downward.

(b) <u>Infinite sequence of roots.</u> We refer to the infinite number of loops of loci that progress downward in the lower-half ζ_e plane in Fig. C-3. For a given value of ω we find there is but one root on

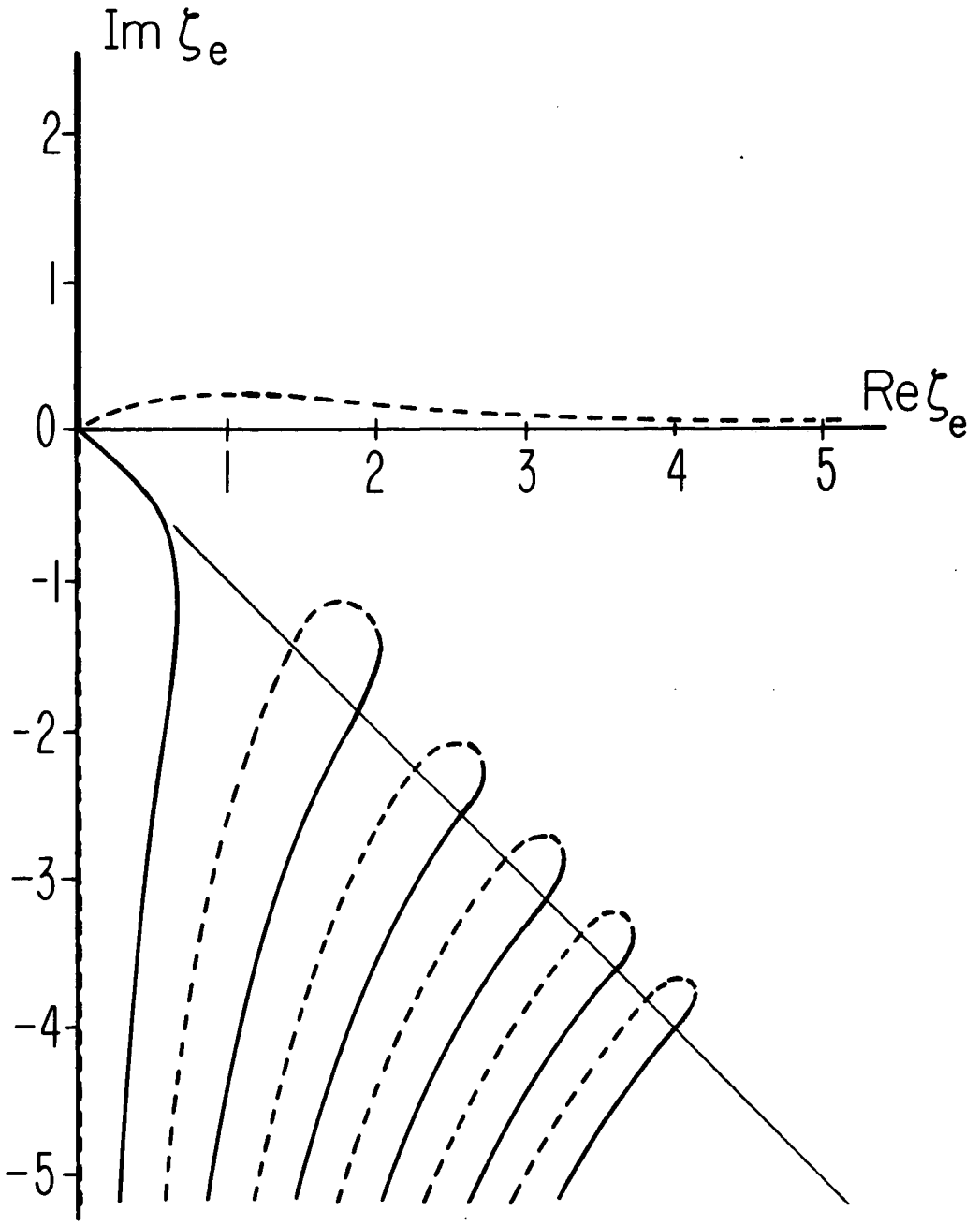

FIGURE C-3. LOCUS OF ROOTS OF THE TRANSVERSE DISPERSION RELATION (C.13) IN THE ζ_e PLANE FOR REAL ω.

The solid lines apply for $\omega<0$ or $\omega>\omega_{ce}$, the dashed lines for $0<\omega<\omega_{ce}$. See text for full discussion.

each loop. And for $|\omega/\omega_{ce}| \lesssim 5$ say, each root lies very close to the $-45°$ line. This will become clearer when we consider specific examples (in Figs. C-7, C-8).

(c) Pure imaginary roots. Note that the whole imaginary ζ_e axis is a locus because every point on it is a solution to (C.13).

More will be said about all of these roots when we consider the corresponding roots in the complex k plane.

Figure C-3 is based on Eq. (C.13) which is valid only when the ζ_e^2 term on the right-hand side of (C.12) is negligible, i.e., when

$$\left| \frac{\left[\frac{\omega(\omega-\omega_{ce})}{\omega_{pe}^2}\right]\zeta_e^2}{\left[\frac{(\omega-\omega_{ce})^2 c^2}{\omega\omega_{pe}^2 a^2}\right]} \right| \ll 1$$

or

$$\left| \zeta_e^2 \right| \ll \frac{(\omega-\omega_{ce})^2 c^2}{\omega^2 a^2} \tag{C.17}$$

This inequality holds for Fig. C-3 (for which $|\zeta_e| \lesssim 5$) except possibly when $\omega \simeq \omega_{ce}$. But using $\zeta_e = (\omega-\omega_{ce})/ka$, (C.17) is

$$\left(\frac{\omega}{kc}\right)^2 \ll 1 \tag{C.18}$$

which we shall find holds when $\omega \simeq \omega_{ce}$. Thus Fig. C-3 is valid for all values of ω .

If we wanted to compute the loci for $|\zeta_e| \gg 5$ we would have to include both terms on the right-hand side of (C.12). In that case we could not easily calculate the loci because it is not possible to

isolate the ζ_e dependence from the ω dependence in (C.12) to obtain an equation in the form of (C.14). Instead, the loci would have to be constructed by actually calculating all the roots of (C.12) for many values of ω. Generally though it is not necessary to know all the loci accurately for $|\zeta_e| \gtrsim 5$. In fact, the least-damped root for $\omega < \omega_L$, $\omega > \omega_R$ (which has $|\zeta_e| >> 5$) has already been computed in (C.9), (C.10). And the approximate values of the roots in the infinite sequences (for $|\zeta_e| \gtrsim 3$) will be obtained in a following section. Thus in general, Fig. C-3 should be sufficient for all applications.

3.2 Roots in the complex k plane.

(i) Cyclotron-damped root (ω slightly below ω_{ce}).

As discussed earlier, the cold plasma result (C.9) with $\text{Im } k = 0$ is a valid representation of the least-damped root of the transverse dispersion relation (C.8) for $0 < \omega < \omega_{ce}$ provided $|\zeta_e| \gtrsim 3$. For $\omega \approx \omega_{ce}$, $|\zeta_e| \lesssim 3$ and (C.8) must be solved numerically. For $\omega \approx \omega_{ce}$ we consider the regions $\omega \leq \omega_{ce}$ and $\omega \geq \omega_{ce}$ separately since our main interest lies in the former ($\omega \leq \omega_{ce}$) for which cyclotron-damping measurements would be made. In the latter ($\omega \geq \omega_{ce}$) the damping is typically so large that it would be difficult to ever measure it experimentally. In this section we present values of the cyclotron-damped root for several cases where ω is slightly below ω_{ce}. In the following section we briefly consider the cyclotron-damped root for ω slightly above ω_{ce}.

We have solved (C.8) numerically using the following Nyquist

complex root finding scheme. We seek solutions in the ζ_e plane of

$$F(\zeta_e) \equiv \left\{ \zeta_e^3 Z_+(\zeta_e) - \left[\frac{(\omega-\omega_{ce})^3 c^2}{\omega \omega_{pe}^2 a^2} \right] + \left[\frac{\omega(\omega-\omega_{ce})}{\omega_{pe}^2} \right] \zeta_e^2 \right\} = 0 \qquad \text{(C.19)}$$

[as in (C.12)]. For each desired value of ω we guess a value for the root ζ_e (such as the cold plasma value or a point on the appropriate locus in Fig. C-3) and then compute

$$N = \frac{1}{2\pi i} \oint \frac{\alpha F(\zeta_e)}{F(\zeta_e)} \qquad \text{(C.20)}$$

on a closed contour in the ζ_e plane that encloses the chosen ζ_e. If we find $N = 0$ there is no root enclosed by the contour whereas if $N = 1$ there is precisely one root enclosed in which case we compute

$$S = \frac{1}{2\pi i} \oint \frac{\zeta_e \alpha F(\zeta_e)}{F(\zeta_e)} \qquad \text{(C.21)}$$

which gives a value for the root better than our original guess. Using this ζ_e and choosing a smaller contour we repeat (C.20), (C.21). After a few such iterations we obtain the correct value of the root ζ_e. Then using

$$k = \frac{\omega - \omega_{ce}}{\zeta_e a} \qquad \text{(C.22)}$$

we compute the value of the corresponding root in the k plane.

These calculations were performed using the Fried, Hedrick, McCune[34] two-pole approximation for the Z function that occurs in (C.19). The results so obtained compared favorably (Re k and Im k

agreed within about 2%) to some sample results for which $Z_+(\zeta_e)$ was computed exactly. Thus use of the two-pole approximation for this case was justified.

In this and the following sections we consider only roots in the right half of the complex k plane since the corresponding roots in the left half and also the roots of $\varepsilon_T(k,\omega) = 0$ are then easily found using the symmetry properties summarized in Fig. B-1. Now consider the first quadrant of the complex k plane wherein (C.19) has only one root for $0 < \omega < \omega_{ce}$, and since the Z function in (C.19) has $\sigma_+(\zeta_e) = 0$ there [using the Z function representation (2.51) of Part I], this root comes from the algebraic part of the Z function. We have calculated this (cyclotron-damped) root for several values of the parameters ω_{pe}/ω_{ce} and c/a with the results displayed in Figs. C-4a,b,c, and C-5. (The parameters of Fig. C-5 are typical values for the UCLA Q machine.)

We note the following features in Figs. C-4a,b,c, and C-5. First consider Re k. If ω_{pe}/ω_{ce} is fixed, then for a finite temperature as ω approaches ω_{ce}, Re kc/ω_{ce} approaches a finite cutoff value instead of becoming infinite as it does for a cold plasma. Moreover, as the temperatures increases (c/a decreases), this cutoff value decreases. If c/a is fixed (as in Fig. C-5) then the cutoff value of Re kc/ω_{ce} increases as ω_{pe}/ω_{ce} decreases. These results are explicitly shown by the cutoff formula

$$\frac{kc}{\omega_{ce}} = \left[\frac{\sqrt{\pi}\,\omega\omega_{pe}^2}{2\omega_{ce}^3}\,\frac{c}{a}\right]^{\frac{1}{3}}\left[\sqrt{3}+i\right]$$

which will be obtained in the next section.

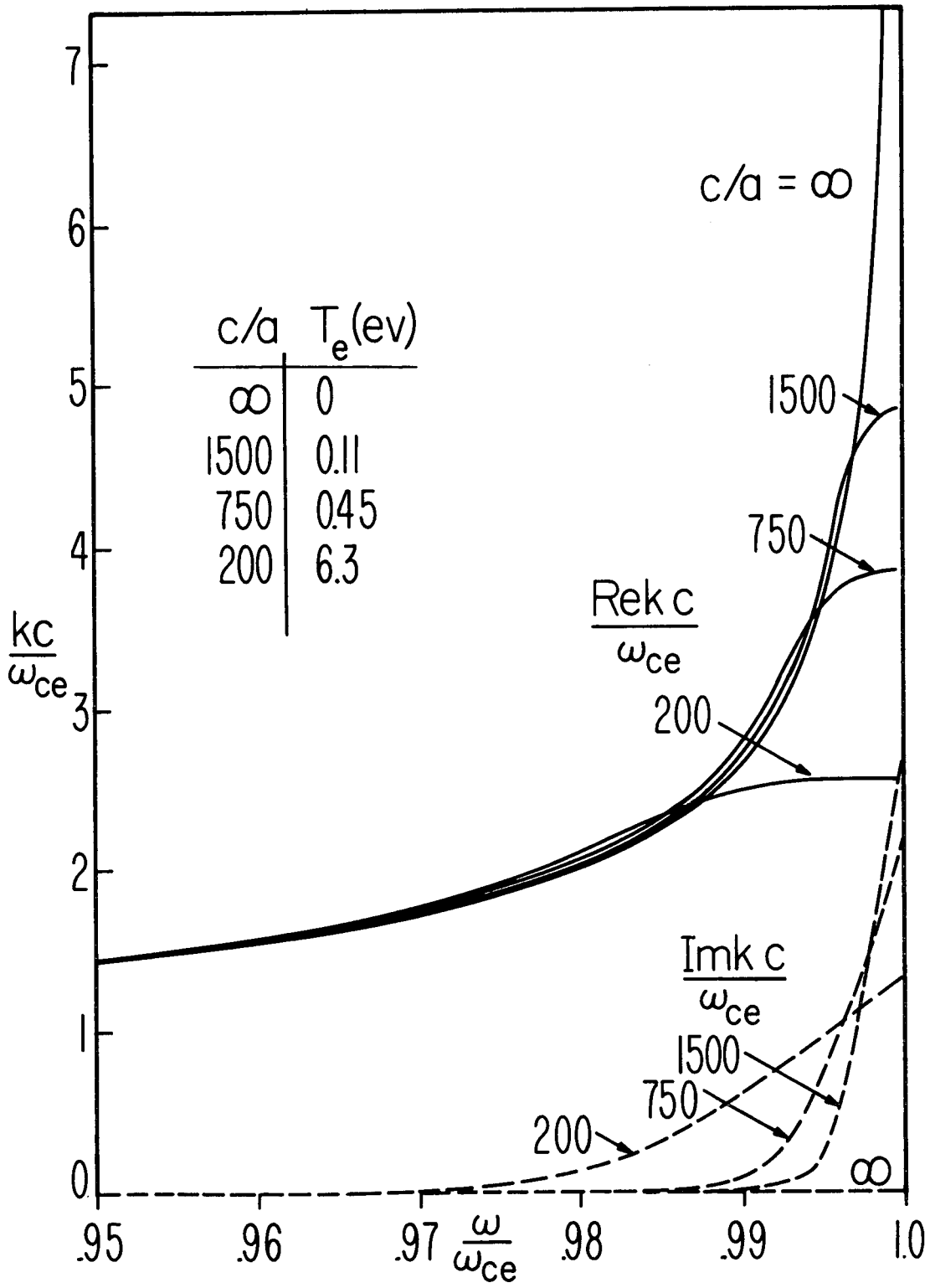

FIGURE C-4a. THE CYCLOTRON-DAMPED ROOT FOR $\omega_{pe}/\omega_{ce} = .25$.

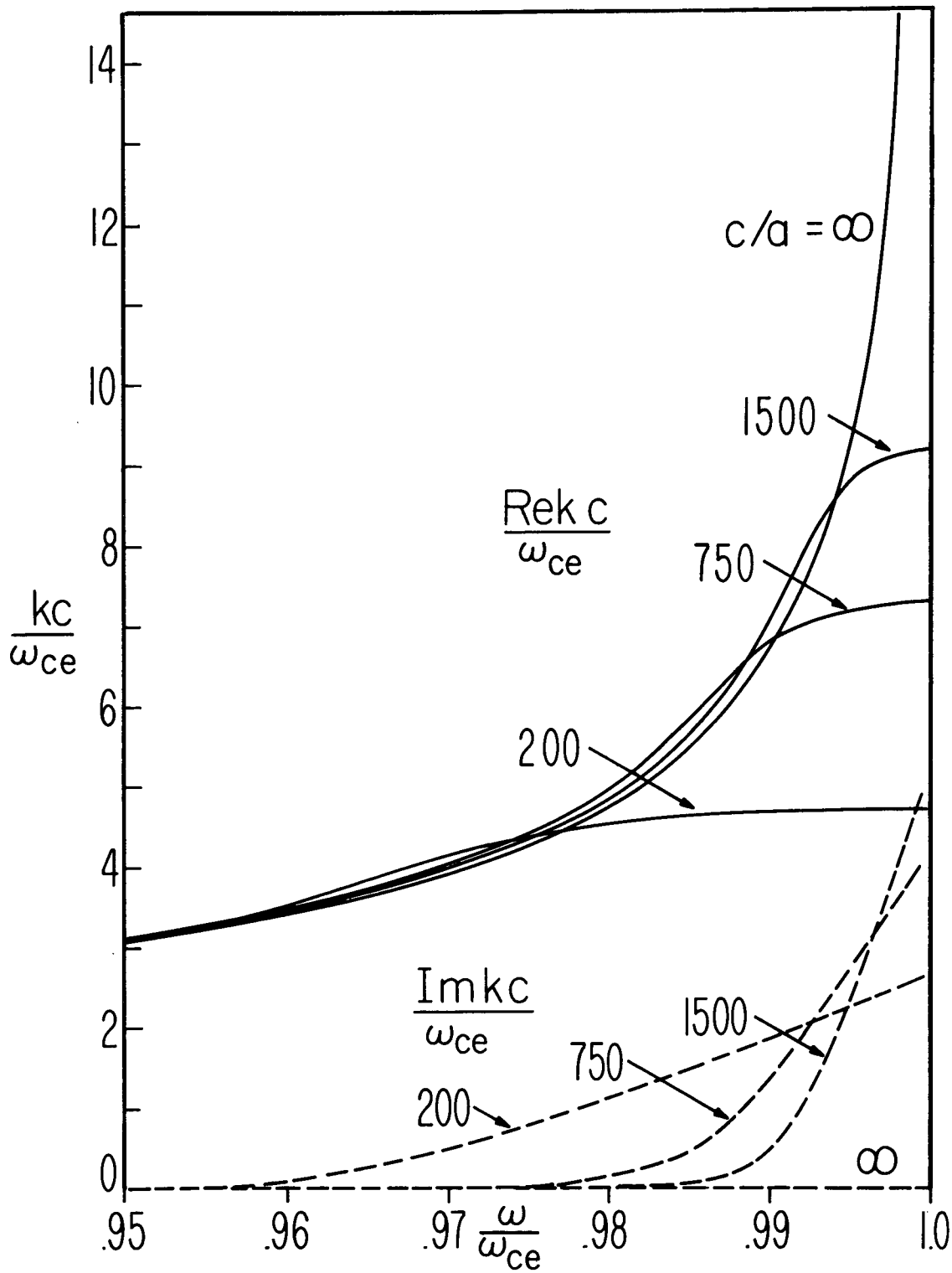

FIGURE C-4b. THE CYCLOTRON-DAMPED ROOT FOR ω_{pe}/ω_{ce} = .6666 .

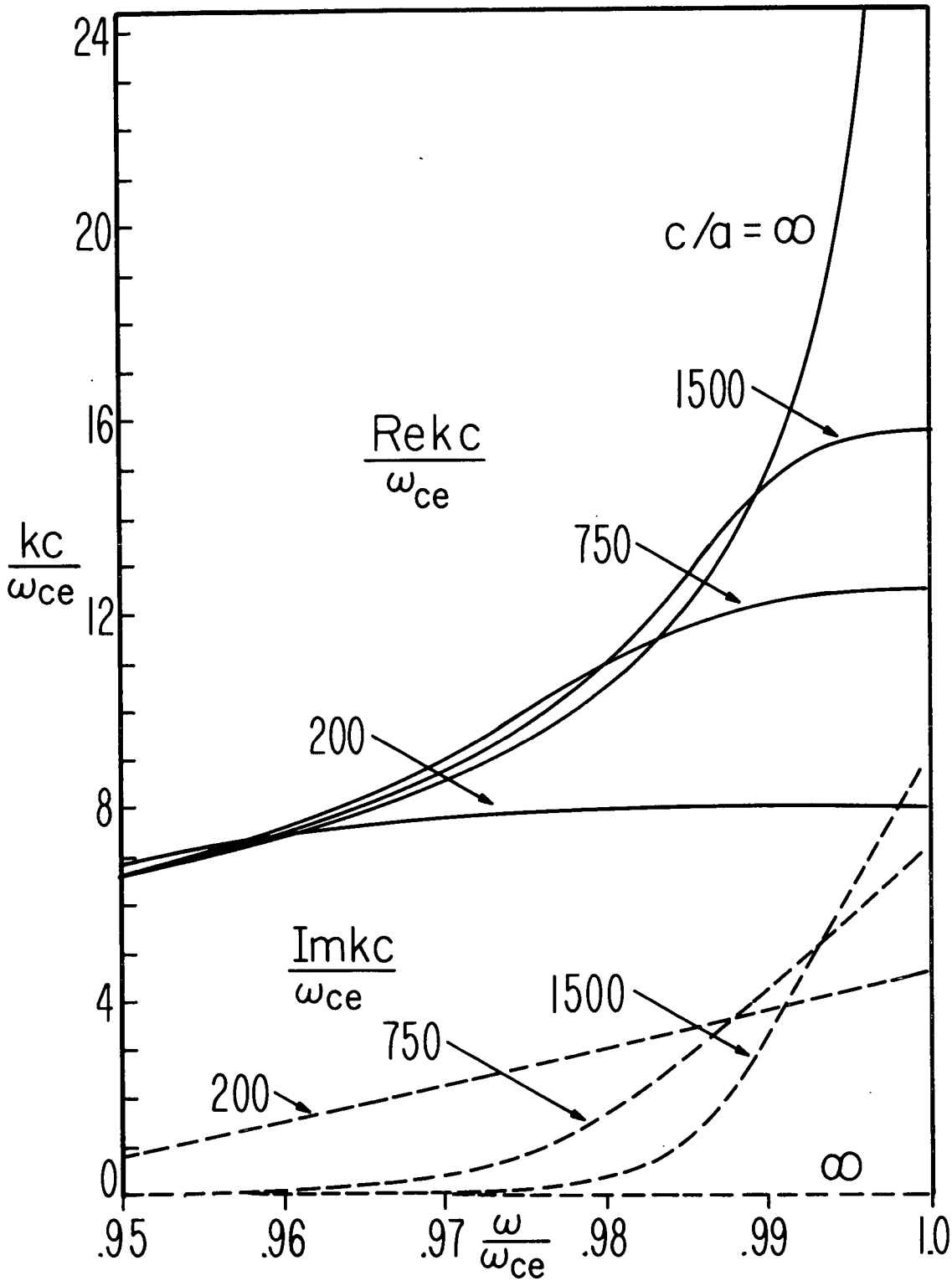

FIGURE C-4c. THE CYCLOTRON-DAMPED ROOT FOR $\omega_{pe}/\omega_{ce} = 1.5$.

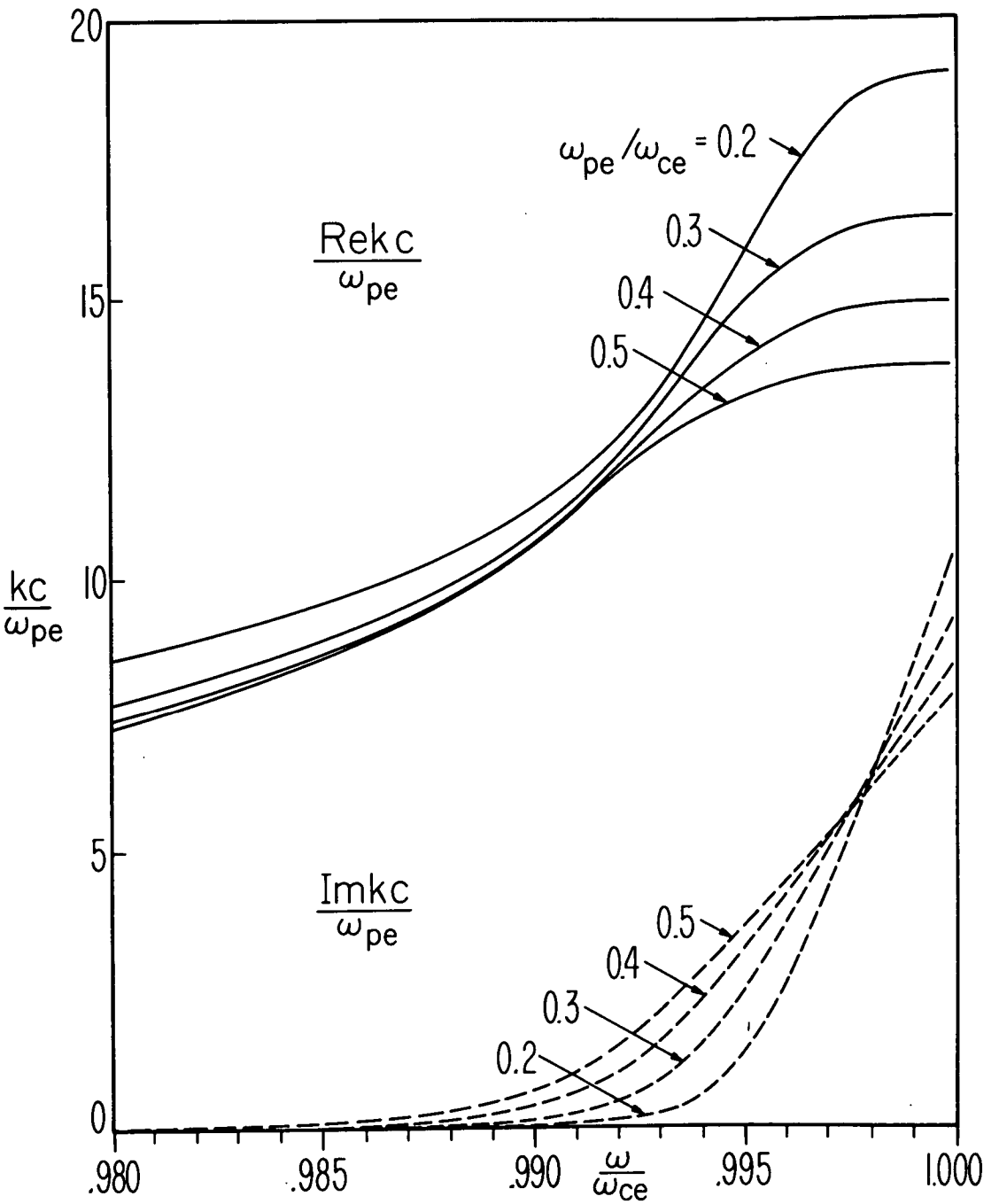

FIGURE C-5. THE CYCLOTRON-DAMPED ROOT FOR c/a = 1120.

Since Re k has a finite cutoff value, the phase velocity $\omega/\mathrm{Re}\ k$ does not approach zero (as it does in the cold plasma case) when ω approaches ω_{ce}. Instead it remains of the order of the speed of light since

$$V_{PHASE} = \frac{\omega}{\mathrm{Re}\,k} = \frac{\frac{\omega}{\omega_{ce}}}{\frac{\mathrm{Re}\,k c}{\omega_{ce}}} c \sim .1\, c \qquad (C.23)$$

where we have noted from Figs. C-4, C-5 that Re kc/ω_{ce} is typically of order 10 for $\omega \approx \omega_{ce}$. Of course the particles that are responsible for cyclotron damping are <u>not</u> those that move at v_{PHASE} but rather those that see a Doppler-shifted frequency $\omega-(\mathrm{Re}\ k)v$ equal to ω_{ce}. Those particles have velocity

$$V = \frac{\omega-\omega_{ce}}{\mathrm{Re}\,k} = \frac{\left(\frac{\omega}{\omega_{ce}}-1\right)}{\left(\frac{\mathrm{Re}\,k c}{\omega_{ce}}\right)} c \qquad (C.24)$$

which, of course, approaches zero as ω approaches ω_{ce}.

Now consider Im k. Note in each of Figs. C-4a,b,c (for ω_{pe}/ω_{ce} fixed) that for weak damping, increasing the temperature causes the damping to increase whereas for strong damping (ω extremely close to ω_{ce}), increasing the temperature causes the damping to actually decrease. A similar effect occurs in Fig. C-5 (for c/a fixed) where for weak damping, increasing ω_{pe}/ω_{ce} increases the damping whereas for strong damping, increasing ω_{pe}/ω_{ce} actually causes the damping to decrease. These effects will be explained physically in Section 4.1.

(ii) Cyclotron-damped root (ω slightly above ω_{ce}).

In the immediate vicinity of $\omega = \omega_{ce}$ the cyclotron-damped root has $\zeta_e \approx 0$. From the power series representation of the Z function,

$$Z_{\pm}(\zeta) = -2\zeta + \frac{4}{3}\zeta^3 - \frac{8}{15}\zeta^5 + \cdots \pm i\sqrt{\pi}\, e^{-\zeta^2} \tag{C.25}$$

we find to good approximation that

$$Z_{+}(\zeta) \approx -2\zeta + i\sqrt{\pi} \tag{C.26}$$

for $|\zeta| \ll 1$. Using (C.26) in (C.12) we find the transverse dispersion relation becomes

$$\left[\frac{kc}{\omega_{ce}}\right]^4 - \left[\frac{kc}{\omega_{ce}}\right]^3\left(\frac{\omega^2}{\omega_{ce}^2}\right) - \left[\frac{kc}{\omega_{ce}}\right]\left(i\sqrt{\pi}\,\frac{\omega\omega_{pe}^2 c}{\omega_{ce}^2 a}\right) + \left(2\frac{\omega_1}{\omega_{ce}}\left\{\frac{\omega_1}{\omega_{ce}} - 1\right\}\frac{\omega_{pe}^2}{\omega_{ce}^2}\frac{c}{a}\right) = 0 \tag{C.27}$$

which is correct provided

$$|\zeta_e| = \left|\frac{\omega - \omega_{ce}}{ka}\right| = \left|\frac{\left(\frac{\omega}{\omega_{ce}} - 1\right)\frac{c}{a}}{\frac{kc}{\omega_{ce}}}\right| \ll 1 \tag{C.28}$$

Since $|kc/\omega_{ce}|$ is of order 10, say (for $\omega \approx \omega_{ce}$), (C.28) holds only for $\left|[(\omega/\omega_{ce}) - 1]\,\frac{c}{a}\right| \ll 1$. Note that (C.27) is a true quartic equation.

For $\omega \approx \omega_{ce}$, i.e., for $\left|[(\omega/\omega_{ce}) - 1]\,\frac{c}{a}\right| \ll 1$ the second and fourth terms in (C.27) may be neglected (as can be justifed a posteriori) leaving

$$\left(\frac{kc}{\omega_{ce}}\right)^3 = \left[i\sqrt{\pi}\,\frac{\omega}{\omega_{ce}}\,\frac{\omega_{pe}^2 c}{\omega_{ce}^2 a}\right] \tag{C.29}$$

In this case the principal root of interest is

$$\frac{kc}{\omega_{ce}} = \left[\frac{\sqrt{\pi}}{2}\frac{\omega}{\omega_{ce}}\frac{\omega_{pe}^2 c}{\omega_{ce}^2 a}\right]^{\frac{1}{3}}(\sqrt{3}+i) \qquad (C.30)$$

which gives the value of the Re k cutoff exactly at $\omega = \omega_{ce}$ as mentioned earlier.

For ω near ω_{ce}, i.e., for $\left|[(\omega/\omega_{ce}) - 1]\frac{c}{a}\right| \lesssim 1$, we have solved the full quartic equation (C.27) analytically and numerically evaluated the solutions (which are quite complicated). We found that Re k was essentially constant near $\omega = \omega_{ce}$ while Im k increased uniformly as ω increased. Thus the cyclotron-damped root is given by (C.30) for $\omega = \omega_{ce}$ and this root is well behaved as ω departs from ω_{ce}.

To study the behavior of the cyclotron-damped root for $\omega > \omega_{ce}$ (i.e., for $[(\omega/\omega_{ce}) - 1]\frac{c}{a} \gtrsim 1$) we must resort back to solving (C.19) numerically. For $\omega \geq \omega_{ce}$ the two-pole approximation for the Z function in (C.19) may not be readily used, as will be explained in Section 4.2. Thus we have used the exact Z function to obtain the results presented in Fig. C-6; shown are the hot plasma results [obtained by solving (C.19)], together with the cold plasma result (C.9). We have considered frequencies in the range $\omega < \omega_{ce}$ to $\omega > \omega_R$ to give a complete picture of the behavior of the cyclotron-damped root in the evanescent region $\omega_{ce} < \omega < \omega_R$. (In Fig. C-6, the cold plasma results duplicate a small portion of Fig. C-2 while the hot plasma results duplicate part of the $\omega_{pe}/\omega_{ce} = 0.4$ curves in Fig. C-5.) The dip (at $\omega \gtrsim \omega_{ce}$) in the hot plasma Re k curve in Fig. C-6

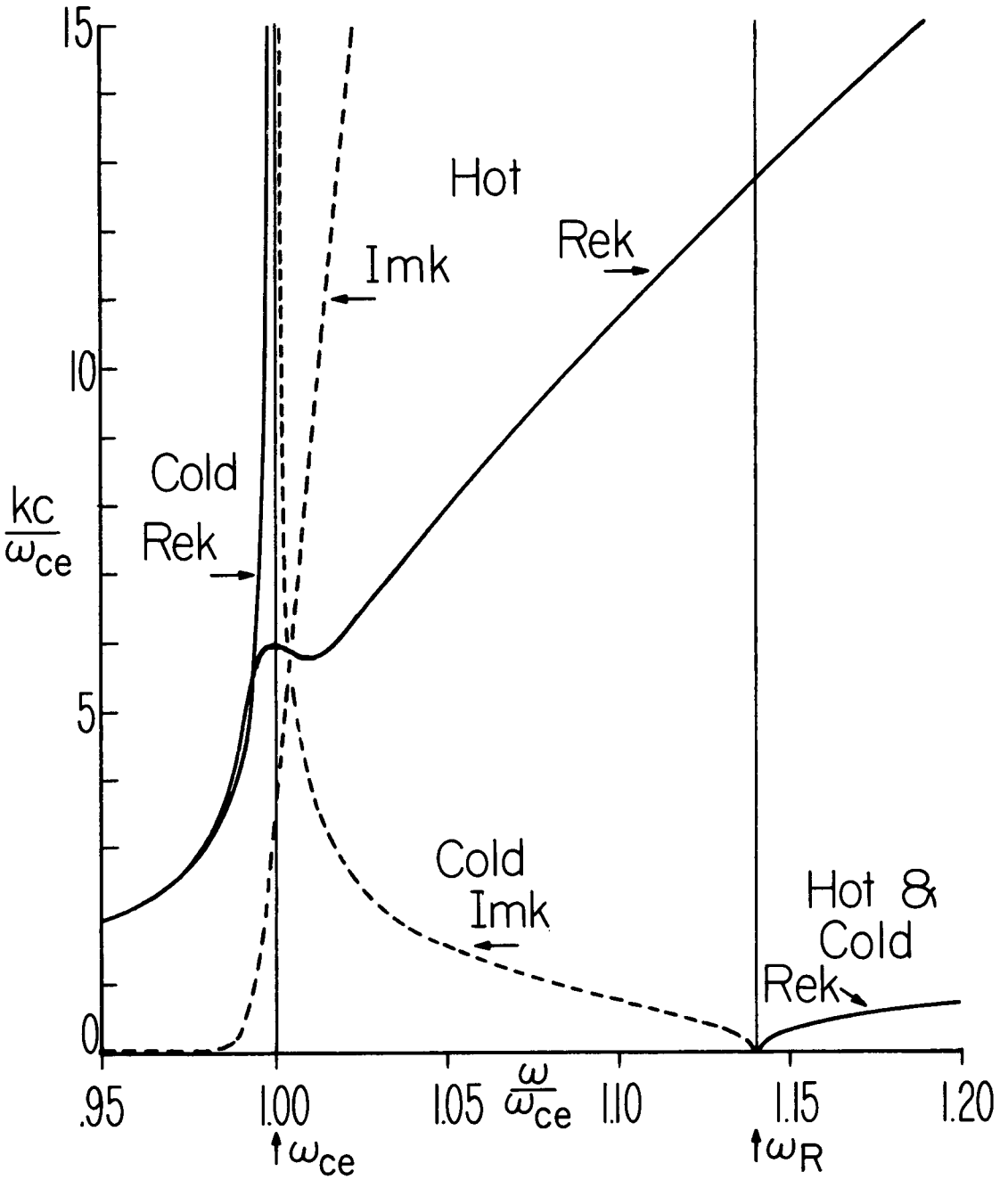

FIGURE C-6. COMPARISON OF HOT PLASMA AND COLD PLASMA ROOTS IN THE EVANESCENT REGION $\omega_{ce} < \omega < \omega_R$.

Comparison of the hot plasma cyclotron-damped root of (C.8) to the cold plasma root (C.9). (c/a=1120, ω_{pe}/ω_{ce}=.4) For $\omega>\omega_{ce}$, Im k of the hot plasma root keeps increasing linearly (even for $\omega>\omega_R$).

flattens out as c/a or ω_{pe}/ω_{ce} decreases.

Note the large difference between the hot plasma root and the cold plasma root for $\omega_{ce} < \omega < \omega_R$ in Fig. C-6. Actually there is no true discrepancy because the "cold" plasma pure imaginary root is also a valid hot plasma root (as will be discussed shortly). And, in fact, both roots are included in the response for a single transverse excitation. [In Fig. 3 of Part I, only the cyclotron-damped root of $\varepsilon_{T_+}(k,\omega_1) = 0$ is shown; actually the pure imaginary ("cold" plasma) root of $\varepsilon_{T_-}(k,\omega_1) = 0$ also produces a residue term for $\omega_{ce} < \omega < \omega_R$.] Since the dominant root is the one with the smallest value of $\text{Im } k$, we see in Fig. C-6 that the "cold" plasma root dominates for most of the region $\omega_{ce} < \omega < \omega_R$; only for $\omega \approx \omega_{ce}$ is the cyclotron-damped root dominant. Thus the sharp transition from pure real k to pure imaginary k that occurs at $\omega = \omega_{ce}$ in the cold plasma case is effectively smoothed out when finite temperature effects are included.

(iii) Infinite sequence of roots.

In the above discussion we examined the cyclotron-damped root of (C.19). For $\omega \gtrsim \omega_{ce}$ this root is on the first curved solid locus in the lower-half ζ_e plane in Fig. C-3. However, note that this branch is just the first of an infinite number of similar branches that progress lower and lower in the ζ_e plane. And it is important to realize that the lower the branch is in the ζ_e plane, the less damped the corresponding roots in the k plane are, because $k \sim 1/\zeta_e$ [see (C.22)]. Accordingly the most-damped root in the ζ_e plane is the least-damped and possibly most significant root in the k plane.

We proceed to examine these roots.

We present first, in Figs. C-7, C-8, the results of two numerical examples which show the infinite sequence of roots in the ζ_e plane and the corresponding infinite sequence of roots in the k plane. For these examples we chose values of ω in the interval $\omega_{ce} < \omega < \omega_R$ although the resultant distributions of roots in the ζ_e and k planes remain qualitatively the same for all values of ω. Note that the roots in Figs. C-7a and C-8a are specific points on the loci of roots given earlier in Fig. C-3. Also note from these figures that as $|\zeta_e| \to \infty$, $|k| \to 0$. Thus as just explained, the most-damped root in the ζ_e plane is the least-damped root in the k plane.

For all values of ω the roots in the k plane approach the origin along a 45° line as $|\zeta_e|$ approaches infinity. There results an infinite number of roots in the k plane whose real and imaginary parts approach zero. This is a rather disturbing result since it seems these roots might dominate the response of a steady-state transverse excitation. Fortunately, however, when the appropriate infinite sum of residues is computed (as is done in Part I) we find that the response is not significantly affected by the infinite sequence of roots except at positions very close to the place of excitation.

Approximate values of infinite-sequence roots.

We now obtain an expression for the approximate value of the roots in the infinite sequence in the ζ_e plane. Considering only $|\zeta_e| \gtrsim 3$ we use the asymptotic expansion of the Z function [as given by (C.3)] in the transverse dispersion relation (C.12). We restrict our attention

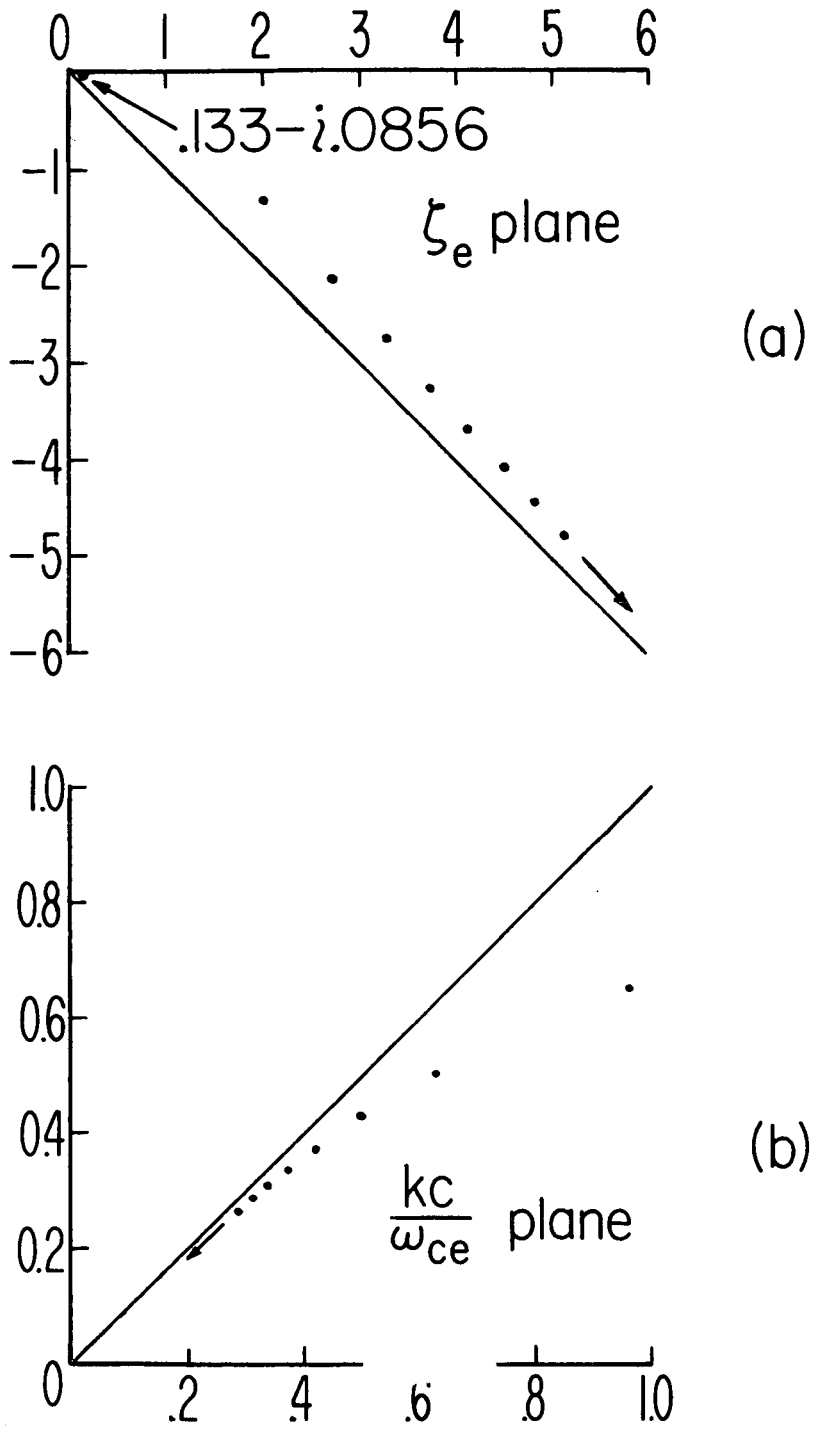

FIGURE C-7. INFINITE SEQUENCE OF ROOTS FOR ω/ω_{ce} = 1.001 . Shown in (a) are the roots in the ζ_e plane and in (b) the corresponding roots in the kc/ω_{ce} plane (c/a=1120, ω_{pe}/ω_{ce}=.4) . Not shown in (b) is the root 14.86+i9.56 that corresponds to the root 0.133-i0.0856 in (a).

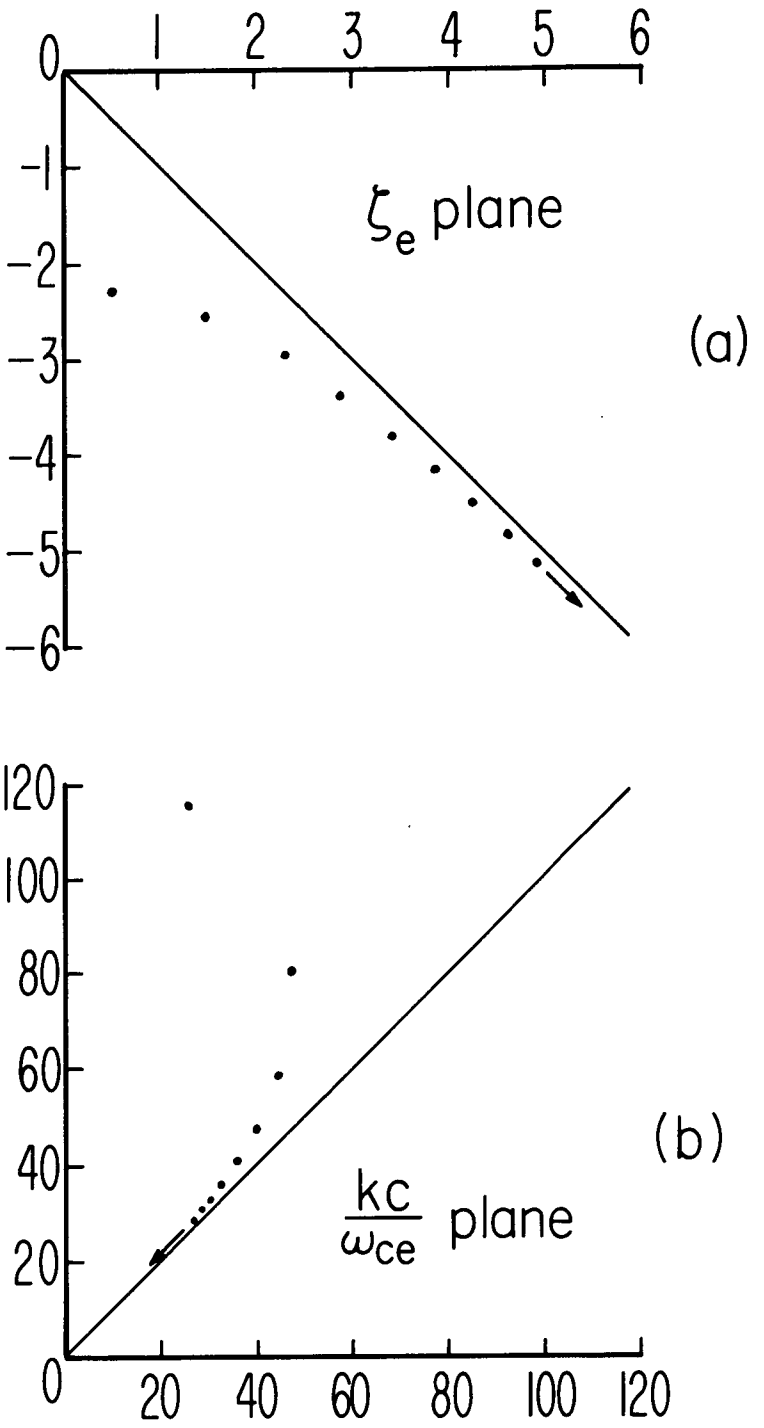

FIGURE C-8. INFINITE SEQUENCE OF ROOTS FOR $\omega/\omega_{ce} = 1.1$.

(c/a=1120 , ω_{pe}/ω_{ce}=.4)

to $\text{Im}\,\zeta_e < 0$ so $\sigma_+(\zeta_e) = 2$ and therefore

$$Z_+(\zeta_e) \approx -\frac{1}{\zeta_e} + 2\sqrt{\pi}\, i\, e^{-\zeta_e^2} \tag{C.31}$$

We shall (1) show that the term $2\sqrt{\pi}i \exp[-\zeta_e^2]$ causes the infinite sequence of roots, (2) obtain an expression for the approximate value of these roots, and (3) obtain an expression for the term $2\sqrt{\pi}i \exp[-\zeta_e^2]$ evaluated at these roots (the latter expression for use in Part I, in calculating the infinite sum of residue terms associated with the infinite sequence of roots).

Using (C.31) in (C.12), the transverse dispersion relation becomes

$$2\sqrt{\pi}\, i\, e^{-\zeta_e^2} = \frac{D}{\zeta_e} + \frac{E}{\zeta_e^3}$$

$$D \equiv \left[1 - \frac{\omega(\omega - \omega_{ce})}{\omega_{pe}^2}\right] \tag{C.32}$$

$$E \equiv \left[\frac{(\omega - \omega_{ce})^3 c^2}{\omega\, \omega_{pe}^2\, a^2}\right]$$

We restrict our attention to the fourth quadrant of the ζ_e plane (since any root ζ_e in the fourth quadrant has the corresponding root $-\zeta_e^*$ in the third quadrant, as follows from Appendix B). Then $\zeta_e = |\text{Re}\,\zeta_e| - i\,|\text{Im}\,\zeta_e|$ and the left-hand side of (C.32) may be written as

$$2\sqrt{\pi}\, i\, e^{-\zeta_e^2} = 2\sqrt{\pi}\, e^{-\left[(\text{Re}\,\zeta_e)^2 - (\text{Im}\,\zeta_e)^2\right]}\, e^{i\left[2(\text{Re}\,\zeta_e)\,|\text{Im}\,\zeta_e| + \frac{\pi}{2}\right]} \tag{C.33}$$

Note that the factor $\exp\left(-[(\text{Re}\,\zeta_e)^2 - (\text{Im}\,\zeta_e)^2]\right)$ equals unity when ζ_e

is on the -45° line in the ζ_e plane, and that this factor changes size very rapidly (for $|\zeta_e| \gtrsim 3$) when ζ_e departs from the -45° line. Thus even though the magnitude of the right-hand side of (C.32) may vary considerably, by only slightly departing from the -45° line, the left-hand side of (C.32) can match it and a root occurs. (This explains why the infinite-sequence roots are always near the -45° line.) Also, at a root the phase factor in (C.33), $[2(\text{Re } \zeta_e)|(\text{Im } \zeta_e)| + \pi/2]$, must equal the corresponding phase factor of the right-hand side of (C.32) plus any integral multiple of 2π. (This last consideration explains the multiplicity of roots.) Thus we have shown qualitatively how the term $2\sqrt{\pi}i \exp[-\zeta_e^2]$ produces the infinite sequence of roots.

To obtain an expression for the approximate value of the roots of (C.32), we note that a root occurs whenever the magnitudes (and phases) of the right- and left-hand sides of (C.32) are equal. From the above discussion we know the roots are near the -45° line. Thus we set $\zeta_e = \rho e^{-i(\pi/4)}$ (ρ real, > 0) everywhere in (C.32), (C.33), except in the factor $\exp\left(-[(\text{Re } \zeta_e)^2 - (\text{Im } \zeta_e)^2]\right)$. Then, at a root, the phases of the two sides of (C.32) must be equal, i.e., we must have

$$\rho^2 + \frac{\pi}{2} = \text{PHASE OF} \left\{ \frac{D e^{i\frac{\pi}{4}}}{\rho} + \frac{E e^{i\frac{3\pi}{4}}}{\rho^3} \right\} + 2m\pi \qquad \text{(C.34)}$$

where $n = 0, \pm 1, \pm 2, \ldots$. For $|n| \geq 3$, we have $\rho^2 \approx 2n\pi$. Alternatively we may say that the roots in the infinite sequence are given by

$$\zeta_e = \rho e^{-i\frac{\pi}{4}}$$

$$\rho = \sqrt{2m\pi} \qquad m = 3, 4, 5, \cdots \qquad \text{(C.35)}$$

and the value of the term $2\sqrt{\pi}i \exp[-\zeta_e^2]$ at such roots is simply given by the right-hand side of (C.32) evaluated at the roots. In (C.35) n starts at $n = 3$ because in using (C.31) we assumed $|\zeta_e| \gtrsim 3$. It follows from Fig. C-3 that only the first two roots of the infinite sequence (which have $|\zeta_e| \lesssim 3$) need to be calculated accurately while the rest of them are given approximately by (C.35).

[In the above, note that it was not necessary to express $Z_+(\zeta_e)$ in terms of Fresnel functions for ζ_e along the -45° line and then use asymptotic expansions for the Fresnel functions to obtain the approximate values of the intercepts of the loci of (C.12) with the -45° line (as was done for the longitudinal case in Refs. 7 and 8) since we were able to obtain approximate values for the roots and even the value of the term $2\sqrt{\pi}i \exp[-\zeta_e^2]$ at these roots by simply considering the asymptotic expansion of the Z function.]

The infinite sequence of roots in the ζ_e plane, as discussed above, occurs only in the lower-half ζ_e plane (Im $\zeta_e < 0$). [For Im $\zeta_e > 0$, $\sigma_+(\zeta_e) = 0$ and there is no $2\sqrt{\pi}i \exp(-\zeta_e^2)$ term to produce the infinite sequence of roots.] We now determine where the corresponding roots in the k plane are. Since $k = (\omega-\omega_{ce})/\zeta_e a$, Im $\zeta_e < 0$ implies Im $k < 0$ for $\omega < \omega_{ce}$ and Im $k > 0$ for $\omega > \omega_{ce}$. Thus the infinite sequence of roots occurs in the lower-half k plane for $\omega < \omega_{ce}$ and in the upper-half k plane for $\omega > \omega_{ce}$.

(iv) Pure imaginary roots.

The hot plasma dispersion relation (C.8) has the pure imaginary root(s)

$$k = \pm i \left[\frac{\omega^2}{c^2} \left(\frac{\omega_{pe}^2}{\omega(\omega - \omega_{ce})} - 1 \right) \right]^{\frac{1}{2}} \qquad \text{(C.36)}$$

(for $\omega_L < \omega < 0$ and $\omega_{ce} < \omega < \omega_R$) but only if the root is in the half of the k plane wherein $\text{Im}\, \zeta_e > 0$. In the half of the k plane wherein $\text{Im}\, \zeta_e < 0$ there may be a pure imaginary root of (C.8) but it is not given by (C.35) because the term $2\sqrt{\pi} i \exp[-\zeta_e^2]$ (which goes as $\exp[+|\zeta_e|^2]$ for ζ_e pure imaginary) was not adequately considered in obtaining (C.36).

For a pure imaginary root, $\zeta_e^2 = -|\zeta_e|^2$ and the hot plasma dispersion relation (C.12) may be written as

$$\zeta_e^3 Z_+(\zeta_e) = \left[\frac{(\omega - \omega_{ce})^3 c^2}{\omega \omega_{pe}^2 a^2} \right] + \left[\frac{\omega(\omega - \omega_{ce})}{\omega_{pe}^2} \right] |\zeta_e|^2 \qquad \text{(C.37)}$$

Note that the right-hand side of (C.37) is positive for $\omega < 0$, $\omega > \omega_{ce}$ and negative for $0 < \omega < \omega_{ce}$. Thus we distinguish the following two cases.

(1) $\omega < 0$, $\omega > \omega_{ce}$: From Fig. C-3 we know that for $\omega < 0$, $\omega > \omega_{ce}$ any allowed pure imaginary root has $\zeta_e = +i|\zeta_e|$ in which case $\sigma_+(\zeta_e) = 0$. And we note in general that the right-hand side of (C.37) is very large (except for ω extremely close to ω_{ce}). Thus any root of (C.37) will have $|\zeta_e| \gtrsim 3$ in which case the cold plasma results are valid; i.e., for $\omega < \omega_L$, $\omega > \omega_R$ there is no pure imaginary root whereas for $\omega_L < \omega < 0$ and $\omega_{ce} < \omega < \omega_R$ there is one pure imaginary root, given by (C.36), that occurs in the half of the

k plane wherein $\text{Im}\,\zeta_e > 0$.

(2) $0 < \omega < \omega_{ce}$: From Fig. C-3 we know that for $0 < \omega < \omega_{ce}$ any allowed pure imaginary root has $\zeta_e = -i|\zeta_e|$ in which case $\sigma_+(\zeta_e) = 2$. In this case (C.37) may be written as

$$e^{+|\zeta_e|^2} = \frac{1}{2\sqrt{\pi}}\left\{\left|\frac{(\omega-\omega_{ce})^3 c^2}{\omega\omega_{pe}^2 a^2}\right|\frac{1}{|\zeta_e|^3} + \left|\frac{\omega(\omega-\omega_{ce})}{\omega_{pe}^2}\right|\frac{1}{|\zeta_e|} + |Z|\right\} \qquad \text{(C.38)}$$

[in which Z represents the principal part integral of $Z_+(\zeta_e)$ as given in (2.51) of Part I]. Since $\exp[+|\zeta_e|^2]$ is a rapidly growing function of $|\zeta_e|$ we note that the root of (C.38) will typically have $|\zeta_e| \lesssim 4$, say. In general, (C.38) must be solved numerically.

Thus cold plasma theory predicts pure imaginary roots only in the two evanescent regions $\omega_L < \omega < 0$ and $\omega_{ce} < \omega < \omega_R$. Hot plasma theory also predicts these roots occur (but only on the side of the k plane wherein $\text{Im}\,\zeta_e > 0$). In addition, hot plasma theory predicts a pure imaginary root for $0 < \omega < \omega_{ce}$.

3.3 Summary of roots in the complex k plane.

The cold plasma dispersion relation (C.9) with negligible hot plasma damping (C.10) is valid in the two propagating regions $\omega < \omega_L$ and $\omega > \omega_R$. In the propagating region $0 < \omega < \omega_{ce}$ except for $\omega \approx \omega_{ce}$ a root is also given by (C.9) but with no damping term. For $\omega \approx \omega_{ce}$ we must solve the full hot plasma dispersion relation (C.8) numerically. Some numerical calculations of this root are given in Figs. C-4, C-5 for ω slightly below ω_{ce} and in Fig. C-6 for ω slightly above ω_{ce} .

In the half of the k plane wherein $\text{Im}\,\zeta_e < 0$ there are an infinite number of roots of (C.8) which asymptotically approach the origin in the k plane along a 45° line. Some numerical results concerning these roots are presented in Figs. C-7, C-8, and the approximate values of these roots are given by (C.35).

Also, pure imaginary roots occur for some values of ω. For $\omega < \omega_L$ and $\omega > \omega_R$ there is no pure imaginary root, whereas for $\omega_L < \omega < 0$ and $\omega_{ce} < \omega < \omega_R$ there is a pure imaginary root given by (C.36) (that occurs in the half of the k plane wherein $\text{Im}\,\zeta_e > 0$). For $0 < \omega < \omega_{ce}$ there is also a pure imaginary root, which can be found by solving (C.38) numerically.

We have summarized these results in Fig. C-9 which shows the roots of $\varepsilon_{T_+}(k,) = 0$ for all choices of ω. We have used the symmetry property (from Appendix B) that all roots in the left-half k plane are mirror images about the imaginary axis of roots in the right-half k plane.

In Fig. C-10 we have summarized the roots of $\varepsilon_{T_+}(k,\omega) = 0$ and of $\varepsilon_{T_-}(k,\omega) = 0$ (shown by crosses) in the upper-half k plane. The roots of $\varepsilon_{T_-}(k,\omega) = 0$ are mirror images across the real axis of the roots of $\varepsilon_{T_+}(k,\omega) = 0$ (this symmetry property was also given in Appendix B).

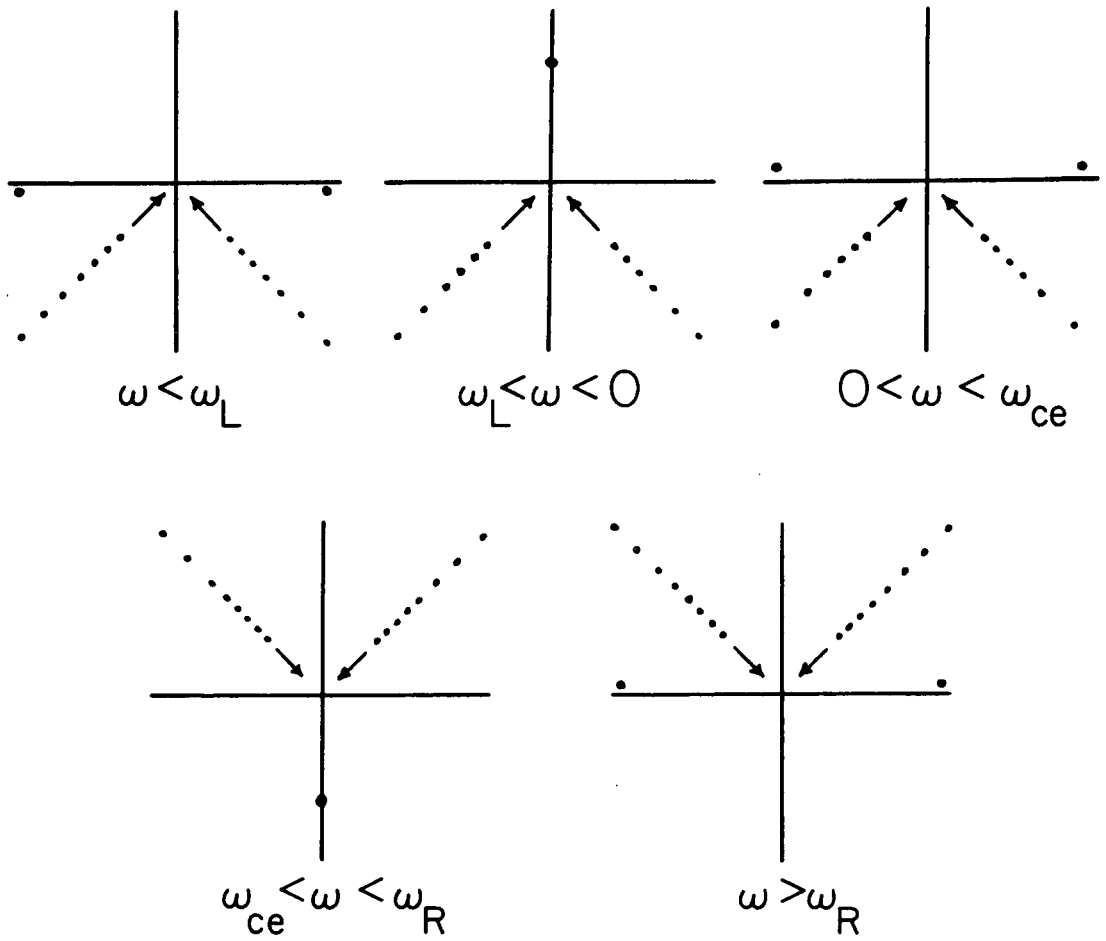

FIGURE C-9. ROOTS OF $\epsilon_{T\pm}(k,\omega) = 0$ [DOTS] IN THE WHOLE COMPLEX k PLANE.

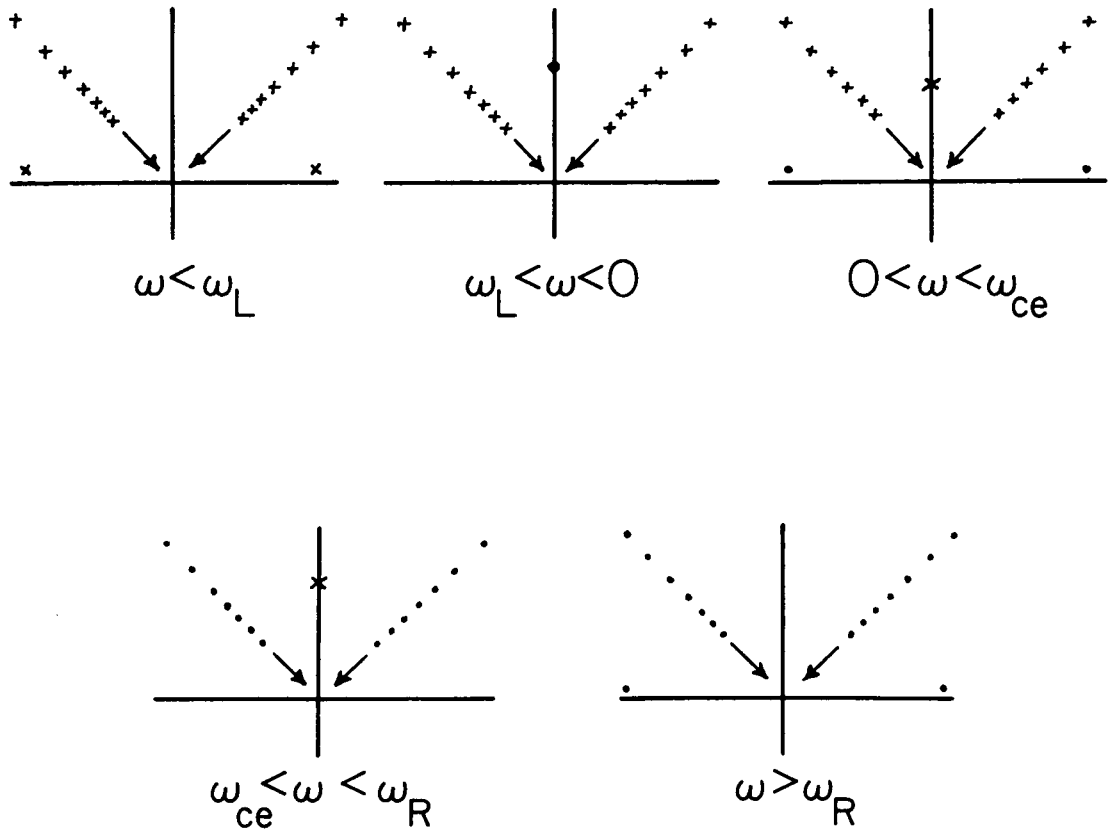

FIGURE C-10. ROOTS OF $\epsilon_{T+}(k,\omega) = 0$ [DOTS] AND ROOTS OF $\epsilon_{T-}(k,\omega) = 0$ [CROSSES] IN THE UPPER-HALF k PLANE.

4. Special Considerations

4.1 Physical explanations of cyclotron-damped root results.

In this section we want to explain physically the (cyclotron-damped) Im k curves of Figs. C-5, C-6. As discussed earlier, cyclotron damping is caused by those particles whose Doppler-shifted frequency is approximately equal to the cyclotron frequency. Roughly, the damping particles are those which have v_z within

$$\left(V - \frac{|\Delta V|}{2}\right) \leq v_z \leq \left(V + \frac{|\Delta V|}{2}\right)$$

where v is defined exactly and Δv approximately by

$$\begin{aligned} \omega - (Re\,k)V &= \omega_{ce} \\ \left[\omega - (Re\,k)(V+\Delta V)\right] - \omega_{ce} &= \alpha\,\omega_{ce} \end{aligned} \tag{C.39}$$

in which α is some small number (like 0.001). Thus

$$\begin{aligned} V &= \frac{\omega - \omega_{ce}}{Re\,k} \\ \Delta V &= \frac{\alpha\,\omega_{ce}}{Re\,k} \end{aligned} \tag{C.40}$$

and the number of damping particles N is roughly

$$N \approx n\, f_0(V)\, \Delta V \tag{C.41}$$

Using a Maxwellian distribution for $f_0(v_z)$

$$f_0(v_z) = \frac{1}{\sqrt{\pi}\,a}\, e^{-\left(\frac{v_z}{a}\right)^2} \tag{C.42}$$

we have

$$N \approx \frac{\alpha\left(\frac{c}{a}\right)n}{\sqrt{\pi}\left(\frac{Re\,k\,c}{\omega_{ce}}\right)} e^{-\left(\frac{v_z}{a}\right)^2} \tag{C.43}$$

In each of Figs. 5a,b,c we consider n and B_o fixed and examine the effects of varying T_e. Using (C.39) - (C.43) we show in Figs. C-11 the particles responsible for the damping. Note that increasing T_e broadens the tails of $f_o(v_z)$ and lowers the center peak. For weak damping, v is out on the tail of $f_o(v_z)$ and therefore increasing T_e increases N. For strong damping ($\omega \simeq \omega_{ce}$) $v \simeq 0$ and therefore increasing T_e actually decreases N. This explains the behavior of the Im k curves in Figs. 5a,b,c.

In Fig. C-6 we consider n and T_e fixed and examine the effects of varying B_o. In this case increasing ω_{pe}/ω_{ce} means decreasing B_o (but to maintain the same horizontal position in Fig. C-5 we must keep ω/ω_{ce} fixed). In Fig. C-12 we show the particles responsible for the damping; note that v and Δv change while $f_o(v_z)$ remains constant. [This may be seen by writing (C.40) as

$$v = \frac{\omega - \omega_{ce}}{Re\,k} = \frac{\left(\frac{\omega}{\omega_{ce}} - 1\right)c}{\left(\frac{Re\,k\,c}{\omega_{ce}}\right)\left(\frac{\omega_{pe}}{\omega_{ce}}\right)}$$

$$\Delta v = \frac{\alpha\,\omega_{ce}}{Re\,k} = \frac{\alpha\ \ c}{\left(\frac{Re\,k\,c}{\omega_{ce}}\right)\left(\frac{\omega_{pe}}{\omega_{ce}}\right)} \tag{C.44}$$

and noting in Fig. C-6 that $(\text{Re } kc/\omega_{pe})(\omega_{pe}/\omega_{ce}) \sim \omega_{pe}/\omega_{ce}$.] For

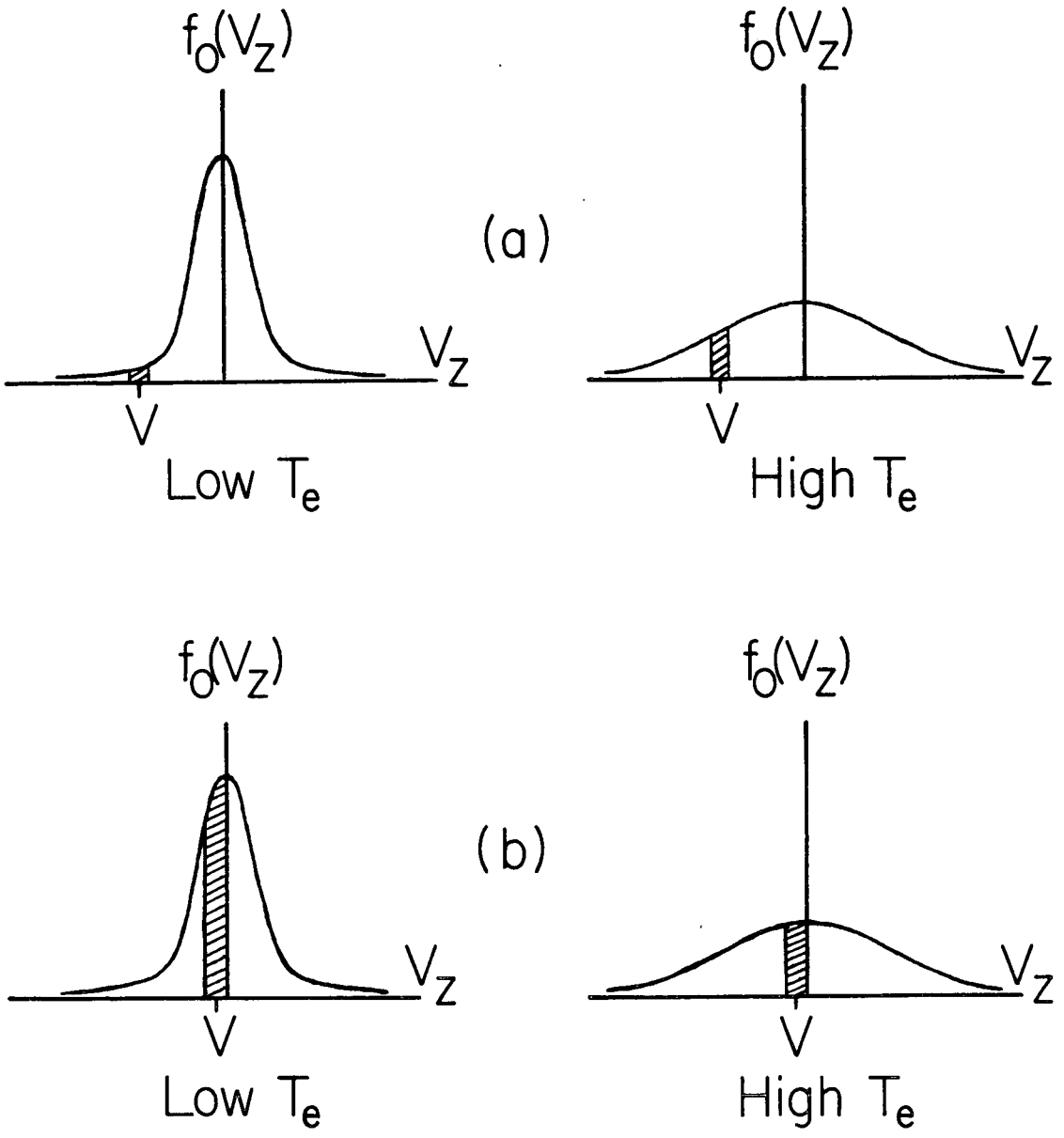

FIGURE C-11. PARTICLES RESPONSIBLE FOR ELECTRON CYCLOTRON DAMPING WHEN n_e AND $\underline{B}_o$ ARE FIXED AND T_e IS VARIED.

(a) Weak damping.
(b) Strong damping.

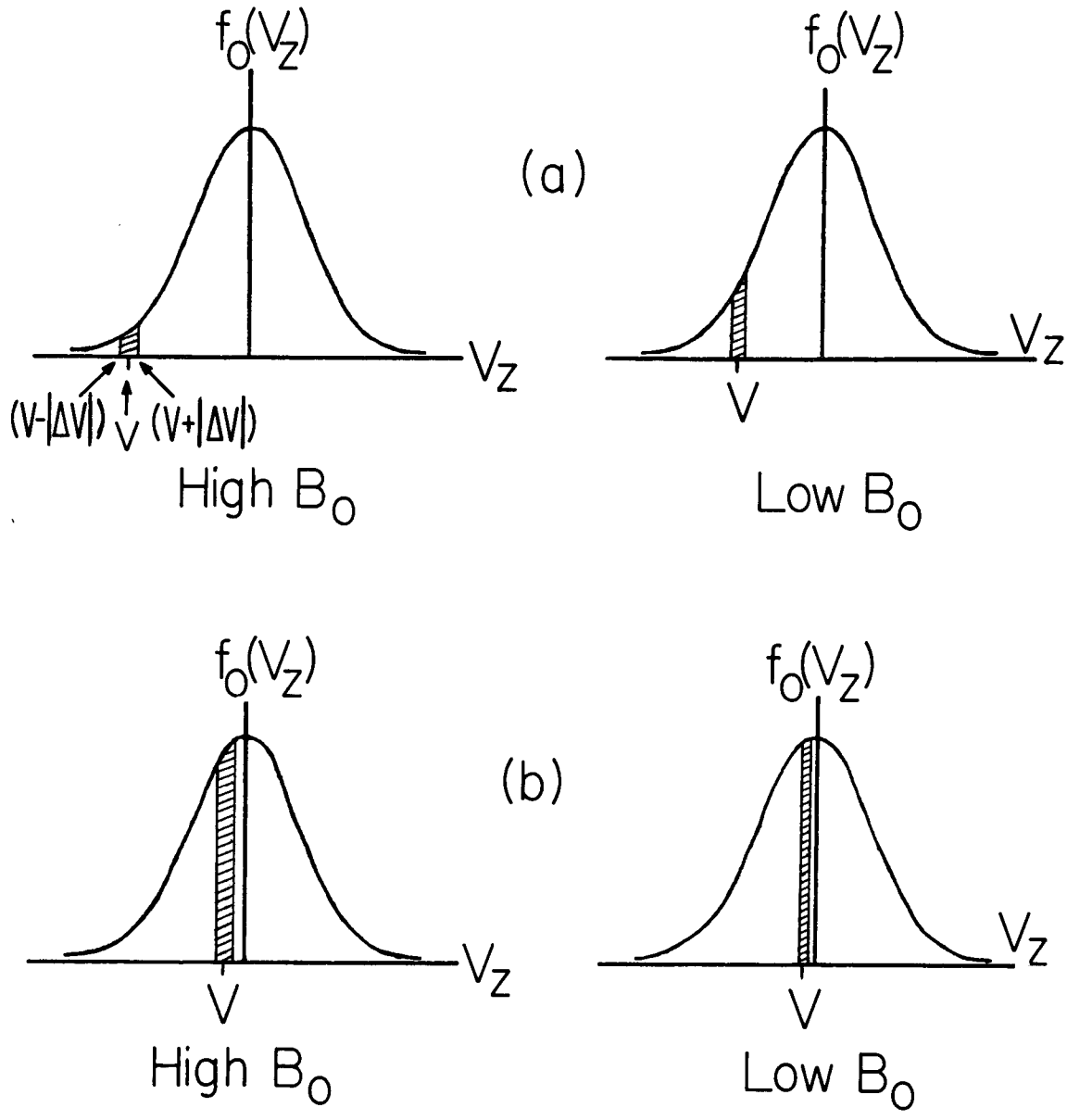

FIGURE C-12. PARTICLES RESPONSIBLE FOR ELECTRON CYCLOTRON DAMPING WHEN n_e AND T_e ARE FIXED AND $\underline{B}_0$ IS VARIED.

(a) Weak damping.
(b) Strong damping.

weak damping, the number of damping particles depends mainly on v which is out on the tail of $f_o(v_z)$. Thus decreasing B_o decreases v thereby increasing N . For strong damping ($\omega \approx \omega_{ce}$) $v \approx 0$ and the number of damping particles depends mainly on the velocity spread width Δv . In this case decreasing B_o decreases Δv thereby decreasing N . This explains the behavior of the Im k curves in Fig. C-6.

4.2 Why the two-pole approximation for $Z(\zeta)$ should not be used in calculating the cyclotron-damped root for $\omega \gtrless \omega_{ce}$.

In this section we explain why the two-pole approximation[34] for $Z(\zeta)$ should not be used in computing the cyclotron-damped root for $\omega \gtrless \omega_{ce}$. As shown in Fig. C-13, the locus of this root begins at $\zeta_e = 0$ (for $\omega = \omega_{ce}$) and progresses downward as ω increases. As will be explained, the two-pole approximation is in error in the region defined by Im $\zeta < 0$ and $|\zeta| \lesssim 3$. Since the cyclotron-damped root passes through this region for $\omega \gtrless \omega_{ce}$, the two-pole approximation should not be used in computing the root in this region.

For Im $\zeta > 0$ the two-pole approximation matches the first two terms in the power series $[Z_+(\zeta) \approx i\sqrt{\pi} - 2\zeta]$ for small ζ and the first term in the asymptotic series $[Z_+(\zeta) \approx -1/\zeta]$ for large ζ . For Im $\zeta < 0$ one is instructed to add on the term $2\sqrt{\pi} i\, e^{-\zeta^2}$. Clearly this is correct only for $|\zeta| \gtrsim 3$ because only the asymptotic series (which is valid for $|\zeta| \gtrsim 3$) has the term $i\sqrt{\pi}\, \sigma_+(\zeta)\, e^{-\zeta^2}$. The power series has no additional term for Im $\zeta < 0$. Thus, as

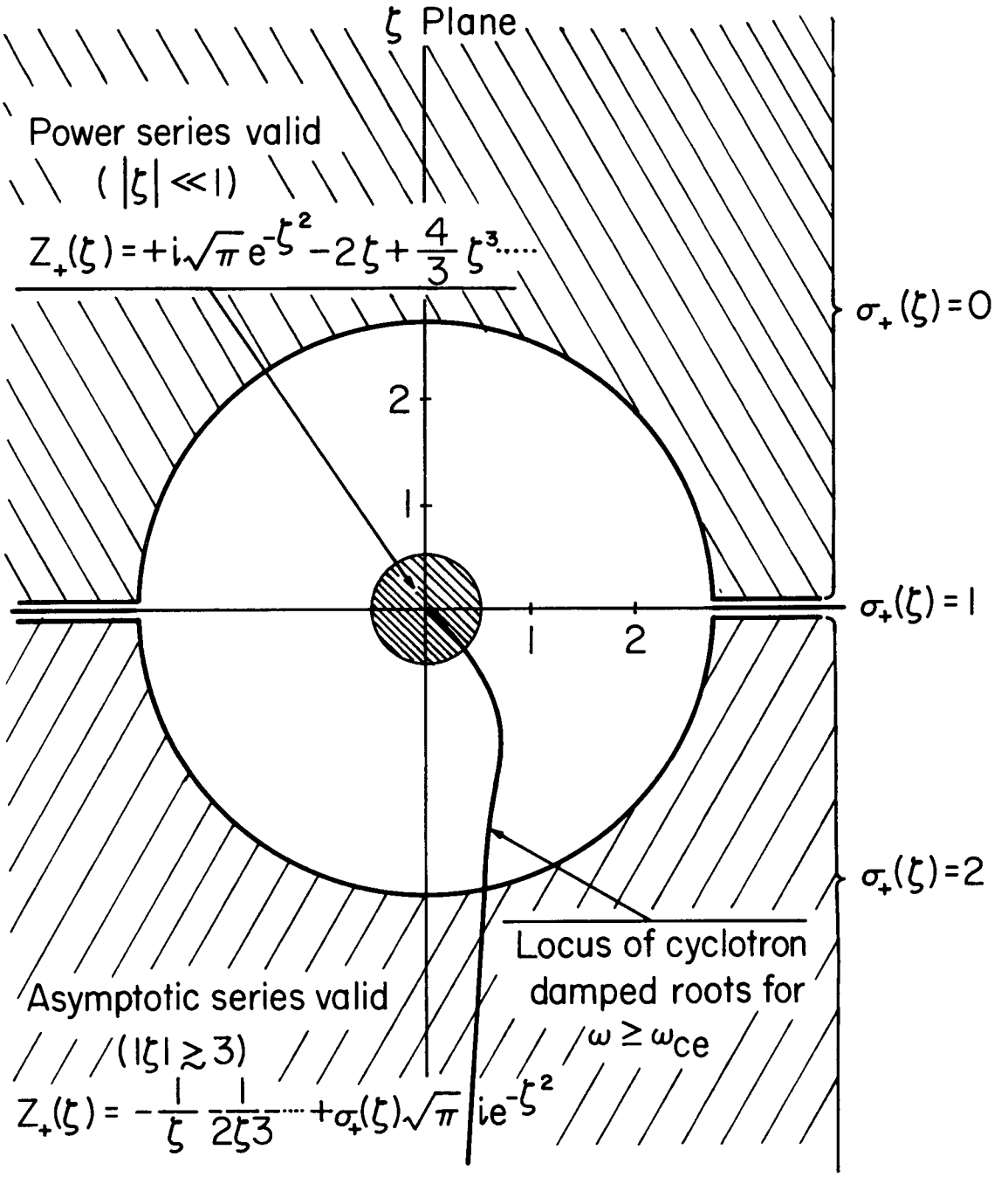

FIGURE C-13. REGION IN THE ζ PLANE WHEREIN THE TWO-POLE APPROXIMATION FOR Z(ζ) SHOULD NOT BE USED.

Shown are regions of the ζ plane wherein the power series and asymptotic series of $Z_+(\zeta)$ are useful approximations. The two-pole approximation[34] for $Z_+(\zeta)$ should not be used for Im $\zeta < 0$ and $1 \leq |\zeta| \leq 3$ (see text). Also shown is the locus of cyclotron-damped roots for $\omega \geq \omega_{ce}$, as given in Fig. C-3.

presented, the two-pole approximation is in error in the region defined by $\mathrm{Im}\,\zeta < 0$ and $|\zeta| \lesssim 3$.

We are left with the problem of deciding specifically when the term $2\sqrt{\pi}i\, e^{-\zeta^2}$ should be added on. (Presumably this should occur for $\mathrm{Im}\,\zeta < 0$ and $|\zeta|$ somewhere between 2 and 3.) Furthermore, at the place where the term is added on, the two-pole approximation for $Z(\zeta)$ will effectively suffer a discontinuity, whereas the true Z function is continuous. To avoid this artificial discontinuity, the exact Z function should be used in the troublesome region. In summary, for $\mathrm{Im}\,\zeta < 0$ and

for $\lvert\zeta\rvert \lesssim 1$	add nothing;
for $1 \lesssim \lvert\zeta\rvert \lesssim 3$	use the exact Z function; and
for $3 \lesssim \lvert\zeta\rvert \gtrsim 3$	add $2\sqrt{\pi}i\, e^{-\zeta^2}$.

In actual practise, such as in computing the cyclotron-damped root for $\omega \gtrsim \omega_{ce}$ it is probably least confusing to use the exact Z function for all $\mathrm{Im}\,\zeta < 0$.

4.3 Effects of anisotropic temperature ($T_\perp \neq T_z$).

All of the above work was done for $T_\perp = T_z$. For $T_\perp \neq T_z$ we have from (2.40) of Part I that, neglecting ions,

$$\epsilon_T(k,\omega) = 1 - \frac{\omega_{pe}^2\,\omega}{(k^2c^2-\omega^2)} \int_{-\infty}^{+\infty} \frac{dv_z\, f_0(v_z)\left[1 - \frac{kv_z}{\omega}\left(1 - \frac{T_\perp}{T_z}\right)\right]}{kv_z - \omega + \omega_{ce}} \qquad \text{(C.45)}$$

Taking $f_0(v_z)$ to be Maxwellian, we obtain

$$\epsilon_{T_\pm}(k,\omega) = 1 - \frac{\omega}{(k^2c^2-\omega^2)}\frac{\omega_{pe}^2}{ka}\left\{Z_\pm(\zeta_e) + \frac{ka\alpha}{2\omega}Z'_\pm(\zeta_e)\right\} \tag{C.46}$$

where $\alpha \equiv 1 - (T_\perp/T_z)$ and $Z'(\zeta) \equiv \frac{\partial}{\partial\zeta}Z(\zeta)$. Assuming $|\zeta_e| \gtrsim 3$ and $|\mathrm{Re}\ k| >> |\mathrm{Im}\ k|$, and proceeding as in (C.3) - (C.7), we find the least-damped root of $\epsilon_{T_+}(k,\omega) = 0$ to have

$$\mathrm{Re}\,k = \frac{\pm\frac{\omega}{c}\left[1 - \frac{\omega_{pe}^2}{\omega(\omega-\omega_{ce})}\right]^{\frac{1}{2}}}{\left[1 - \frac{\alpha}{2}\left(\frac{a}{c}\right)^2\frac{\omega_{pe}^2}{(\omega-\omega_{ce})^2}\right]^{\frac{1}{2}}} \tag{C.47}$$

$$\mathrm{Im}\,k = \frac{\frac{\sqrt{\pi}\,\omega\omega_{pe}^2}{2c^2(\mathrm{Re}\,k)^2a}\sigma_+(\zeta_e)e^{-\zeta_e^2}\left\{1 - \alpha\frac{\omega-\omega_{ce}}{\omega}\right\}}{\left[1 - \frac{\alpha}{2}\left(\frac{a}{c}\right)^2\frac{\omega_{pe}^2}{(\omega-\omega_{ce})^2}\right]^{\frac{1}{2}}} \tag{C.48}$$

If we assume

$$\left\{1 - \alpha\frac{\omega-\omega_{ce}}{\omega}\right\} > 0$$

$$\left[1 - \frac{\alpha}{2}\left(\frac{a}{c}\right)^2\frac{\omega_{pe}^2}{(\omega-\omega_{ce})^2}\right] > 0 \tag{C.50}$$

then as we found earlier for (C.10), Eq. (C.48) is valid only for $\omega < \omega_L$ or $\omega > \omega_R$. For $0 < \omega < \omega_{ce}$ $(\omega \neq \omega_{ce})$ we must ignore (C.48) and conclude that the root is undamped and given by (C.47).

In general, the only situation of real concern is if α is such that

$$\left[1 - \frac{\alpha}{2}\left(\frac{a}{c}\right)^2 \frac{\omega_{pe}^2}{(\omega-\omega_{ce})^2} \right] \leq 0 \tag{C.51}$$

which is

$$\left(1 - \frac{T_\perp}{T_z}\right) \geq 2\left(\frac{c}{a}\right)^2 \left(\frac{\omega-\omega_{ce}}{\omega_{pe}}\right)^2 \tag{C.52}$$

For $\omega \approx 0$ this is

$$\left(1 - \frac{T_\perp}{T_z}\right) \geq 2\left(\frac{c}{a}\right)^2 \left(\frac{\omega_{ce}}{\omega_{pe}}\right)^2 \tag{C.53}$$

which is the usual criterion for obtaining the firehose instability.[18]

In (C.46) note that the coefficient of $Z'(\zeta_e)$

$$\frac{k\alpha a}{2\omega} = \frac{\left(\frac{kc}{\omega_{ce}}\right)\alpha}{2\left(\frac{\omega}{\omega_{ce}}\right)} \frac{a}{c} \tag{C.54}$$

is typically very small, in which case the roots of (C.46) are essentially the same as the roots of the isotropic case ($T_\perp = T_z$). Only if $\omega \approx 0$ does (C.54) become significant, in which case the roots of (C.46) would differ significantly from those of the isotropic case.

4.4 The transverse dispersion relation for $B_0 = 0$.

In the limit of no external magnetic field, the transverse dispersion relation (C.1) becomes

$$\epsilon_{T_+}(k,\omega) = 1 - \frac{\omega}{(k^2c^2-\omega^2)}\left\{ \frac{\omega_{pe}^2}{ka} Z_+\left(\frac{\omega}{ka}\right) + \frac{\omega_{pi}^2}{kA} Z_+\left(\frac{\omega}{kA}\right)\right\} = 0 \tag{C.55}$$

Neglecting the ions and proceeding as in (C.3) - (C.7) we find the least-damped root to have

$$Re\, k = \pm \frac{\omega}{c}\left[1 - \frac{\omega_{pe}^2}{\omega^2}\right]^{\frac{1}{2}} \tag{C.56}$$

$$Im\, k = \frac{\sqrt{\pi}\,\omega\,\omega_{pe}^2}{2c^2 (Re\, k)^2 a}\left[\sigma_+\left(\frac{\omega}{ka}\right)\right] e^{-\left(\frac{\omega}{ka}\right)^2} \tag{C.57}$$

Equation (C.56) is plotted in Fig. C-14a. Note that both $\omega > 0$ and $\omega < 0$ have the same dispersion characteristics. From (C.56) we have

$$\left|\frac{\omega}{ka}\right| \approx \frac{\frac{c}{a}}{\left[1 - \frac{\omega_{pe}^2}{\omega^2}\right]^{\frac{1}{2}}} \tag{C.58}$$

and this is displayed in Fig. C-14b. Since c/a is typically very large ($\gg 3$) we note that $|\omega/ka|$ is also very large (except if $\omega \approx 0$); this justifies our use of the asymptotic expansion (C.3) to obtain (C.56) - (C.57) and it also means that the damping as given by (C.57) is zero for all practical purposes.

4.5 Roots of $\varepsilon_{T_+}[(\omega-\omega_{ce}/v_z),\omega] = 0$ in the complex ω plane and roots of $\varepsilon_{T_+}(k, kv_z+\omega_{ce}) = 0$ in the complex k plane (for v_z real).

Substituting $k = (\omega-\omega_{ce})/v_z$ in (C.8) we find

$$\epsilon_{T_+}\left(\frac{\omega-\omega_{ce}}{v_z}, \omega\right) = 0 \tag{C.59}$$

is

5 e

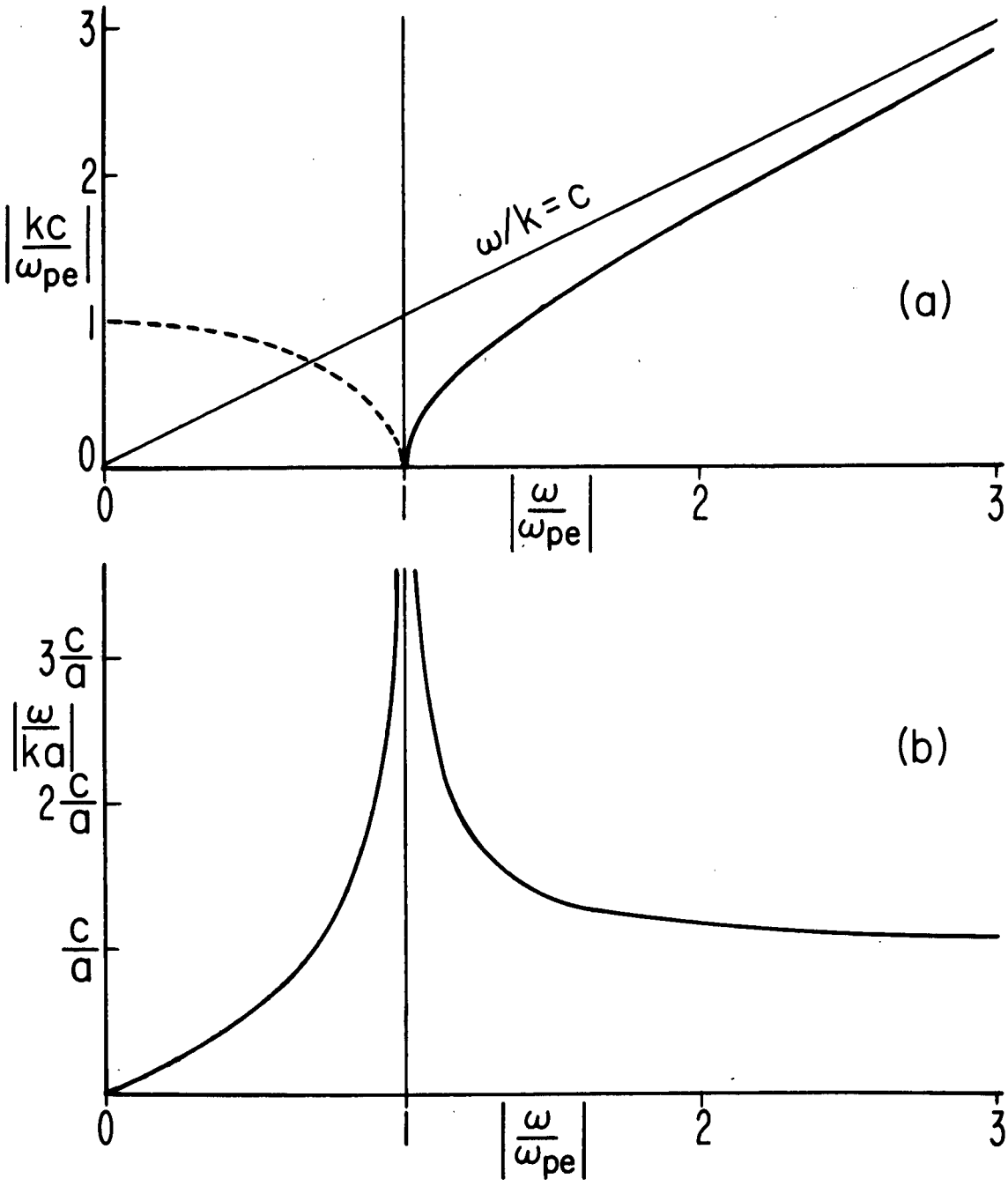

FIGURE C-14. THE LEAST-DAMPED ROOT OF THE TRANSVERSE DISPERSION RELATION FOR $\underline{B}_o = 0$.

(a) Plot of (C.56); the solid line applies for $(\mathrm{Re}\ k)^2 > 0$, the dashed line for $(\mathrm{Re}\ k)^2 < 0$.

(b) Plot of (C.58).

$$(\omega-\omega_{ce})^3-\omega^2(\omega-\omega_{ce})\frac{v_z^2}{c^2}-\omega\omega_{pe}^2\frac{v_z^3}{c^2 a}Z_+\left(\frac{v_z}{a}\right)=0 \tag{C.60}$$

Note that the argument of the Z function in (C.60) is real (v_z is real) and has no ω dependence. Thus, given a value for v_z, (C.60) is a cubic equation in ω which has three exact analytic solutions. In the cold plasma limit ($a \to 0$), and for $|v_z/c| \ll 1$ all three roots of (C.60) are $\omega \approx \omega_{ce}$. For a hot plasma, we have calculated the locus of roots of (C.60) for a typical case in Fig. C-15b; note that all three roots remain very close to $\omega = \omega_{ce}$.

Substituting $\omega = kv_z + \omega_{ce}$ in (C.8) we find

$$\epsilon_{T_+}(k, kv_z+\omega_{ce})=0 \tag{C.61}$$

is

$$k^3(-c^2+v_z^2)+k^2(2\omega_{ce}v_z)+k\left[\omega_{ce}^2+\omega_{pe}^2\frac{v_z}{a}Z_+\left(\frac{v_z}{a}\right)\right]+\left[\frac{\omega_{pe}^2\omega_{ce}}{a}Z_+\left(\frac{v_z}{a}\right)\right]=0 \tag{C.62}$$

which is a cubic equation in k. In the cold plasma limit all three roots of (C.62) are $k \approx 0$. For the hot plasma parameter values used in Fig. C-15b we have plotted the locus of roots of (C.62) in Fig. C-15a. Note that the roots of (C.62) may be obtained from the roots of (C.60), or vice versa, by use of the change of variable

$$k \longleftrightarrow \frac{\omega-\omega_{ce}}{v_z} \tag{C.63}$$

In particular Fig. C-15a may be obtained from Fig. C-15b, or vice versa, by use of (C.63).

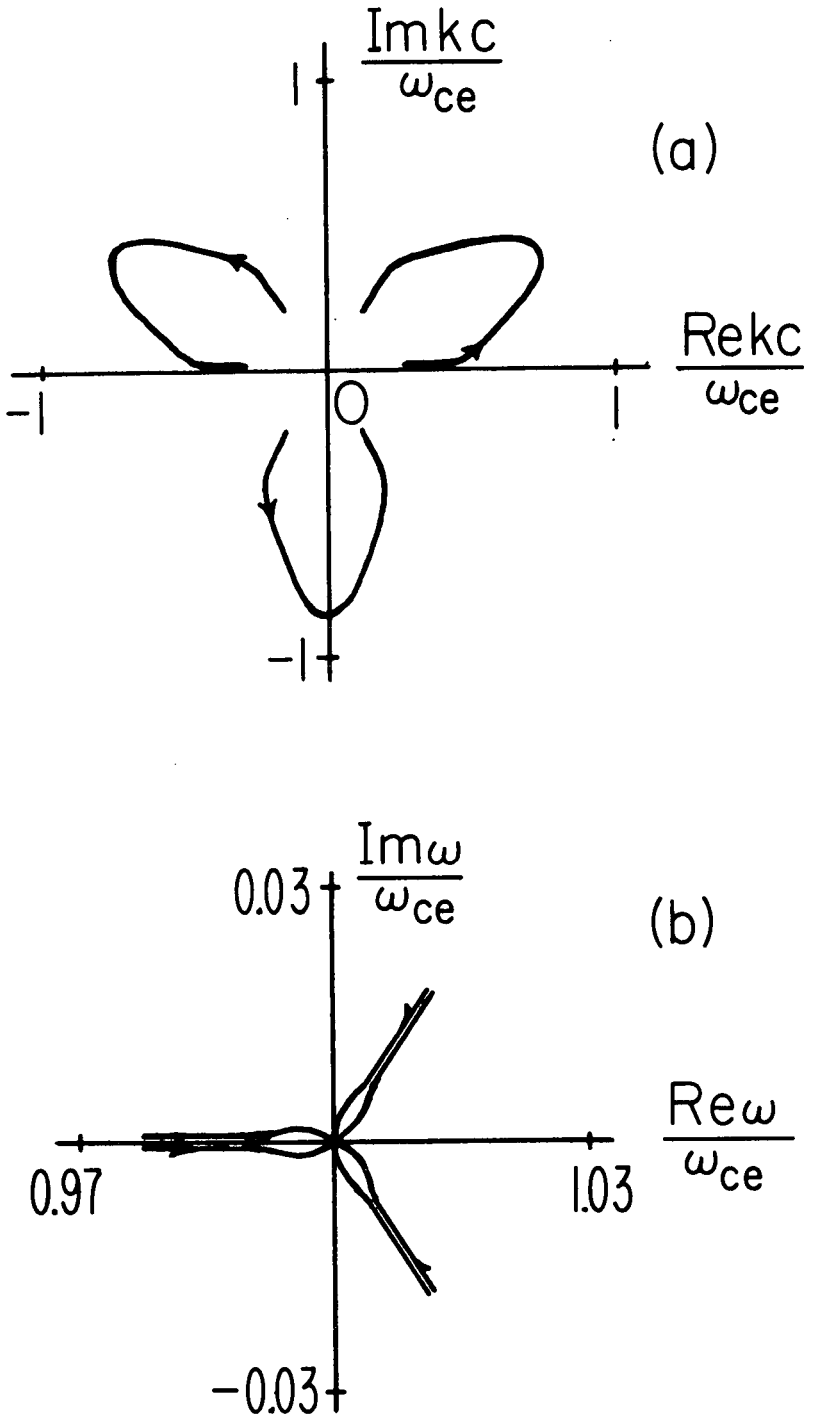

FIGURE C-15. (a) LOCUS OF ROOTS OF (C.62).
(b) LOCUS OF ROOTS OF (C.60).

[c/a=1120, ω_{pe}/ω_{ce}=.4, v_z/a=-10→+10]

The arrows indicate the directions the roots move as v_z/a progresses from -10 to +10.

APPENDIX D

ROOTS OF THE LONGITUDINAL DISPERSION RELATION FOR REAL ω AND COMPLEX k

From the symmetry properties discussed in Appendix B we find it is sufficient to obtain only the roots of

$$\epsilon_{\ell_+}(k,\omega) = 1 - \frac{\omega_{pe}^2}{k^2a^2} Z_+'\left(\frac{\omega}{ka}\right) - \frac{\omega_{pi}^2}{k^2A^2} Z_+'\left(\frac{\omega}{kA}\right) = 0 \tag{D.1}$$

Using the asymptotic expansion of the Z function

$$Z_+(\zeta) \approx -\frac{1}{\zeta} - \frac{1}{2\zeta^3} + i\sqrt{\pi}\,\sigma_+(\zeta)\, e^{-\zeta^2} \tag{D.2}$$

and proceeding exactly as in (C.1) - (C.7) we obtain

$$Re\, k = \pm \left\{ \frac{2\omega^4}{3(\omega_{pe}^2a^2+\omega_{pi}^2A^2)} \left[1 - \frac{\omega_{pe}^2}{\omega^2} - \frac{\omega_{pi}^2}{\omega^2} \right] \right\}^{\frac{1}{2}} \tag{D.3}$$

$$Im\, k = \frac{2\sqrt{\pi}\,\omega^5\sigma_+}{3(\omega_{pe}^2a^2+\omega_{pi}^2A^2)(Re\,k)^4} \left\{ \frac{\omega_{pe}^2}{a^3} e^{-\zeta_e^2} + \frac{\omega_{pi}^2}{A^3} e^{-\zeta_i^2} \right\} \tag{D.4}$$

where $\sigma_+ = \sigma_+(\zeta_e) = \sigma_+(\zeta_i)$ and $\zeta_e = \omega/ka$, $\zeta_i = \omega/kA$. None of the problems associated with $\sigma_+(\zeta_e)$ of the transverse case occur in this, the longitudinal case.

Considering $Im\,\zeta_e < 0$ so $\sigma_+(\zeta_e) = 2$ and neglecting the ion terms in (D.3) - (D.4) we find

$$\frac{Re\,k}{k_d} = \frac{1}{\sqrt{3}} \frac{\omega}{\omega_{pe}} \left[\frac{\omega^2}{\omega_{pe}^2} - 1 \right]^{\frac{1}{2}} \tag{D.5}$$

$$\frac{\mathrm{Im}\,k}{k_d} = \frac{3\sqrt{\frac{\pi}{2}}\,\frac{\omega}{\omega_{pe}}}{\left[\frac{\omega^2}{\omega_{pe}^2}-1\right]^2}\, e^{-\frac{3}{2}\left[\frac{\omega^2}{\omega_{pe}^2}-1\right]^{-1}} \tag{D.6}$$

where $k_d = \sqrt{2}\,(\omega_{pe}/a)$ is the electron Debye wavenumber. Equations (D.5) - (D.6) are valid only for $|\zeta_e| \gtrsim 3$ since the asymptotic expansion of the Z function (D.2) was used in their derivation. From (D.5) we have

$$|\zeta_e| = \left|\frac{\omega}{ka}\right| = \left|\frac{\sqrt{\frac{3}{2}}}{\left(\frac{\omega^2}{\omega_{pe}^2}-1\right)^{\frac{1}{2}}}\right| \tag{D.7}$$

Setting $\zeta_e = 3$ in (D.7) and solving for ω we find $\omega = 1.08\,\omega_{pe}$. Thus only for the narrow range $\omega_{pe} \lesssim \omega \lesssim 1.08\,\omega_{pe}$ are the asymptotic formulas (D.5) - (D.6) valid.

For $\omega \gtrsim 1.08\,\omega_{pe}$ we must solve (D.1) numerically. Neglecting the ion term, (D.1) is

$$\zeta_e^{\,2} Z'(\zeta_e) = \frac{\omega^2}{\omega_{pe}^2} \tag{D.8}$$

Kuehl, Stewart, and Yeh[8] have plotted Re k/k_d and Im k/k_d vs. ω/ω_{pe} corresponding to the first four least-damped roots of (D.8) in the ζ_e plane. Also, Derfler and Simonen[9] have numerically tabulated the first four roots of (D.8). In both cases, for $\omega \gtrsim 1.4\,\omega_{pe}$ the damping of the higher-order roots becomes comparable to, and even less than, that of the "least-damped" root. However, Gould[2] has evaluated

the first few residue terms that occur for a longitudinal excitation and concluded that use of just the "least-damped" root is probably a valid approximation.

For computational purposes, it is especially useful to know the value of the least-damped root for ω near ω_{pe}. Since for $\omega_{pe} \leq \omega \lesssim 1.25\,\omega_{pe}$ the graphs of Kuehl, Stewart, and Yeh may not be read accurately (especially Im k/k_d) we have also calculated the least-damped root of (D.8) for $\omega_{pe} \leq \omega \leq 1.5\,\omega_{pe}$ and this is displayed in the top of Fig. D-1. Also shown are the asymptotic results, (D.5) - (D.6). In the bottom of Fig. D-1 we have plotted $|\zeta_e|$ vs. ω/ω_{pe} for the true least-damped root of (D.8). Note that as deduced above, the asymptotic results (D.5) - (D.6) as shown in Fig. 10 are good approximations only for $\omega_{pe} \leq \omega \lesssim 1.08\,\omega_{pe}$.

To obtain the results in Fig. D-1, the true least-damped root of (D.8) was calculated using the correct function $Z'(\zeta)$ rather than the two-pole approximation.[34] The latter was tried but found to be very poor in this case. More specifically, when the two-pole approximation was used in (D.8) for $1.15\,\omega_{pe} \leq \omega \leq 1.5\,\omega_{pe}$ we found the least-damped root had Re k/k_d in error from its true value by 3%-18% and Im k/k_d in error from its true value by 15%-40%; and when ω went below $1.15\,\omega_{pe}$, Im k even went negative. The reason for this poor behavior is presumably due to the fact that the two-pole approximation for $Z'(\zeta)$ matches only the first term of the asymptotic series for $Z'(\zeta)$ accurately whereas the basic asymptotic form of the longitudinal dispersion relation (D.5) - (D.6) requires for its derivation the first <u>two</u> terms in the asymptotic series of $Z'(\zeta)$.

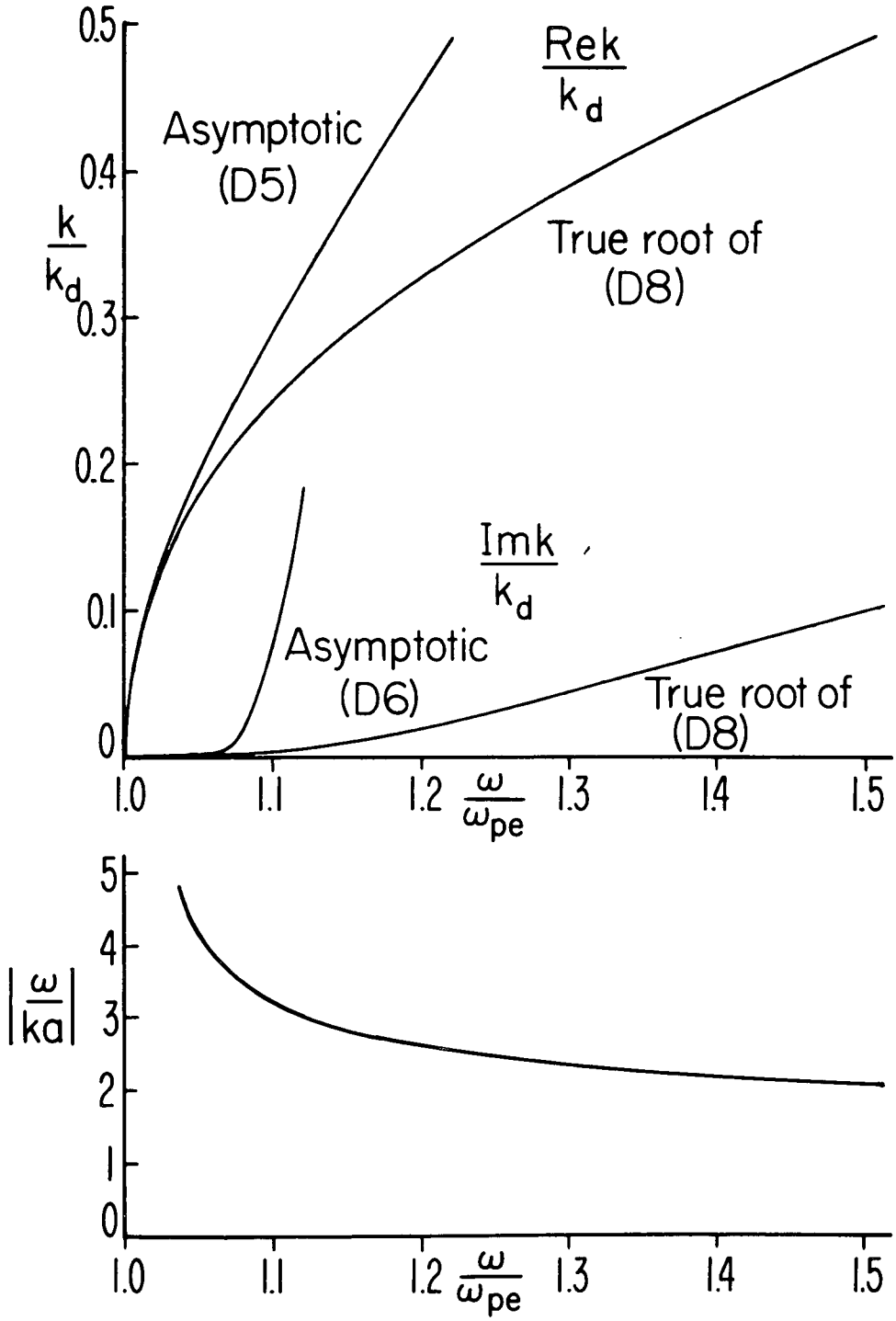

FIGURE D-1. THE LEAST-DAMPED ROOT OF THE LONGITUDINAL DISPERSION RELATION FOR REAL ω AND COMPLEX k.

Top: Comparison of true and asymptotic results.
Bottom: Plot of $|\omega/ka|$ for the true root.

APPENDIX E

METHOD OF STEEPEST DESCENT AS USED IN EVALUATING BRANCH-CUT AND PHASE-MIXING INTEGRALS

We present here a brief summary of the method of steepest descent[35] as used in both Sections I and II.

Consider an integral of the form

$$I = \int_C F(w)\, e^{+\phi(w)}\, dw \tag{E.1}$$

where $F(W)$ is a slowly-varying function of W and $\phi(W)$ is a rapidly-varying function of W. Then the integrand of (E.1) has saddle points at W_o where

$$\phi'(w_o) = 0 \tag{E.2}$$

We assume the initial contour C is along the real axis in the complex W plane. Then rewriting (E.1) as

$$I\, e^{-\phi(w)} = \int_C F(w)\, e^{\phi(w) - \phi(w_o)}\, dw \tag{E.3}$$

we note that if we deform the contour C through the saddle point at $W = W_o$ along a path such that

$$\mathrm{Im}\left\{\phi(w) - \phi(w_o)\right\} = 0 \tag{E.4}$$

i.e., a path of constant phase, then the integral in (E.3) may be approximated as follows.

We first expand $\phi(W)$ about $W = W_o$

$$\phi(w) = \phi(w_0) + \frac{1}{2!}\phi''(w_0)(w-w_0)^2 + \frac{1}{3!}\phi'''(w_0)(w-w_0)^3 + \cdots \tag{E.5}$$

so

$$\phi(w) - \phi(w_0) \approx \frac{1}{2}\phi''(w_0)(w-w_0)^2 \tag{E.6}$$

We then specify the desired path of constant phase C' by imposing the transformation of variable

$$\frac{1}{2}\phi''(w_0)(w-w_0)^2 = -T^2 \tag{E.7}$$

where T is a real variable. Thus (E.3) becomes

$$Ie^{-\phi(w_0)} = \frac{1}{\sqrt{-\frac{1}{2}\phi''(w_0)}} \int dT\, F(T) e^{-T^2} \tag{E.8}$$

where the integration contour runs along the real axis in the complex T plane. [Note that the integrand of (E.8) decreases rapidly as $|T|$ increases; had we chosen $+T^2$ in (E.7) the integrand of (E.8) would have increased rapidly as $|T|$ increased.] Assuming F(T) is sufficiently slowly varying, and extending the limits of the T integration to $T = \pm\infty$ we may write

$$\int dT\, F(T) e^{-T^2} \approx F(T=0) \int_{-\infty}^{+\infty} dT\, e^{-T^2}$$

$$= F(w_0)\sqrt{\pi} \tag{E.9}$$

since the exponential peaks the integrand of (E.8) about $T = 0$. Actually the limits at $T = \pm\infty$ are not required; the result of (E.9) will be obtained as long as T covers the range $-3 \lesssim T \lesssim +3$ and

F(T) is approximately constant over the same range. Combining (E.8), (E.9) we obtain finally

$$I \approx \frac{\sqrt{2\pi}}{\sqrt{-\phi''(W_0)}} F(W_0)\, e^{+\phi(W_0)} \qquad \text{(E.10)}$$

This result is the first term of an asymptotic expansion for I , more terms of which may be obtained (at least in principle) by keeping more terms in the Taylor series expansion for $\phi(W)$ in (E.5).

Returning to the original integral (E.1), we note that the change of variable used in (E.7) for the approximate case suggests that we use the change of variable

$$\phi(W) - \phi(W_0) = -T^2 \qquad \text{(E.11)}$$

(with T real as before) in the exact case (E.1). The path of constant phase defined by (E.11) for $-\infty \leq T \leq +\infty$ is the path of steepest descent. [The path obtained by using $+T^2$ in place of $-T^2$ in (E.11) is the path of steepest ascent.] To obtain an analytic expression for I we must first invert (E.11) to obtain W as a function of T . Then this W(T) is used in F(W) and dW to give

$$I = \int F\left[W(T)\right] e^{-T^2} d\left[W(T)\right] \qquad \text{(E.12)}$$

where the integration contour runs along the real axis in the complex T plane. Presumably the integrand of (E.12) could be written as a power series in T times e^{-T^2} and the integration could be performed analytically term by term.

In actual practise the required inversion of (E.11) may be

difficult and one often resorts back to using (E.10) as an approximation for I. In this case some comment should be made on the range of validity of (E.10). To this end we consider values of W that are near W_o and on the path of steepest descent in the range defined by

$$\left| \frac{1}{2} \phi''(W_o)(W-W_o)^2 \right| \leq 1 \tag{E.13}$$

Then (E.10) is a good approximation to I provided:

(i) Any singularities of $\phi(W)$ occur for values of W far from those defined by (E.13).

(ii) $F(W)$ varies negligibly, i.e.,

$$\left| \frac{F(W) - F(W_o)}{F(W_o)} \right| \ll 1 \tag{E.14}$$

for values of W within the range defined by (E.13).

(iii) The terms in the Taylor series expansion of $\phi(W)$ past those terms used in (E.6) must be negligibly small. Using the first term dropped to represent the error, we must have

$$\left| \frac{\phi'''(W_o)(W-W_o)}{3\phi''(W_o)} \right| \ll 1 \tag{E.15}$$

which, combined with (E.13), requires

$$\left| \sqrt{2}\, \phi'''(W_o) \right| \ll \left| 3 \left\{ \phi''(W_o) \right\}^{3/2} \right| \tag{E.16}$$

We now apply the above results to some specific cases as used in Sections I and II.

Branch-cut integral in the k plane.

We consider Eq. (2.58) of Part I which is of the form

$$I = \int F(k)\, e^{\phi(k)}\, dk$$
$$\phi(k) = ikz - \left(\frac{\omega-\omega_{ce}}{ka}\right)^2 \tag{E.17}$$

This form of $\phi(k)$ occurs generally in the branch-cut integral that arises in a spatial problem (with a zero-order Maxwellian velocity distribution) when the inverse transform of $f_1(k,\omega)$ [or $\underline{E}_1(k,\omega)$, etc.] is computed, so the following results should be of general interest. The integrand of (E.17) has three saddle points given by the three roots of

$$k_s^3 = \left[\frac{2(\omega-\omega_{ce})^2}{2a^2}\right] e^{i\frac{\pi}{2}} \tag{E.18}$$

where k_s represents a saddle point. The paths of steepest descent defined by (E.11), i.e., by

$$\phi(k) - \phi(k_s) = -T^2$$

are given by the roots of

$$K^3 - K^2\left\{k_s + i\,\frac{Z^2}{k_s^2} + i\,T^2\right\} + i\,Z^2 = 0 \tag{E.19}$$

where

$$K \equiv k_z = \left(\frac{kc}{\omega_{ce}}\right)\frac{z}{\frac{c}{\omega_{ce}}}$$
$$Z \equiv \frac{z(\omega-\omega_{ce})}{a} \tag{E.20}$$

and T runs along the real axis from $T = -\infty$ to $T = +\infty$. The quantity Z is the characteristic dimensionless parameter associated with (E.17). In terms of Z, the saddle points are given by the three roots of

$$K_s^3 = (K_s z)^3 = 2 Z^2 e^{i\frac{\pi}{2}} \tag{E.21}$$

The paths of steepest descent are calculated as follows. We choose a value for Z and then select a specific saddle point from the three given by (E.21). We then solve the cubic equation (E.19) analytically which gives three values of K for each value of T; two of these roots are points on the desired path of steepest descent while the third root is extraneous [for $T = 0$ the three roots of (E.19) are K_s, K_s, and $-\frac{1}{2}K_s$, the latter being extraneous]. Then by numerically evaluating the expressions for the two desired roots for several values of T $(-\infty < T < +\infty)$ we are able to plot the desired path of steepest descent.

We now display the results of our calculations. In Fig. E-1 we show the paths of steepest descent for $z = \pm 1$. Note that according to (E.21) any specific saddle point for $z = +1$ changes its phase by $2\pi/3$ radians as z changes to $z = -1$. Thus the resultant distribution of saddle points and paths of steepest descent are the same for $z = +1$ and $z = -1$. To see how the contours actually shift as z goes through zero, we have performed the following calculation. We let $z = e^{i\theta}$ with $0 \leq \theta \leq 2\pi$ so z takes on values of points on a unit circle centered at the origin in the complex z plane. We then calculated the saddle point contours for several significant values of θ

with the results displayed in Fig. E-2. The contours for $\theta = 0°, 180°$ are of course the same as the contours for $\tilde{z} = \pm 1$ given in Fig. E-1. Note that as θ increases from $0°$ to $180°$ all three saddle points rotate rigidly in the counterclockwise direction.

Of special significance in Fig. E-2 are the cases $\theta = 45°$ and $\theta = 135°$ where in each case one of the contours violently changes shape. Consider the case $\theta = 135°$. Then suppose we had been using contour 2 (which has one endpoint at infinity) to evaluate some integral for $0° \leq \theta < 135°$. We note that as θ crosses $\theta = 135°$ the endpoint at infinity of contour 2 is diverted back to the origin and therefore contour 2 is no longer suitable for evaluating the integral; we must therefore change to contour 1 as θ crosses $\theta = 135°$. This behavior is known as Stokes phenomenon and the lines in the $\tilde{z}$ plane defined by $\tilde{z} = r\, e^{i(\pi/4)}$, $r\, e^{i(3\pi/4)}$ (r real and $0 \leq r \leq \infty$) are called Stokes lines. Note that for $0° \leq \theta \leq 180°$ contour 1 in Fig. E-2 never exhibits Stokes phenomenon and may therefore be used for all values of θ within the given interval.

Thus, in Part I, in evaluating (2.58) we have chosen to use contour 1 of Fig. E-2. The first term of the asymptotic expansion, (E.10), then gives the result (2.61). We now estimate the errors involved in using (E.10) as discussed with (E.13) - (E.16).

First we construct a graph to aid in establishing over what values of K, $F(K)$ [as defined by (E.17)] must be essentially constant. We scale (E.19) appropriately by dividng it by $\tilde{z}^2$ to give

$$\tilde{\kappa}^3 - \tilde{\kappa}^2 \left\{ \tilde{\kappa}_s + i \frac{1}{\tilde{\kappa}_s^2} + i \tilde{\gamma}^2 \right\} + i = 0 \qquad \text{(E.22)}$$

where

$$\tilde{K} \equiv \frac{K}{Z^{2/3}}$$

$$\tilde{T} \equiv \frac{T}{Z^{1/3}} \qquad \text{(E.23)}$$

We consider only Z real so $\tilde{T}$ is real. Then in Fig. E-3 we have plotted "contour 1" of (E.22) for $Z > 0$. (For $Z < 0$ the contour is just mirrored about the imaginary axis.) With the aid of Fig. E-1 one may easily estimate the range of $\tilde{K}$ over which $F(\tilde{K})$ should be approximately constant. The dominant portion of the integral comes from $|T| \lesssim 2$ say [see (E.12)]. Thus we set $|T| = 2$. Then given a value for Z we calculate $|\tilde{T}|$ from (E.23) and find the two corresponding points on the contour in Fig. E-3. The segment of the contour between these two points is the range of $\tilde{K}$ over which $F(\tilde{K})$ should be approximately constant. In particular for $Z = 1$ (cutoffs at $|\tilde{T}| = 2$) a large portion of the contour is needed whereas for large Z, say $Z = 27$ (cutoffs at $|\tilde{T}| = 0.66$) a smaller portion is needed.

Upon examining $F(k)$ of (2.58) of Part I with the aid of Fig. E-3, one notes that the only poles of $F(k)$ that may be troublesome are those in the infinite sequence of poles that come in along the 45° line (see Appendix C) in the k plane (and therefore also in the $\tilde{K}$ plane). But $|(\omega-\omega_{ce})/ka|$ is very large at these poles so the exponential in (E.17) should make any pole effects negligible. The slowly varying behavior of $F(k)$ is roughly like $1/k^3$ (for $\omega/k \ll c$), so using $F(k_s)$ instead of $F(k)$ in (E.9) does of course introduce an error, which becomes negligible for large Z. Thus, preferably, we should have $|Z| \gg 1$.

Lastly we find that the requirement (E.16)

$$\frac{\left| \frac{3}{2} \left\{ \phi''(k_s) \right\}^{3/2} \right|}{\left| \sqrt{2}\, \phi'''(k_s) \right|} \gg 1$$

by direct calculation from (E.19) reduces to the requirement $|z| \gg 1$. This means that the asymptotic expansion method used to derive (E.10) breaks down when $|z|$ becomes less than a characteristic length $|a/(\omega-\omega_{ce})|$, in which case (2.58) would have to be evaluated numerically (along the path of steepest descent for convenience) to obtain an accurate result.

Thus, in Part I, (2.61) is an accurate result for $|z| \gg 1$ and it is still a good order-of-magnitude estimate of (2.58) for $|z| \simeq 1$.

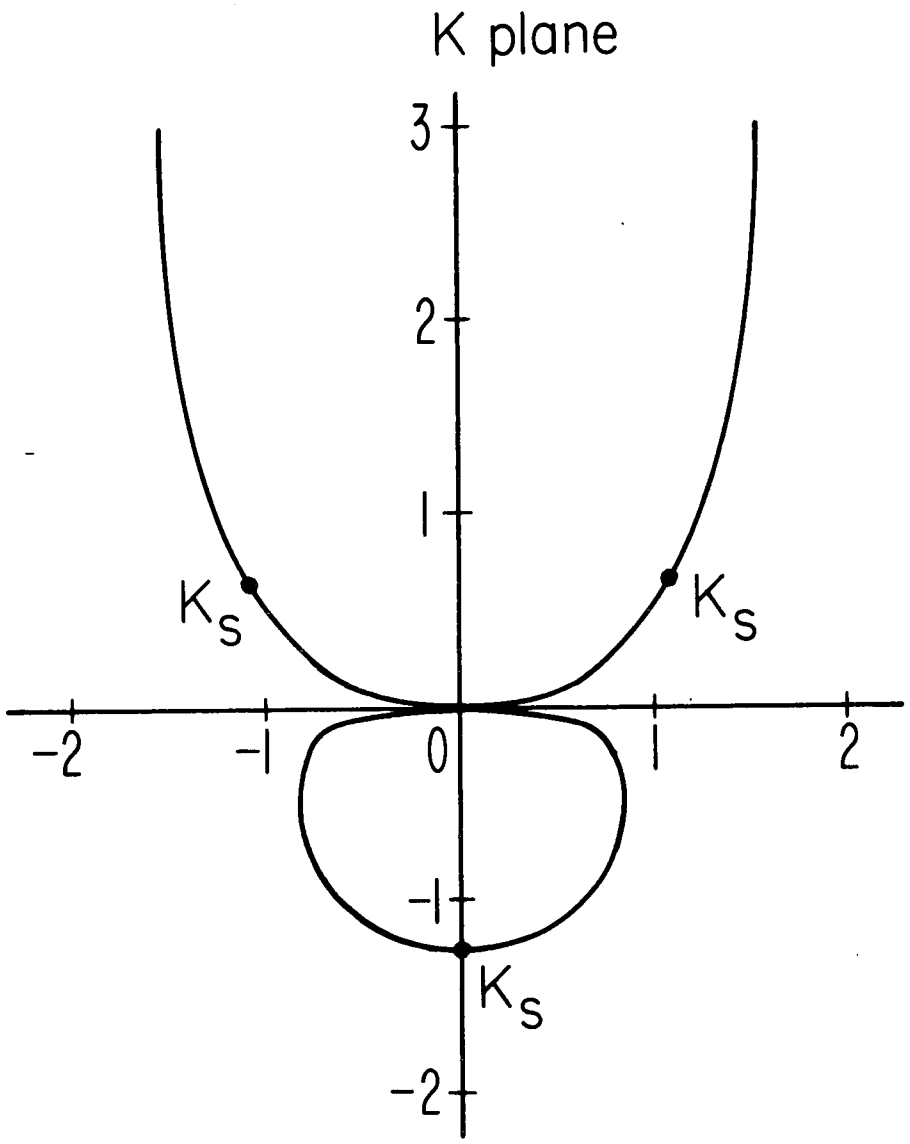

FIGURE E-1. SADDLE-POINT CONTOURS OF (E.17) FOR $\hat{z}=\pm 1$.

Shown are the saddle points of (E.17) as given by (E.21) and the paths of steepest descent as given by (E.19) for $\hat{z}=\pm 1$. This figure holds for $\hat{z}=+1$ or $\hat{z}=-1$ although any specific saddle point rotates through $2\pi/3$ radians when $\hat{z}$ goes through zero, as is shown in the next figure.

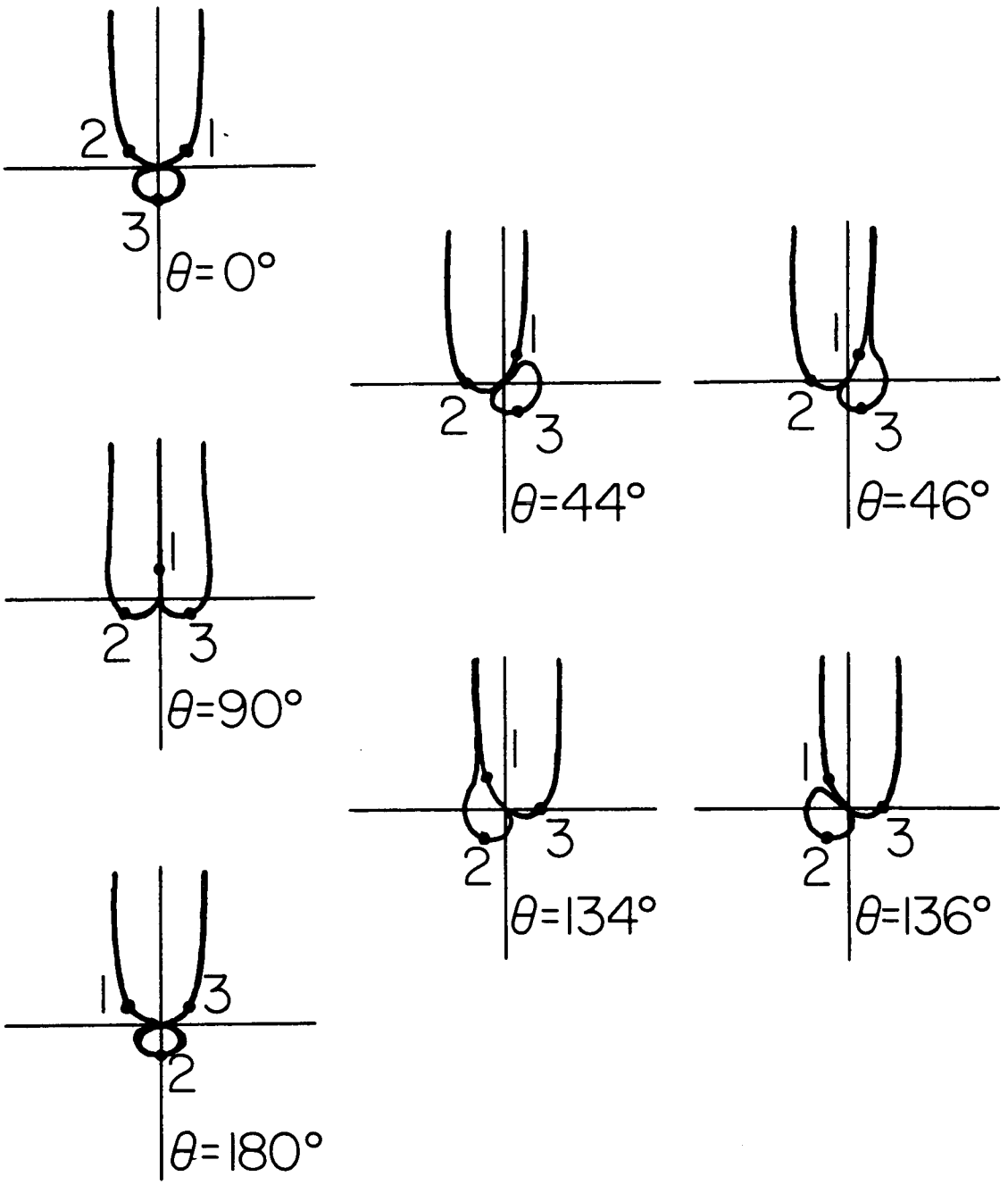

FIGURE E-2. EVOLUTION OF THE SADDLE-POINT CONTOURS OF (E.17) FOR $z = e^{i\theta}$ AS θ VARIES FROM 0° TO 180°.

Saddle points and paths of steepest descent are as given by (E.21), (E.19) respectively. Note Stokes phenomenon that occurs when $\theta = 45^\circ$ and $\theta = 135^\circ$.

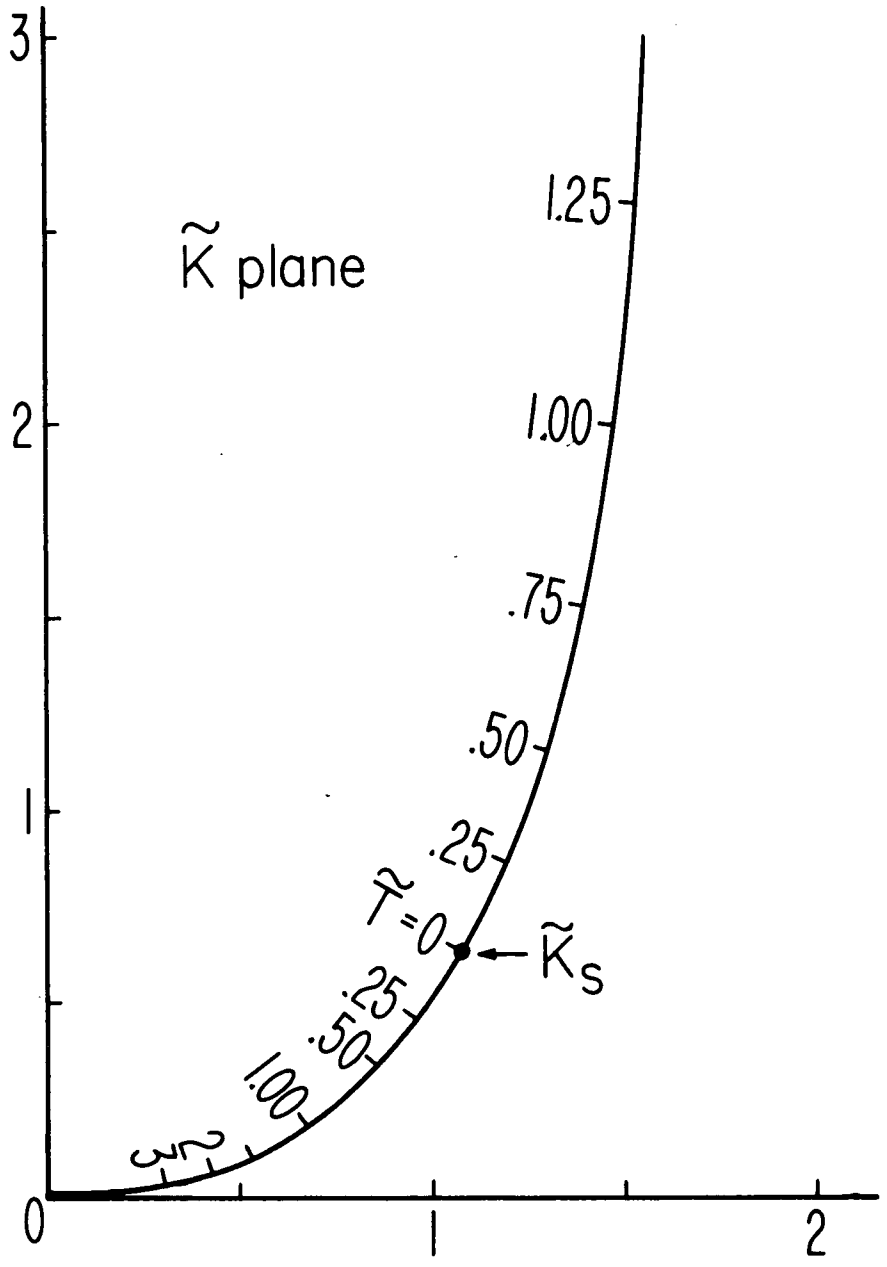

FIGURE E-3. SADDLE-POINT CONTOUR OF (E.17) IN THE $\tilde{K}$ PLANE WITH $\tilde{T}$ SPECIFIED ALONG THE CONTOUR.

Shown is the path of steepest descent of (E.17) in the $\tilde{K}$ ($=K/z^{2/3}$) plane for z real and with values of $\tilde{T}$ ($=T/Z^{1/3}$) specified along the contour [see (E.22),(E.23)]. This plot is useful in estimating the range of the variable $\tilde{K}$ over which $F(\tilde{K})$ should be approximately constant.

Phase-mixing integrals in the v_z plane.

We consider Eq. (2.80) of Part I and Eq. (4.4) of Part II, both of which are of the form

$$I = \int F(v_z)\, e^{\phi(v_z)}\, dv_z$$

$$\phi(v_z) = i\left(\frac{\omega-\omega_{ce}}{v_z}\right) z - \frac{v_z^2}{a^2} \tag{E.24}$$

This form of $\phi(v_z)$ occurs generally in a spatial problem (with a zero-order Maxwellian velocity distribution) when the free-streaming part of $f_1(z,\underline{v},t)$ is integrated over v_z to give $\underline{J}_1(z,t)$ (or $\underline{E}_1$, etc.). Thus again the following results should be of general interest.

We note immediately that $\phi(v_z)$ in (E.24) may be obtained from $\phi(k)$ in (E.17) by the transformation

$$k \longrightarrow \frac{\omega-\omega_{ce}}{v_z} \tag{E.25}$$

so all of the graphs for the previous case apply to the new variable $[(\omega-\omega_{ce})/v_z]$. Of course we want graphs in terms of v_z directly, so we would have to invert the previous graphs point by point according to (E.25) to obtain the desired graphs. Instead, we shall write out the appropriate equations in terms of v_z and solve them, although at any stage we can check our results by comparing them to the previous case using (E.25).

The integrand of (E.17) has three saddle points given by the three roots of

$$v_s^3 = \left[\frac{(\omega-\omega_{ce})z\,a^2}{2}\right] e^{-i\frac{\pi}{2}} \tag{E.26}$$

where v_s is a saddle point. The paths of steepest descent defined by (E.11), i.e., by

$$\phi(v_z) - \phi(v_s) = -T^2$$

are given by the roots of

$$V^3 + V\left\{ i\frac{Z}{V_s} - V_s^2 - T^2 \right\} - iZ = 0 \qquad \text{(E.27)}$$

where

$$V \equiv \frac{v}{a}$$

$$Z \equiv \frac{z(\omega - \omega_{ce})}{a} \qquad \text{(E.28)}$$

and T runs along the real axis from $-\infty$ to $+\infty$. Once again the quantity Z is the characteristic dimensionless parameter. In terms of Z the saddle points are given by the three roots of

$$V_s^3 = \frac{Z}{2} e^{-i\frac{\pi}{2}} \qquad \text{(E.29)}$$

We note for reference that in terms of $K = kz$ as in (E.20), the transformation (E.25) is

$$K \longrightarrow \frac{Z}{V} \qquad \text{(E.30)}$$

The paths of steepest descent are calculated from (E.27) by the method used in the previous case. As earlier, given Z and a specific choice of V_s two of the roots of (E.27) are points on the desired path of steepest descent while the third root is extraneous [for T = 0 the three roots of (E.27) are V_s, V_s, $-2V_s$, the latter being

extraneous].

In Fig. E-4 we show the saddle-point contours for $\tilde{z} = +1$ and $\tilde{z} = -1$. Note that the contours for the two cases are not the same but are mirror images about the real axis of each other. In Fig. E-5 we let $\tilde{z} = e^{i\theta}$ with $0 \leq \theta \leq 2\pi$ as earlier. We see that as θ goes from 0° to 180° all three saddle points rotate rigidly in the counter-clockwise direction, but only through $\pi/3$ radians. Also we find contours 2 and 3 exhibit Stokes phenomenon at $\theta = 45°$ and $\theta = 135°$, respectively. Note that contour 1 does not exhibit any Stokes phenomenon for $0° \leq \theta \leq 180°$ and therefore this is the contour we choose to use.

To aid in establishing over what values of V, F(V) must be essentially constant, we construct a graph similar to Fig. E-3. We scale (E.27) appropriately by dividing it by $\tilde{z}$ to obtain

$$\tilde{V}^3 + \tilde{V}\left\{\frac{i}{\tilde{V}_s} - \tilde{V}_s^2 - \tilde{T}^2\right\} - i = 0 \tag{E.31}$$

where

$$\tilde{V} \equiv \frac{V}{\tilde{z}^{1/3}}$$

$$\tilde{T} \equiv \frac{T}{\tilde{z}^{1/3}} \tag{E.32}$$

As earlier, we consider only $\tilde{z}$ real so $\tilde{T}$ is real. Then in Fig. E-6 we have plotted "contour 1" of (E.31) for $\tilde{z} < 0$ (for $\tilde{z} > 0$ the contour is just mirrored about the real axis). Also, as earlier, we may set $|T| = 2$ and then given $\tilde{z}$ we can compute $|\tilde{T}|$ from (E.32) to obtain the cutoffs on the contour in Fig. E-6.

Thus using contour 1 and the first term of the asymptotic expansion (E.10), (2.80) of Part I becomes (2.82). Similarly in Part II, Eq. (4.4) becomes (4.8). Roughly the integrand of the first case goes $\sim 1/V$ while the integrand of the second case goes $\sim 1/V^3$. Thus with the aid of Fig. E-6 we conclude that $F(\tilde{V})$ in each case is sufficiently constant provided $|\tilde{z}| \gg 1$ but that even if $|\tilde{z}| \approx 1$ the errors involved should not change the results greatly.

Lastly we note that the requirement (E.16)

$$\frac{\left| 3\left\{\phi''(V_s)\right\}^{3/2} \right|}{\left| \sqrt{2}\,\phi'''(V_s) \right|} \gg 1$$

by direct calculation from (E.24) reduces to the requirement $|\tilde{z}| \gg 0.12$. Thus the asymptotic expansion method used to derive (E.10) breaks down in this case only when $|\tilde{z}|$ becomes much smaller than a characteristic length $|a/(\omega-\omega_{ce})|$.

Thus the free-streaming term in (2.85) of Part I and the echo saddle-point contribution (4.8) of Part II are accurate for $|\tilde{z}| \gg 1$ but still good approximations for $|\tilde{z}| \approx 1$; these results lose their validity only for $|\tilde{z}|$ significantly less than one.

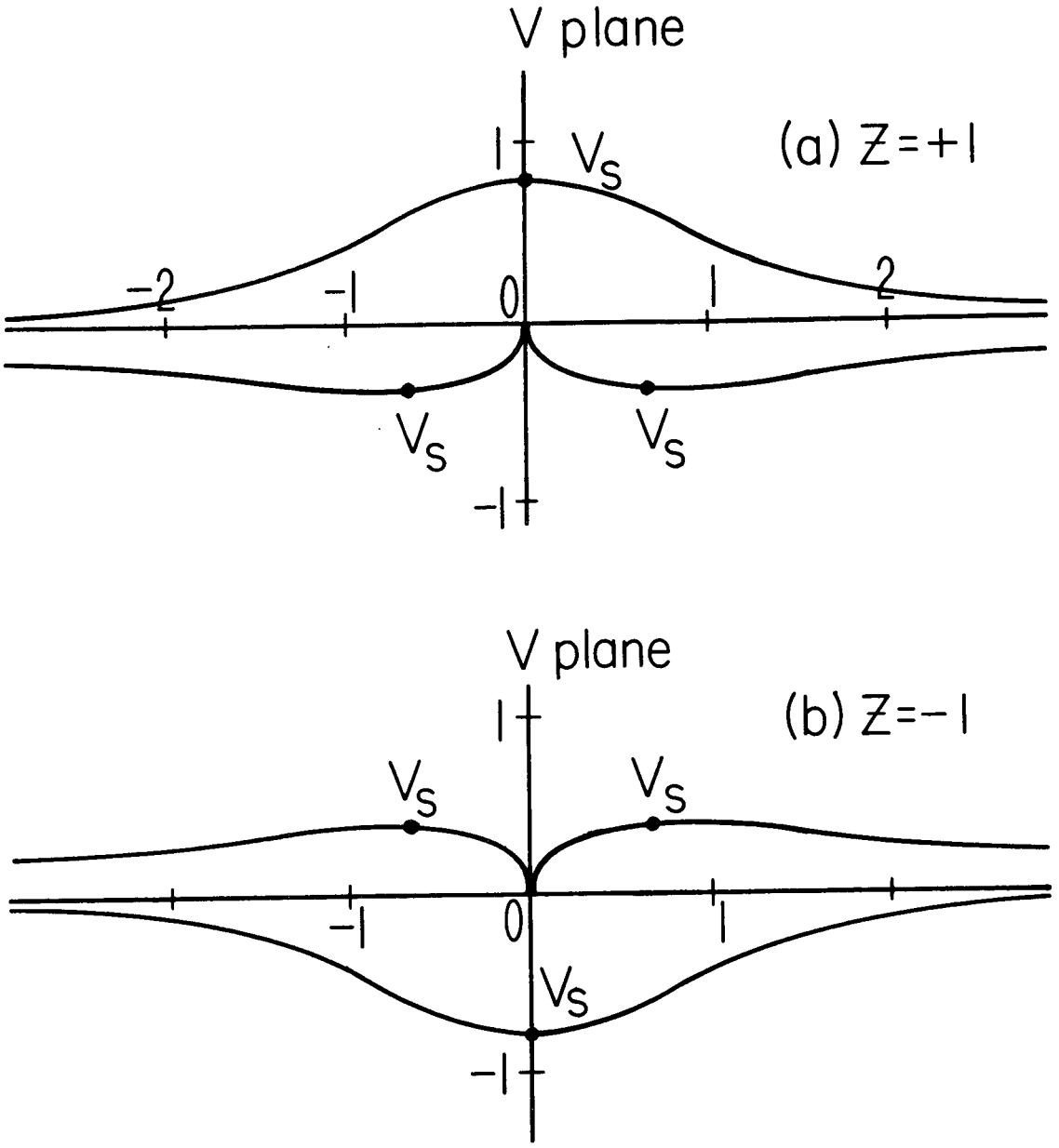

FIGURE E-4. SADDLE-POINT CONTOURS OF (E.24) FOR $Z=\pm 1$.

Shown are the saddle points of (E.24) as given by (E.29) and paths of steepest descent as given by (E.27) for $Z=+1$ and $Z=-1$.

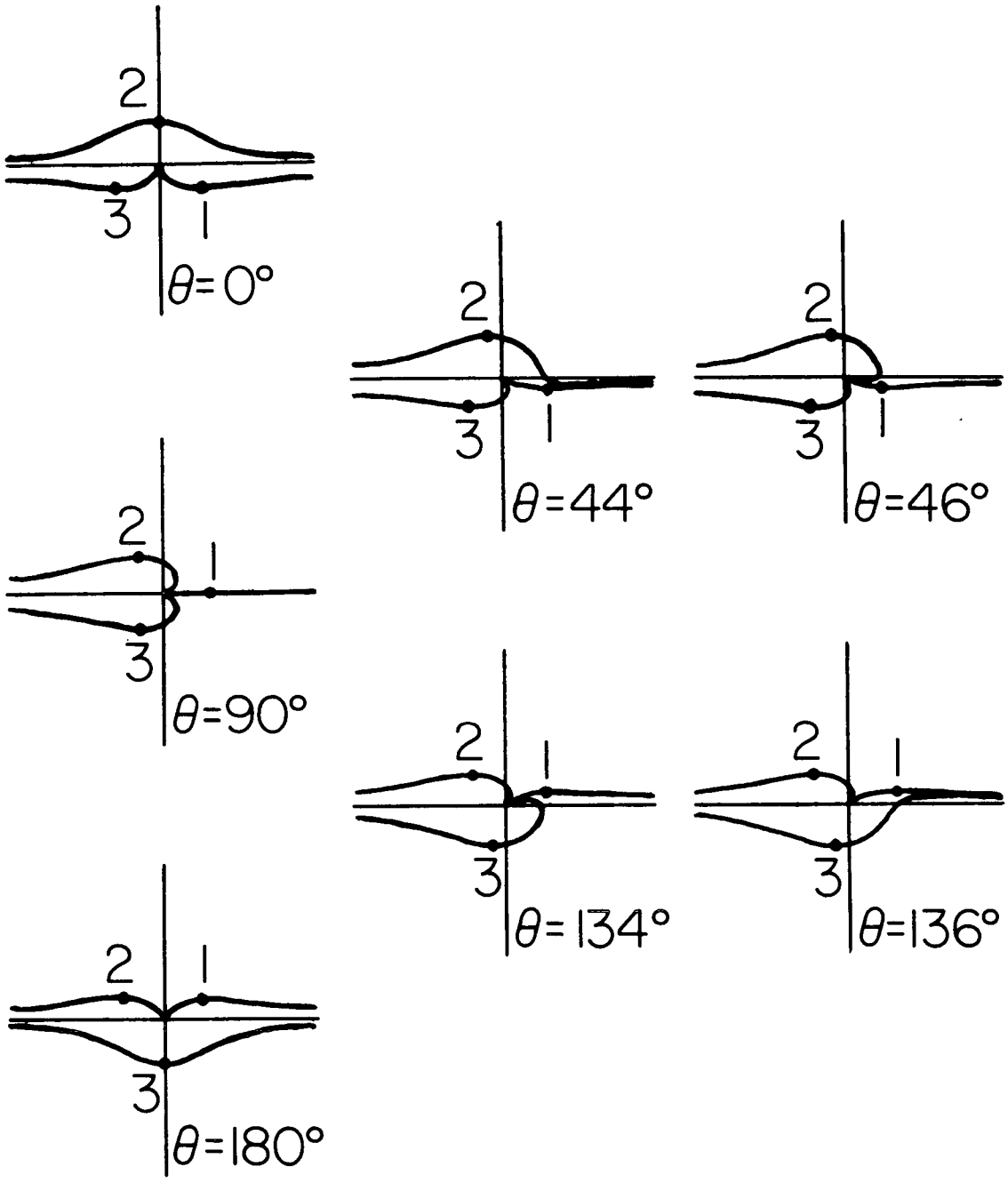

FIGURE E-5. EVOLUTION OF THE SADDLE-POINT CONTOURS OF (E.24) FOR $z = e^{i\theta}$ AS θ VARIES FROM 0° TO 180°.

Saddle points and paths of steepest descent are as given by (E.29), (E.27) respectively. Note Stokes phenomenon that occurs when $\theta = 45^\circ$ and $\theta = 135^\circ$.

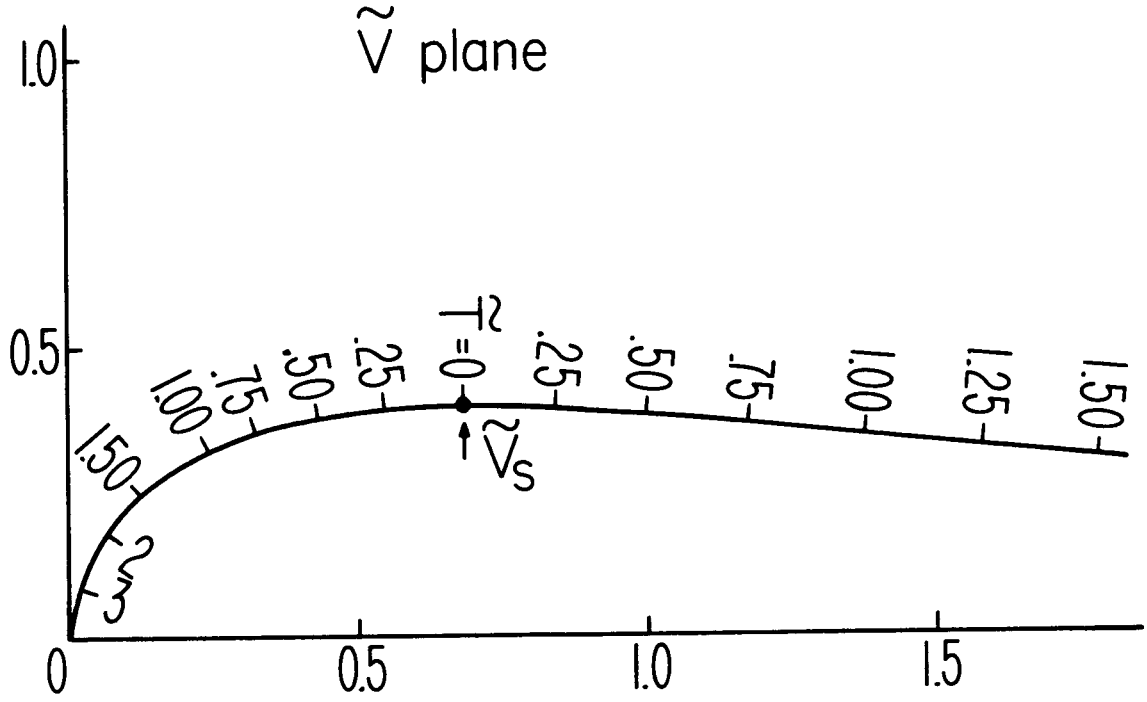

FIGURE E-6. SADDLE-POINT CONTOUR OF (E.24) IN THE $\tilde{V}$ PLANE WITH $\tilde{T}$ SPECIFIED ALONG THE CONTOUR.

Shown is the path of steepest descent of (E.24) in the $\tilde{V}$ ($=V/Z^{1/3}$) plane for Z real and with values of $\tilde{T}$ ($=T/Z^{1/3}$) specified along the contour [see (E.31),(E.32)]. This plot is useful in estimating the range of the variable $\tilde{V}$ over which $F(\tilde{V})$ should be approximately constant.

BIBLIOGRAPHY

1. L. Landau, J. Phys., USSR, X, 25 (1946).

2. R. W. Gould, Phys. Rev. 136, A991 (1964).

3. G. L. Johnston, Ph.D. Thesis, University of California (1967).

4. W. E. Drummond, Rev. Sci. Instr. 34, 779 (1963).

5. M. Feix, Phys. Letters 9, 123 (1964).

6. A. Y. Wong, N. D'Angelo, and R. W. Motley, Phys. Rev. Letters 9, 415 (1962); Phys. Rev. 133, A436 (1964).

7. B. D. Fried and R. W. Gould, Phys. Fluids 4, 139 (1961).

8. H. H. Kuehl, G. E. Stewart, and C. Yeh, Phys. Fluids 8, 723 (1965).

9. H. Derfler and T. C. Simonen, Phys. Fluids 12, 269 (1969).

10. B. D. Shafranov, Soviet Phys.-JETP 7, 1019 (1958).

11. D. L. Sachs, Phys. Fluids 8, 1520 (1965).

12. P. M. Platzman and S. J. Buchsbaum, Phys. Rev. 128, 1004 (1962).

13. J. C. Lee, T. J. Fessenden, and F. W. Crawford, 9th International Conference on Phenomena in Ionized Gases, Bucharest, Romania, p. 475 (1969).

14. T. Pradham, Phys. Rev. 107, 1222 (1957).

15. N. L. Varma, Acta Physica Austriaca 21, 262 (1966).

16. S. K. Majumdar, Indian J. Phys. 39, 511 (1965).

17. T. H. Stix, The Theory of Plasma Waves (McGraw-Hill, N.Y., 1962).

18. D. C. Montgomery and D. A. Tidman, Plasma Kinetic Theory (McGraw-Hill, N.Y., 1964).

19. Ginzburg, Propagation of EM Waves in Plasma (Gordon & Breach, N.Y., 1961).

20. T. Kamimura and A. Hasegawa, Phys. Fluids 12, 1480 (1969).

21. B. D. Fried and S. D. Conte, The Plasma Dispersion Function (Academic Press, Inc., N.Y., 1961).

22. S. C. Brown, Basic Data of Plasma Physics (M.I.T. Press, Cambridge, 1967).

23. L. Spitzer, Jr., Physics of Fully Ionized Gases (Interscience Publishers, Inc., New York, 1962).

24. A. N. Kaufman, "Dissipative Effects", in Plasma Physics in Theory and Application, W. B. Kunkel, Ed. (McGraw-Hill, N.Y., 1966).

25. B. S. Tanenbaum, Plasma Physics (McGraw-Hill, N.Y., 1967).

26. T. M. O'Neil and R. W. Gould, Phys. Fluids 11, 134 (1968).

27. J. H. Malmberg, C. B. Wharton, R. W. Gould, and T. M. O'Neil, Phys. Rev. Letters 20, 95 (1968); and Phys. Fluids 11, 1147 (1968).

28. D. R. Baker, N. R. Ahern, and A. Y. Wong, Phys. Rev. Letters 20, 318 (1968).

29. H. Ikezi and N. Takahashi, Phys. Rev. Letters 20, 140 (1968).

30. T. M. O'Neil, Phys. Fluids 11, 2420 (1968).

31. W. B. Thompson, An Introduction to Plasma Physics (Addison-Wesley, Inc., Massachusetts, 1964).

32. Abramowitz and Stegun (Eds.), Handbook of Mathematical Functions (National Bureau of Standards, Washington, D.C., 1968).

33. B. D. Fried and C. L. Hedrick, Festschrift for Gregor Wentzel (University of Chicago Press, 1969).

34. B. D. Fried, C. L. Hedrick, and J. McCune, Phys. Fluids 11, 250 (1968).

35. G. F. Carrier, M. Krook, and C. E. Pearson, Functions of a Complex Variable (McGraw-Hill, N.Y., 1966).